N-truncated Aβ4-x peptides in Alzheimer's disease: generation, degradation, and relationship with neuropathological hallmarks

Dissertation
for the award of the degree
"**Doctor rerum naturalium**"
of the Georg-August-Universität Göttingen

within the doctoral program
"Molecular and Cellular Physiology of the Brain"
of the Georg-August University School of Science (GAUSS)

submitted by
Silvia Zampar
from Monza, Italy

Göttingen, 2021

Thesis Committee

Prof. Dr. Oliver Wirths
Department of Psychiatry and Psychotherapy, University Medical Center Göttingen

Prof. Dr. Tiago F. Outeiro
Department of Experimental Neurodegeneration, University Medical Center Göttingen

Prof. Dr. Fred S. Wouters
Department of Neuropathology, University Medical Center Göttingen

Members of the Examination Board

Reviewer: **Prof. Dr. Oliver Wirths**
Department of Psychiatry and Psychotherapy, University Medical Center Göttingen

Second Reviewer: **Prof. Dr. Tiago F. Outeiro**
Department of Experimental Neurodegeneration, University Medical Center Göttingen

Further members of the Examination Board:

Prof. Dr. Fred S. Wouters
Department of Neuropathology, University Medical Center Göttingen

Prof. Dr. Thomas Dresbach
Department of Anatomy and Embryology, University Medical Center Göttingen

Prof. Dr. med. Christine Stadelmann-Nessler
Department of Neuropathology, University Medical Center Göttingen

Prof. Dr. mult. Thomas Meyer
Department of Psychosomatic Medicine and Psychotherapy, University Medical Center Göttingen

Date of the oral examination: 10.11.2021

"Knowledge has a beginning but no end"

Geeta Iyengar

List of publications:

Publications included in this thesis:

Zampar S., and Wirths O. 2021. "Characterization of a Mouse Model of Alzheimer's Disease Expressing Aβ4-42 and Human Mutant Tau." International Journal of Molecular Sciences 22 (10):5191. doi: 10.3390/ijms22105191.

Zampar S., Klafki H. W., Sritharen K., Bayer T. A., Wiltfang J., Rostagno A., Ghiso J., Miles L. A., and Wirths O. 2020. "N-terminal heterogeneity of parenchymal and vascular amyloid-beta deposits in Alzheimer's disease." Neuropathol Appl Neurobiol 46 (7):673-685. doi: 10.1111/nan.12637.

Hornung K.*, **Zampar S.***, Engel N., Klafki H., Liepold T., Bayer T. A., Wiltfang J., Jahn O., and Wirths O. 2019. "N-Terminal Truncated Abeta4-42 Is a Substrate for Neprilysin Degradation in vitro and in vivo." J Alzheimers Dis 67 (3):849-858. doi: 10.3233/jad-181134.
* Equal contribution

Publications not included in this thesis:

Zampar S., and Wirths O. 2020. "Immunotherapy Targeting Amyloid-beta Peptides in Alzheimer's Disease." In Alzheimer's Disease: Drug Discovery, edited by X. Huang. Brisbane (AU), doi: 10.36255/exonpublications.alzheimersdisease.2020.ch2.

Wirths O., and **Zampar S.** 2020. "Neuron Loss in Alzheimer's Disease: Translation in Transgenic Mouse Models." Int J Mol Sci 21 (21). doi: 10.3390/ijms21218144.

Klafki H. W., Rieper P., Matzen A., **Zampar S.**, Wirths O., Vogelgsang J., Osterloh D., Rohdenburg L., Oberstein T. J., Jahn O., Beyer I., Lachmann I., Knölker H.-J., and Wiltfang J. 2020. "Development and Technical Validation of an Immunoassay for the Detection of APP(669-711) (Aβ(-3-40)) in Biological Samples." International journal of molecular sciences 21 (18):6564. doi: 10.3390/ijms21186564.

Wirths O., and **Zampar S.** 2019. "Emerging roles of N- and C-terminally truncated Aβ species in Alzheimer's disease." Expert Opinion on Therapeutic Targets 23 (12):991-1004. doi: 10.1080/14728222.2019.1702972.

Wirths O., **Zampar S.**, and Weggen S. 2019. "N-Terminally Truncated Abeta Peptide Variants in Alzheimer's Disease." In Alzheimer's Disease, edited by T. Wisniewski. Brisbane (AU), doi: 10.15586/alzheimersdisease.2019.ch7.

Gerberding A. L., **Zampar S.**, Stazi M., Liebetanz D., and Wirths O. 2019. "Physical Activity Ameliorates Impaired Hippocampal Neurogenesis in the Tg4-42 Mouse Model of Alzheimer's Disease." ASN Neuro 11:1759091419892692. doi: 10.1177/1759091419892692.

Walter S., Jumpertz T., Hüttenrauch M., Ogorek I., Gerber H., Storck S. E., **Zampar S.**, Dimitrov M., Lehmann S., Lepka K., Berndt C., Wiltfang J., Becker-Pauly C., Beher D., Pietrzik C. U., Fraering P. C., Wirths O., and Weggen S. 2019. "The metalloprotease ADAMTS4 generates N-truncated Aβ4–x species and marks oligodendrocytes as a source of amyloidogenic peptides in Alzheimer's disease." Acta Neuropathologica 137 (2):239-257. doi: 10.1007/s00401-018-1929-5.

ABSTRACT

Amyloid pathology in Alzheimer's disease (AD) is characterized by a heterogeneity of amyloid-β peptides (Aβ) variants. The N-terminally truncated $A\beta_{4\text{-}42}$ peptides are among the most abundant species and were reported having an enhanced aggregation propensity and comparable toxicity to full-length Aβ peptides. Employing transgenic mouse models of AD, we aim to address the importance of this particular Aβ isoform in AD pathology. We questioned if an alteration of their degradation or generation affects the course of the pathology and how $A\beta_{4\text{-}42}$ peptides and the two main neuropathological hallmarks of AD, extracellular amyloid deposits and tau pathology, are interrelated *in-vivo*.

We showed that $A\beta_{4\text{-}42}$ is a substrate of the enzyme Neprilysin (NEP) *in-vitro*, and that *in-vivo*, the absence of endogenous NEP in the Tg4-42^{het} mouse model of AD, exclusively expressing $A\beta_{4\text{-}42}$ peptides preferentially in the CA1 region of the hippocampus, led to an increased deposition of this isoform in hippocampal CA1 pyramidal neurons. The removal of ADAMTS4, a metalloprotease able to generate $A\beta_{4\text{-}x}$ peptides in oligodendrocytes, from the 5xFAD mouse model of familial AD, caused an improvement in the motor deficits characterizing this transgenic line, concomitant to reduced $A\beta_{4\text{-}x}$ levels in the spinal cord.

To investigate the relationship between $A\beta_{4\text{-}42}$ peptides and extracellular amyloid pathology, the FAD/Tg4-42^{hom} line was generated crossing the Tg4-42^{hom} transgenic model, characterized by the sole expression of the $A\beta_{4\text{-}42}$ isoform and time-dependent behavioral deficits and neurodegeneration, with the plaque-bearing 5xFAD mouse model of AD, demonstrating no impairment or hippocampal loss of neurons at the age employed here. While an aggravation of deficits in motor performance and an increased loss of spinal α-motoneurons was detected in the filial line, cognitive performance was unaltered. Surprisingly, a rescue of recognition memory could even be observed in

FAD/Tg4-42^{hom} mice, accompanied by an increased number of pyramidal neurons in the distal portion of the CA1 region of the hippocampus compared to Tg4-42^{hom} controls. Together with increased levels of insoluble Aβ_{4-x} peptides in the hippocampus of FAD/Tg4-42^{hom} mice, these results support the hypothesis of extracellular amyloid plaques possessing buffering properties towards soluble Aβ_{4-42} peptides.

In the classical amyloid cascade hypothesis, Aβ is considered to act upstream of tau pathology. This hypothesis is supported by several studies on APP-overexpressing lines that have been crossed with mouse models of tauopathy. We crossed the Tg4-42^{hom} line with the MAPT (PS19) transgenic tau model to investigate whether soluble N-truncated Aβ_{4-42} variants affect the phosphorylation and aggregation of tau. Although the co-expression of Aβ_{4-42} and transgenic human tau caused an aggravation of spatial memory deficits, neurodegeneration, and tau hyperphosphorylation remained unaltered in MAPT/Tg4-42^{hom} mice compared to the transgenic parental lines.

CONTENTS

1 INTRODUCTION

1.1 Alzheimer's Disease

Named after Alois Alzheimer who first characterized this pathology in 1906 (Alzheimer 1907), Alzheimer's disease (AD) is an irreversible and progressive neurodegenerative disorder which constitutes the most common form of dementia. An estimation from the World Health Organization suggests that worldwide around 50 million people suffer from dementia, of which two thirds attributed to AD (WHO 2017). A number projection sees a triplication of total dementia cases by 2050, with possibly 152 million people affected (WHO 2019), especially in the developing nations. The tolls of this disease have detrimental effects on finances and economies, but foremost on communities, families and individuals involved. The lack of an effective medical treatment after more than 100 years from its discovery leaves unmet medical needs and a substantial burden for health care systems.

1.1.1 Clinical features of AD

Clinically, patients suffering from AD display a gradual loss of memory and impairment of cognition. The progression of the disease is slow and can be differentiated into stages (Reisberg et al. 1982). During the initial preclinical stage, which can last several years, no obvious clinical symptoms can be observed but neurodegenerative processes begin to take place in the brain, specifically in the hippocampus and entorhinal cortex (medial temporal lobe) (Backman et al. 2004). A prodromal phase follows, during which the patients start to develop a mild memory loss that could be interpreted as normal forgetfulness. Neurodegeneration then progresses to the point where the established mild cognitive impairment (MCI) stage can be revealed through neuropsychological tests. At this stage. despites the ability to still live independently, the patients' memory declines, affecting their performance at work and in social settings. Further cognitive

decline leads to the moderate stages of AD. At this point, patients start to forget details about their personal history and short-term events with the neuropathology spreading further to frontal and parietal lobes. Subsequently, AD patients can no longer execute complex tasks and display language impairments, disorientation, and motor deficits up to the point of requiring help in their daily lives. At the severe dementia stage, the patients are unaware of their surroundings, fail to recognize family members and need constant care. At this point the neuropathology affects at this point the entire brain. Changes in personality and behavior can be observed, with increased aggressiveness, suspiciousness, and delusions (Forstl and Kurz 1999). Additionally, an aggravation of language and motor deficits becomes evident with apathy, rigidity, and bradykinesia (Scarmeas et al. 2004). At the very late stage, all verbal abilities are lost, the patients require assistance in toileting, in eating and become prone to infections (Forstl and Kurz 1999).

1.1.2 Etiology

Alzheimer's disease can be considered a multifactorial disease. Affecting older people (> 65 years), ageing-related biological processes are believed to be implicated in the pathogenesis of the disease. The incidence rate of AD increases almost exponentially with increasing age until 85 years of age. The strong age-dependent association of AD could be the result of cumulative effects of several risks and protective factors over the lifespan, such as genetic susceptibility, psychosocial situation, biological factors, and environmental exposures experienced (Qiu, Kivipelto, and von Strauss 2009). Based on the age of onset and genetic predisposition, two forms of AD can be distinguished: an early-onset familial form (EO-FAD), which affects only 2-5% of all cases and develops before the age of 65, and a sporadic late-onset form (LOAD), which accounts for most of all diagnosed cases (~95-98%) (Campion et al. 1999, Reitz and Mayeux 2014).

1.1.2.1 Genetic risk factors

More than 200 mutations in the genes encoding for the β-amyloid precursor protein (*APP*), presenilin 1 (*PSEN1*) and its homologue presenilin 2 (*PSEN2*) have been identified and linked to the development of EO-FAD (Tanzi 2012). Most of these mutations are inherited in an autosomal-dominant manner and exhibit a high penetrance (>85%). Because of such mutations, the production of total Aβ, the $A\beta_{42}$ to $A\beta_{40}$ ratio and Aβ aggregation increases, leading to the development of the pathology (Holtzman, Morris, and Goate 2011, Reitz and Mayeux 2014). LOAD, on the other hand, has no consistent mode of transmission and multiple factors are believed to contribute (Bertram and Tanzi 2005). Recent genome-wide association studies (GWAS) have reported more than 20 risk loci in AD patients (Marioni et al. 2018, Jansen et al. 2019a, Kunkle et al. 2019). The main genetic risk factor is associated with the lipid/cholesterol carrier apolipoprotein E (APOE). The APOE gene encodes for three allelic variants (ε2, ε3, and ε4), of which the ε4 allele constitutes the susceptibility factor for AD development. The frequency of this variants is 40% in AD patients, in contrast to 15% in the general population (Farrer et al. 1997). APOEε4 is associated with a dose-dependent decrease in age of onset, with a 3-fold and 15-fold increase of the risk to develop AD if one or two copies of the allele are carried, respectively (Corder et al. 1993, Pastor et al. 2003). The ε2 variant, on the other hand, has been associated with a reduced risk of developing LOAD (Corder et al. 1994). The mechanism by which APOEε4 predisposes to AD is not fully unraveled. It has been shown that the ε4 variant could modulate Aβ accumulation and clearance in the brain (Castellano et al. 2011), and might impair synaptic and mitochondrial function, contributing to the early events of the disease (Valla et al. 2010). Among the other genetic risk loci, independent studies employing whole genome sequencing and *in-vivo* validations reported common or rare functional variants in the following genes: *CR1*, *BIN1*, *TREM2*, *CLU*, *PILRA*, *SORL1*, *ADAM10*, *ABCA7*, and *CD33* (Pimenova, Raj, and Goate 2018). Being involved with inflammatory response, APP processing, tau pathology,

cell migration, lipid metabolism, and endocytosis, these studies remark the importance of these physiological processes in the development of the disease.

1.1.2.2 Non-genetic risk factors

While aging is the primary risk factor for AD, the risk of developing the disease is increased by several acquired factors. Cerebrovascular diseases, hypertension, obesity, diabetes, and dyslipidemia are among the most renown health conditions linked with AD (Mayeux and Stern 2012). Cerebrovascular changes, causing strokes, brain hypoxia, and changes in cerebral white matter, are indeed known to increase the probability of dementia. Cerebral amyloid angiopathy (CAA) is found in more than 50% of post-mortem analyses on AD brains (Reitz, Brayne, and Mayeux 2011, Love and Miners 2016). Hypertension contributes to cerebrovascular diseases and might lead to brain-blood barrier dysfunctions (Skoog and Gustafson 2006). Several epidemiological studies suggest an association between type II diabetes and AD. Insulin resistance and insulin deficiency result in cerebrovascular damage and vascular inflammation and are believed to be the mechanisms linking the two pathologies (Li, Song, and Leng 2015). Along with metabolic and cardiovascular diseases, the person's psychological status was found to play a role in the development of AD. Stress, depression, and inadequate sleep have been associated with an increased risk of developing the pathology (Ownby et al. 2006, Huang et al. 2009). Other modifiable health factors (e.g. smoking, alcohol consumption) were also associated with the etiology of the disease (Cataldo, Prochaska, and Glantz 2010). Additionally, traumatic brain injuries in early adulthood were associated with an increased risk of developing AD later in life (Plassman et al. 2010). While many co-morbidities could influence the beginning and progression of AD, many factors are preventable. A healthy diet and an active and socially integrated lifestyle could have a positive influence on cognitive functions and might delay the onset of AD (Fratiglioni, Paillard-Borg, and Winblad 2004).

1.2 Neuropathological hallmarks

1.2.1 Amyloid pathology

One of the main neuropathological hallmarks of AD is the deposition of β-amyloid (Aβ) peptides in extracellular deposits, known as senile amyloid plaques. According to their morphology, amyloid plaques can be classified into diffuse plaques and dense-core/neuritic plaques. Diffuse plaques are constituted of Aβ peptides in a non β-sheet conformation (non-fibrillar), while in neuritic plaques Aβ is aggregated in a β-sheet conformation (fibrillar) (Fig. 1.1A,B). The latter are believed to cause detrimental effects by increasing dystrophic neurites, synaptic and neuron loss, activation of astrocytes and microglial cells in their surroundings (Itagaki et al. 1989, Masliah et al. 1994, Pike, Cummings, and Cotman 1995, Knowles et al. 1999, Urbanc et al. 2002). Diffuse plaques, on the other hand, can be found also in brains of cognitive normal elderly and might not have direct negative effects in the brain (Masliah et al. 1990, Delaere et al. 1990, Dickson et al. 1992). The spatio-temporal progression pattern of amyloid pathology in the brain has been classified in stages (A-C) by Braak and Braak (Braak and Braak 1991). A more recent classification by Thal and coworkers identifies five phases of Aβ accumulation which follow a descendent progression (Thal et al. 2002). Starting in the neocortex, Aβ pathology later involves allocortical brain regions in phase two, reaching diencephalic nuclei, the putamen, the caudate nucleus, the substantia innominata, and the basal forebrain in the following phases. Finally, accumulation of Aβ is found in the brainstem and the cerebellum. Despite amyloid deposits being a major hallmark of the disease, a poor correlation between amyloid plaques and cognitive status has been reported (Katzman et al. 1989, Hulette et al. 1998). Concomitant to amyloid deposition in the brain parenchyma, accumulation of Aβ peptides can be observed also within the vessel walls (Fig. 1.1C). The majority of AD patients exhibits cerebral amyloid angiopathy (CAA), but accumulation of Aβ in brain vessels has been reported also in the healthy aging brain

(Lewis et al. 2006, Kalaria 2001). Aβ-CAA is believed to derive from neuronal sources and accumulate in the vessels as consequence of a failure in perivascular lymphatic drainage. CAA results in decreased vascular reactivity, affecting the blood supply and preventing the elimination of fluid and solutes from the brain (Weller et al. 2009).

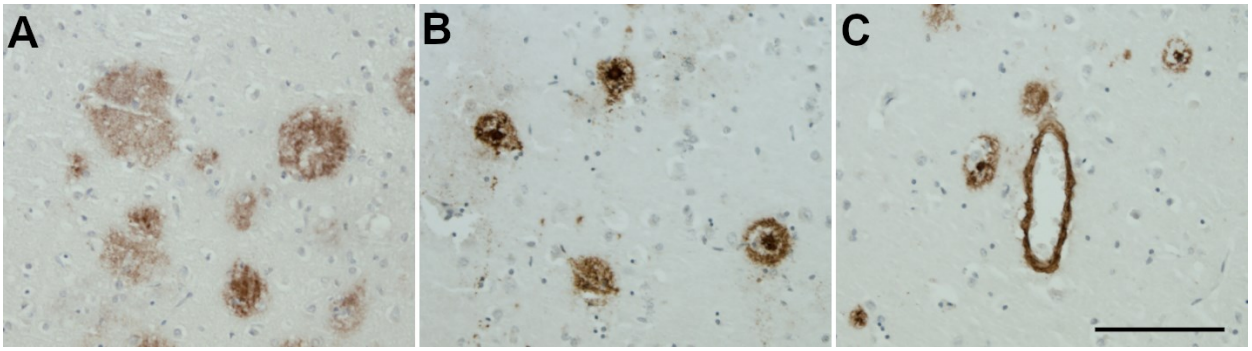

Fig. 1.1 Amyloid deposition in AD brain.
(A) Diffuse plaques, (B) neuritic plaques, and (C) cerebral amyloid angiopathy visualized by immunohistochemistry employing an antibody detecting $A\beta_{42}$ in the cortex of an AD brain. Scale bar: 100 μm

1.2.2 Neurofibrillary tangles

The second major neuropathological hallmark of AD are neurofibrillary tangles (NFTs) (Fig. 1.2). Despite being first described by Alois Alzheimer at the beginning of the 20th century (Alzheimer 1907), their composition has been unraveled only approximately 80 years later. NFTs are constituted of paired helical filaments (PHFs) predominantly made of hyperphosphorylated and misfolded forms of the microtubule-associated protein tau (MAPT) (Grundke-Iqbal et al. 1986, Kosik, Joachim, and Selkoe 1986). The protein tau is predominantly expressed in neurons and its main physiological functions involve microtubule assembly thus influencing the stability of the cytoskeleton and axonal transport (Drechsel et al. 1992). In AD brains, tau is found in a hyperphosphorylated state, which impairs its ability to bind to microtubules and enhances its aggregation into tangles (Lindwall and Cole 1984, Alonso et al. 2001). Hyperphosphorylated tau has been linked with alteration in mitochondrial respiration and axonal transport, and negatively

affect neuronal integrity (Ittner and Gotz 2011). Compared to amyloid deposits, NFTs appear at younger age in AD patients (Braak and Braak 1997) and their pattern of progression is quite predictable. Inclusions are initially observed in the transentorhinal (perirhinal) region, later spreading to the entorhinal cortex and CA1 region of the hippocampus. Limbic structures are subsequently affected with a final involvement of isocortical, primary sensory, motor, and visual areas (Braak and Braak 1991). The spreading pattern has been classified and divided into six stages (I-VI), which are widely used as a neuropathological criterion for AD. Unlike extracellular amyloid deposits, NFTs have shown a strong correlation with the cognitive decline of AD patients (Gomez-Isla et al. 1997, Giannakopoulos et al. 2003, Nelson et al. 2012).

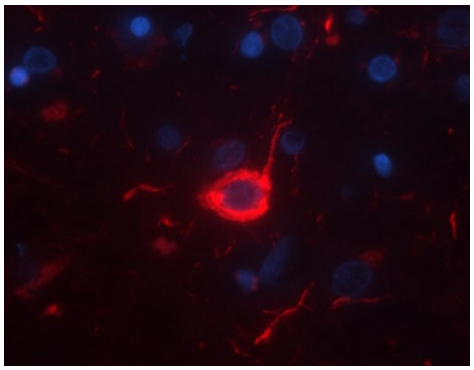

Fig. 1.2 Neurofibrillary tangle in AD brain.
Fluorescent immunohistochemical staining of a NFT in the cortex of an AD brain using the AT8 antibody.

1.2.3 Neuron loss and brain atrophy

Loss of neurons is a key feature in AD pathology (Coleman and Flood 1987, Hof, Cox, and Morrison 1990). Neurodegeneration can be observed already at preclinical stages when the above-mentioned neuropathological hallmarks are not yet evident (Gomez-Isla et al. 1996, West et al. 1994). Neuron loss in the Cornu Ammonis area 1 (CA1) region of the hippocampus (Simic et al. 1997) and in the entorhinal cortex appears to correlate with the severity of the cognitive deficits (Giannakopoulos et al. 2003), but also other brain regions are affected by neurodegeneration, with the involvement of the entire brain at

late stages of the pathology (Mountjoy et al. 1983). Because of the loss of neuronal cells, brain atrophy is observed in AD (Fig. 1.3). Magnetic resonance imaging (MRI) showed reduction of brain volumes and weights already at early stages of the pathology and could be a predictive measure for the progression from MCI to AD (Jack et al. 2005). Atrophic changes had been observed in the medial temporal lobe, in the inferior temporal and the superior and middle cortices (Duyckaerts, Delatour, and Potier 2009, Halliday et al. 2003). Consequently, ventricles become enlarged, the cortical sulci widen, and the gyri shrink. The mechanisms underlying neuronal death and the resulting atrophy in AD are not fully understood. Both amyloid and tau pathology have been found causative of neurodegeneration. Senile Aβ plaques might contribute to focal neuronal toxicity in their immediate environment (Urbanc et al. 2002, Xie et al. 2003), although they do not correlate with the cognitive decline in diseased patients. On the other hand, soluble Aβ oligomers and intraneuronal Aβ have been linked to neurodegeneration (Haass and Selkoe 2007, Wirths and Zampar 2020). Aβ peptides may interact and disrupt the endoplasmic reticulum (Mukhin, Pavlov, and Klimenko 2017), or directly trigger apoptosis (Bancher et al. 1997). A direct correlation between NFTs and neuronal loss (Gomez-Isla et al. 1997, Giannakopoulos et al. 2003) and grey matter atrophy (Jack et al. 2002, Whitwell et al. 2008) was observed in AD patients. Hyperphosphorylated tau was associated with the disruption of the glutamate receptors NMDA and AMPA at the post-synapses (Hoover et al. 2010). Synaptic pathology also contributes to the atrophic changes in diseased brains. Reduced synapses were observed in the CA1 region of the hippocampus of mild AD patients when compared to controls and MCI patients (Scheff et al. 2007). Interestingly, loss of synapses could be one of the first pathological alteration in AD, preceding neuron loss (Serrano-Pozo et al. 2011a). Synapse loss and disrupted synaptic transmission have been associated with the detrimental effects of both Aβ and tau proteins (Spires-Jones and Hyman 2014).

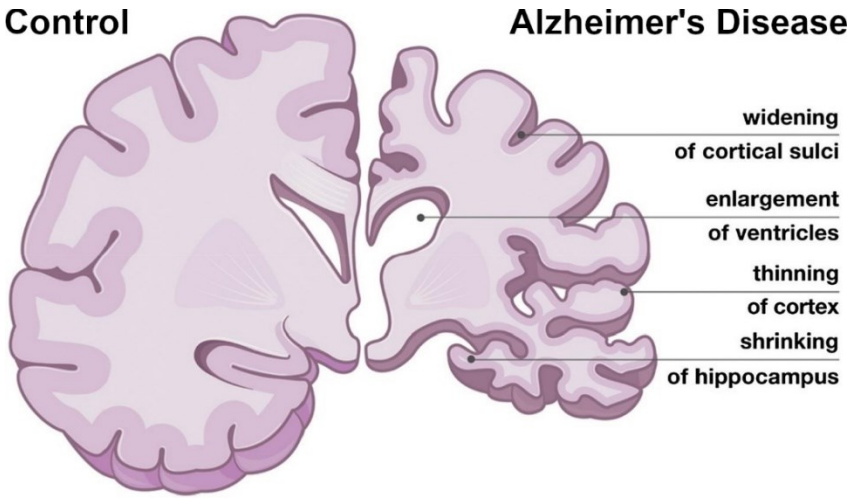

Fig. 1.3 Brain atrophy in AD.
While a healthy brain (left) preserves intact volume and weight, an AD brain (right) presents with general atrophy, enlargement of ventricles, widening of cortical sulci and shrinkage of gyri. Adapted from (Sungura et al. 2021).

1.2.4 Inflammation

Neuroinflammation is a feature found in both human AD brains and transgenic mouse models of the pathology (Hoozemans et al. 2006, Schwab, Klegeris, and McGeer 2010). Aβ is considered the main driver of a glial response, as activated microglia and reactive astrocytes are predominantly present in close proximity of neuritic plaques (Itagaki et al. 1989). Recent observations suggest also a relationship between tau pathology and neuroinflammation (Serrano-Pozo et al. 2011b). It is still a matter of debate if a neuroinflammatory response is beneficial or detrimental to the pathogenesis of AD. While some studies suggest a protective role of microglia and astrocytes because of the potential endocytosis and degradation of Aβ by glial cells, the activation of the inflammatory response may cause the formation of proinflammatory and potentially neurotoxic substances (e.g. cytokines, complement factors, reactive oxygen intermediates, and chemokines) (Wyss-Coray 2006, Wyss-Coray and Rogers 2012).

1.3 Amyloid Precursor Protein (APP)

The Aβ peptides constituting senile amyloid plaques derive from a larger precursor protein named Amyloid Precursor Protein (APP) (Kang et al. 1987, Goldgaber et al. 1987). APP is member of a family of highly conserved type I single-pass transmembrane proteins and is encoded by a gene located on chromosome 21 (Yoshikai et al. 1990). Different isoforms of APP can be generated through alternative splicing, which differ by the total number of amino acids (639–770). APP695 is the primary isoform expressed in neurons, while the longer APP751 and APP770 isoforms, containing a protease inhibitor domain in the extracellular sequence, can be found in other tissues and cell types (Kang et al. 1987, Tanaka et al. 1988, Sola et al. 1993). The synthesis of APP takes place in the ER, where it can undergo post-translational modification before being transported and integrated into the cellular membrane (Weidemann et al. 1989). The physiological role of uncleaved APP is unknown, but its involvement in cell growth, synapse formation and neural plasticity has been hypothesized (Saitoh et al. 1989, Priller et al. 2006, Turner et al. 2003). Once in the cytoplasmatic membrane, if not promptly cleaved, APP is internalized and trafficked into endosomes to be recycled (Marquez-Sterling et al. 1997) or is subjected to lysosomal degradation (Haass et al. 1992).

1.3.1 Amyloidogenic and non-amyloidogenic APP processing

The transmembrane protein APP can undergo two competing types of processing, called amyloidogenic and non-amyloidogenic, the first resulting in production of Aβ peptides (Fig. 1.4). In the non-amyloidogenic pathway, APP is cleaved at first by α-secretases within the Aβ domain (between residues Lys16 and Leu17), thus preventing the generation of Aβ peptides. This proteolysis leads to the release of a large soluble fragment called sAPPα into the extracellular space, while the 83-residue α-carboxyl-terminal fragment (CTF) remains in the cytoplasmatic membrane. The main constitutive α-secretase activity in the brain is mediated by the zinc metalloproteases member of "a

disintegrin and metalloprotease" (ADAM) ADAM10, but also other members of the family, such as ADAM9 and ADAM17, can function as α-secretases (Allinson et al. 2003, Kuhn et al. 2010). The C83 fragment is later cleaved by γ-secretase, with the release of the soluble p3 and the APP intracellular domain (AICD) fragment in the lumen and in the cytoplasm, respectively. The 3-kD p3 fragment is rapidly degraded and appears to have no important biological functions (Haass et al. 1993). The function of intracellular AICD is unclear but its involvement in gene expression regulation has been hypothesized (Cao and Südhof 2001, von Rotz et al. 2004).

In the amyloidogenic processing pathway, APP is initially cleaved by the aspartic protease β-secretase named β-site APP cleaving enzyme (BACE1), releasing a soluble APP fragment (sAPP-β) and a slightly longer APP CTF fragment (C99) (Vassar et al. 1999). BACE1 is a type 1 transmembrane aspartyl protease, able to cleave APP at the Asp1 and Glu11 positions of the Aβ domain (Liu, Doms, and Lee 2002). The consecutive action of γ-secretase causes the release of Aβ peptides into the extracellular space and AICD fragment inside the cell. The activity of γ-secretase can occur at slightly different positions on the APP protein, which are known as the ε-, ζ-, and γ-sites. These cleavage sites distance approximately three amino acids from each other and lead to the generation of Aβ peptides with different lengths at the C-terminus (Lichtenthaler et al. 1999). The proteolytic activity of γ-secretase leads to the production of ~90% of $A\beta_{1\text{-}40}$ and less than 10% of $A\beta_{1\text{-}42}$ under basal conditions (Dovey et al. 1993), but shorter and slightly elongated Aβ peptides ($A\beta_{37}$ – $A\beta_{43}$) have also been described (Steiner et al. 2018). γ-Secretase is a larger protein complex formed by either PSEN1 or PSEN2, Nicastrin, Anterior Pharynx Defective 1 and presenilin enhancer 2 (PEN2) (Oikawa and Walter 2019).

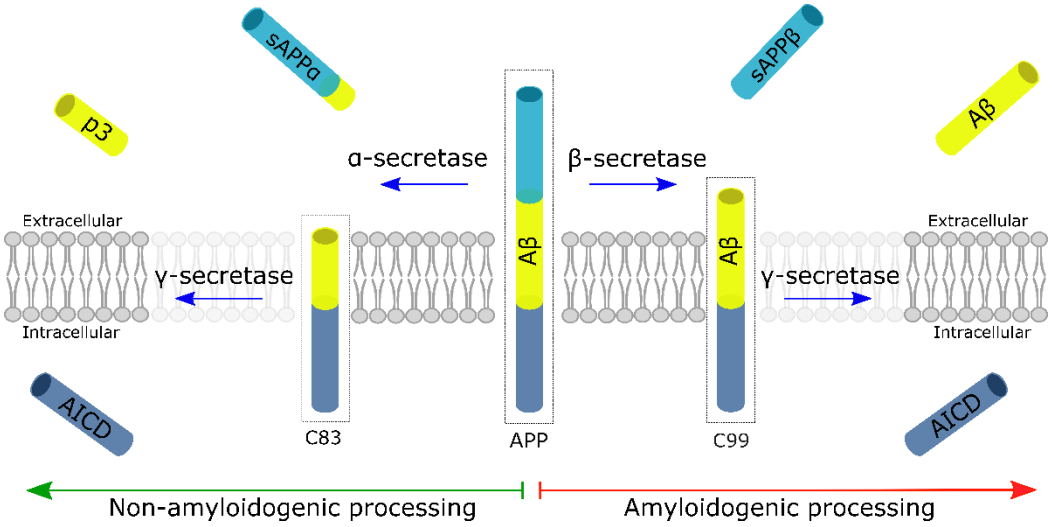

Fig. 1.4 APP processing pathways.
During the non-amyloidogenic pathway (left), APP is sequentially cleaved by α- and γ-secretase, resulting in the release of p3 and AICD. The Aβ-liberating amyloidogenic way (right) is initiated by a BACE1 cleavage of APP. Subsequently, the γ-secretase complex induces the release of Aβ and AICD. Adapted from (Wirths and Zampar 2019).

1.3.2 Classical amyloid cascade hypothesis

The aggregation and deposition of Aβ peptides in senile plaques as the main event triggering AD pathology is at the base of the amyloid cascade hypothesis, according to which extracellular fibrillary amyloid deposits are the upstream event causing NFTs formation, neurodegeneration, brain atrophy, and the consequent cognitive deficits in AD patients (Hardy and Allsop 1991) (Fig. 1.5). This hypothesis is strongly supported by the genetic risk factors of AD (Hardy and Selkoe 2002). Several mutations or duplications on the *APP* and *PSEN* genes connected with the familial form of AD (FAD) cause increased production and aggregation of Aβ (Rovelet-Lecrux et al. 2006, Reitz and Mayeux 2014). Moreover, people affected by Down syndrome (DS) possessing a third copy of the APP-containing chromosome 21 are at greater risk of developing AD pathology at young ages (Wisniewski, Wisniewski, and Wen 1985). On the other hand, a mutation recently discovered on the *APP* gene (A673T) was found to protect against AD (Maloney et al. 2014). The main genetic risk factor for LOAD, APOEε4, is associated with

an enhanced aggregation of Aβ peptides as a consequence of a reduced clearance (Kim, Basak, and Holtzman 2009). Transgenic mouse models of AD harboring FAD mutations further support the amyloid hypothesis, as they present several characteristics of AD pathology, such as Aβ plaque deposition, gliosis, and memory deficits (Duyckaerts, Potier, and Delatour 2008). Extracellular amyloid pathology is considered the trigger of NFT formation. Several transgenic mouse models over-expressing mutant APP and tau showed increased hyperphosphorylation of tau and NFTs while amyloid pathology remained unaffected (Lewis et al. 2001). This is also supported by the lack of amyloid deposition in patients suffering from mutant-tau-induced tauopathies, such as frontotemporal dementia (FTD) (Poorkaj et al. 1998, Goedert and Spillantini 2000).

The amyloid cascade hypothesis remains nevertheless controversial. The finding that amyloid burden poorly correlates with the cognitive status in AD argues against the hypothesis. Abundant amyloid deposits can be found also in *post mortem* brains of cognitively normal elderly (Hulette et al. 1998, Price and Morris 1999). An additional con-argument is the failure of several clinical trials aiming to a reduction of amyloid burden (Harrison and Owen 2016, Zampar and Wirths 2020). These and other considerations led to an adjustment of the amyloid hypothesis, putting the emphasis on soluble Aβ oligomers.

1.3.3 Soluble amyloid hypothesis

The central role of fibrillary Aβ plaques in the amyloid cascade hypothesis has been questioned. The amount and localization of these insoluble deposits indeed did not correlate with the disease state as about 40% of non-demented individuals meet the criteria for a neuropathological diagnosis of AD (Hulette et al. 1998, Price and Morris 1999). *In-vivo* imaging techniques demonstrated that the plaque burden in non-demented patients was equivalent to those of AD patients, who reached a plateau despite of the ongoing cognitive decline (Aizenstein et al. 2008). These and other considerations arose

the need for an adjustment of the amyloid hypothesis. It has therefore been proposed that soluble Aβ oligomers (AβOs), rather than insoluble fibrillar Aβ deposits, may be the crucial players in AD etiology (Fig. 1.5). Soluble Aβ oligomers (e.g., dimers, trimers, dodecamers and higher oligomers larger than 100kDa) have been described in *post mortem* tissues from AD patients (Roher et al. 1996, Shankar et al. 2008, Esparza et al. 2013) and have been found to better correlate with the risk and severity of the disease than insoluble amyloid plaques (McLean et al. 1999, Wang et al. 1999, Esparza et al. 2013). The hypothesis of soluble oligomeric Aβ forms causing direct adverse effects in contrast to fibrillary Aβ being less harmful is supported by several *in-vitro* (Selkoe 2008, Lambert et al. 1998, Wang et al. 2002, Dahlgren et al. 2002) and *in-vivo* studies (Walsh et al. 2002, Cleary et al. 2005, Lesne et al. 2006, Shankar et al. 2008). The Osaka familial AD mutation of Aβ (APP E693*Δ*) interestingly presents with severe cognitive impairment concomitant with extremely low levels of fibrillary amyloid plaques but elevated levels of AβOs in the cerebrospinal fluid (CSF) (Tomiyama et al. 2008, Tomiyama et al. 2010, Shimada et al. 2011, Kutoku et al. 2015). The contribution of fibrillary amyloid plaques and their relationship with soluble Aβ oligomers have been addressed by several groups but is still a matter of debate. While it was proposed that insoluble amyloid deposits might sequester toxic Aβ oligomers thus preventing their toxicity, others suggest that amyloid plaques might be the source of these toxic species. A popular line of thinking hypotheses a combination of both, with amyloid plaques acting as reservoirs at the beginning of the pathology, but with disease progression and saturation of the reservoirs the amyloid deposits start to release soluble Aβ aggregates (Brody et al. 2017, Maggio et al. 1992).

1.3.4 Intraneuronal amyloid hypothesis

Intracellular Aβ deposition was described as the preceding step to fibrillary amyloid plaques shortly after the discovery of Aβ as the main component of extracellular deposits (Masters et al. 1985a, Grundke-Iqbal et al. 1989). In the following decades, several studies

reported that intraneuronal accumulation of $A\beta_{42}$ peptides occurs in vulnerable brain regions, such as the hippocampus and the entorhinal cortex, and might initiate AD pathology (Fig. 1.5). Indeed, in AD patients intracellular Aβ accumulation was observed prior to the appearance of NFTs and extracellular Aβ plaques (Gouras et al. 2000, Fernandez-Vizarra et al. 2004). Interestingly, the accumulation of the peptide inside neurons appeared attenuated with the increase of cognitive dysfunction and plaque deposition (Gouras et al. 2000). Similarly, people with DS showed strong intraneuronal accumulation of $A\beta_{42}$ at young ages, which declined with the formation and maturation of senile amyloid plaques (Mori et al. 2002). The contribution of intraneuronal Aβ to AD pathology is still questioned. The main argument against a relevant role of intraneuronal Aβ lies on the fact that the intracellular deposition of the peptides could be the product of a normal neuronal metabolism which is present throughout lifespan rather than a predictor of brain amyloidosis (Wegiel et al. 2007). A later study on *post mortem* brains from the temporal neocortex of AD patients, on the other hand, supported a correlation between intracellular and membrane-associated $A\beta_{42}$ and dementia severity at the last examination before death (Steinerman et al. 2008). Additionally, using laser-capture microdissection, Aoki and coworkers showed that increased $A\beta_{42}$ could be found in CA1 pyramidal neurons of AD patients compared to controls (Aoki et al. 2008). This data was later confirmed by sensitive ELISA measurements in Purkinje cell neurons from sporadic AD patients (Hashimoto et al. 2010). It has been hypothesized that an excessive intracellular accumulation of the peptide might result in neuronal lysis, contributing to the deposition into extracellular plaques and to neuron loss (D'Andrea et al. 2001).

Intraneuronal Aβ accumulation has been reported in several single, double, and triple transgenic AD mouse models overexpressing human APP and tau, as well as lines overexpressing only human Aβ peptides [reviewed in (Wirths and Zampar 2020)]. Interestingly, the accumulation of Aβ inside pyramidal neurons of these transgenic

mouse models has been associated with neuronal loss. Immunoelectron microscopy revealed that the sub-cellular localization of $A\beta_{1-42}$ in mouse, rat, and human brains was predominantly in endosomal multivesicular bodies (MVBs) within pre- and post-synaptic compartments (Takahashi et al. 2002). The accumulation of $A\beta_{1-42}$ within endosomes and lysosomes was described also by other studies on neuron cultures and AD brains (Takahashi et al. 2004, Cataldo et al. 2004). Next to an intracellular production of Aβ, the peptide could be re-uptaken from the extracellular space and contribute to the intraneuronal accumulation. Possible internalization mechanisms have been linked to the *α*7 nicotinic acetylcholine receptors (Nagele et al. 2002), APOE receptors (Bu, Cam, and Zerbinatti 2006), *N*-methyl-D-aspartate (NMDA) (Bi et al. 2002) or advanced glycation end products (RAGE) receptors (Takuma et al. 2009). Passive diffusion of Aβ peptides through the cellular membrane has also been proposed as a way through which the peptides could enter cells (Nagele et al. 2002).

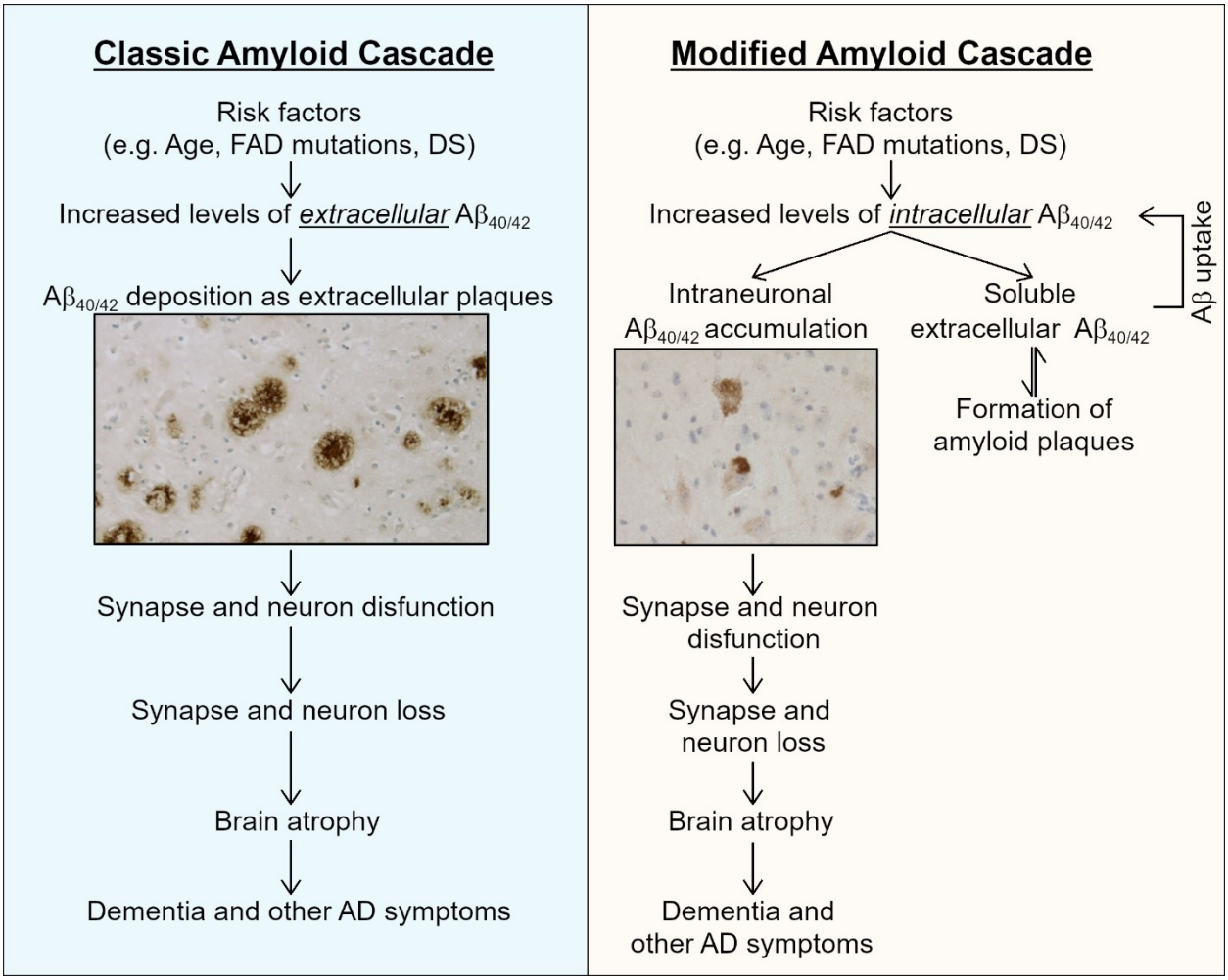

Fig. 1.5 Classic and modified amyloid cascade hypothesis.
Extracellular Aβ plaques are believed to be the causative event of AD pathology in the classic amyloid cascade (left), while intracellular accumulation of Aβ is considered the key event during AD pathology in the modified amyloid cascade (right). Adapted from (Wirths, Multhaup, and Bayer 2004)

1.3.5 Physiological and pathological functions of Aβ

In healthy brains, Aβ peptides are found at low picomolar concentrations in the extracellular space (Cirrito et al. 2003) and their formation and secretion is believed to be secondary to the dynamic activity of neurons and synapses, which trigger APP trafficking in the cell membrane towards β-secretase cleavage sites (Kamenetz et al. 2003, Cirrito et al. 2005). *In-vitro* studies suggest that the physiological function of Aβ may be related to neuronal growth and survival (Whitson, Selkoe, and Cotman 1989, Yankner, Duffy, and Kirschner 1990, Plant et al. 2003), but the most supported role of physiological Aβ is

probably the one related to synaptic activity-related learning and neuroplasticity. Picomolar levels of synthetic $A\beta_{1-42}$ indeed improved hippocampal long-term potentiation (LTP) and learning in mice lacking endogenous Aβ (Garcia-Osta and Alberini 2009, Puzzo et al. 2011, Puzzo et al. 2008). Functional α7 nicotinic acetylcholine receptors (α7nAChRs) appear to be required for Aβ-induced neuroplasticity (Puzzo et al. 2008, Dougherty, Wu, and Nichols 2003). Additionally, the turnover of synaptic vesicles (SVs) at presynaptic sites is influenced by Aβ under physiological conditions. Picomolar concentration of human $A\beta_{1-40}$ increased presynaptic release probability when applied on primary hippocampal neurons (Fogel et al. 2014). $A\beta_{1-42}$ peptides were later also correlated with an increased SVs turnover and α7nAChRs were further confirmed to play an important role in the process (Lazarevic et al. 2017).

On the other hand, elevated concentration of Aβ (high nanomolar - low micromolar) are correlated with an inhibition of synaptic function, neurotoxicity, and subsequent neuron loss. At the postsynaptic level, high levels of the peptide interfered with neurotransmission with disruption of the glutamatergic signaling pathway by internalization or desensitization of glutamatergic receptors (Walsh et al. 2002, Hsieh et al. 2006). The inhibitory effects of Aβ on synaptic activity takes place also at the presynaptic site as endocytosis of SVs is influenced by nanomolar concentrations of the peptide (Park, Jang, and Chang 2013). The synaptic depression derived from elevated Aβ concentration is suggested to be one of the mechanisms causing synaptic loss in AD (Walsh et al. 2002, Chapman et al. 1999, Hsia et al. 1999, Palop and Mucke 2010). Aβ-related synaptic toxicity was linked specifically to the detrimental effects of soluble Aβ oligomers (Lacor et al. 2004, Moreno et al. 2009, Shankar et al. 2007), but the contribution of the different Aβ conformations and species still needs extensive research. Synaptic dysfunction and neurodegeneration caused by Aβ oligomers was associated with the disruption of several receptors, including NMDA receptors (Snyder et al. 2005) or its

downstream signaling pathways [reviewed in (Yamin 2009),(Zhao, Watson, and Xie 2004)]. The inhibition of LTP was associated with an increased NMDA response through NR2B-containing NMDA receptors (Li et al. 2009). Other receptors through which Aβ oligomers might exert their toxicity include the nerve growth factor (NGF) receptors, neuronal insulin receptors, frizzled receptors, and the cellular prion protein (PrP^C) [reviews in (Kayed and Lasagna-Reeves 2013)]. The disruption of membrane permeability by the generation of pores/ion channels is also a known mechanism of Aβ toxicity (Kayed and Lasagna-Reeves 2013). The enhanced membrane permeability results in an increase of the intracellular calcium concentration and disruption of calcium homeostasis (Mattson et al. 1992, Mattson 1994, Arispe, Pollard, and Rojas 1993). The Aβ-induced disruption of calcium and other ions homeostasis might accelerate neuronal death by increasing degenerative processes, such as formation of free radicals and tau phosphorylation (Yatin et al. 1998, Takashima et al. 1993). Besides the adverse effects of extracellular Aβ, intraneuronal Aβ accumulation has been linked to synaptic disfunction (D'Andrea et al. 2001, Skovronsky, Doms, and Lee 1998, Almeida et al. 2005, Casas et al. 2004, Mori et al. 2002, Mucke et al. 2000, Spires et al. 2005). The exact mechanisms of intracellular Aβ toxicity are not clear. Intraneuronal accumulation could cause an inhibition of the proteasome and deubiquitinating enzymes (Almeida, Takahashi, and Gouras 2006). Diminished mitochondrial activity and rate of oxygen consumption (Caspersen et al. 2005) were observed as consequence of Aβ accumulation in the mitochondria. Additionally, Aβ accumulation in lysosomes is correlated with the extensive disruption of this system and altered autophagy in AD (Nixon and Cataldo 2006, Nixon et al. 2005, Chyung, Raper, and Selkoe 2005).

1.4 Heterogeneity of Aβ peptides

Besides the presence of the full-length $A\beta_{1-40}$ and $A\beta_{1-42}$ peptides, deriving predominantly from BACE1 cleavage during the APP amyloidogenic processing, a huge variety of

shortened and elongated peptide variants at either the C- or N-terminus have been described in human and transgenic mouse samples [reviewed in (Wirths and Zampar 2019)]. The first N-terminally truncated Aβ variants have been described in 1985 with amino-terminal solid phase protein sequencing, which identified $A\beta_{4\text{-}x}$ starting with phenylalanine (Phe), $A\beta_{8\text{-}x}$ starting with serine (Ser), and $A\beta_{9\text{-}x}$ starting with glycine (Gly) in amyloid plaque cores extracts from AD cases (Masters et al. 1985a, Masters et al. 1985b). More recent studies showed that more than 70% of all Aβ peptides in human brain actually consists of N-terminal truncated species and broadened the spectrum of the known N-truncated variants (Portelius et al. 2010, Moore et al. 2012). A variety of C-truncated Aβ species, deriving from different stepwise APP-processing by γ-secretase, have additionally been detected in human brain, plasma, and CSF samples using mass spectrometry methods (Moore et al. 2012, Zakharova et al. 2018). Moreover, several post-translational modifications on the Aβ sequence have been identified. N-terminal pyro-glutamylation at Glu3 and phosphorylation at Ser8 and Ser26 are among the most studied modifications, but several others have been described [reviewed in (Schaffert and Carter 2020)]. The diverse Aβ variants might contribute differently to the pathogenesis of the disease. The loss of charged amino acids at the N-terminus and the presence of post-translational modifications are indeed linked to altered aggregation and toxicity profiles because of the consequent changes of the Aβ peptides' biophysical properties (Wirths, Zampar, and Weggen 2019, Schaffert and Carter 2020).

1.4.1 N-terminal truncated Aβ peptides

N-terminally truncated species account for the majority of total Aβ in the aged human brain. The entire range of peptides between $A\beta_{1\text{-}x}$ and $A\beta_{pE11\text{-}x}$ has been detected in cortex samples of sporadic AD patients and people with a *PSEN1* mutated FAD form of the disease (Miravalle et al. 2005). Further studies showed that insoluble Aβ aggregates are mainly composed of N-truncated variants starting at positions 2, 3, pE3, 4, 5, 8, or 9 and

ending at position 42 (Sergeant et al. 2003). Among the different N-truncated variants, isoforms such as $A\beta_{pE3-42}$ or $A\beta_{4-42}$ were detected with relative high abundance, comparable or even exceeding the one of full-length $A\beta_{1-42}$ peptides (Portelius et al. 2010, Wildburger et al. 2017). Next to the presence in extracellular amyloid plaques, N-truncated variants, such as $A\beta_{2-x}$ and $A\beta_{4-x}$, have been described in brain vessels (Savastano et al. 2016, Wirths et al. 2017) but only few N-truncated species could be detected in plasma and CSF samples (Zakharova et al. 2018). The mechanism by which the different N-terminal truncated Aβ isoforms are generated is still not fully understood and several enzymes have been proposed to cleave the Aβ sequence at specific positions (Fig. 1.6) [reviewed in (Wirths, Zampar, and Weggen 2019)]. The loss of charged amino acids from the Aβ sequence is believed to alter the aggregation properties of N-truncated peptides. Several *in-vitro* and *in-vivo* studies demonstrated an increased aggregation propensity to form soluble oligomers and fibrillar, high-molecular weight aggregates, and comparable or increased neurotoxicity compared to full-length Aβ peptides for the two most abundant isoforms, $A\beta_{pE3-x}$ or $A\beta_{4-x}$ (Schilling et al. 2006, Bouter et al. 2013, Cabrera et al. 2018, Galante et al. 2012, Tekirian et al. 1999). N-terminally truncated peptides have been described also in mouse models of AD overexpressing the *APP* gene (Savastano et al. 2016, Wirths et al. 2017, Reinert et al. 2016, Schilling et al. 2008). Nevertheless, contrary to the high abundance of N-truncated Aβ peptides in human AD brains, the N-terminally shortened isoforms are greatly underrepresented in transgenic models harboring the APP_{SWE} mutation. The Swedish mutation increases APP affinity for BACE1, thus leading to a preferential production of Aβ peptides starting at position 1 (Weggen and Beher 2012). Nevertheless, a reduction of the $A\beta_{pE3–42}$ burden in 5xFAD mice resulted in a rescue of behavioral deficits (Jawhar et al. 2011), supporting the elevated toxicity of these truncated isoforms. The toxicity of $A\beta_{pE3-42}$ and $A\beta_{4-42}$ peptides was additionally demonstrated by the cognitive deficits and neurodegeneration that

characterized mouse models exclusively expressing these N-truncated Aβ variants (Wirths et al. 2009, Bouter et al. 2013).

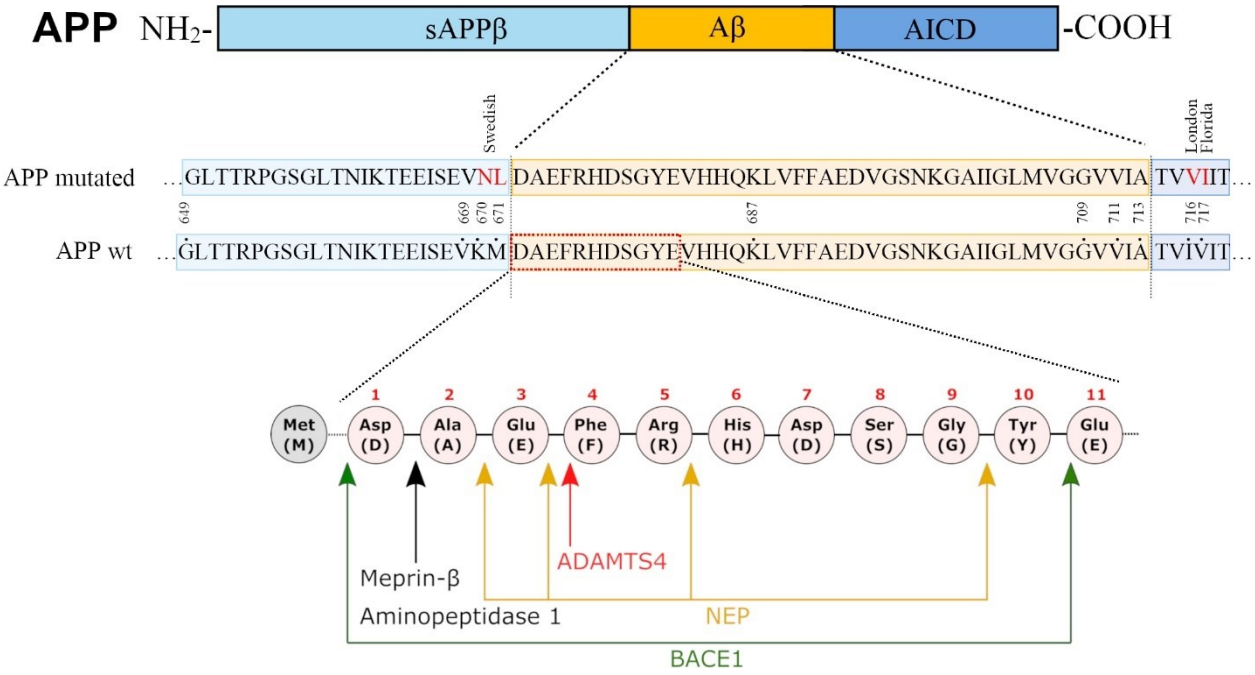

Fig. 1.6 Schematic representation of the sequence of the Aβ N-terminus.
APP mutated shows the Swedish, London, and Florida mutations present in the most common mouse models of AD. The arrows indicate the relevant cleavage site and putative enzymes involved in the generation of N-truncated Aβ species. Adapted from (Wirths, Zampar, and Weggen 2019, Klafki et al. 2020)

1.4.2 Aβ4-x peptides

Aβ species starting with phenylalanine at position 4 were firstly described in amyloid plaque cores of patients with sporadic AD and DS by Masters and colleagues in 1985 (Masters et al. 1985b). Surface-enhanced laser desorption/ionization time-of-flight (SELDI-TOF) mass spectrometry revealed that Aβ4-42 was the major N-truncated species in *post mortem* brain samples from non-demented aged individuals, patients with vascular dementia, and AD patients (Lewis et al. 2006). More recent mass spectrometry analyses confirmed that the Aβ4-42 isoform, together with AβpE3-42 and full-length peptides, was the most prominent in three brain regions of sporadic AD, FAD patients and non-demented controls (Portelius et al. 2010). In particular, Aβ1-42 and Aβ4-42 were the

predominant variants in the hippocampal and cortical regions. Despite the presence of the truncated variant in non-demented patients, $A\beta_{4-42}$ was found to be approximately 4-fold higher in AD patients (Portelius et al. 2015). Immunohistochemical staining confirmed the location of $A\beta_{4-x}$ peptides in the plaque cores and revealed the presence of these truncated isoforms within blood vessels of the majority of the analyzed AD cases (Wirths et al. 2017, Cabrera et al. 2018). Due to the loss of negatively charged amino acids, $A\beta_{4-x}$ peptides present with increased aggregation propensity and tendency to form higher molecular mass oligomers than full-length peptides counterparts, as shown by several *in-vitro* studies (Bouter et al. 2013, Cabrera et al. 2018). Evident neurotoxicity was observed in primary neuronal cultures, where $A\beta_{4-42}$ peptides displayed a toxicity comparable to $A\beta_{1-42}$ and $A\beta_{pE3-42}$. The neurotoxicity was further confirmed *in-vivo*, as intraventricular injection of $A\beta_{4-42}$ peptides into wildtype mouse brain induced working memory deficits (Bouter et al. 2013). The detrimental effects of $A\beta_{4-42}$ were extensively studied in the Tg4-42 mouse model of AD, where the N-truncated Aβ isoform exclusively is expressed under the control of the murine Thy1-promoter. Hippocampal neurodegeneration, cognitive deficits, and altered synaptic transmission could be observed in this transgenic mouse model (described in detail in paragraph 1.6.1) (Bouter et al. 2013, Dietrich et al. 2018).

1.4.3 Generation and degradation of $A\beta_{4-x}$ peptides

Little information is available on the mechanism through which $A\beta_{4-x}$ peptides are generated and degraded. The metalloprotease neprilysin (NEP) has been proposed as a putative enzyme responsible for the generation of the N-truncated variant (Fig. 1.6). Analysis of cleavage products resulting from the enzymatic activity of NEP on full-length Aβ peptides showed that one of the cleavage sites is located between Glu-3 and Phe-4 (Mital et al. 2018). Under the studied *in-vitro* conditions, the observed fragments starting at position 4 were however shorter than the complete Aβ sequence (e.g., $A\beta_{4-9}$ or $A\beta_{4-16}$)

because of the presence of several other cleavage sites. *In-vivo* studies indicated that the cleavage of the Gly-9–Tyr-10 bond is rate-limiting step in the proteolysis of Aβ by NEP (Iwata et al. 2000). These observations suggest that a production of $A\beta_{4-40}$ or $A\beta_{4-42}$ peptides from NEP activity is unlikely and that the metalloprotease could actually be involved in the degradation of these variants. Recently, the metalloprotease ADAMTS4, was proven to be able to cleave APP between Glu-3 and Phe-4 of the Aβ sequence (Walter et al. 2019) (Fig. 1.6). The disintegrin-like and metalloprotease with thrombospondin type 1 motif (ADAMTS) is a member of the secreted Zn^{2+}-metalloproteases family, involved in the degradation and modification of components of the extracellular matrix (Apte 2009). The metalloprotease appeared to be able to generate N-truncated $A\beta_{4-x}$ peptides in a BACE1-independent manner. In the adult murine brain, the ADAMTS4 enzyme appears to be expressed exclusively in oligodendrocytes and *in-vitro* studies on murine oligodendrocyte cultures revealed that the metalloprotease is responsible for generation of $A\beta_{4-40}$ peptide in this particular cell type (Walter et al. 2019). The removal of endogenous ADAMTS4 from the 5xFAD mouse model of AD resulted in a 50% reduction of $A\beta_{4-40}$ levels, suggesting that, although the metalloprotease is indeed involved in the generation of the N-truncated peptides *in-vivo*, other generation mechanisms must exist (Walter et al. 2019). ADAMTS4 was recently linked to AD risk, which underscores the interesting role of this metalloprotease in AD pathology (Jansen et al. 2019b).

1.5 Tauopathy in AD

1.5.1 Genetic and physiological role of tau

The protein tau is encoded by the microtubule-associated protein tau (MAPT) gene, located on chromosome 17. The hydrophilic protein is formed by four primary N-terminal domains, a proline-rich domain, a microtubule-binding domain (MBD), and a C-terminal region (Fig. 1.7). In the CNS, alternative splicing ,affecting predominantly the N-terminal domains and the MBD, produces six different isoforms with molecular

weights ranging from 58 kDa to 66 kDa and one of 110 kDa (Goedert et al. 1989, Andreadis 2005). The two main isoforms containing 4-repeat (4R) and 3-repeat (3R) tau are present in a 1:1 ratio in the healthy adult human brain, with 3R tau being produced mainly during development and the 4R tau isoforms being mostly generated during adulthood (Hong et al. 1998).

In-vitro studies suggest that the main physiological role of tau protein is the promotion of microtubule assembly and stability (Weingarten et al. 1975). Tau knock-out transgenic lines and primary neuronal culture, however, showed no impairment of microtubule assembly or axonal transport (Qiang et al. 2006, Vossel et al. 2010), suggesting that the presence of other microtubule associated proteins (e.g., MAP1A, MAP1B, MAP2, etc.) could be sufficient to compensate the lack of tau (Dawson et al. 2001, Harada et al. 1994). A clear neuron-specific function of this protein has not yet been found. As a driver of axonal microtubule assembly, tau has been deemed responsible for the maintenance of proper neuronal projections and synaptic function. Indeed, impairment of synaptic potentials has been observed in tau-null mice (Ahmed et al. 2014, Regan et al. 2015). No physiological tau was observed in the presynaptic compartment through analysis of the synaptic vesicle proteome in the murine brain, but a putative role in the postsynaptic compartment has been proposed (Frandemiche et al. 2014).Although tau is mainly associated with axonal microtubules, its recruitment at the dendrites and the postsynaptic density was recently described (Ittner and Ittner 2018). The phosphorylation state of the protein moreover affects its biological and pathological function.

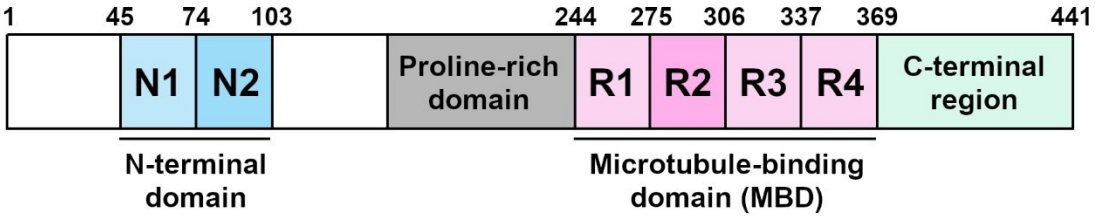

Fig. 1.7 Domains of 2N4R tau.
Tau protein is comprised of four primary domains, the N-terminal domain (blue), the proline-rich domain (grey), the microtubule-binding domain (pink), and the C-terminal region (green). Alternative splicing of the N-terminal and microtubule-binding domains yields six isoforms in the CNS. The 2N4R tau isoform is here depicted. Adapted from (Naseri et al. 2019).

1.5.2 Tau in AD pathology

Hyperphosphorylation of tau is a distinct alteration observed in AD. NFTs purified from AD brains are indeed enriched with hyperphosphorylated form of the protein. The phosphorylation reduces tau's ability to bind to microtubules and enhances tau self-assembly into tangles and filaments (Lindwall and Cole 1984, Bramblett et al. 1993, Yoshida and Ihara 1993, Alonso et al. 2001, Kellogg et al. 2018), possibly because of an alteration of the charge and structure of the MBD (Fischer et al. 2009, Jho et al. 2010). Numerous pathological tau phospho-sites have been identified and experimentally reported in the context of AD pathology (Morris et al. 2011, Wang and Mandelkow 2016, Medina and Avila 2015). Different kinases have been found to contribute to tau phosphorylation, ultimately leading to its aggregation in NFTs. Glycogen synthase kinase-3β (GSK-3β) and cyclin dependent kinase 5 (CDK5) are among the most studied and characterized ones (Kitagishi et al. 2014, Shukla, Skuntz, and Pant 2012). Tau hyperphosphorylation and aggregation is associated with impaired long- and short-term synaptic plasticity. Reduction of hippocampal long-term potentiation (LTP) was observed in several tau transgenic mouse lines (Boekhoorn et al. 2006, Chong et al. 2011, Sydow et al. 2011, Hatch et al. 2017, Polydoro et al. 2009, Levenga et al. 2013, Van der Jeugd et al. 2012), which could be restored after the reduction of tau phosphorylation by inhibition of the responsible kinases (Van der Jeugd et al. 2012, Seo et al. 2017). As already

mentioned in paragraph 1.1.2, NFTs appear at earlier stages than amyloid plaques and they are characterized by a predictable pattern of progression. It is still unclear which are the toxic species among insoluble NFTs, soluble tau oligomers or fragments of already-formed aggregates. Recent evidence suggests that hyperphosphorylated soluble tau species, rather than the insoluble NFTs aggregates, could be the neurotoxic variants in AD. Synapse loss and cognitive deficits were indeed observed in tau transgenic mice prior to the formation of NFTs (Wang and Mandelkow 2016, Kruger and Mandelkow 2016). The mechanisms by which pathological tau impairs synaptic plasticity are not fully understood. Hyperphosphorylated tau was found to stably interact with synaptic vesicles purified from AD brains thus interfering with their normal release (Fein et al. 2008, Henkins et al. 2012, Tai et al. 2012, Zhou et al. 2017, Ait-Bouziad et al. 2017). At the dendrites, hyperphosphorylated tau was associated with spine loss, aberrant postsynaptic activity, and ultimately cognitive deficits, representing a possible crosstalk point between Aβ and tau (Fein et al. 2008, Ittner and Ittner 2018, Hoover et al. 2010, Thies and Mandelkow 2007, Zhao et al. 2016, Bories et al. 2017). The regulation of NMDA or AMPA receptors is one of the proposed mechanisms by which tau mediates its toxicity (Spires-Jones and Hyman 2014, Ittner et al. 2010). Additionally, abnormal phosphorylated tau possibly leads to mitochondrial dysfunction by impairing mitochondrial transports and dynamics (Eckert et al. 2014).

1.5.3 Aβ and tau crosstalk

The discoveries of the past decades indicate that soluble forms of Aβ and tau are the toxic elements causing neuronal death and cognitive impairment in AD. Although separate mechanisms of the two proteins can result in singular detrimental effects, it is popular belief that their interaction leads to toxicity. According to the classic amyloid hypothesis, Aβ is considered upstream in the pathogenesis of AD, triggering tau hyperphosphorylation and the subsequent aggregation into NFTs (Bloom 2014). The

hypothesis is supported by several *in-vivo* studies. Intraventricular injection of synthetic Aβ in tau transgenic mice lead to a 5-fold increase of tangle number near the injection sites (Gotz et al. 2001). On the same trend, when transgenic mice overexpressing mutant human APP, thus possessing abundant amyloid pathology, were crossed with tau transgenic mice an increase of hyperphosphorylated tau and NFTs formation was generally reported (Hurtado et al. 2010, Saul et al. 2013a, Stancu et al. 2014a, Lewis et al. 2001). In these mouse models, amyloid pathology was overall unaffected, supporting the upstream position of Aβ in the cascade of events. Whether tau is fundamental for Aβ toxicity is still a matter of debate. An essential role of tau is supported by the positive effects that the reduction of tau levels causes on Aβ-induced synaptic plasticity and behavioral abnormalities in transgenic mouse models. hAPPJ20 mice (overexpressing human APP containing 2 mutations), characterized by learning and memory deficits and excitotoxicity, presented with improved performances when endogenous tau was removed (Roberson et al. 2007). Similarly, by knocking out the tau genes in an APP/PSEN1 mouse model of AD, protective effects were reported against memory deficits, synapse and neuron loss, and premature death (Leroy et al. 2012). *In-vitro* studies on primary neuronal cultures also supported the importance of tau for Aβ toxicity. Exposure to fibrils assembled from synthetic Aβ caused neurite degeneration and extensive cell death in wild type but not in tau knockout neurons (Rapoport et al. 2002). Later studies with AβOs reported increased toxicity with these soluble species compared to fibrillary Aβ and additionally showed that the soluble AβOs were responsible for tau-dependent microtubule disassembly, impaired LTP, and mitochondrial transport inhibition (King et al. 2006, Vossel et al. 2010, Jin et al. 2011, Lambert et al. 1998, Shankar et al. 2007, Shankar et al. 2008). *In-vivo* studies with soluble Aβ species gave, on the other hand, conflicting results. Intracerebral injection of $A\beta_{1-42}$ peptides induced tau phosphorylation and aggregation in the P301S transgenic tau model (Hu et al. 2014),

while the co-expression of $A\beta_{1-42}$ and transgenic human tau did not affect tau pathology (Gomes et al. 2019).

As already mentioned, tau proteins appear to be important for proper synaptic function and pre- and post-synaptic compartments might be particularly sensitive to possible Aβ-induced tau toxicity. Several studies in rodent models suggest that Aβ and tau indeed co-operate at the synaptic level leading to LTP impairments and resulting in behavioral deficits (Shipton et al. 2011, Pickett et al. 2019, Ittner et al. 2010). Plausible interaction mechanisms between the two proteins include calcium dysregulation and calcineurin activation (Wu et al. 2010, Hudry et al. 2012, Kuchibhotla et al. 2008, Mattson et al. 1992, Zempel et al. 2010, Yin et al. 2016). Additionally, abnormal activation of synaptic receptors by Aβ leads to activation of kinases known to be involved in tau phosphorylation (Purro, Dickins, and Salinas 2012, Small and Duff 2008, Ittner et al. 2010, Roberson et al. 2011, Sellers et al. 2018). The kinase Fyn, and the related NMDA receptor activity, was proposed as point of interaction between Aβ and tau (Ittner et al. 2010, Roberson et al. 2011).

Other studies on neuronal culture proved, however, that not all effects of Aβ on neurons are tau dependent. Activation of some kinases (such as Fyn, PKA, and CaMKI) were observed after exposure to AβOs also in primary neuronal culture derived from tau knockout mice (Seward et al. 2013). Recent studies question if tau is indeed necessary for Aβ toxicity, or if the two proteins actually act in parallel by possessing common toxicity mechanisms (Gulisano et al. 2018). In this scenario, APP appeared to be an essential protein for both Aβ and tau detrimental effects on LTP and memory (Takahashi et al. 2015, Puzzo et al. 2017).

1.6 Mouse models of AD

1.6.1 Tg4-42

The Tg4-42 mouse model of AD exclusively expresses the human N-truncated $A\beta_{4-42}$ peptide. The peptide sequence is fused to the Thyrotropin-releasing hormone (TRH) signal peptide under the control of the Thy1 promoter, which ensures a neuron-specific extracellular secretion of $A\beta_{4-42}$ (Bouter et al. 2013) (Fig.1.8).

The line is characterized by intraneuronal accumulation of the N-terminally truncated peptide with almost absent extracellular amyloid pathology. $A\beta_{4-42}$ intracellular deposits can be predominantly observed in the CA1 pyramidal neurons of the hippocampus, but Aβ is also found in the occipital cortex, striatum, superior colliculus, and piriform cortex (Bouter et al. 2013). Accumulation of Aβ was observed also in the motoneurons of the spinal cord (Lopez-Noguerola et al. 2018b). Aβ accumulation starts at early ages as abundant intraneuronal deposition can be observed already at 2-3 months in both the hemizygous and the homozygous lines. The $A\beta_{4-42}$ soluble neurotoxic oligomers secreted in Tg4-42 mice induce severe neuron loss in the CA1 region of the hippocampus in an age- and dose-dependent manner. An approximate 50% loss of CA1 pyramidal neuron is observed at 12 months in the hemizygous line and at 6 months in the homozygous line (Bouter et al. 2013, Antonios et al. 2015). After 6 months of age, the neurodegeneration in the homozygous line reaches a plateau, as by 8 months the loss of CA1 pyramidal neurons increases by only 15%, reaching approximately 65% compared to age-matched WT controls (Antonios et al. 2015). Synaptic hyperexcitability, altered synaptic short-term plasticity, and decreased hippocampal glucose metabolism were additionally described in young Tg4-42 mice (Dietrich et al. 2018, Bouter et al. 2019). Alongside, alteration in the expression of miRNA associated with synaptic functions and memory decline were measured in 8-month-old mice (Bouter et al. 2020).

The severe hippocampal neurodegeneration is accompanied by behavioral deficits. Spatial reference learning and memory deficits in the Morris Water Maze (MWM) task have been reported in 12-month-old Tg4-42^{het} mice and in 6-month-old Tg4-42^{hom} mice (Antonios et al. 2015, Bouter et al. 2013). Recognition memory is also impaired in this mouse model of AD, as deficits were observed in the Novel Object Recognition (NOR) task at 6 and 12 months for the homozygous and hemizygous lines, respectively (Hüttenrauch et al. 2016, Stazi and Wirths 2021). Impaired contextual learning was also described in aged Tg4-42^{het} mice (Bouter et al. 2014). Next to cognitive deficits, Tg4-42 mice display alteration of sensorimotor behaviors. A reduction of acoustic startle response, pre-pulse inhibition and worsened performances in motor tasks, such as the accelerating rotarod and balance beam, were described (Sichler et al. 2019, Wagner et al. 2019).

Differently to most APP/PSEN mouse models of AD, the Tg4-42 line lacks APP-overexpression and AD-related mutations, which make this transgenic model a suitable tool to study the predominant sporadic form of AD.

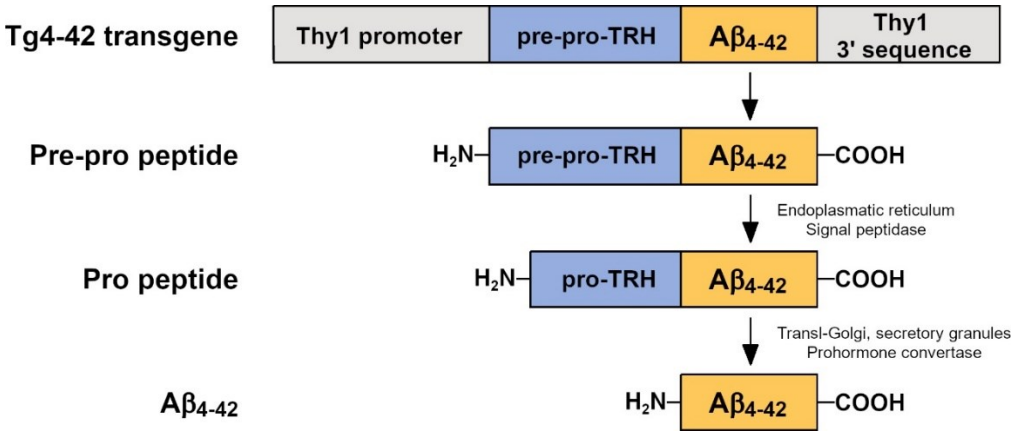

Fig. 1.8 Schematic diagram of Tg4-42 transgene.
Thy1 promoter induces the neuronal expression of the pre-pro-TRH-Aβ$_{4-42}$ fusion peptide. The fusion peptide is directed into the Endoplasmic Reticulum (ER) where signal peptidases liberate the pro-TRH-Aβ$_{4-42}$ peptide. In the trans-Golgi network and secretory granules, prohormone convertases cleave the remaining pro-TRH sequence liberating the Aβ$_{4-42}$ peptide (Alexandru et al. 2011). Figure generated after (Wittnam et al. 2012)

1.6.2 5xFAD

The 5XFAD mouse model is an extensively studied and utilized line in AD research. This transgenic murine line co-expresses a total of five FAD mutations and was firstly described by Oakley and colleagues (Oakley et al. 2006). The human APP695 isoform, harboring the Swedish K670N/M671L, Florida I716V, and London V717I FAD mutations, and the human PSEN1, containing the M146L and L286V mutations, are over-expressed under the control of the murine neuron specific Thy1 promoter (Fig 1.9). The Swedish mutation enhances the production of total Aβ, with a preference for the generation of peptides starting at position 1 (Weggen and Beher 2012), while the APP Florida/London, and PSEN1 M146/L286V mutations promote the generation of Aβ at the 42nd amino acid. These mutations lead to an increased production of Aβ peptides and to an accelerated formation of amyloid plaques, which can be detected in the animals' brains already at young ages. Intraneuronal accumulation of $A\beta_{x-42}$ can be detected in pyramidal neurons of the 5th cortical layer and subiculum at 1.5 months, prior to amyloid deposits formation. Intraneuronal accumulation of Aβ peptides is associated with the neurodegeneration observed in this brain region at 9 months. No loss of neurons can be detected in the CA1 region of the hippocampus, a sub-field where no intracellular accumulation of Aβ can be observed (Jawhar et al. 2012). Amyloid pathology increases in an age-dependent manner spreading to different brain regions including the cortex and the hippocampus, as well as in the spinal cord (Jawhar et al. 2012, Chu et al. 2017). Here, loss of neurons can be detected after 8 months of age (Li et al. 2013). Concomitant and proportional to amyloid pathology, an increase of astro- and microgliosis is present in this line (Oakley et al. 2006). Besides full-length $A\beta_{1-x}$ peptides, N-truncated isoforms, such as $A\beta_{2-x}$, $A\beta_{pE3-x}$, and $A\beta_{4-x}$ were described in this mouse model (Jawhar et al. 2011, Savastano et al. 2016, Wirths et al. 2017).

Because of the abundant amyloid pathology and neurodegeneration, behavioral deficits develop in the transgenic line. Hippocampus-dependent spatial working memory deficits, analyzed by the Y-maze task, were reported between 4 and 5 months of age (Oakley et al. 2006). Additional learning and memory deficits were observed in other behavioral paradigms, such as the Morris Water Maze (MWM), the conditioned taste aversion task, the Cross Maze, and the contextual fear conditioning tests (Ohno et al. 2007, Devi et al. 2010, Jawhar et al. 2012). Sensorimotor deficits can be observed in the balanced beam and string suspension tasks starting from 9 months of age (Jawhar et al. 2012, O'Leary et al. 2020). A reduced anxiety-like phenotype furthermore characterizes this transgenic line, as altered behavioral performances become evident at 6 months (Jawhar et al. 2012).

The 5xFAD line displays several neuropathological hallmarks of AD. Abundant amyloid pathology, neurodegeneration, inflammation, and behavioral alterations can be detected at some point in the transgenic animals. The presence of FAD mutation makes it a suitable tool to study EO-FAD but less appropriate to understand the pathological mechanisms responsible for the more prevalent sporadic forms of AD. Additionally, the overproduction of full-length Aβ peptides at the expenses of N-truncated isoforms is not representative of the amyloid heterogeneity in the human AD brain. The 5xFAD line is nevertheless important to unravel the pathological alterations occurring in AD, but its limitations should be considered when employing this mouse model for research purposes.

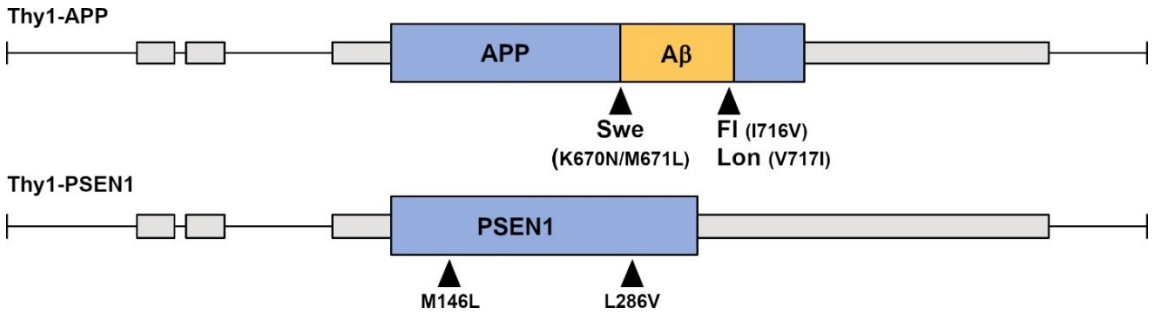

Fig. 1.9 Schematic diagram of 5xFAD transgenes.
5XFAD mice co-express the human APP695 and PSEN1 transgenes under the control of the neuron specific Thy1 promoter. Arrow heads indicated mutations in Thy1-APP and Thy1-PSEN1 transgenes. Swe: Swedish mutation; Lon: London mutation; Fl: Florida mutation. Figure generated after (Oakley et al. 2006)

1.6.3 MAPT (PS19)

MAPT (PS19) is a widely-used murine transgenic model of tauopathy, firstly described by Yoshiyama and colleagues in 2007 (Yoshiyama et al. 2007). The transgenic line harbors the T34 isoform of microtubule-associated protein tau (MAPT), expressing one N-terminal insert and four microtubule binding repeats (1N4R). The transgene encodes the human disease associated P301S mutation and is driven by the mouse prion protein promoter.

The original PS19 line was bred on a mixed background and showed an age-dependent accumulation of tau with evident intracellular fibrillary inclusions starting at 6 months of age. From this time point, NFTs were present in the neocortex, amygdala, hippocampus, brain stem, and spinal cord, and were accompanied by microgliosis and astrocytosis (Yoshiyama et al. 2007). Neuronal loss and brain atrophy were reported by 8 months of age. The neurodegeneration was primarily observed in the hippocampus, where neurons of CA3 and Dentate Gyrus (DG) but not CA1 subfields were affected, but also in other brain regions, such as the neocortex and entorhinal cortex (Yoshiyama et al. 2007). The PS19 line presents changes in cognition as well as in sensorimotor behaviors. Spatial learning and memory impairments could be detected in the MWM task at 6 months (Takeuchi et al. 2011). From a motor point of view, clasping, limb retraction and weakness

progressed to paralysis between 7 to 10 months, with 80% mortality by 12 months when on a mixed background (Yoshiyama et al. 2007).

The more recently generated congenic line on a C57BL/6J background showed similar tau pathology, with clear NFTs inclusion visible in the brain stem, spinal cord, hippocampus, and cortex at 9 months (Maruyama et al. 2013, Saul et al. 2013b). A delayed onset of neurodegeneration was however observed in the congenic line compared to the mixed background, with an onset around 9 months of age (Maruyama et al. 2013). A hyperactive phenotype was described in 6-month-old animals and no obvious motor impairments were observed between 3.5 to 9 months of age (Takeuchi et al. 2011, Mikhail et al. 2015, Sun et al. 2020). Cognitive impairments were, on the other hand, reported for the congenic line. The transgenic mice presented with clear working memory deficits in the Y-maze (Takeuchi et al. 2011, Van der Jeugd et al. 2016) while the presence of spatial memory impairments is controversial. Some studies described the development of deficits in the MWM test starting at 5-6 months (Takeuchi et al. 2011, Eckenweber et al. 2020), while in other studies no deficits could be detected until 10-12 months (Sun et al. 2020, Chalermpalanupap et al. 2018).

Although tau transgenic lines, such as the PS19 line employed in this thesis, successfully modelled NFTs pathology and are widely used in AD research, a couple of considerations must be made. Firstly, mutations in the *MAPT* gene are not found in AD but are linked to the development of subtypes of frontotemporal lobar degeneration (Gendron and Petrucelli 2009). Overexpression of mutant tau appears to be required for phospho-tau and NFT pathology to manifest in murine models. Additionally, the expression of the tau transgene might not recapitulate the spreading pattern of NFTs that occurs in AD patients (Jankowsky and Zheng 2017).

1.7 Project objectives

1.7.1 PROJECT I: Assessment of N-terminal heterogeneity of parenchymal and vascular amyloid-β deposits in autopsied Alzheimer's disease brains

Next to full-length Aβ peptides, a variety of N- and C-terminal truncated Aβ variants have been identified by mass spectrometry analysis in human brains, with $A\beta_{4\text{-}42}$ peptides being among the most abundant species (Moore et al. 2012, Portelius et al. 2010, Wildburger et al. 2017). In the first project we aim to further analyze the heterogeneity of Aβ peptides in human brains from AD and non-demented control (NDC) *post mortem* samples to address the precise spatial localization and distribution of full-length and N-terminally truncated Aβ peptides through immunohistochemical staining.

The objectives of PROJECT I are the following:

- Characterize the employed antibodies' specificity by capillary isoelectric focusing immunoassay.
- Investigate and compare the abundance and staining pattern of full-length and $A\beta_{4\text{-}x}$ peptides in the brain parenchyma of AD, NDC, and DS cases.
- Investigate and compare the deposition of full-length and $A\beta_{4\text{-}x}$ peptides in parenchymal and meningeal vessels of AD, NDC, and DS cases.

1.7.2 PROJECT II: *In-vitro* and *in-vivo* activity of enzymes involved in the degradation and generation of $A\beta_{4\text{-}x}$ peptides: an outlook on neprilysin and ADAMTS4

Little information is known about the generation and degradation of N-truncated $A\beta_{4\text{-}x}$ peptides and how changes in their production and catabolism affect the course of AD pathology. As the metalloprotease neprilysin (NEP) is known to be involved in the degradation of full-length Aβ peptides (Howell, Nalbantoglu, and Crine 1995, Iwata et al. 2000, Zou et al. 2006), we questioned whether $A\beta_{4\text{-}x}$ peptides could be substrates for

NEP hydrolyzation. We will address this issue in part I of PROJECT II through *in-vitro* experiments and *in-vivo* analysis of the Tg4-42 mouse model lacking endogenous NEP.

The following objectives will be investigated in PROJECT II - part I:

- Are $A\beta_{4\text{-}x}$ peptides subjected to degradation by recombinant NEP *in-vitro*?
- Does the lack of endogenous NEP affect $A\beta_{4\text{-}42}$ accumulation in the Tg4-42^{het} mouse model of AD?

The metalloprotease ADAMTS4 was recently reported as an enzyme capable of generating $A\beta_{4\text{-}x}$ peptides *in-vitro* and *in-vivo* (Walter et al. 2019). Depletion of ADAMTS4 in the widely used 5xFAD mouse model of AD caused a reduction of the N-truncated peptide levels. The aim of the second part of PROJECT II is to further characterize the effects of an ADAMTS4 knock-out background on the 5xFAD line from a behavioral and pathological point of view.

The objectives of PROJECT II-part II can be summarized in the following questions:

- Does an ADAMTS4 deficiency alter the motor and cognitive deficits of the 5xFAD mouse model?
- Does the lack of ADAMTS4 lead to a reduction of amyloid pathology?

1.7.3 PROJECT III: *In-vivo* relationship of $A\beta_{4\text{-}42}$ peptides and amyloid-β plaques

Soluble Aβ oligomers, rather than insoluble fibrillar Aβ deposits, may be the crucial players in AD etiology (Walsh et al. 2002, Cleary et al. 2005, Lesne et al. 2006, Shankar et al. 2008). The relationship between insoluble amyloid plaques and soluble Aβ oligomers is at present not fully understood. In PROJECT III we aim to investigate the relationship between the highly abundant $A\beta_{4\text{-}42}$ peptides and insoluble extracellular deposits *in-vivo* by crossing the plaque-bearing 5xFAD mouse model of AD with the Tg4-42^{hom} line exclusively expressing intraneuronal N-truncated peptides.

The FAD/Tg4-42^{hom} line was thus generated and will be studied at two time points to answer the following questions:

- Are motor performances and cognition affected by the co-occurrence of extracellular amyloid pathology and intraneuronal accumulation of Aβ$_{4-42}$ peptides?
- Is neurodegeneration in the hippocampal CA1 region and in the spinal cord of Tg4-42^{hom} mice increased by the presence of extracellular amyloid deposits?
- Does extracellular amyloid pathology from the 5xFAD background have an influence on soluble Aβ$_{4-42}$ accumulation in Tg4-42^{hom} mice and *vice versa*?

1.7.4 PROJECT IV: *In-vivo* relationship of Aβ$_{4-42}$ peptides and protein tau

In the classical amyloid cascade hypothesis, Aβ is regarded as a trigger for the formation of NFTs and the subsequent neurodegeneration (Bloom 2014). Studies on transgenic mouse models mostly reported an aggravation of tau pathology in the presence of extracellular Aβ deposits (Hurtado et al. 2010, Saul et al. 2013b, Stancu et al. 2014a), but little is known about the contribution of soluble Aβ peptides. In PROJECT IV we aim to understand the role of N-truncated Aβ$_{4-42}$ peptides on tau pathology and the *in-vivo* relationship between the two proteins by crossing the Tg4-42^{hom} mouse model of AD with the MAPT (PS19) transgenic mouse model of tauopathy.

The resulting MAPT/Tg4-42^{hom} line will be characterized at three different time points to address the following objectives:

- Understand if motor and cognitive deficits are enhanced after the co-expression of Aβ$_{4-42}$ and transgenic human tau.
- Investigate if soluble Aβ$_{4-42}$ peptides aggravate hippocampal tau pathology and confirm that tau does not influence Aβ pathology.

- Determine if the co-expression of the N-truncated peptide and transgenic tau results in an increased loss of CA1 pyramidal neurons.

2 MATERIALS AND METHODS

2.1 Chemicals, reagents, and kits

The chemicals and reagents used in the thesis are listed in Table 2.1, kits used are listed in Table 2.2.

Table 2.1 Chemicals and reagents

Chemical/Reagent	Manifacturer
Agarose	Lonza, Basel, Switzerland
Aqua	Braun, Melsungen, Germany
Benzonase	Merck, Darmstadt, Germany
Bovine serum albumin (BSA)	Roth, Karlsruhe, Germany
Citric Acid	Roth, Karlsruhe, Germany
Chloroform	Merck, Darmstadt, Germany
Complete Mini-Phosphatase Inhibitor Tablets	Roche, Basel, Switzerland
Complete Mini-Protease Inhibitor Tablet	Roche, Basel, Switzerland
Diluent 100	Meso Scale Discovery, Rockville, USA
Diluent 35	Meso Scale Discovery, Rockville, USA
Dimethyl sulfoxide (DMSO)	Roth, Karlsruhe, Germany
DNA ladder 100 bp	Bioron, Ludwigshafen, Germany
DNAse 10X reaction buffer with $MgCl_2$	Thermo Fisher Scientific, Waltham, USA
DNAse	Thermo Fisher Scientific, Waltham, USA
dNTPs	Invitrogen, Carlsbad, CA, USA
Dynabeads M-270 Epoxy	Thermo Fisher Scientific, Waltham, USA
Dulbecco's Phosphate Buffered Salt Solution (DPBS)	Bio & SELL GmbH, Nuremberg, Germany
Ethanol 99%	Chemsolute, Renningen, Germany
Ethylendiaminetetraacetic acid (EDTA)	Sigma-Aldrich, St. Louis, USA
Fetal Calf Serum (FCS)	Biochrom, Berlin, Germany
Formic Acid 98%	Roth, Karlsruhe, Germany
Haematoxylin Solution	Roth, Karlsruhe, Germany
HD green plus DNA stain	Intas, Göttingen, Germany
Hydrogen peroxide (H_2O_2)	Roth, Karlsruhe, Germany
Isopropanol	Roth, Karlsruhe, Germany
Ketamine 10%	Medistar, Ascheberg, Germany

Methanol	AppliChem, Darmstadt, Germany
$MgCl_2$ (25 mM)	Axon, Kaiserslautern, Germany
Molecular-grade water	Braun, Melsungen, Germany
MSD GOLD 96-well Small Spot Streptavidin SECTOR Plate	Meso Scale Discovery, Rockville, USA
MSD GOLD Read Buffer	Meso Scale Discovery, Rockville, USA
MSD Gold SULFO-TAG NHS-Ester	Meso Scale Discovery, Rockville, USA
Non-fat Dry Milk Powder	Roth, Karlsruhe, Germany
Paraffine	Roth, Karlsruhe, Germany
Paraformaldehyde (PFA)	Roth, Karlsruhe, Germany
PCR 10X reaction buffer	Axon, Kaiserslautern, Germany
Phosphoramidon	Enzo Life Sciences, Farmingdale, USA
Proteinase K	Peqlab, Erlangen, Germany
Recombinant human Neprilysin	R&D Systems, Minneapolis, USA
ROTI®Histofix with 4% formalin	Roth, Karlsruhe, Germany
ROTI®Histokitt	Roth, Karlsruhe, Germany
ROTI®Mount FluorCare DAPI	Roth, Karlsruhe, Germany
Sodium chloride (NaCl)	Roth, Karlsruhe, Germany
Sodium dodecyl sulfate (SDS)	Roth, Karlsruhe, Germany
Sodium hydroxide (NaOH)	AppliChem, Darmstadt, Germany
Sucrose	Roth, Karlsruhe, Germany
Synthetic Aβ peptides	AnaSpec, Fremont, USA
Taq polymerase	Axon, Kaiserslautern, Germany
Trifast®	Peqlab, Erlangen, Germany
Tris(hydroxymethyl)aminomethane (Tris)	Roth, Karlsruhe, Germany
Triton X-100	Roth, Karlsruhe, Germany
Tween 20	Roth, Karlsruhe, Germany
Xylazine (Xylariem)	Ecuphar, N.V. Oostkamp, Belgium
Xylol	Roth, Karlsruhe, Germany
Zeba Spin Desalting column 40 K MWCO	Thermo Fisher Scientific, Waltham, USA

Table 2.2 Kits

Kit	Manifacturer
Amplified Mouse Secondary Antibody Detection Kit	ProteinSimple, San Jose, USA
Amplified Rabbit Secondary Antibody Detection Kit	ProteinSimple, San Jose, USA
Biozym Blue S'Green qPCR Kit Separate ROX	Biozym Scientific GmbH, Hessisch Oldendorf, Germany
DAB Substrate Kit, Peroxidase (HRP), with Nickel, (3,3'-diaminobenzidine)	Vector Laboratories, Burlingame, USA
EZ-Link Micro Sulfo-NHS-LC Biotinylation kit	Thermo Fisher Scientific, Waltham, USA
Pierce BCA Protein assay Kit	Thermo Fisher Scientific, Waltham, USA
RevertAid First Strand cDNA Synthesis Kit	Thermo Fisher Scientific, Waltham, USA
R-PLEX Human Aβ (total) Antibody Set	Meso Scale Discovery, Rockville, USA
Vectastain ABC Kit	Vector Laboratories, Burlingame, USA
XDR Charge Separation Master Kit for Peggy Sue	ProteinSimple, San Jose, USA

2.2 Analyses on synthetic Aβ peptides

2.2.1 Preparation of synthetic Aβ peptides

The synthetic Aβ peptides $A\beta_{1–40/42}$, $A\beta_{2–40/42}$, $A\beta_{3–40/42}$, pyroglutamate $A\beta_{pE3-40/42}$, $A\beta_{4–40/42}$, $A\beta_{5–40}$, and $A\beta_{11–40}$ were purchased from AnaSpec (Fremont, CA, USA). The synthesis of $A\beta_{-3–40/42}$ has been previously described (Beyer et al. 2016) (generous gift of Dr H.-J. Knölker, Dresden). Stock solutions were solubilized in DMSO, or in 0.1% NH_3(aq) (~0.1% NH_3(w/v)) for $A\beta_{pE3-40}$, at a final concentration of 1 mg/mL. Volumes of 20 µL were aliquoted in 0.5 mL low binding microcentrifuge tubes (Eppendorf®, Hamburg, Germany) and stored at -80°C. Working aliquots were thawed only once.

2.2.2 Proteolysis of synthetic Aβ peptides by neprilysin

$A\beta_{4-40}$, $A\beta_{4-42}$, $A\beta_{1-40}$, and $A\beta_{1-42}$ were incubated for 2 h at 37°C with neprilysin (NEP, R&D Systems) in the presence or absence of the neprilysin inhibitor Phosphoramidon (PA,

Enzo Life Sciences). The reactions (20 µL reaction volume) were prepared in low bind 1.5 mL Eppendorf reaction vials by mixing 4 µL of each single synthetic peptide (0.1 mg/mL) and 2 µL of neprilysin (10 ng/µL) with or without 2 µL of PA, prediluted to 0.1 mM with 20 mM HEPES, pH 7.0. Appropriate volumes of 20 mM HEPES, pH 7.0 were added to reach the reaction volume. Control reactions contained 16 µL of 20 mM HEPES, pH 7.0 and 4 µL of synthetic peptide. After the incubation, two technical replicates were mixed with 1 µL of 10% trifluoroacetic acid (TFA), stored at 4°C to be analyzed by mass spectrometry. Other 2 replicates were each mixed with 20 µL of 2 x SDS-sample buffer and analyzed by SDS-PAGE.

2.2.2.1 SDS-polyacrylamide gel electrophoresis and quantification of silver staining

For each digestion condition, 15 µL were mixed with 15 µL of 2 × SDS-sample buffer (0.72 M bistris, 0.32 M bicine, 30% (w/v) sucrose, 2% (w/v) SDS and 0.015% bromophenol blue) and heated at 95°C for 5 min. The samples were loaded and separated on a 15% T / 5% C bicine / Tris SDS-gel followed by fixation with 30% ethanol/10% acetic acid for 1 h. The peptides were visualized by silver staining (Wiltfang et al. 1997). The silver-stained gels were scanned on a Bio-5000 Plus scanner (Microtek International) and evaluated with the Quantity One basic software (BioRad). For quantification, the volume within each band (measured as intensity*mm^2) was adjusted by global background subtraction.

2.2.2.2 Mass spectrometry

To determine the masses of the intact Aβ peptides and their cleaved products mass spectrometry analyses were performed (Haußmann et al. 2013). An Anchor-Chip target (Bruker Daltonics) was precoated with 2-cyano-4-hydroxycinnamic acid (CHCA) and 1 µL of 1% TFA/0.1% octyl β-D-glucopyranoside was deposited on the anchor position. To these droplets, 0.5 µL of the NEP reaction mixture were added to allow adsorption on the CHCA surface for 3 min. The samples were washed twice with ammonium dihydrogen phosphate ($NH_4H_2PO_4$, 10 mM in 0.1% TFA) and analyzed by mass spectrometry using

an UltrafleXtreme MALDI TOF/TOF instrument (Bruker Daltonics). Positively charged ions in the *m*/*z* range 300-6000 were analyzed in the reflector mode under the control of the FlexControl 3.4 operation software. A mixture of Peptide Calibration Standard II (*m*/*z* 757-3147, Bruker Daltonics) and Peptide calibration Mix 2 (*m*/*z* 1673-5730, LaserBio Labs) was used for calibration (Hornung et al. 2019).

2.2.3 Capillary Isoelectric Focusing (CIEF) Immunoassay

Automated capillary isoelectric focusing immunoassays were performed with a PeggySue system (Protein Simple). Synthetic Aβ peptides at a stock conc. of 1 mg/mL DMSO were diluted in in 20 mM bicine, pH 7.6, 0.6% CHAPS to obtain a final conc. of 100 ng/μL in the assay and mixed 1:4 with G2 Premix containing a pH gradient ranging from pH 5−8 (nested, with a pH 2−4 plug), fluorescent pH standards (Standard Ladder 3 (pH 4.9, 6.0, 6.4, 7.0, 7.3) + pH standard 5.5) and a DMSO inhibitor mix (all reagents were obtained from ProteinSimple). Samples, primary antibodies (also used in immunohistochemistry and listed in Table 2.19, diluted in ProteinSimple antibody diluent), biotinylated secondary antibodies (anti-mouse – ProteinSimple, anti-human – DAKO; all 1:100), streptavidin coupled horseradish peroxidase (ProteinSimple, 1:100), and a 1:1 solution of luminol/peroxide were loaded onto a 384 well sample plate, and the automated assay was programmed in the Compass software (ProteinSimple). The automated assay comprises the load of the sample for 5 sec, separation of the analytes for 40 min with 21’000 μW, immobilization within 100 s, followed by two washing steps (load, 20 s; soak, 150 s) prior to the load of the primary antibodies which stay in incubation for 120 min. The secondary antibodies were incubated for 60 min, followed by 60 min incubation of the streptavidin-HRP conjugate, each of which was preceded by two washing steps. After two final washing steps, luminol/peroxide was loaded for 2 s, and chemiluminescence signals were detected at six exposure times (30, 60, 120, 240, 480, and 960 s).

2.3 Human brain samples

Paraffin-embedded human brain samples from sporadic AD, non-demented controls (NDC) and Down's syndrome (DS) cases were obtained from the Netherlands Brain Bank. Samples exclusively from the medial frontal gyrus region of the brain were used in the analysis. The current study was approved by the ethical committee of the University Medicine Göttingen (UMG).

2.4 Laboratory animals

2.4.1 Animal care and general conditions

All animals used for these studies were of the species *Mus musculus* and were maintained in the central animal facility of the University Medicine Göttingen (UMG), under specific-pathogen-free (SPF) conditions. All mouse lines were generated or maintained on a C57Bl/6J genetic background by backcrossing for at least 10 generations. Animals were housed in controlled environment conditions with 12 hours/12 hours inverted dark/light cycle (light from 8 p.m. to 8 a.m.) and grouped housing up to 5 mice in standardized individually ventilated cages (33 cm x 18 cm x 14 cm), where food and water were provided *ab libitum*. Handling and behavioral testing were performed during the dark phase. All animal experiments were conducted in accordance with the guidelines of the 'Federation of European Laboratory Animals Science' (GV-SOLAS) and the guidelines of the 'Federation of European Laboratory Animals Science Association' (FELASA). The 'Lower Saxony State Office for Consumer Protection and Food Safety' (LAVES) approved all animal experiments. All efforts were made to minimize the number and the suffering of the animals used in the present study. If not stated otherwise, both female and male mice were used in the experiments.

2.4.2 Tg4-42 transgenic mice

The Tg4-42 mice express the human $A\beta_{4\text{-}42}$ sequence fused to the thyrotropin-releasing hormone (TRH) signal peptide sequence, ensuring secretion through the secretory pathway, under the control of the neuronal murine Thy1 promoter. The generation of the heterozygous line (Tg4-42^{het}) was previously described (Bouter et al. 2013). The hemizygous line was used in project II. A homozygous line (Tg4-42^{hom}) was further generated in our group and was used in projects III and IV.

2.4.3 5xFAD transgenic mice

The 5xFAD mice overexpress the 695 amino acids isoform of the human amyloid precursor protein (APP695) carrying the Swedish, Florida, and London mutations under the control of the neuronal murine Thy1 promoter. This promoter additionally drives the expression of the human presinilin-1 (PSEN1), carrying the M146L and L286V mutations (Oakley et al. 2006). To obtain an incipient congenic line on a C57Bl/6J genetic background (Jawhar et al. 2012), the 5xFAD mice used in these studies were backcrossed for more than 10 generations to C57Bl/6J wild-type mice (WT) (Jackson Laboratories). As mentioned in the result session, only female 5xFAD mice were used in the studies.

2.4.4 MAPT transgenic mice

The heterozygous MAPT (PS19) mice express the mutant P301S human microtubule-associated protein tau (MAPT), driven by the mouse prion protein promoter (Prnp). The generation of the line was described by Yoshiyama and colleagues (Yoshiyama et al. 2007). The mice were purchased from Jackson laboratories (B6;C3-Tg(Prnp-MAPT*P301S)PS19Vle/J) and were backcrossed for more than 10 generations to C57Bl/6J WT mice.

2.4.5 Neprilysin gene-disrupted mice

The neprilysin gene-disrupted mouse model, a generous gift of Dr. Takaomi Saido (RIKEN Brain Institute, Japan), has been initially generated and described by Lu and

colleagues (Lu et al. 1995). The mice were backcrossed with C56Bl/6J WT mice for at least 5 generations and kept as a homozygous line (NEP$^{-/-}$). NEP$^{-/-}$ mice were bred with hemizygous Tg4-42 mice to obtain Tg4-42^{het}/NEP$^{-/-}$ mice. Genotypes were checked by means of PCR and qRT-PCR.

2.4.6 ADAMTS4$^{-/-}$ transgenic mice

ADAMTS4$^{+/-}$ mice were obtained from the Jackson laboratories. The gene encoding for the disintegrin-like and metallopeptidase with thrombospondin type 1 motif 4 (ADAMTS4) was disrupted by the insertion of a bacterial lacZ gene, such that the endogenous gene promoter drives expression of β-galactosidase. ADAMTS4$^{+/-}$ mice were backcrossed to C56Bl/6J WT mice for at least 5 generations and were bread to obtain a homozygous ADAMTS4 KO line (ADAMTS4$^{-/-}$). ADAMTS4$^{-/-}$ mice were crossed with 5xFAD to finally obtain 5xFAD mice on a homozygous ADAMTS4 KO background (5xFAD/ADAMTS4$^{-/-}$) as previously described (Walter et al. 2019). Genotypes were checked by means of PCR and qRT-PCR.

2.4.7 FAD/Tg4-42^{hom} transgenic mice

In project III, the 5xFAD and Tg4-42 lines were crossed to finally obtain heterozygous 5xFAD mice on a homozygous Tg4-42 background (FAD/Tg4-42^{hom}). Genotypes were checked by means of PCR and qRT-PCR. All animals were maintained on a C57Bl/6J background. Only female mice were used.

2.4.8 MAPT/Tg4-42^{hom} transgenic mice

In project IV, the MAPT and Tg4-42 lines were crossed to finally obtain heterozygous MAPT mice on a homozygous Tg4-42 background (MAPT/Tg4-42^{hom}). Genotypes were checked by means of PCR and qRT-PCR. All animals were maintained on a C57Bl/6J background.

2.5 Behavioral Analysis

2.5.1 General considerations

Behavioral phenotyping of mice was performed during the dark phase (between 8 a.m. and 8 p.m.). All mice underwent a onetime battery of behavioral testing within a 3-week period. To avoid excessive stress and undermine the outcome of the cognitive tasks, the mice performed only one motor and one cognitive task during a single day of testing. The apparatuses used in the behavioral tests were cleaned with 70% Ethanol between each trial to avoid odor cues. All motor tasks, the Elevated Plus Maze and the Cross Maze tasks were performed under red light conditions to reduce stress and increase the focus on performances. Due to the higher physical demand requested in the Morris Water Maze, the test was the last one performed with no other in parallel. Weight gain of mice was monitored as part of a general physical assessment.

2.5.2 Motor phenotype assessment

2.5.2.1 Balance Beam

The balance beam test was conducted to assess balance and fine motor coordination (Luong et al. 2011). A 1 cm wide, 50 cm long wooden beam was attached to two grey plastic support columns at a height of 44 cm. At both ends of the beam, a 9 x 15 cm escape platform was attached. Mice were placed on the center of the beam facing either one of the platforms and gently released. To prevent possible fall injuries, the ground surface underneath the beam was padded. The latency to fall from the beam or to reach one of the platforms was recorded. During a single day of testing, each mouse performed three consecutive 60 seconds trials with at least 10 minutes intervals in between. If a mouse remained on the beam for the whole 60-seconds trial or escaped to one of the platforms, the maximum time of 60 seconds was given.

2.5.2.2 Inverted Grip

The inverted grip task was used to test neuromuscular abilities, vestibular function, and muscle strength (Wirths and Bayer 2008). The testing apparatus consisted of a metallic wire grid (45 cm in length, 30 cm in width with a grid spacing of 1 cm). The mouse was positioned in the center of the grid, which was then inverted and suspended 40 cm above a padded surface. Each animal underwent a single 60-seconds trial and the latency to fall was recorded. If the mouse was able to stay on the grid for the entire trial the maximum time of 60 seconds was assigned.

2.5.2.3 Accelerating Rotarod

Motor performance and motor learning were tested using the rotarod task. A computer controlled Rotarod system (TSE System, Bad Homburg, Germany) was used to perform the task, which consisted of 2 days of testing with 4 trials per day with 10 minutes intervals in between. Each mouse was placed on the rod, which accelerated from 4 to 40 rpm over a maximum trial time of 300 seconds. The latency to fall off the rod was recorded and used as indicator of motor performances.

2.5.3 Elevated Plus Maze

The elevated plus maze task allowed the test of anxiety-like behavior in rodents (Karl, Pabst, and von Horsten 2003). The apparatus consisted of a "+" shaped maze, elevated 75 cm from the ground. Two opened arms (15 cm in length, 5 cm in width) and two closed arms (15 cm in length, 5 cm in width, 15 cm in height) alternated extending from a central platform (5 cm in length, 5 cm in width). Each mouse was individually placed on the central platform facing one of the closed arms and let to freely explore the maze for 5 minutes in a single trial, while they were tracked using the ANY-maze™ video tracking system (Stoelting Co., Wood Dale, IL, USA). The percentage of time spent exploring the open arms was recorded and used as an indicator of anxiety-like behavior, as the test is

based on the conflict of the animals between the desire of exploring a novel environment and the avoidance of elevated open spaces due to the anxiety to fall.

2.5.4 Cross Maze

The cross maze task was performed to investigate working memory by measuring spontaneous alternation rate (Jawhar et al. 2012). The apparatus consisted of a black cross-shaped plastic maze. The four arms (30 cm in length, 8 cm in width, and 15 cm in height) were arranged in a 90° position opening in a 64 cm^2 central space. Each mouse was randomly placed in one of the four arms and allowed to freely explore the maze for 10 minutes, in a single test trial. The sequence of the arm entries, the average speed as well as the total distance travelled were recorded using the ANY-maze™ video tracking system (Stoelting Co., Wood Dale, IL, USA). Alternation was defined as successive entries into the four arms in overlapping quadruple sets (e.g., 1, 3, 2, 4 or 2, 3, 4, 1 but not 1, 2, 3, 1) (Arendash et al. 2001). The alternation percentage was calculated as the percentage of actual alternations to the possible number of arm entries (Wietrzych et al. 2005).

2.5.5 Open Field

The open field (OF) test was performed to evaluate motor performances as well as anxiety-like behavior, utilizing the rodent natural fear for open spaces. The apparatus consisted of a grey plastic arena of 50 cm × 50 cm surface area and 38 cm-high walls. Each mouse was placed in the center of the arena and allowed to explore the field freely in a single 5-minute trial. Mice were tracked using the ANY-maze™ video tracking system (Stoelting Co., Wood Dale, IL, USA). The software also allowed the delineation of a virtual 20 cm x 20 cm central area of the field. Average speed and average distance were recorded and used as indicators of motor abilities. Moreover, the time spent in the virtual central part was recorded and used as an assessment of anxiety-like behavior of the mice.

2.5.6 Novel Object Recognition

To test for recognition memory, the novel object recognition (NOR) task was performed. The test consisted of single training test trials, 5 minutes each, performed on two consecutive days (24 hours apart). The NOR task took place 24 hours after the OF test, which served as a habituation trial. On the training trial, two identical objects were placed in the arena. In the test trial the following day, one of the two familiar identical objects was substituted with a new object, different in shape, color, and texture. The mice freely explored the object on both trials and exploration time for each object was recorded manually. Based on the innate preference of rodents for novelty, a mouse that remembers the familiar object will spend more time exploring the novel object. The recognition performances were quantified using the Discrimination Index (DI), measured as the differences between novel (T_{novel}) and familiar ($T_{familiar}$) object exploration times in proportion to the animal's total exploration time (T_{total}): (T_{novel} - $T_{familiar}$) / T_{total}. A DI equivalent to 0 indicates an equal exploration of the novel and familiar objects, while a preference for the novel or familiar object is represented by a positive or a negative DI, respectively.

2.5.7 Morris Water Maze

The Morris Water Maze (MWM) was used to assess spatial reference memory (Morris 1984). The MWM apparatus consisted of a circular pool of 110 cm diameter filled with tap water, which was made opaque by adding a white non-toxic paint. The temperature of the water was maintained between 20-22 °C for the entire duration of the task. The aim of the task is for mice to learn the position of a hidden circular platform (approximately 10 cm diameter), located below water level, and using distal and proximal cues. The pool was divided into 4 virtual quadrants with the ANY-Maze video tracking software. The quadrants were defined according to their spatial location compared to the hidden

platform as follows: left (L), right (R), opposite (O), and target quadrant (T), which contained the goal platform.

At first, the animals performed a three-day cue training to learn the aim of the task and to evaluate general health and intact vision of the mice. During this stage, the submerged platform was marked with a triangular flag and its position in the pool varied between trials. Only distal visual cues were applied during this first phase. The mice were introduced into the water at the edge of the pool facing the wall, starting from a different given position in subsequent trials. Each trial lasted a maximum of 60 seconds. If the mice failed to reach the platform within the given time, they were gently guided to it and allowed to sit on the platform for a few seconds before being placed back to their cages. Each mouse received four cued training trials per day with an inter-trial interval of at least 10 minutes.

Forty-eight hours after the last cued training, a five-day acquisition training began. The platform was submerged and invisible for the animals during this entire phase and its position remained stationary. In addition to distal cues attached on the walls, proximal cues were placed to the outside of the pool. Mice were introduced into the water from different given starting locations in each trial (Vorhees and Williams 2006). As with the cue training, the mice performed four trials each day, each lasting a maximum of 60 second and with a 10-minute break. During both cue and acquisition training, the average speed, the average distance, and the latency to reach the platform were recorded for each trial.

At last, twenty-four hours after the last acquisition trial, a single probe trial was performed. The hidden platform was removed from the pool and mice were placed into the water from a novel position. The trial lasted 60 seconds and mice were freely allowed to swim. The time spent in each quadrant was recorded, as well as average speed, and distance, and used to assess spatial reference memory. After each trial, the mice were kept in cages in front of heat lamps to prevent hypothermia.

2.6 Tissue collection and preservation

2.6.1 Preparation of tissues for biochemical analyses

Mice were deeply anesthetized with carbon dioxide and sacrificed via cervical dislocation. After decapitation, brain and spinal cord tissues were rapidly and carefully dissected on ice. For the brains, the skin and tissue surrounding the skull were removed with fine surgical scissors. A first incision at the midline, followed by lateral incisions along the temporal bones were performed to remove the skull bones. The skull fragments were removed with tweezers before the whole brain was expelled from the skull basis with a small spatula. The cerebellum and olfactory bulbs were removed before the two hemispheres were separated for storage or for further dissection. When further processing was not needed, the left and right hemispheres were quickly frozen on dry ice and stored at -80°C. Otherwise, each hemisphere was placed with the medial side facing up and the thalamus, the septum, and the underlying striatum were removed with a spatula to expose the hippocampus. The clearly visible hippocampus was rolled out starting from the ventral part with the tip of a spatula and separated from the cerebral cortex. Hippocampi and cortexes from both hemispheres were rapidly frozen on dry ice and stored at -80°C until further processing. Sections of cervical/thoracic spinal cord were also collected for biochemical analysis. After decapitation, the spine was exposed to perform careful lateral incision of the vertebra. Subsequently, the spinal cord was removed from the spine, frozen on dry ice and stored at -80°C until use.

2.6.2 Preparation of tissues for immunohistochemical analyses

Mice were sacrificed and the brain dissected as described in section 2.6.1 to obtain the intact left and right hemispheres. The right and/or left hemispheres were positioned into embedding cassettes (Simport) and post-fixed in a light protected 4% phosphate-buffered formaldehyde solution (Roti®-Histofix 4%, Roth, Karlsruhe, Germany) at 4°C for at least a week. Eventually, the samples were embedded in paraffin (Section 2.9.1).

When brain samples were needed for stereological analysis or blood removal was preferred for immunohistochemistry, the mice underwent a perfusion procedure. Therefore, mice were deeply anesthetized with a mixture of 10% ketamine (Medistar, Ascheberg, Germany) and 2% xylazine (Ecuphar, N.V. Oostkamp, Belgium) diluted in molecular-grade water. The anesthetic was administered intraperitoneally at a dosage of 100 mg/kg ketamine and 10 mg/kg xylazine body weight. Once the animals did no longer display a pedal withdrawal reflex, they were pinned on the perfusion board. The abdominal wall was opened with surgical scissors, the diaphragm was carefully cut, and the rib cage was split with two lateral cuts and lifted to reveal the beating heart. An incision was made to the right atrium to allow the drainage of blood from the circulatory system. Subsequently, a sterile needle attached to the tubing system of a peristaltic pump was inserted into left ventricle and the mice were perfused with approximately 20 mL of ice-cold 0.01 M PBS. Discoloring of the liver was used as indicator of a successful perfusion. Following perfusion, the mice were decapitated, and the brain/spinal cord dissected as described in section 2.6.1. The right brain hemisphere and the cervical/thoracic spinal cord were placed into embedding cassettes and post-fixated with a light-protected 4% formalin Histofix solution (Roth, Karlsruhe, Germany) at 4°C for at least one week before embedding in paraffin (Section 2.9.1). The left hemisphere, used for stereological analyses, was post-fixated in 4% PFA in 0.01 M PBS for additional 24h before being transferred in a 30% sucrose solution prepared in 0.01 M PBS for cryo-protection. The brain tissue was left in sucrose until it sunk to the bottom of its container, subsequently frozen on dry ice and stored at -80°C until further use.

2.7 Genotyping of transgenic animals

2.7.1 Isolation of genomic DNA

Mice were genotyped before behavioral analysis and tissue collection. Tail or ear biopsies were used to isolate genomic DNA. The biopsies were first digested overnight at 55°C

under shaking conditions (450 rpm) in a Thermomixer Compact (Eppendorf, Hamburg, Germany). For this purpose, each biopsy was incubated with a volume of 500 µL lysis buffer (100 mM Tris/HCl [pH 8.5], 5 mM EDTA, 0.2% dodecyl sulfate (SDS) and 200 mM NaCl) supplemented with 5 µL proteinase K (20 mg/ml stock; Peqlab, Erlangen, Germany). Samples were then centrifuged for 20 min at 17'000 rpm at 4°C (Heraeus Biofuge Stratos) and the supernatant transferred to a new 1.5 mL reaction tube. In each microtube 500 µL ice-cold isopropanol (Roth, Karlsruhe, Germany) were added and the tube inverted to allow the precipitation of genomic DNA. After an additional centrifugation at 13'000 rpm for 10 min at room temperature (RT), the supernatant was discarded, and the remaining pellets were washed, twice with 500 µL of ice-cold 70% absolute ethanol. After each washeing step, the pellets were centrifuged for 10 min at 13'000 rpm (RT conditions). Following the last centrifugation, the supernatant was discarded, and the DNA pellets were dried at 37°C in a Thermomixer Compact (Eppendorf, Hamburg, Germany) for 45 min. Genomic DNA was re-suspended in 30 µL molecular-grade (Braun, Melsungen, Germany) water and dissolved at 55°C overnight in a Thermomixer Compact before being stored at 4°C until further usage.

2.7.2 Determination of nucleic acid concentration

DNA and RNA concentrations were determined using a spectrophotometer (NanoDrop One C, Thermo Fischer Scientific). According to which samples were read (DNA or RNA), different applications on the device were used. The blank for the photometry was achieved by reading 1 µL of molecular-grade water for DNA or DNAse free Water for RNA, prior to sample measurements. For each DNA or RNA sample, 1 µL of sample solution were loaded to the lower pedestal to allow the reading. After the blanking and each sample reading, the lower and upper pedestal were cleaned with a laboratory wipe. For each DNA and RNA sample, the 260/230 and 260/280 absorbance ratios were

measured. Concentration measurements were considered accurate if the 260/230 and 260/280 absorbance ratios were between 1.6 and 2.0.

2.7.3 Polymerase chain reaction (PCR)

The genomic DNA samples were further diluted to 20 ng/μL with molecular grade (Braun, Melsungen, Germany) prior to the genotyping by standard polymerase chain reaction (PCR). The reaction mixtures and the thermal cycling program for DNA amplification are given in the Tables 2.3, 2.4, 2.5, 2.6, 2.7 and Tables 2.8, 2.9, 2.10 respectively. To corroborate the presence of the transgenes in the samples, the PCR products were identified by agarose gel-electrophoresis. A 2% agarose gel was prepared by mixing 0.7 g of agarose (Lonza, Basel, Switzerland) with 35 mL of 1X TBE (prepared from a 5X TBE stock solution: Tris/Borat/EDTA buffer) and boiled in a microwave before 2 μL of HD Green Plus DNA stain (Intas Science Imaging, Göttingen, Germany) were added to the gel. The agarose solution was poured into a casting tray with a comb to form the wells under the hood. After solidification of the gel, 10 μL of the PCR product were mixed with 2 μL of 10X loading buffer and added into the wells. For size identification, 6 μL of 100 bp DNA ladder (Bioron, Ludwigshafen, Germany) were loaded into the first well and gel electrophoresis was conducted at 135 mV for 30 min in 1X TBE buffer. The PCR product bands were then visualized in an UV-chamber (BlueCube 300L, Serva, Heidelberg, Germany).

Table 2.3 Reaction mixture for hAPP genotyping.
(Performed for genotyping of 5xFAD, FAD/Tg4-42^{hom} and 5xFAD/ADAMTS4$^{-/-}$)

Reagent	Volume (μL)
DNA (20 ng/μL)	1.0
Primer hAPP forward	0.5
Primer hAPP reverse	0.5
dNTP's (2 mM)	2.0
$MgCl_2$ (25 mM)	3.2
10X Reaction buffer	2.0
Taq Polimerase (5U/μL)	0.2

Molecular-grade water	10.6
Total reaction volume per sample	**20**

Table 2.4 Reaction mixture for MAPT genotyping.
(Performed for genotyping of MAPT and MAPT/Tg4-42^{hom}).

Reagent	Volume (μL)
DNA (20 ng/μL)	1.0
Primer oIMR8080	1.8
Primer oIMR8081	1.8
Primer oIMR8744	1.2
Primer oIMR8745	1.2
dNTP's (2 mM)	1.9
10X Reaction buffer PeqLAb	2.4
Taq Polimerase PeqLAb (5U/μL)	0.12
Molecular-grade water	12.6
Total reaction volume per sample	**24**

Table 2.5 Reaction mixture for Tg4-42 transgene genotyping.
(Performed for genotyping of FAD/Tg4-42^{hom} and MAPT/ Tg4-42^{hom})

Reagent	Volume (μL)
DNA (20 ng/μL)	1.0
Primer Aβ3-42 forward	0.5
Primer Aβ3-42 reverse	0.5
dNTP's (2 mM)	2.0
$MgCl_2$ (25 mM)	3.2
10X Reaction buffer	2.0
Taq Polimerase (5U μL)	0.2
Molecular-grade water	10.6
Total reaction volume per sample	**20**

Table 2.6 Reaction mixture for ADAMTS4 genotyping.
(Performed for genotyping of ADAMTS4$^{-/-}$ and 5xFAD/ADAMTS4$^{-/-}$).

Reagent	Volume (μL)
DNA (20 ng/μL)	1.0
Primer Adam-Neo	1.2
Primer Adam forward	1.8
Primer Adam reverse	1.2
dNTP's (2 mM)	1.9

10X Reaction buffer PeqLab	2.5
Taq Polimerase PeqLAb (5U/μL)	0.125
Molecular-grade water	14.2
Total reaction volume per sample	**24**

Table 2.7 Reaction mixture for NEP genotyping.
(Performed for genotyping of $NEP^{-/-}$ and $Tg4\text{-}42^{het}/NEP^{-/-}$).

Reagent	Volume (μL)
DNA (20 ng/μL)	1.0
5′-ex12 primer	0.4
3′-ex13 primer	0.2
3′-neo(3) primer	0.5
dNTP's (2 mM)	2.5
$MgCl_2$ (25 mM)	2.5
10X Reaction buffer	2.5
Taq Polimerase (5U/μL)	0.2
Molecular-grade water	15.2
Total reaction volume per sample	**25**

Table 2.8 Thermal cycling program for hAPP, NEP and Tg4-42 transgene genotyping.

Step	Temperature [°C]	Duration [s]
1	94	180
2	94	45
3	58	60
4	72	60
5	Repetition of cycled 2-4 (40 cycles)	
6	72	300
7	4	∞

Table 2.9 Thermal cycling program for MAPT genotyping.

Step	Temperature [°C]	Duration [s]
1	94	180
2	94	30
3	57	60
4	72	60
5	Repetition of cycled 2-4 (34 cycles)	
6	72	120
7	4	∞

Table 2.10 Thermal cycling program for ADAMTS4 genotyping.

Step	Temperature [°C]	Duration [s]
1	95	420
2	94	30
3	60	30
4	68	90
5	Repetition of cycled 2-4 (34 cycles)	
6	68	420
7	6	∞

2.7.4 Quantitative Real-Time PCR for Genotyping

A quantitative Real-Time PCR (qRT-PCR) was performed to determine the heterozygous/homozygous state for the Tg4-42 transgene in Tg4-42 and 5xFAD/Tg4-42 lines. The Biozym Blue S'Green qPCR Mix, containing SYBR Green as the intercalating fluorescent dye, was used for this purpose. ROX was added to the Mix as internal reference dye, following the manufacturer's instructions. The reaction mix and the thermal cycling program for amplification are shown in Table 2.11 and Table 2.12 respectively. The DNA dilutions (20 ng/µL) were mixed with the qPCR reaction mix in 200 µL PCR tubes (Biozym, Oldendorf, Germany) in duplicates, and briefly centrifuged in a Spectrafuge Mini (Labnet Inc., Edison, NJ, USA). qRT-PCRs were performed in the MX3000P Real-Time Cycler (Stratagene, Santa Clara, CA, USA) and data collected using the MxPro Mx3000P software (Stratagene, Santa Clara, CA, USA). The CT-values were

measured and averaged from the duplicates. For relative quantification, CT-values of the human Aβ4-42 target gene were normalized to those of murine APP (reference gene) and calibrated to a known heterozygous control mouse using the $2^{-\Delta\Delta CT}$ method (Schmittgen and Livak 2008). For both the test mouse (test) and the control mouse (calibrator), the CT of the target gene was normalized to that of the reference gene.

$$\Delta CT(test) = CT(target, test) - CT(reference, test)$$

$$\Delta CT(calibrator) = CT(target, calibrator) - CT(reference, calibrator)$$

Then, the ΔCT of the test mouse was normalized to the ΔCT of the calibrator:

$$\Delta\Delta CT = \Delta(test) - \Delta CT(calibrator)$$

Finally, the gene amount of the target gene in the test mouse is $2^{-\Delta\Delta CT}$ times of the control mouse. Homozygous mice are recognized as having double amount of transgene compared to the heterozygous controls.

Table 2.11 Reaction mixture for Tg4-42 transgene qRT-PCR genotyping.

Reagent	Volume (µL)
DNA (20 ng/µL)	1.0
Primer Aβ3-42 forward	1.5
Primer Aβ3-42 reverse	1.5
Blue S'Green Mix	10
Molecular grade water	6.0
Total reaction volume per sample	**20**

Table 2.12 Thermal cycling program for Tg4-42 transgene genotyping.

Step	Temperature [°C]	Duration [s]
1	95	600
2	95	15
3	60	60
4	Repetition of cycled 2-3 (40 cycles)	
5	95	15
6	60	60
7	95	15

2.7.5 Primers used in genotyping

The primers were used at a concentration of 10 pmol/µL (1:10 dilution prepared in ddH_2O from the 100 pmol/µL stock). All primers were purchased from Eurofins (Ebersberg, Germany) and are listed in Table 2.13.

Table 2.13 List of primers used for mouse genotyping in alphabetical order.

Name	Sequence (5′ → 3′)	Usage
5′-ex12	GCC TAT TCT TAC CAA ATA TTC TCC CAG	PCR
3′-ex13	TTG CGG AAA GCA TTT CTG GAC TCC TTG	PCR
3′-neo	CTA TCG CCT TCT TGA CGA GTT CTT CT	PCR
Aβ3-42 forward	TCC GGC CAG AAC GTC GAT TC	qRT-PCR
Aβ3-42 reverse	GGA GAA GCA AGA CCT CTG C	qRT-PCR
AdamTS4-Neo	GGG TGG GAT TAG ATA AAT GCC TGC TCT	PCR
AdamTS4 forward	GGA CAC GGG ATG GAC CCT CTA GAT G	PCR
AdamTS4 reverse	ACA TGG AGG ACT CAG TGT GGC CCA C	PCR
Human APP forward	GTA GCA GAG GAA GAA GTG	PCR
Human APP reverse	CAT GAC CTG GGA CAT TCT C	PCR
Murin APP forward	TCT TGT CTT TCT CGC CAC TGG C	qRT-PCR
Murin APP reverse	GCA GTC AGA AGT TCC TAG G	qRT-PCR
oIMR8080	GGG GAC ACG TCT CCA CGG CAT CTC AGC AAT GTC TCC	PCR
oIMR8081	TCC CCC AGC CTA GAC CAC GAG ACT	PCR
oIMR8744	CAA ATG TTG CTT GTC TGG TG	PCR
oIMR8745	GTC AGT CGA GTG CAC AGT TT	PCR

2.8 Molecular biology

2.8.1 RNA Isolation and nucleic acid concentration determination

RNA was isolated from deep frozen hippocampus, cortex, and spinal cord samples. The tissues were weighted, supplied with 1 mL of Trifast® reagent per 100 mg of sample and homogenized using a glass-Teflon homogenizer with 15 strokes at 800 rpm. The homogenates were transferred in 1.5 mL tubes and were incubated at RT for 5 min for dissociation of nucleoprotein complexes. To each sample, 0.2 mL of chloroform were added per each mL of Trifast® used. The mixtures were vortexed for 15 seconds and

incubated at RT for 10 min. The samples were centrifuged at 12'000 x g for 15 min at 4°C to separate the RNA from the other cellular components. The upper RNA-containing aqueous phase was transferred to fresh sterile 1.5 mL tube and 0.5 mL isopropanol per 1 mL Trifast® was added. The samples were gently mixed and incubated at -20°C for 20 min to allow RNA precipitation. The tubes were later centrifuged at 12'000 x g for 10 min at 4°C. The supernatant was carefully discarded, and the RNA pellets were washed twice with an equivalent volume to that of isopropanol with 75% absolute ethanol. After each washing step, the pellets were centrifuged at 7'500 x g for 10 min at 4°C. The remaining ethanol was later removed, and the pellets air-dried for 30 min at RT. Once dry, 30 µL of molecular grade water were added to each sample to dissolve the RNA pellets. The tubes were left for 1 hour on ice before storing them at -80 °C. The RNA concentration of the samples was determined as described in section 2.7.2

2.8.2 Reverse transcription

To remove possible genomic DNA from the RNA samples, RNA was firstly subjected to digestion with DNAse I. For this purpose, 1 µg of RNA was mixed with 1 µL of 10x DNAse reaction buffer (+$MgCl_2$) and 1 µL DNase I (1 U/µL) and brought to a final volume of 10 µL with nuclease-free water. The dilutions were incubated at 37°C for 30 min in a LabCycle (SensoQuest). The digestion was then deactivated by addition of 1 µL of EDTA (25 mM) to each reaction mixture and incubated for 10 min at 65°C. The resulting 11 µL of DNAse digested RNA mixture were used as template for cDNA synthesis.

The RevertAid RT Kit (Thermo Fisher Scientific) was used to perform the reverse transcription, following to the manufacturer's instructions. Briefly, the 11 µL of DNAse digested RNA sample were mixed with 1 µL of random hexamer primer, 4 µL 5x reaction buffer, 1 µL RiboLock® RNAse inhibitor (20 u/µL), 2 µL of 10 mM dNTP mix and 2 µL M-MuLV reverse transcriptase (20 u/µL). The reactions were incubated in a LabCycler

(SensoQuest) for 5 min at 25°C, 1 h at 37°C and 5 min at 70°C. The 21 µL of cDNA mixtures were then stored at -20°C until further use.

2.8.3 Quantitative real-time polymerase chain reaction (qRT-PCR)

The Biozym Blue S'Green qPCR Mix, containing SYBR Green as the intercalating fluorescent dye, was used to perform gene expression analysis. ROX was added to the Mix as internal reference dye, following the manufacturer's instructions. cDNA samples were diluted 1:10 with molecular-grade water before being used as qPCR template. cDNA dilutions were pipetted into 200 µL qRT-PCR tubes (Biozym Scientific) followed by the qRT-PCR reaction mix. Each reaction was performed in duplicate. Before the start of the qRT-PCR reactions in the Mx3000P cycler (Stratagene), the tubes were briefly centrifuged using a Spectrafuge Mini (Labnet Inc.). The reaction mix and the cycling program are given in Table 2.11 and Table 2.12, respectively. Raw data were collected using the MxPro Mx3000P software (Stratagene). The average Ct value was calculated from the duplicate for each sample. The relative expression of the genes of interest (GOIs) was performed using murine β-Actin as reference gene for normalization, and were calibrated to a selected control group using the ΔΔCt method (Schmittgen and Livak 2008):

$$Amount_{\mathrm{GOI}} = 2^{-\Delta\Delta Ct}$$

For each animal (q) the relative expression level of a GOI, normalized to the expression of murine β-Actin from the sample animal and calibrated to a control group (cb), is calculated as follows:

$$\Delta C_{t,\mathrm{q}} = C_{t,GOI\text{-}\mathrm{q}} - C_{t,\beta\text{-}Actin\text{-}\mathrm{q}}$$

$$-\Delta\Delta C_t = -(\Delta C_{t,q} - \Delta C_{t,cb})$$

Table 2.14 qRT-PCR reaction mixture.

Reagent	Volume (µL)
cDNA 1:10	1.0
Primer forward	0.8
Primer reverse	0.8
Blue S'Green Mix	10
Molecular grade water	7.4
Total reaction volume per sample	**20**

Table 2.15 qRT-PCR cycling program.

Step	Temperature [°C]	Duration [s]
1	95	120
2	95	10
3	60	30
4	Repetition of cycled 2-3 (40 cycles)	
5	95	60
6	60	30
7	95	30

2.8.4 Primers

All primers were purchased from Eurofins Genomics (Ebersberg, Germany) and used at a final concentration of 10 pmol/µL (1:10 dilution of the 100 pmol/µL primer stock prepared in ddH_2O). The primers are listed in alphabetical order.

Table 2.16 List of primers.

Name	Sequence (5′ → 3′)
Aβ3-42 forward	TCC GGC CAG AAC GTC GAT TC
Aβ3-42 reverse	GGA GAA GCA AGA CCT CTG C
Actin-β forward	ATG GAG GGG AAT ACA GCC C
Actin-β reverse	TTC TTT GCA GCT CCT TCG TT
CNP forward	TTT ACC CGC AAA AGC ACA ACA
CNP reverse	CAC CGT GTC CTC ATC TTG AAG
Human APP forward	GTA GCA GAG GAA GAA GTG
Human APP reverse	CAT GAC CTG GGA CAT TCT C
Human MAPT forward	CCA AGT GTG GCT CAT TAG GCA

Human MAPT reverse	CCA ATC TTC GAC TGG ACT CTG T
MBP forward	ACA CGA GAA CTA CCC ATT ATG GC
MBP reverse	CCA GCT AAA TCT GCT GAG GGA
Plp1 forward	TGA GCG CAA CGG TAA CAG G
Plp1 reverse	TTC CCA AAC AAT GAC ACA CCC

2.8.5 Protein isolation

Frozen samples were weighted and 200 µl TBS buffer (120 mM NaCl, 50 mM Tris, pH 8.0) per 100 mg tissue were provided. The protease inhibitor cocktail cOmplete™ (1 tablet per 10 mL) and Phosphatase inhibitor cocktail (1 tablet per 10 mL) were added to the TBS buffer prior to use. According to the size and weight of the sample, two different homogenization procedures were used. In case of protein isolation from cortex samples, the tissues were homogenized using a R50D homogenizer at 800 rpm (10 strikes). The homogenates were then transferred to 1.5 mL tubes. When hippocampus and spinal cord tissues were homogenized, the procedure was performed in 1.5 mL Eppendorf using a Sonicator (Sonitrome) while incubating the samples on ice. The following settings were used:

Tip MS: 1.5
Amplitute 80%
Time: 30s
Pulse: 0.05s – 1s pause

After both types of homogenizations, the samples were centrifuged at 17’000 x g for 20 min at 4°C (Heraeus Biofuge Stratos). The supernatant, corresponding to the TBS-soluble protein fraction, was transferred into a fresh tube, and stored at -80°C until further use. A 2% SDS solution was later added to the remaining pellets (800 µL for cortex samples, 200 µL for hippocampus and spinal cord samples) and sonicated (Sonitrom) on ice with the following settings:

Tip MS: 1.5

Amplitute 80%
Time: 20s
Pulse: 0.05s – 1s pause

After sonication, 1 µL of Benzonase was added to each sample, which were incubated at RT for 5 min to remove DNA. The samples were then centrifuged at 17'000 x g for 20 min at 4°C (Heraeus Biofuge Stratos). The supernatants containing the SDS-soluble fraction were transferred in new tubes. Both supernatant and remaining pellets were stored at -80°C until further use.

2.8.6 Protein concentration determination

The protein concentration of the TBS- and SDS-soluble fractions was determined using the Pierce™ BCA Protein Assay Kit (Thermo Fischer Scientific), according to the manufacturer's protocol. Briefly, a stock solution of 10 mg/mL albumin fraction V in 0.01 M PBS was diluted in ddH_2O and TBS buffer or 2% SDS for the generation of two standard curves (2, 1.5, 1.0, 0.75, 0.5, 0.25, 0.10, 0.05, 0.025 mg/mL), one for each protein fraction. TBS-soluble fraction samples were diluted 1:5, while SDS-soluble fraction samples 1:8, in ddH_2O before the measurement. 25 µL of each diluted sample and standard curve sample were loaded in duplicate in a 96-wells plate. The BCA Working Reagent (WR) was prepared by mixing 50 parts of BCA Reagent A with 1 part of BCA Reagent B. 200 µL of WR were added to each well and the plate was incubated at 37°C for 30 minutes protected from light. Protein concentrations were measured at 562 nm using a Synergy HTX multi-mode reader (BioTek Instruments, Inc.) combined with the Gen5 software (BioTek Instruments, Inc).

2.8.7 Electrochemiluminescent Assay

To determine Aβ levels in hippocampus and spinal cord protein samples, an electrochemiluminescent assay obtained from Meso Scale Discovery (MSD) was used. The determination of total Aβ was achieved using the Human Aβ (total) R-PLEX™

Antibody Set, which employs monoclonal antibody 6E10 (directed against an amino terminal epitope of Aβ) for capture and monoclonal antibody 4G8 (directed against Aβ17-26) for detection on MSD GOLD 96-well Small Spot Streptavidin Plates. To measure the levels of specific Aβ variants ($A\beta_{1-x}$, $A\beta_{4-x}$, $A\beta_{4-42}$), antibodies with known specificity were biotinylated and sulfo-tagged, as described in section 2.8.7.1, and used as capture and detection antibodies on MSD GOLD 96-well Small Spot Streptavidin Plates. The combination of antibodies, their epitopes, and the concentrations used in the assay are listed in table 2.17. The assay was performed according to the protocol for the Human Aβ Antibody Set of the manufacturer and readout on an MSD QuickPLex SQ 120. Briefly, the MSD GOLD 96-well Small Spot Streptavidin Plate was coated with the biotinylated capture antibody by adding 25 µL of biotinylated antibody diluted in Diluent 100 (MSD) in each well. The plate was incubated for 1h at RT at 700 rpm. After 3 washing with 150 µL/well of 0.05% PBS-Tween, the plate was blocked by adding 150 µL/well of Diluent 35 (MSD). After incubation at RT for 1h under shaking conditions, the plate was again washed three times with 150 µL/well of PBS-T. In each well, 25 µL of detection antibody and 25 µL of sample were added and left for 2h at RT under shaking conditions. Finally, the plate was washed 3 times with 150 µL/well with PBS-T and, after the addition of 150 µL/well of Gold Read Buffer, read on an MSD QuickPLex SQ 120.

Table 2.17 Aβ-directed antibodies used in MSD chemiluminescent assay.

Detected Aβ	Biotinylated Captured Ab (epitope) – Conc.	SulfoTAG Captured Ab (epitope) – Conc.
$A\beta_{1-x}$	82E1 ($A\beta_{1-x}$) - 1 µg/ml	4G8 ($A\beta_{18-22}$) – 1:50 (manufacturer instruction)
$A\beta_{4-x}$	18H6 ($A\beta_{4-x}$) - 0.6 µg/ml	4G8 ($A\beta_{18-22}$) – 1:50 (manufacturer instruction)

2.8.7.1 Preparation of biotinylated antibodied

Preparation of biotinylated antibodies used in the Electrochemiluminescent Assay was performed following the instruction recommended by MSD in the MSD Biotin Conjugation Quick Guide. 50 µL of a 1 mg/mL stock solution of mAb 18H6 and mAb 82E1 were at first buffer-exchanged into MSD conjugation buffer (PBS, pH 7.9, preservative-free) on a Zeba Spin Desalting column 40 K MWCO, 0.5 mL (Thermo Scientific). For biotinylation, a 0.9 nmol/µL Sulfo-NHS-LC biotin solution (EZ-link(™) Micro Sulfo-NHS-LC-biotinylation kit, Thermo Scientific) was added to approximately 50 µg of IgG to have a challenge ratio of 10:1 and mixed immediately by vortexing. After 2 hours incubation at 23°C, excess biotin was removed by buffer exchange into MSD conjugate storage buffer (PBS, pH 7.4 containing 0.05% sodium azide) on a Zeba Spin Desalting column (40 K MWCO, 0.5 mL). Glycerol was added to a final concentration of 50% (v/v) and the biotinylated antibodies were stored at -20°C until use.

2.9 Immunohistochemistry

2.9.1 Paraffin embedding of mouse brain and spinal cord tissues

Brain and spinal cord samples were fixated as described in paragraph 2.6.2. Subsequently, the samples were dehydrated and immersed in paraffin with a TP Automatic Tissue Processor (Leica). The steps performed by the Automatic Tissue Processor are displayed in Table 2.18

Table 2.18 Tissue dehydration protocol.

Reagent	Time
4% Histofix	5 min
Tap Water	30 min
50%, 60%, 70%, 80%, 90% EtOH	1 h each
100% EtOH	2 x 1 h
Xylol	1 h
Melted paraffin	2 x 1 h

After dehydration, each sample was processed using an EG1140 H Embedding Station (Leica) and embedded in paraffin blocks. 4 µm sagittal brain sections and spinal cord cross sections were cut with a HM 335E microtome (Thermo Fisher Scientific). Sections were transferred to a RT ddH_2O water bath, mounted onto Superfrost® slides (Thermo Fisher Scientific) and defolded in a 55°C ddH_2O bath (Medax). Each slide was left at RT for 30 min before incubating them O/N at 37°C to permanently fix them onto the slides.

2.9.2 3, 3'-Diaminobenzidine (DAB) immunohistochemistry

To perform a DAB staining the sections were firstly deparaffinized with xylol (2 x 5 min) and subsequently rehydrated with a decrescent ethanol series (100% - 10 min, 95% - 5 min, 70% - 5 min). After 1 min incubation in ddH_2O, the sections were treated with 0.3% H_2O_2 in 0.01 M PBS to block endogenous peroxidases and later boiled in 0.01 M citrate buffer pH 6.0 (2 min at 800 W, 8 min at 200 W) to retrieve the antigen. The sections were cooled down for 15 min, dipped in ddH_2O for 1 min and membrane permeabilization was achieved with a 15 min incubation in 0.1% Triton X-100 in 0.01 M PBS. In case of Aβ staining, the slides were additionally incubated for 3 min in 88% formic acid to reveal the epitope. Non-specific binding sites were blocked by incubation with 4% skim milk and 10% fetal calf serum (FCS) in 0.01 M PBS for 1 h. After removal of the blocking solution and without any further washing step, the primary antibodies were applied and left in incubation O/N at RT in a humid chamber. The primary antibodies were diluted to the desired concentration in 0.01 M PBS with 10% FCS and are listed in Table 2.19. The sections were washed in 0.1% Triton X-100 in 0.01 M PBS for 15 min and, after a 1 min wash in 0.01 M PBS, the respective biotinylated secondary antibodies, diluted in 0.01 M PBS with 10% FCS, were applied (Table 2.20) and the slides were left in a humid incubation chamber for 1 h at 37°C. The Avidin-biotin complex (ABC) solution was prepared using the Vectastain Elite ABC Kit according to the instructions of the manufacturer at least 30 min prior to use, and stored at 4°C. Following 3 x 5 min washings

in 0.01 M PBS, the sections were incubated with the ABC solution for 1.5 h at 37°C in a humid chamber. The slides were later washed for 3 x 5 min with 0.01 M PBS and the staining was visualized using 3,3'-diaminobenzidine (DAB) as a chromogen. The DAB solution was prepared by mixing 100 µL DAB stock solution (25 mg/mL DAB in 50 mM Tris/HCl) with 5 mL 50 mM Tris/HCl and 2.5 µL 30% H_2O_2. After the staining development, the slides were washed for 15 min in 0.01 M PBS and the eventual counterstaining with hematoxylin was performed. Slides were incubated in hematoxylin for 40 sec, then rinsed in ddH_2O and washed under running tap water for 5 min. Finally, the slides were dehydrated with a crescent ethanol series (70% - 1 min, 95% - 5 min, 100% - 10 min) followed by 2 x 5 min incubations in xylol. Each section received 2 drops of Roti®-Histokitt mounting medium, and a cover slip was applied to the slide.

2.9.2.1 Semiquantitative analysis of DAB immunoreactivity in human samples

The stained human sections were evaluated in a blinded fashion using a BX51 microscope (Olympus, Hamburg, Germany) equipped with a Moticam Pro 282 camera (Motic, Wetzlar, Germany). For each antibody used, a semi-quantitative scoring was assigned to parenchymal plaques, parenchymal and meningeal CAA staining as follow: 0 = no staining, 0.5 = barely detectable staining, 1 = weak staining, 2 = moderate staining, 3 = extensive staining.

2.9.2.2 Quantification of DAB immunoreactivity in mouse samples

An Olympus BX-51 microscope equipped with a Moticam Pro 282A camera (Motic) was used to capture images in selected brain regions and in the spinal cord for the analyzed protein. For each sample three sections, at least 30 µm apart from each other, were used. The immunoreactivity was analyzed using the ImageJ software package where pictures were binarized to 8-bit black and white images and a fixed intensity threshold was applied defining the DAB signal. The percentage area covered by DAB staining was calculated and compared within the considered groups.

2.9.3 Fluorescent immunohistochemistry

In case of fluorescent immunohistochemistry, the followed protocol for the first day of staining is equivalent to DAB immunohistochemistry (paragraph 2.8.2), besides the incubation in 0.3% H_2O_2 in 0.01 M PBS to block endogenous peroxidases is omitted. After the overnight incubation with primary antibodies, the slides were washed for 15 min in 0.1% Triton X-100 in 0.01 M PBS before incubation with the fluorescent secondary antibodies (Table 2.20). The secondary antibodies were diluted in 0.01 M PBS with 10% FCS and applied for 1.5 h at 37°C in a humid chamber. The slides were later washed 3 x 5 min in 0.01 M PBS, protected from light. Each section received 2 drops of Fluorescent Roti®-Histokitt mounting medium containing 4',6-diamidin-2-phenylindol (DAPI) and a cover slip was applied to the slide.

2.9.3.1 Quantification of fluorescent immunoreactivity

Fluorescent images were recorded using a Nikon TiE microscope (Nikon) and analyzed with NIS Elements imaging software (Nikon). A fixed intensity threshold was applied, and the percentage area covered by fluorescent staining was recorded.

2.9.4 Primary antibodies used in immunohistochemistry

Table 2.19 Primary antibodies used in immunohistochemistry.

Antibody	Host	Isotope	Immunogen	Working dilution	Manufacturer
029-2	guinea pig	polyclonal	$A\beta_{4\text{-}x}$	1:500	Department of Psychiatry and Psychotherapy (Wirths et al. 2017)
18H6	mouse	monoclonal	$A\beta_{4\text{-}x}$	1:500	Gift from Prof. Jorge Ghiso (Cabrera et al. 2018)
24311	rabbit	polyclonal	Pan-Aβ	1:500	Department of Psychiatry and Psychotherapy (Saul et al. 2013b)
80C2	mouse	monoclonal	$A\beta_{1\text{-}16}$	1:500	Synaptic Systems
82E1	mouse	monoclonal	$A\beta_{1\text{-}16}$	1:1000	IBL International
AT8	mouse	monoclonal	Tau pSer202/T205	1:500	Perbio
ChAT	goat	polyclonal	Choline Acetyltransferase	1:500	Chemicon International
D3E10	rabbit	polyclonal	$A\beta_{1\text{-}42}$	1:1000	Cell Signaling
Iba1	guinea pig	polyclonal	Microglia	1:500	Synaptic Systems
NeuN	guinea pig	polyclonal	Neurons	1:500	Synaptic Systems
pAb 77	rabbit	polyclonal	$A\beta_{2\text{-}x}$	1:500	Department of Psychiatry and Psychotherapy (Savastano et al. 2016)

2.9.5 Secondary antibodies used in immunohistochemistry

Table 2.20 Secondary antibodies used in immunohistochemistry.

Antibody	Host	Conjugate	Working dilution	Manufacturer
Anti-guinea pig	donkey	biotinylated	1:200	Dianova
Anti-mouse	goat	biotinylated	1:200	Dianova
Anti-rabbit	goat	biotinylated	1:200	Dianova
Fluorescent Anti-goat	donkey	Dylight™-650	1:750	Thermo Fisher Scientific

Fluorescent Anti-guinea pig	donkey	Alexa Fluor®-488	1:750	Dianova
Fluorescent Anti-mouse	goat	Dylight™-594	1:750	Thermo Fisher Scientific
Fluorescent Anti-rabbit	goat	Dylight™-488	1:750	Thermo Fisher Scientific
Fluorescent Anti-rabbit	goat	Dylight™-594	1:750	Thermo Fisher Scientific

2.10 Quantification of neuron numbers

The quantification of neuron numbers was performed on sagittal brain sections from paraffin samples, while quantification of motoneurons was performed in the cervical spinal cord of paraffin samples. The preparation of brain and spinal cord samples and paraffin embedding are described in paragraphs 2.6.2 and 2.9.1 respectively.

2.10.1 Hematoxylin staining of CA1 pyramidal neurons

Paraffin brain sections were firstly deparaffinized with xylol (2 x 5 min) and subsequently rehydrated with a decrescent ethanol series (100% - 10 min, 95% - 5 min, 70% - 5 min). After 1 min incubation in ddH_2O, the slides were incubated in hematoxylin for 10 min to stain the nuclei. The sections were briefly rinsed in ddH_2O and washed for 5 min under running tap water. The slides were dehydrated with a crescent ethanol series (70% - 1 min, 95% - 5 min, 100% - 10 min) followed by 2 x 5 min incubations in xylol. Each section received 2 drops of Roti®-Histokitt mounting medium, and a cover slip was applied to the slide.

2.10.2 Quantification of CA1 pyramidal neuron numbers

Images from the CA1 pyramidal layer were captured with 400x magnification using an Olympus BX-51 microscope equipped with a Moticam Pro 282A camera (Motic). Images were analyzed using the ImageJ software package: neuronal nuclei, distinguishable from other cellular population by size and color intensity, were manually counted using the

multi-point function. For each sample, three sections at least 50 μm apart from each other, were analyzed. For all analyzed brains, the sections were selected between bregma 0.60 and 1.08.

2.10.3 Quantification of spinal motoneuron numbers

In Project III, Motoneurons (MNs) were counted in the ventral horns of cervical spinal cord paraffin samples. The tissue samples were stained as described in paragraph 2.9.3 and 200x magnification images were taken using a Nikon TiE microscope (Nikon). Fluorescent-stained $ChAT^+$-MNs were manually counted using the multi-point function in the ImageJ software package. α-MNs were recognized through fluorescent NeuN staining and size. In the NIS Elements imaging software (Nikon), a fixed intensity threshold was applied, and automatic object counting was performed after applying a size cut-off to considered only nuclei having a diameter longer than 20 μm. β-MNs were recognized as ChAT-positive and NeuN-negative and were manually counted using the multi-point function in the ImageJ software package. For each animal sample, three sections at least 30 μm apart from each other were analyzed.

2.11 Statistical analyses

Details of statistical analysis are given in the respective results section and in the figure legends. Data exploration was performed to assess the assumptions for parametric testing. In case of parametric testing, differences between groups were tested with unpaired t-test, one-way analysis of variance (ANOVA) followed by Bonferroni multiple comparison or two-way ANOVA followed by Bonferroni multiple comparison. When sample size was too little or assumptions for parametric tests were not met, differences between the groups were tested with Mann-Whitney test or Kruskal-Wallis test followed by Dunn's multiple comparison test. Significance levels were given as follows: ***$p < 0.001$; **$p < 0.01$; *$p < 0.05$. The number of animals used for behavioral experiments as

well as sample sizes used for biochemical or stereological analysis are given in the figure legends (n). All data were given as means ± standard deviation (SD). All statistics were performed using GraphPad Prism version 8.0 for Windows (GraphPad Software, San Diego, CA, USA).

3 RESULTS

3.1 PROJECT I: Assessment of N-terminal heterogeneity of parenchymal and vascular amyloid-β deposits in autopsied Alzheimer's disease brains.

In this study, immunohistochemical staining were performed to qualitatively compare the staining profiles of several antibodies detecting either full-length or N-terminally truncated Aβ species in autopsied brain samples from sporadic AD and non-demented control cases. Additionally, two Down syndrome cases were included in the analysis. The paraffin-embedded human brains used in this analysis comprised samples exclusively from the medial frontal gyrus region of the brain (Zampar et al. 2020). The demographic and pathological data of the analyzed cases are reported in Table 3.1.

3.1.1 Antibody characterization by capillary isoelectric focusing immunoassay

The selectivity of antibodies detecting either the full-length or specific N-terminal truncated variants of Aβ was evaluated with a capillary isoelectric focusing immunoassay (CIEF-immunoassay) using synthetic Aβ peptides. The polyclonal antibody 24311, considered a pan-Aβ antibody with a preference towards N-truncated species (Saul et al. 2013b), indeed detected the entire set of employed $A\beta_{40}$ peptides, with the exception of the N-elongated peptide $A\beta_{3\text{-}40}$, and only weakly recognized the full length $A\beta_{1\text{-}40}$ (Fig.3.1). Antibodies presumed to detect specifically the full-length Aβ peptide starting with Asp at position 1 or directed against the N-truncated variant starting with phenylalanine at position 4 were subsequently analyzed. The mouse monoclonal antibodies 80C2 and 82E1 targeted the intact N-terminus of the peptide and showed a clear signal for $A\beta_{1\text{-}40}$ without detectable cross-reactivity with the additional N-truncated Aβ peptides used in the analysis. The lack of reactivity towards both N-

Data published in (Zampar et al. 2020)

elongated and N-truncated species suggests that the two antibodies require a free aspartic acid at position 1 of the Aβ peptide sequence for detection (Fig. 3.1).

Table 3.1 Demographic and pathological data of sporadic Alzheimer's disease (AD) cases, non-demented control subjects (NDC) and Down syndrome (DS) cases.

Case	Age *(years)*	Gender	ApoE	Braak stage	Amyloid	PMI *(h)*	CAA
Sporadic AD cases							
AD 1	86	f	3/3	IV	B	04:10	no
AD 2	90	f	4/4	VI	C	04:00	severe
AD 3	85	f	3/3	VI	C	04:00	mild
AD 4	88	f	3/3	IV	C	03:30	mild
AD 5	87	f	4/3	VI	C	06:15	distinct
AD 6	92	m	3/3	IV	C	03:30	n.d.
AD 7	91	f	3/3	IV	C	03:45	distinct
AD 8	73	m	4/4	IV	C	05:30	severe
AD 9	93	f	3/3	IV	C	06:15	no
AD 10	92	f	3/3	IV	C	05:10	n.d.
AD 11	78	m	4/3	V	C	06:00	distinct
AD 12	82	f	3/3	V	C	04:25	severe
AD 13	82	f	4/4	V	C	03:05	distinct
AD 14	77	m	4/3	V	C	04:30	distinct
AD 15	89	m	3/3	V	C	04:05	no
AD 16	81	m	n.d.	IV	C	04:50	mild
AD 17	91	f	4/3	IV	B	04:15	mild
AD 18	79	f	4/3	IV	B/C	05:20	distinct
AD 19	70	f	3/3	VI	C	05:20	severe
AD 20	83	f	4/3	VI	C	04:30	mild
Non-demented control cases							
NDC 1	82	f	3/3	I	0	11:30	no
NDC 2	72	f	4/3	II	B	05:30	no
NDC 3	89	f	n.d.	III	0	03:52	no
NDC 4	78	f	3/3	I	A	04:50	no
NDC 5	73	m	3/3	0	0	24:45	no
NDC 6	70	m	3/2	0	0	07:30	n.d.
NDC 7	84	m	3/3	I	0	09:00	no
NDC 8	87	f	n.d.	II	0	05:30	no
NDC 9	93	f	3/3	II	0	05:50	no
NDC 10	87	m	3/3	III	A	06:10	no
NDC 11	90	f	3/3	III	A	06:05	no
Down syndrome cases							
DS 1	64	f	3/3	V	C	04:15	distinct
DS 2	58	m	4/3	VI	n.d.	06:10	distinct

Abbreviations: ApoE - Apolipoprotein E, n.d. – not determined

Data published in (Zampar et al. 2020)

In a similar fashion, the mouse monoclonal antibody 18H6 (Cabrera et al. 2018) displayed selectivity towards the free phenylalanine residue at position 4, giving a clear signal only with the N-truncated Aβ4-40 synthetic peptide without any noticeably cross-reactivity with shorter or longer Aβ variants (Fig. 3.1).

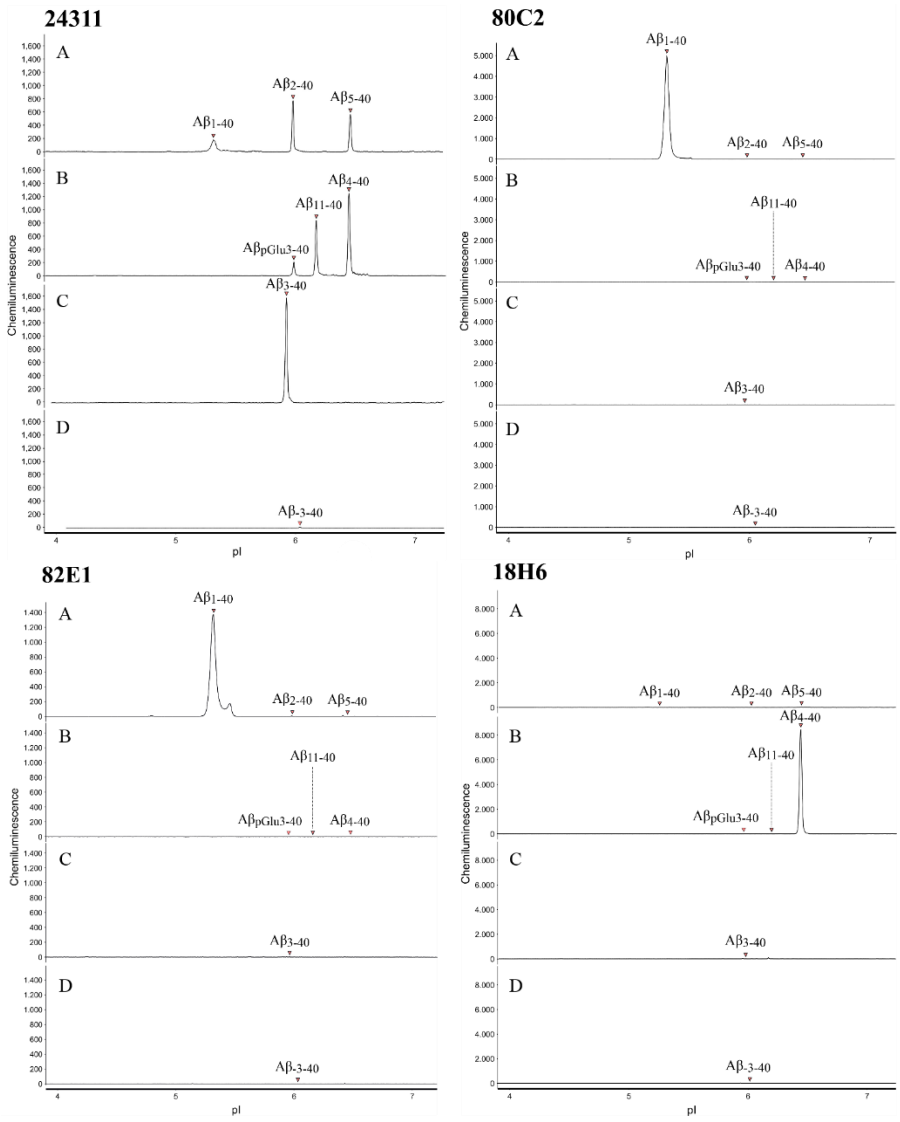

Fig. 3.1 Assessment of antibody selectivity by capillary isoelectric focusing immunoassay.
Synthetic Aβ peptides with different N-termini were separated by isoelectric focusing and probed with the indicated primary antibodies. For each indicated primary antibody, a mixture of $A\beta_{1–40}$, $A\beta_{2–40}$, and $A\beta_{5–40}$ (electropherogram A), a mixture of $A\beta_{pGlu3-40}$, $A\beta_{4–40}$ and $A\beta_{11–40}$ (B), $A\beta_{3–40}$ (C) and N-terminally elongated $A\beta_{-3–40}$ (APP669-711) (D) were assessed. The electropherograms were scaled for each primary antibody according to the maximum signal that was observed.

Data published in (Zampar et al. 2020)

The selectivity of the mAbs 80C2 and 18H6 was also tested against a set of synthetic Aβ peptides ending at position 42, as the different C-terminus ending might influence the conformation of the peptides, possibly resulting in altered immunoreactivity towards the N-terminal epitopes. As shown in Fig. 3.2, the two antibodies displayed qualitatively the same detection profile observed with $A\beta_{40}$ peptides.

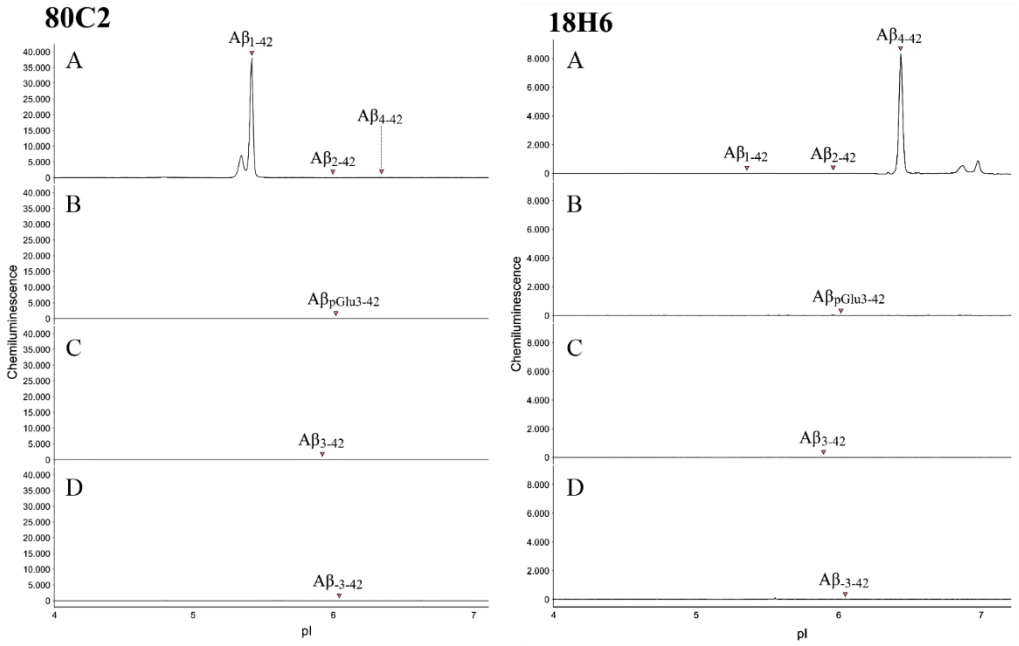

Fig. 3.2 Assessment of antibody selectivity by capillary isoelectric focusing immunoassay towards synthetic Aβ42 peptides with different N-termini.
The peptides were separated by isoelectric focusing and probed with the indicated primary antibodies. For each indicated primary antibody, a mixture of $A\beta_{1–42}$, $A\beta_{2–42}$, and $A\beta_{4–42}$ (electropherogram A), $A\beta_{pGlu3-42}$ (B), $A\beta_{3–42}$ (C) and N-terminally elongated $A\beta_{-3–42}$ (APP669-713) (D) was assessed. The electropherograms were scaled for each primary antibody according to the maximum signal that was observed.

3.1.2 Comparative Aβ staining profiles in human sporadic AD, NDC, and DS cases

The heterogeneity of Aβ variants in human brain samples was assessed by means of immunohistochemistry. The pan-Aβ antibody 24311, the $A\beta_{42}$-targeting antibody D3E10 as well antibodies selectively binding to different N-termini were employed. In particular, antibodies directed towards $A\beta_{1-x}$ (mAbs 80C2 and 82E1), $A\beta_{2-x}$ (pAb 77 (Savastano et al. 2016)) and $A\beta_{4-x}$ (pAb 029-2 (Wirths et al. 2017), mAb 18H6 (Cabrera et

Data published in (Zampar et al. 2020)

al. 2018)) were analyzed. Semi-quantitative scorings were given for each tested antibody with regard to parenchymal plaques, parenchymal CAA, and meningeal CAA (Fig. 3.3).

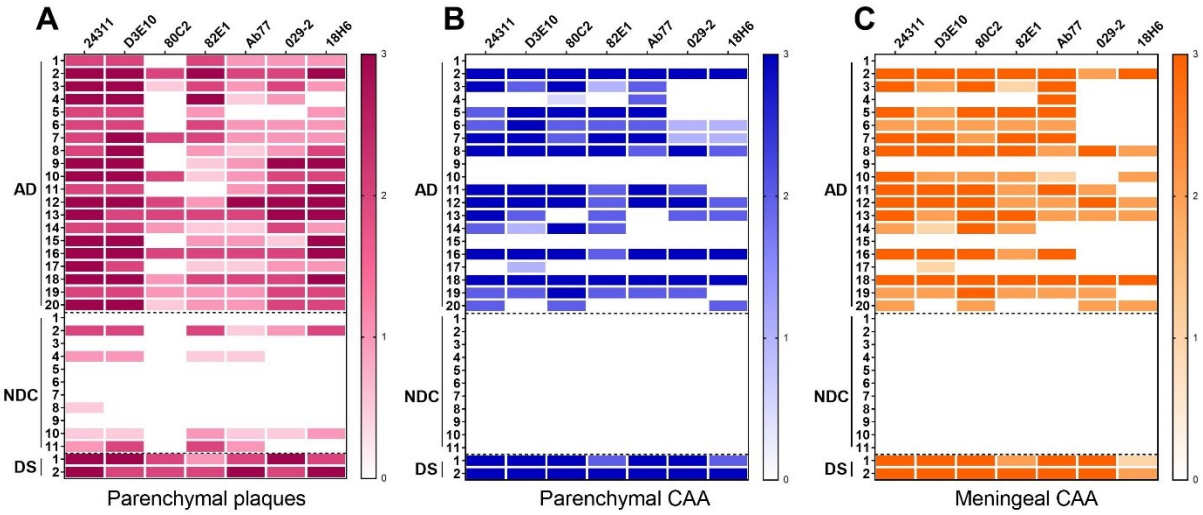

Fig. 3.3 Semi-quantitative analyses of Aβ immunostaining on human brain samples.
Heat maps illustrating the results of the immunostaining of parenchymal plaques (A), parenchymal (B) and meningeal CAA (C). AD, sporadic Alzheimer's disease; NDC, non-demented control; DS, Down syndrome; CAA, cerebral amyloid angiopathy.

Abundance of extracellular plaques and vascular deposits was observed with the pan-Aβ antibody 24311 (Fig. 3.4A, 3.5A) as well as with the $A\beta_{42}$-selective antibody D3E10 (Fig. 3.4B, 3.5B) in most of the AD cases (Fig. 3.3). On the other hand, staining of $A\beta_{1-x}$ peptides with the 80C2 (Fig. 3.4C) and 82E1 (Fig. 3.4D) antibodies showed weaker overall amyloid plaque profiles in the sporadic AD cases, while a strong cerebrovascular immunoreactivity was still detected (Fig. 3.5C,D). The staining profiles for parenchymal and meningeal vascular amyloid accumulation overlapped between the two antibodies directed against Asp-1, with 82E1 generally detecting a more widespread pattern of parenchymal plaques. Similarly, pAb77, directed against $A\beta_{2-x}$ starting with an alanine residue, detected only few plaques in most of the AD cases, still maintaining a strong immunoreactivity in parenchymal and meningeal CAA (Fig. 3.4E and 3.5E).

Data published in (Zampar et al. 2020)

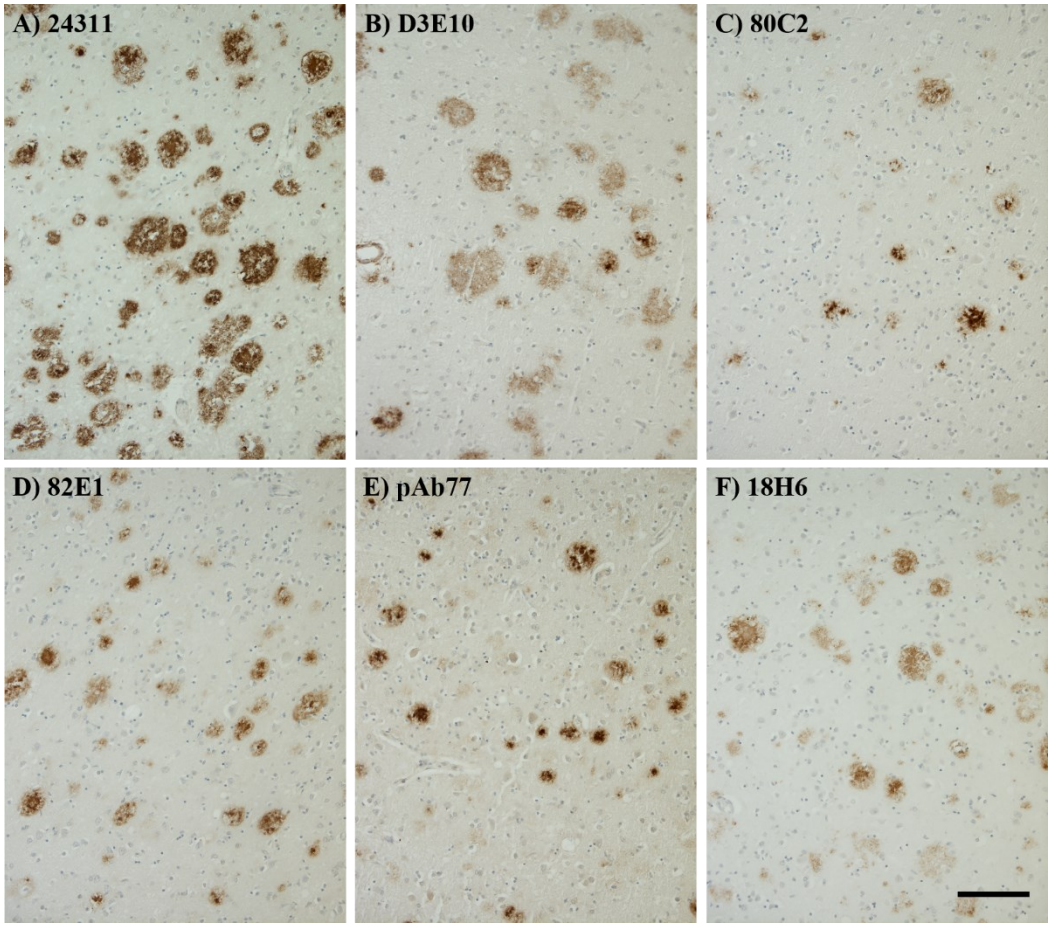

Fig. 3.4 Immunohistochemical staining of extracellular amyloid-β peptides in a sporadic Alzheimer's disease (AD) case.
Parallel sections of the frontal cortex of sporadic AD case 20 were stained with the pan-Aβ antibody 24311 (A), the $A\beta_{42}$-specific antibody D3E10 (B), the $A\beta_{1-x}$-specific antibodies 82E1 (C) and 80C2 (D), the $A\beta_{2-x}$-specific antibody Ab 77 (E), the $A\beta_{4-x}$-specific antibody 18H6 (F). Scale bar: A–H = 100 μm.

The two antibodies selectively detecting N-truncated Aβ peptides starting with phenylalanine at position 4, 029-2 and 18H6, displayed abundant amyloid plaque immunoreactivity in the sporadic AD brain samples (Fig. 3.4, 3.3). Vascular deposits containing $A\beta_{4-x}$ were detected to a lesser extent compared to the immunoreactivity displayed with the pan-Aβ, $A\beta_{1-x}$, and $A\beta_{2-x}$ specific antibodies (Fig. 3.3), appearing in half of the sporadic AD cases analyzed. In the two selected DS cases, a strong immunoreactivity was observed with no clear differences in staining profiles between extracellular plaques and vascular deposits among the tested antibodies (Fig 3.6, 3.3). The

Data published in (Zampar et al. 2020)

immunoreactivity was overall negative in the non-demented control cases, with only 4 out of 11 samples displaying a weak to moderate parenchymal plaque staining with 24311 (pan-Aβ) and D3E10 ($A\beta_{42}$) antibodies, confirming their neuropathological amyloid scores (Table 3.1). The NDC cases were largely negative with the antibodies recognizing N-terminal truncated Aβ variants and parenchymal and meningeal vascular deposits were absent with all the analyzed antibodies (Fig. 3.3).

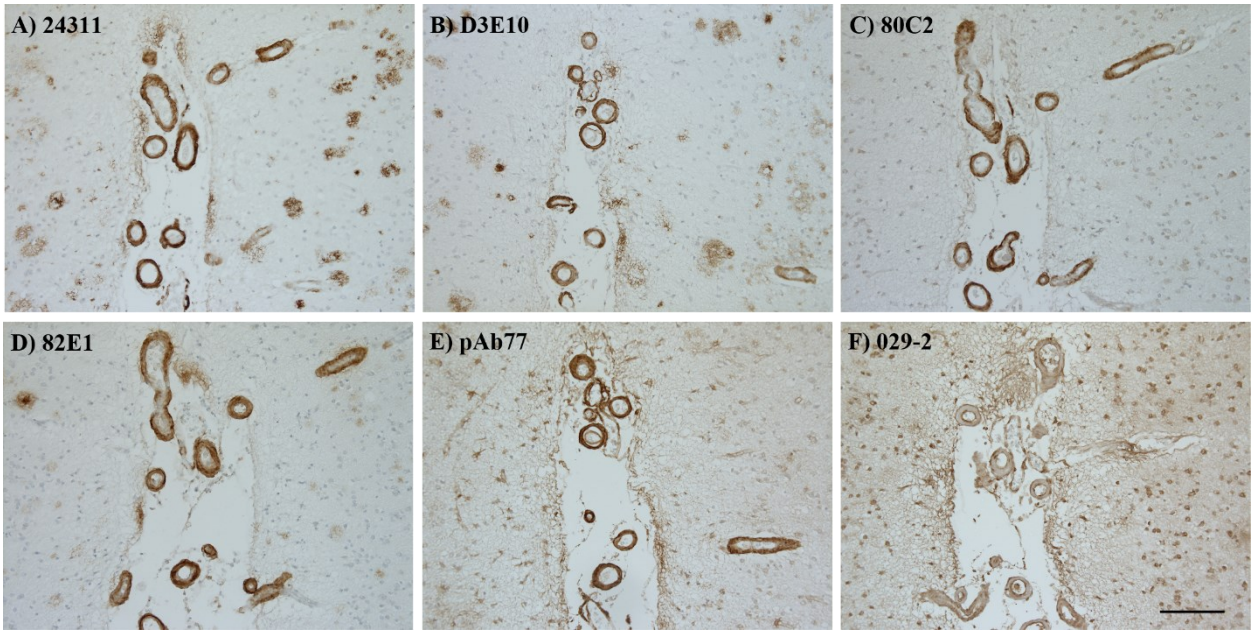

Fig. 3.5 Immunohistochemical staining of parenchymal vessels in a sporadic Alzheimer's disease (AD) case.

Parallel sections of the frontal cortex of the sporadic AD case 5 were stained with the pan-Aβ antibody 24311 (A), the $A\beta_{42}$-specific antibody D3E10 (B), the $A\beta_{1-x}$-specific antibodies 82E1 (C) and 80C2 (D), the $A\beta_{2-x}$-specific antibody pAb77 (E), the $A\beta_{4-x}$-specific antibody 18H6 (F). Scale bar: A–H = 100 μm.

Data published in (Zampar et al. 2020)

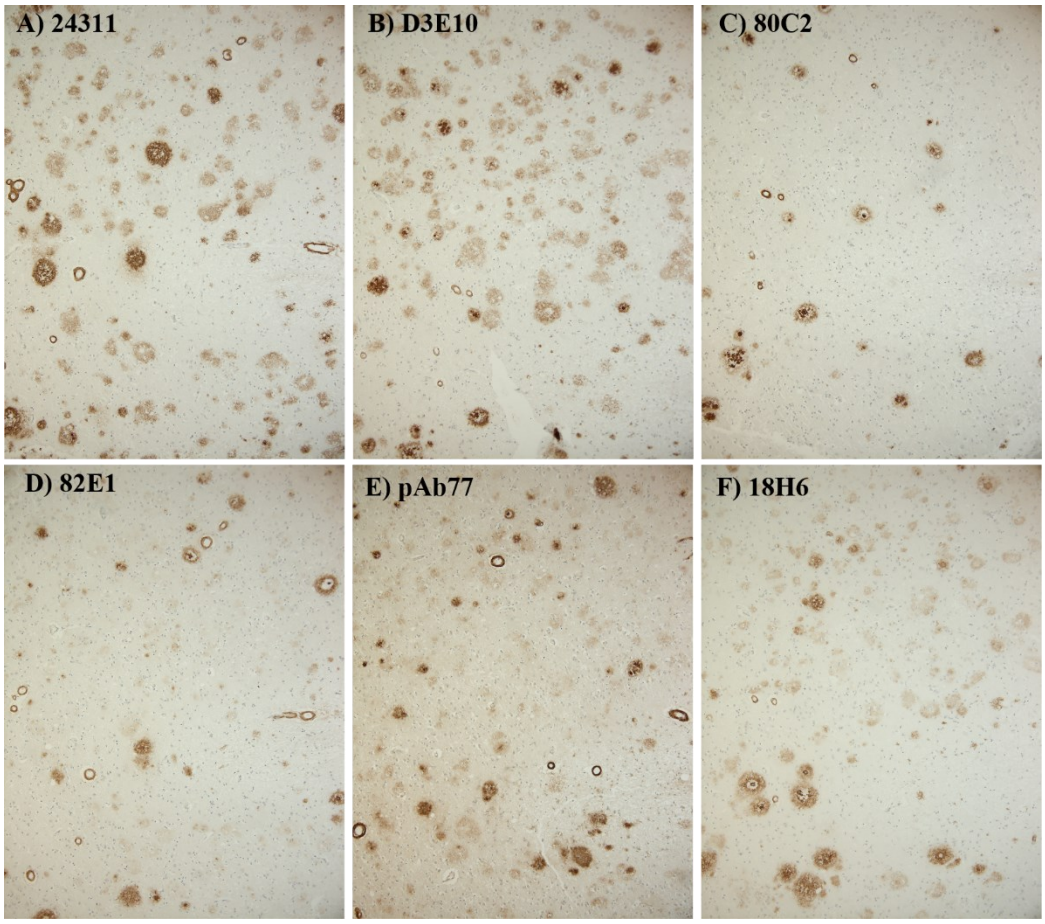

Fig. 3.6 Immunohistochemical staining of parenchymal vessels in a sporadic Down syndrome (DS) case. Parallel sections of the frontal cortex of DS case 1 were stained with the pan-Aβ antibody 24311 (A), the $A\beta_{42}$-specific antibody D3E10 (B), the $A\beta_{1-x}$-specific antibodies 82E1 (C) and 80C2 (D), the $A\beta_{2-x}$-specific antibody pAb77 (E), the $A\beta_{4-x}$-specific antibody 18H6 (F). Scale bar: A–H = 100 μm.

Data published in (Zampar et al. 2020)

3.2 PROJECT II: *In-vitro* and *in-vivo* activity of enzymes involved in the digestion and generation of Aβ4-x peptides: an outlook on neprilysin and ADAMTS4

3.2.1 Part I: *In-vitro* and *in-vivo* degradation of N-terminal truncated Aβ4-42 by neprilysin

The protease neprilysin (NEP) is known to be involved in the degradation of full-length Aβ peptides (Howell, Nalbantoglu, and Crine 1995, Iwata et al. 2000, Zou et al. 2006) but it is unclear if NEP could also hydrolyze N-truncated Aβ variants, such as Aβ4-x peptides. To understand whether Aβ4-x peptides are substrates for the NEP protease, at first an *in-vitro* digestion of synthetic Aβ peptides was performed with recombinant NEP and cleavage products were analyzed by means of mass spectrometry. *In-vivo*, the effects of the lack of endogenous NEP on Aβ4-42 peptides accumulation were evaluated in the Tg4-42^{het} mouse model of AD after crossing with homozygous NEP-knock-out mice (NEP$^{-/-}$) (Hornung et al. 2019).

3.2.1.1 Aβ4-40 and Aβ4-42 are degraded by recombinant neprilysin *in-vitro*

A pilot experiment investigating the hydrolysis of synthetic Aβ4-40 and Aβ4-42 peptides by recombinant NEP in a time-dependent fashion showed that 2h incubation at 37°C resulted in an efficient digestion of the peptides, with longer incubation times resulting in signal loss in the control reactions probably due to aggregation or surface adsorption (Hornung et al. 2019). This incubation time was thus chosen to analyze the peptides digestion pattern in detail. Full-length peptides Aβ1-40 and Aβ1-42 were included in the analysis for comparison. Additionally, control reactions lacking the recombinant enzyme and reactions containing NEP in combination with the NEP inhibitor Phosphoramidon (PA) were added to the analysis to confirm the specificity of NEP activity.

Data published in (Hornung, Zampar et al. 2019)

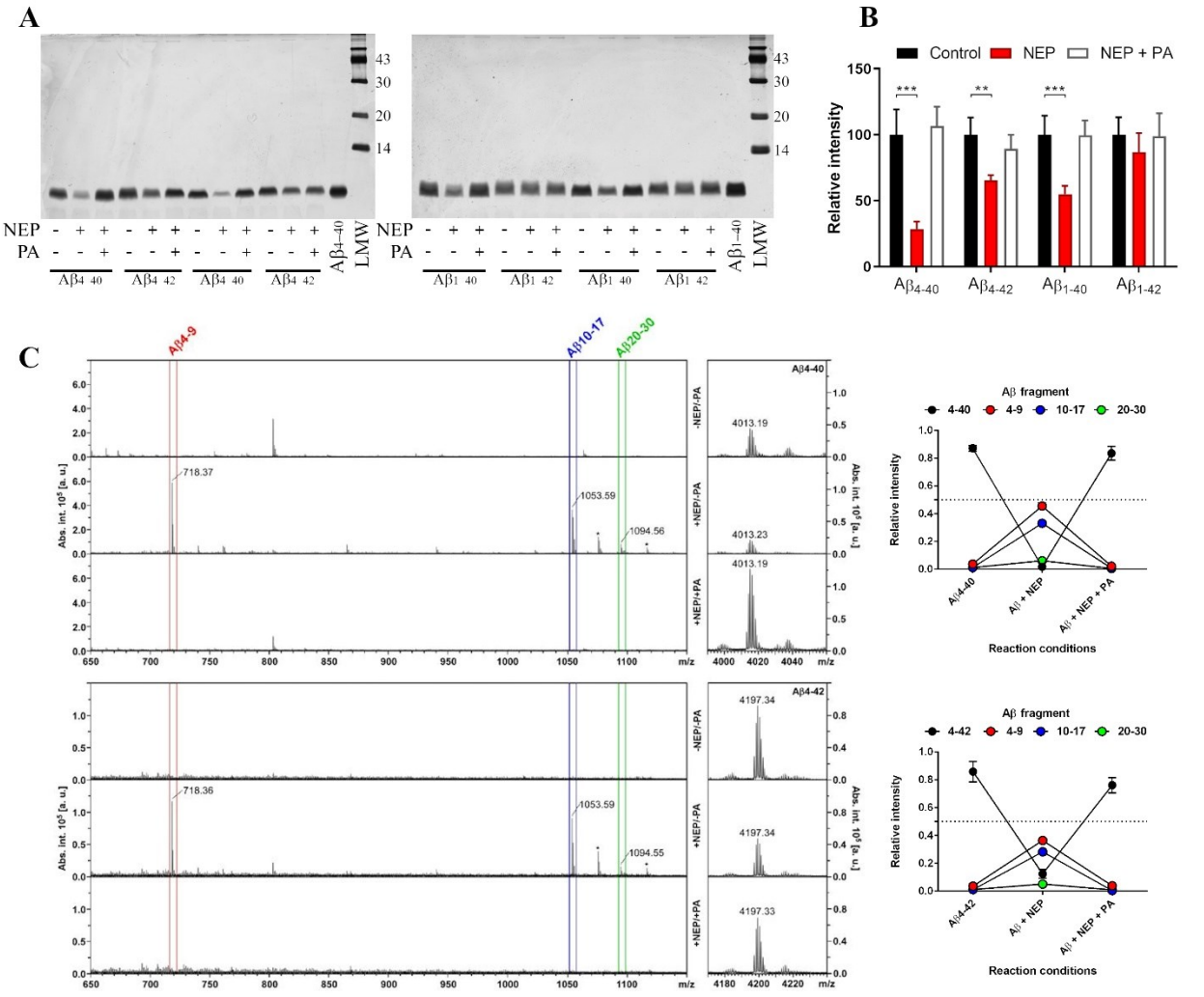

Fig. 3.7 *In-vitro* hydrolysis of synthetic Aβ peptides by NEP and mass spectrometric detection of Aβ$_{4-x}$ peptides and their NEP cleavage products.

(A) Silver-stained SDS polyacrylamide gels of synthetic Aβ peptides after 2h incubation at 37°C under control conditions or in presence or absence of NEP and/or PA. LMW, low molecular weight marker (GE Healthcare), Aβ$_{1-40}$ and Aβ$_{4-40}$, 75 ng prepared in SDS-sample buffer. (B) Densitometric quantification of silver-stained gels shown in A. All data are given as means ± SD. Two-way ANOVA followed by Bonferroni's multiple comparison test: **p<0.01, ***p<0.001. (C) Left: mass spectrometric of Aβ$_{4-40}$ (upper panel group; [M+H]$^+$calc = 4013.0491) or Aβ$_{4-42}$ (lower panel group; [M +H]$^+$calc = 4197.1702) incubated under control conditions or in presence or absence of NEP and/or PA. Only the major cleavage products Aβ$_{4-9}$ (red), Aβ$_{10-17}$ (blue), and Aβ$_{20-30}$ (green) are annotated. Asterisks indicate the sodium adducts of Aβ$_{10-17}$ and Aβ$_{20-30}$, respectively. Right: semi-quantitative comparison of mass spectra signals of intact peptides and cleavage products under the three reaction conditions (Mass spectrometry analysis was performed by Dr. Olaf Jahn).

Data published in (Hornung, Zampar et al. 2019)

Silver-stained SDS-polyacrylamide gels of the digested reactions showed a clear degradation of $A\beta_{4-40}$ and $A\beta_{4-42}$ by NEP, which was no longer visible in control reactions containing the inhibitor PA. Confirming previous findings (Shirotani et al. 2001), NEP also hydrolyzed the full-length $A\beta_{1-40}$ and $A\beta_{1-42}$ peptides (Fig. 3.7A). Densitometric quantification of the silver staining (4 replicates for each peptide) revealed a reduction of approximately 73% of $A\beta_{4-40}$, 31% of $A\beta_{4-42}$, 45% of $A\beta_{1-40}$ and 18% of $A\beta_{1-42}$ compared to the respective control reactions after incubation with recombinant NEP. Co-incubation with PA completely inhibited NEP activity (Fig. 3.7B). The degradation rate for the analyzed synthetic peptides was $A\beta_{4-40}$ > $A\beta_{1-40}$ > $A\beta_{4-42}$ > $A\beta_{1-42}$. Two-way ANOVA analysis followed by Bonferroni's multiple comparison test reported statistically significant differences between NEP treated and the respective control reactions for $A\beta_{4-40}$ ($p<0.001$), $A\beta_{4-42}$ ($p<0.01$) and $A\beta_{1-40}$ ($p<0.001$) (Fig. 3.7B). No shorter Aβ fragments were however visible on the silver-stained gels. To investigate the presence of degradation products that might have escaped gel electrophoretic detection, parallel reactions were subjected to MALDI mass spectrometry analyses. After NEP incubation, signals for the major enzymatic cleavage products $A\beta_{4-9}$, $A\beta_{10-17}$, and $A\beta_{20-30}$ were detected in the reactions containing $A\beta_{4-x}$ peptides, with no signals in the no-enzyme control reactions or in the presence of PA (Fig. 3.7C). A semi-quantitative comparison of the mass spectra showed a decreased signal for the intact $A\beta_{4-40}$ and $A\beta_{4-42}$ peptides with concomitant increase of the cleavage products signals when the peptides were incubated with NEP. The gel electrophoresis and mass spectrometry analyses indicated that $A\beta_{4-40}$ and $A\beta_{4-42}$ are substrates for NEP digestion *in-vitro* and identified $A\beta_{4-9}$, $A\beta_{10-17}$, and $A\beta_{20-30}$ as the major cleavage products. This is in agreement with a mass spectrometry analysis of NEP hydrolysis products recently performed on $A\beta_{1-40}$ (Mital et al. 2018).

Data published in (Hornung, Zampar et al. 2019)

3.2.1.2 Intraneuronal accumulation of Aβ$_{4-42}$ in Tg4-42^{het} and Tg4-42^{het}/NEP$^{-/-}$ mice

To investigate whether NEP is involved in the digestion of Aβ$_{4-x}$ peptides *in-vivo*, the Tg4-42^{het} mouse model of AD, expressing exclusively Aβ$_{4-42}$ peptides, was crossed with homozygous neprilysin ko mice (NEP$^{-/-}$) to achieve a lack of endogenous NEP. DAB immunohistochemical staining were performed on paraffin sagittal sections at 3 and 12 months of age to compare Aβ$_{4-42}$ accumulation in the CA1 region of the hippocampus between Tg4-42^{het} and Tg4-42^{het}/NEP$^{-/-}$ mice. The rabbit polyclonal pan-Aβ antibody 24311 was used, and a semi-quantitative analysis was performed using three sections per animal. In young animals, an intracellular accumulation of Aβ$_{4-42}$ was detectable in the Tg4-42^{het} line (Fig. 3.8A), while at 12 months almost no immunoreactivity was observed (Fig. 3.8B). This finding had been previously described for this model and is believed to be related to the massive neuron loss in the CA1 region of the hippocampus at this time point (Bouter et al. 2013). At 3 months of age, Tg4-42^{het}/NEP$^{-/-}$ mice displayed an enhanced Aβ immunoreactivity (Fig. 3.8C), which was significantly increased compared to age-matched Tg4-42^{het} when a two-way ANOVA followed by Bonferroni's multiple comparison test was performed ($p<0.001$) (Fig. 3.8E). The lack of endogenous NEP led approximately to a doubled Aβ accumulation in CA1 pyramidal neurons in young Tg4-42^{het}. No increase was observed in aged animals ($p>0.05$), which could be explained by the age-dependent significant reduction in immunoreactivity in general (Tg4-42^{het}: $p<0.01$, Tg4-42^{het}/ NEP$^{-/-}$: $p<0.001$) (Fig. 3.8E) observed in both lines (Fig. 3.8B,D).

Data published in (Hornung, Zampar et al. 2019)

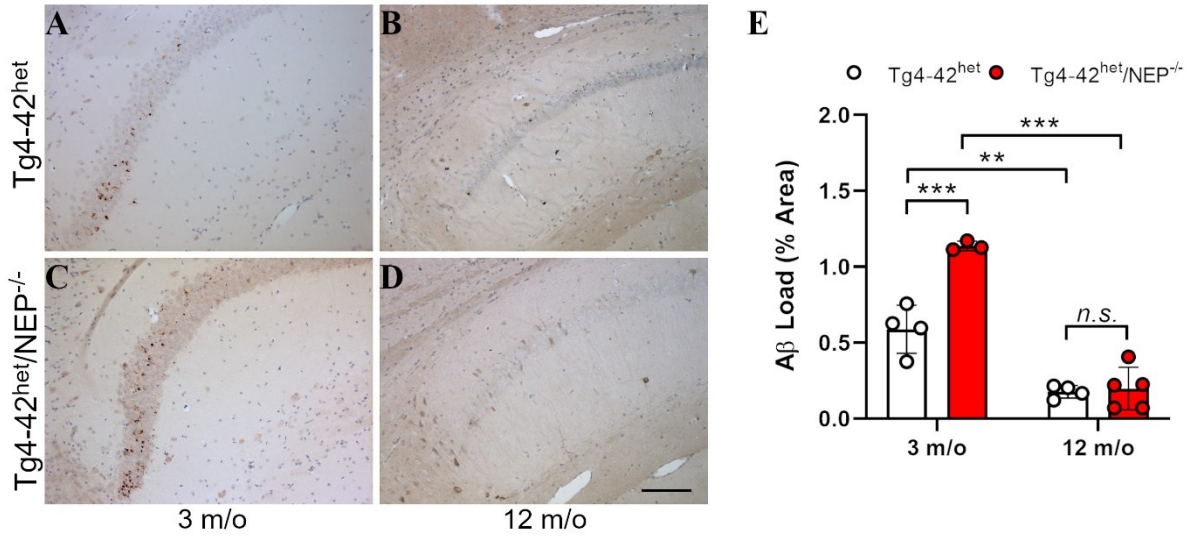

Fig. 3.8 Immunohistochemical staining, and Aβ$_{4-42}$ load analysis in Tg4-42^{het} and Tg4-42^{het}/NEP$^{-/-}$ mice. Intraneuronal Aβ$_{4-42}$ accumulation in hippocampal CA1 pyramidal neurons of young (A,C) and old (B,D) Tg4-42^{het} (A,B) and Tg4-42^{het}/NEP$^{-/-}$ (C,D) mice after DAB immunostaining with pan-Aβ 24311 antibody. (E) Quantification of Aβ load of 3 sections per animal (n=3-5). All data are given as means ± SD. Two-way ANOVA followed by Bonferroni's multiple comparison test: **p<0.01, ***p<0.001. Scale bar (A-D) 100 μm (Load analysis of 3-month-old groups performed by Karen Hornung)

Data published in (Hornung, Zampar et al. 2019)

3.2.2 Part II: *In-vivo* role of ADAMTS4 in the generation of Aβ$_{4-x}$ peptides

The metalloprotease ADAMTS4 is one of the enzymes involved in the generation of Aβ$_{4-x}$ peptides and was found to be expressed exclusively in oligodendrocytes in the adult murine brain (Walter et al. 2019). To understand the role of ADAMTS4 *in-vivo*, the 5xFAD mouse model of AD, showing the presence of peptides in mass spectrometry analysis and immunohistochemical staining (Reinert et al. 2016), was crossed with homozygous ADAMTS4 knock-out mice (ADAMTS4$^{-/-}$) to obtain a total lack of the endogenous metalloprotease in 5xFAD mice. 5xFAD/ADAMTS4$^{-/-}$ presented a significantly reduced amount of brain Aβ$_{4-x}$ peptides (Walter et al. 2019). In this study, we aimed to further characterize the effects of Aβ$_{4-x}$ peptides in the 5xFAD line through a more thorough behavioral and pathological assessment of 5xFAD/ADAMTS4$^{-/-}$ mice.

3.2.2.1 Behavioral characterization of 5xFAD/ADAMTS4$^{-/-}$ mice: the lack of ADAMTS4 rescues motor deficits in the 5xFAD mouse model of AD

A series of behavioral tasks were performed on 3- and 9- month-old mice to assess motor and cognitive performances. WT and ADAMTS4$^{-/-}$ littermates were included as control groups. In good agreement with previous findings (Wagner et al. 2019, Jawhar et al. 2012), no alteration in terms of motor abilities were observed in 3-month-old 5xFAD mice when tested in the accelerating rotarod, balance beam or inverted grid tasks (Fig. 3.9A-C). No differences in bodyweight were detected among the young groups (Fig. 3.9D). As expected, at 9 months of age 5xFAD displayed clear motor deficits in the balance beam and inverted grid tasks, with a significantly reduced latency to fall compared to WT littermates ($p<0.001$ and $p<0.05$, respectively) (Fig. 3.9F,G). Interestingly, removal of endogenous ADAMTS4 resulted in an amelioration of the observed motor deficits.

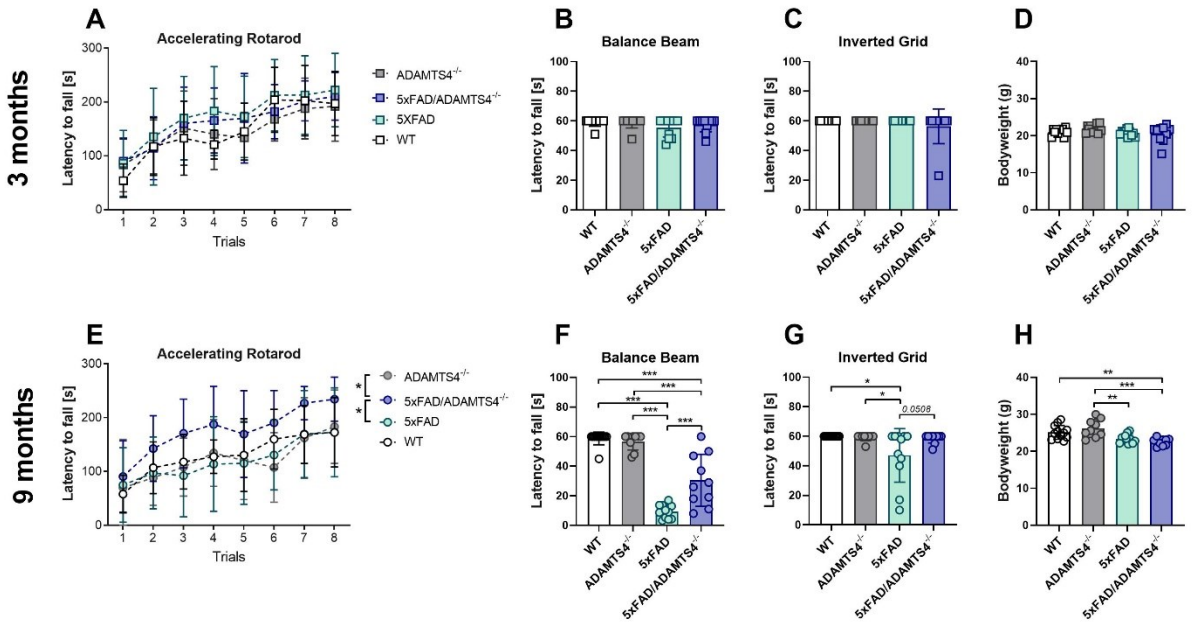

Fig. 3.9 Motor assessment of 3- and 9-month-old 5xFAD/ADAMTS4$^{-/-}$ mice, transgenic and WT controls. Female WT, ADAMTS4$^{-/-}$, 5xFAD and 5xFAD/ADAMTS4$^{-/-}$ mice (n=9-12) were tested at 3 (A-C) and 9 (E-G) months in the accelerating rotarod (A,E), balance beam (B,F) and inverted grid (C,G) tasks. No differences were detected in motor abilities at the 3 months' time point, and no differences in bodyweight were recorded (D). At 9 months, a rescue of motor deficits in 5xFAD was observed when endogenous ADAMTS4 was lacking. In the older group, significant differences in bodyweight were observed in 5xFAD and 5xFAD/ADAMTS4$^{-/-}$ mice compared to WT and ADAMTS4$^{-/-}$ littermates (H). All data are given as means ± SD. (A,E) Two-way ANOVA RM followed by Bonferroni's multiple comparison test, (B-D, F-H) One-way ANOVA followed by Bonferroni's multiple comparison test: *p<0.05, **p<0.01,***p<0.001.

In the balance beam task, 5xFAD/ADAMTS4$^{-/-}$ mice performed significantly better than 5xFAD (p<0.001), although still presenting a significant reduced latency to fall compared to WT and ADAMTS4$^{-/-}$ mice (p<0.001) (Fig 3.9F). In the inverted grid test, contrary to 5xFAD littermates, the 5xFAD/ADAMTS4$^{-/-}$ group performed comparability to WT and ADAMTS4$^{-/-}$, and with a trend towards significant increase when the latency to fall was compared to 5xFAD mice (p=0.0508) (Fig. 3.9G). Additionally, the performance of 5xFAD/ADAMTS4$^{-/-}$ mice in the accelerating rotarod task at 9 months was significantly improved compared to 5xFAD littermates (p<0.05) (Fig 3.9E), supporting a general amelioration of motor abilities in 5xFAD mice lacking the metalloprotease ADAMTS4. In the aged groups, significantly reduced bodyweights were observed in 5xFAD and

5xFAD/ADAMTS4$^{-/-}$ mice compared to WT and ADAMTS4$^{-/-}$ littermates (Fig. 3.9H), but with no differences between the two AD lines. No motor deficits were observed in ADAMTS4$^{-/-}$ within the used tests.

Locomotor activity was furthermore analyzed in the open field (OF) test, which can additionally be used to assess anxiety-like behavior in rodents. In young animals, a significantly reduced average speed and average travelled distance was observed in ADAMTS4$^{-/-}$ ($p<0.05$) and 5xFAD/ADAMTS4$^{-/-}$ ($p<0.01$) compared to WT mice (Fig. 3.10B,C). This might look in contrast to the afore-described motor performances in the 3-month-old group. A deeper analysis of exploratory behavior in the OF showed that 5xFAD/ADAMTS4$^{-/-}$ mice displayed an increased immobility time compared to WT littermates ($p<0.01$) (Fig. 3.10D), which could indicate that the observed alterations in speed and distance are caused by a decreased exploration of the arena rather than by actual motor deficits. In aged mice, no alteration of average speed and distance were observed in the ADAMTS4$^{-/-}$ group (Fig. 3.10F,G), supporting a lack of motor deficits in this line at both time points. In contrast, 5xFAD mice at 9 months displayed a reduced average speed and average distance compared to WT and ADAMTS4$^{-/-}$ ($p<0.05$), corroborating the previously described motor deficits in this line. As observed at the 3 months' time point, aged 5xFAD/ADAMTS4$^{-/-}$ mice showed a reduced average speed and distance compared to WT and ADAMTS4$^{-/-}$ ($p<0.001$), which was accompanied by a significant increase in immobility time when compared to the other three mouse lines (Fig. 3.10H). Since the motor assessment at 9 months showed an improvement of motor performances in 5xFAD lacking ADAMTS4 (Fig 3.10), the reduced locomotor parameters in the OF could be thus partially explained by the lowered exploratory activity of the line observed in this behavioral task. The time spent in the center of the OF arena was used to analyze anxiety-like behavior in the lines. In young mice, no differences were found among the groups (Fig. 3.10A), while at 9 months of age, 5xFAD mice spent more time in

the center of the arena compared to WT and ADAMTS4$^{-/-}$ mice ($p<0.001$), indicating a reduced anxiety-like behavior (Fig3.10E). This phenotype was not observed in aged 5xFAD/ADAMTS4$^{-/-}$ mice, which presented a significantly reduced time spent in center compared to 5xFAD ($p<0.05$) (Fig3.10E).

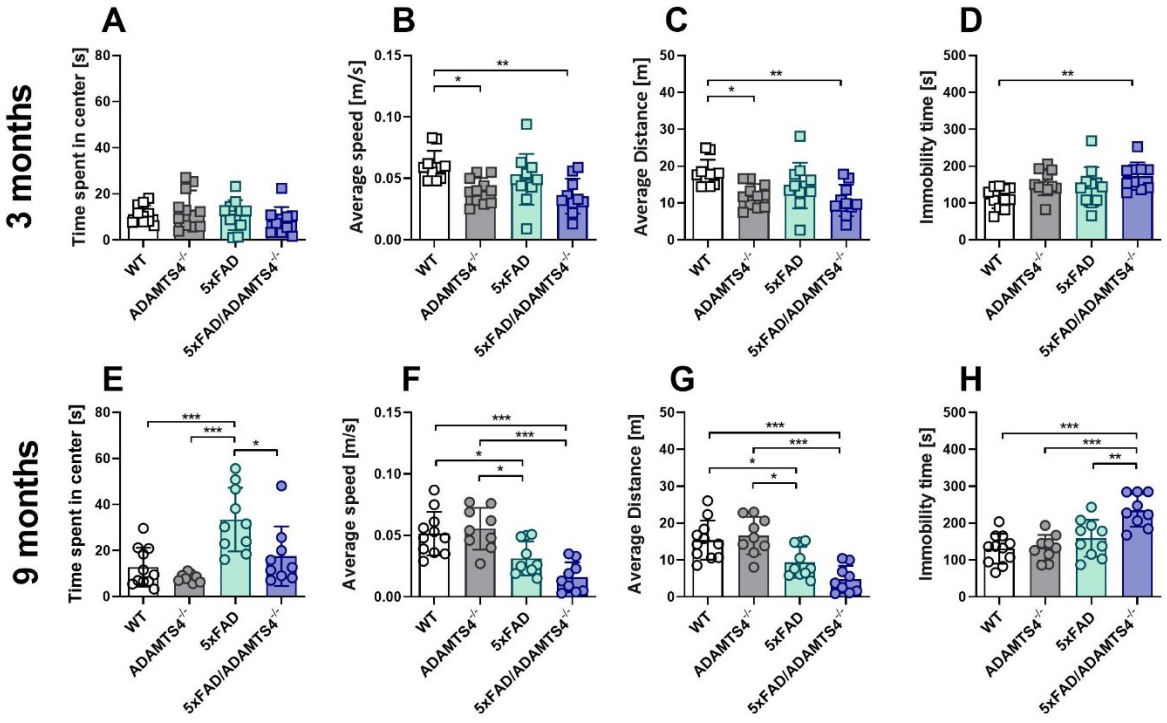

Fig. 3.10 Open field task on 5xFAD/ADAMTS4$^{-/-}$ mice, transgenic and WT controls.
Female WT, ADAMTS4$^{-/-}$, 5xFAD, and 5xFAD/ADAMTS4$^{-/-}$ mice (n=9-12) were tested at 3 (A-D) and 9 (E-H) months. Reduced average speed and distance were observed in young ADAMTS4$^{-/-}$ and 5xFAD/ ADAMTS4$^{-/-}$ mice (B,C), which was accompanied by an increased immobility time in the latter (D). Significantly decreased speed and distance were observed in aged 5xFAD and 5xFAD/ADAMTS4$^{-/-}$ mice (F,G), the latter still displaying a reduced mobility as indicated by an increased immobility time (H). No differences in time spent in the center became obvious in young mice (A), while a reduced anxiety-like behavior was observed in 5xFAD at 9 months (D). All data are given as means ± SD. One-way ANOVA followed by Bonferroni's multiple comparison test: *p<0.05, **p<0.01, ***p<0.001.

Anxiety-like behavior was also assessed with the elevated plus maze task (EPM). In young mice, no alteration in behavior was detected among the groups (Fig. 3.11A), confirming the observations seen in the OF test. In aged mice, ADAMTS4$^{-/-}$ performed comparably to WT, while 5xFAD mice displayed a reduced anxiety-like behavior

compared to WT and ADAMTS4$^{-/-}$ littermates ($p<0.001$). This is shown by an increased time spent in open arms (Fig 3.11E), which is in good agreement with previous findings (Jawhar et al. 2012). In contrast to the OF task, a reduced anxiety-like behavior in 5xFAD/ADAMTS4$^{-/-}$ mice was observed in the EPM. 5xFAD mice lacking ADAMTS4 explored the open arms comparably to 5xFAD mice, with a significantly increased time compared to WT and ADAMTS4$^{-/-}$ ($p<0.001$). This observation might suggest that the reduced time spent in the center of the OF is due to a general decreased exploration of the arena, as indicated by the increased immobility time, and that the lack of endogenous ADAMTS4 does not influence anxiety-like behavior in 5xFAD at this time point.

Working memory was assessed through the Cross Maze task. While no deficits were observed at 3 months of age (Fig. 3.11C), 9-month-old 5xFAD showed significantly reduced correct spontaneous alternation compared to WT controls ($p<0.001$) (Fig. 3.11G). The working memory impairment was observed also in aged 5xFAD/ADAMTS4$^{-/-}$ mice, with no difference compared to the 5xFAD parental line.

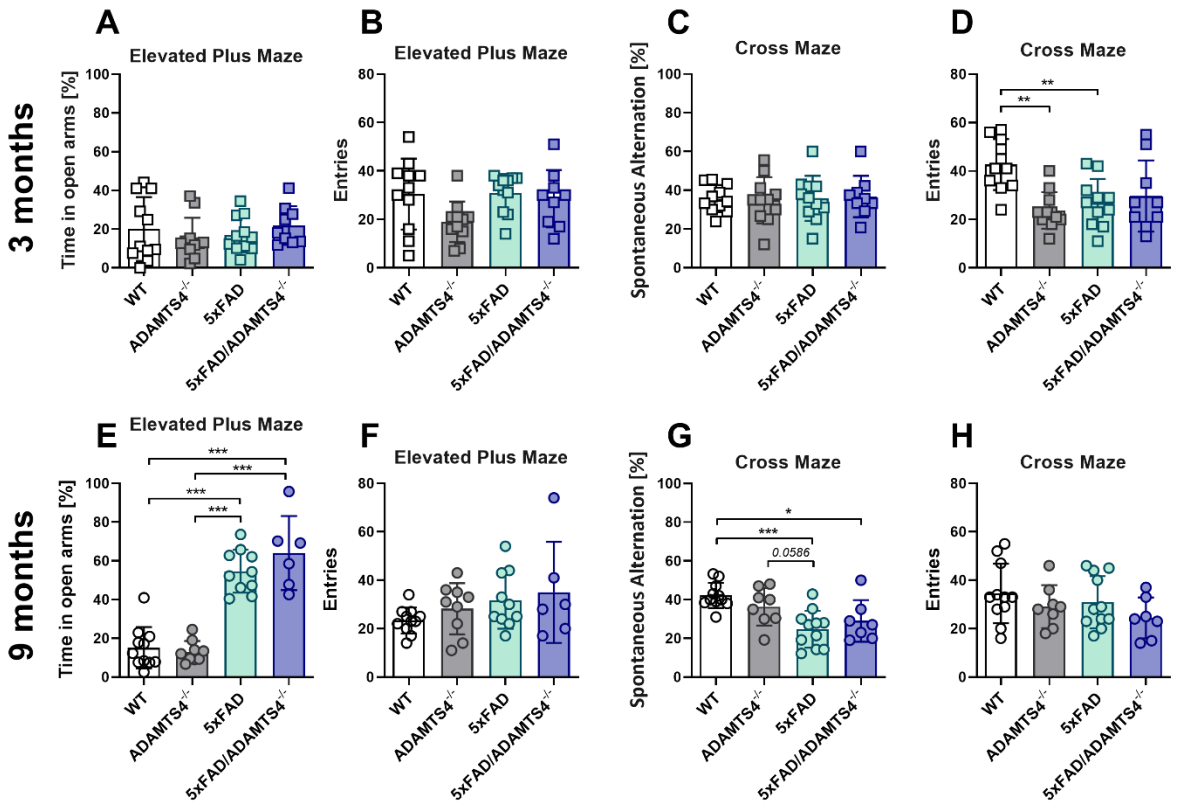

Fig. 3.11 Elevated plus maze and cross maze tasks on 5xFAD/ADAMTS4$^{-/-}$ mice, transgenic and WT controls.
Female WT, ADAMTS4$^{-/-}$, 5xFAD, and 5xFAD/ADAMTS4$^{-/-}$ mice (n=7-12) were tested at 3 (A-D) and 9 (E-H) months in the Elevated Plus Maze (A,B,E,F) and Cross Maze (C,D,G,H) tasks. No differences in anxiety-like behavior (A) or working memory (C) were found at 3 months. 5xFAD and 5xFAD/ADAMTS4$^{-/-}$ mice at 9 months displayed decreased anxiety-like behavior (E) and working memory deficits (G). All data are given as means ± SD. One-way ANOVA followed by Bonferroni's multiple comparison test: *p<0.05, **p<0.01, ***p<0.001.

3.2.2.2 Reduced Aβ$_{4-x}$ pathology in the spinal cord of 5xFAD mice lacking endogenous ADAMTS4

Since the major behavioral effects of the lack of ADAMTS4 in 5xFAD mice were observed on a motor level in aged mice, amyloid pathology was analyzed in spinal cord paraffine tissues of 9-month-old 5xFAD and 5xFAD/ADAMTS4$^{-/-}$ by means of immune-histochemistry. DAB staining was performed using the mouse mAb 80C2, directed against Aβ$_{1-x}$ peptides, and two N-truncated Aβ$_{4-x}$ specific antibodies: mouse mAb 18H6 and guinea-pig pAb 029-2. Abundant amyloid pathology was present in 5xFAD spinal

cords sections when stained with the abovementioned antibodies (Fig. 3.12A,D,G). In contrast, 5xFAD/ADAMTS4$^{-/-}$ mice presented reduced immunoreactivity for $A\beta_{4\text{-}x}$ peptides (Fig. 3.12B,E). Amyloid load quantifications revealed a significant reduction of $A\beta_{4\text{-}x}$ pathology in the spinal cords grey matter of 5xFAD/ADAMTS4$^{-/-}$ mice compared to 5xFAD ($p<0.01$) (Fig. 3.12C,F). No difference in Aβ load was found about full-length ($A\beta_{1\text{-}x}$) peptides between the two lines (Fig. 3.12I).

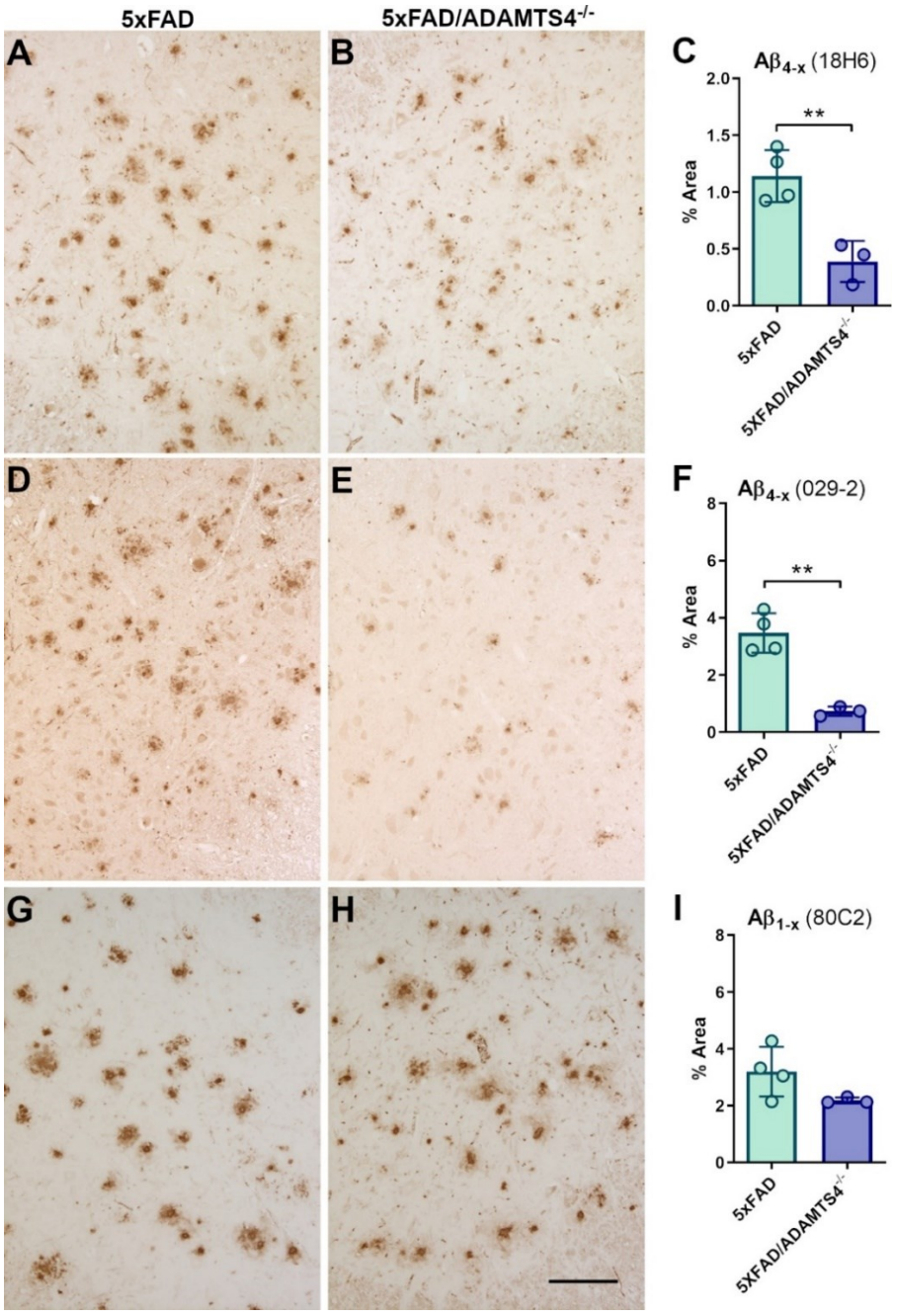

Fig. 3.12 Spinal cord immunohistochemical staining and load analysis of Aβ$_{4-x}$ and Aβ$_{1-x}$ in 9-month-old 5xFAD/ADAMTS4$^{-/-}$ and 5xFAD mice.

Cervical spinal cord paraffin sections from 9-month-old female 5xFAD (A,D,G) and 5xFAD/ADAMTS4$^{-/-}$ (B,E,H) mice (n=3-4) were stained with 18H6 (A,B), 029-2 (D,E) and 80C2 (G,H) antibodies. Load analysis revealed a reduced Aβ$_{4-x}$ pathology in 5xFAD lacking ADAMTS4 (C,F) while no significant differences were detected in Aβ$_{1-x}$ immunoreactivity (I). All data are given as means ± SD. Unpaired t-test: **p<0.01. Scale bar: 100 μm.

$A\beta_{42}$-positive thread-like structures were observed by Chu and co-workers in spinal cord grey and white matter of 5xFAD mice and are potentially correlated with the development of axonopathy in the spinal cord (Chu et al. 2017). During the immunohistochemical staining with $A\beta_{1\text{-}x}$ and $A\beta_{4\text{-}x}$ specific antibodies, we observed and further analyzed these structures (Fig. 3.13). In the spinal cord grey matter of aged 5xFAD, both $A\beta_{4\text{-}x}$- (Fig. 3.13A,B) and $A\beta_{1\text{-}x}$-positive (Fig 3.13C) threads could be visualized. While the antibodies directed towards $A\beta_{4\text{-}x}$ peptides gave strong staining of both the plaques core and threads structures, $A\beta_{1\text{-}x}$ immunoreactivity revealed fewer and weaker thread-like structures while maintaining strong plaque staining. In sagittal sections of the spinal cord, clear $A\beta_{4\text{-}x}$-positive threads were present in the white matter (Fig. 3.13G,H), while no $A\beta_{1\text{-}x}$-positive structure could be detected (Fig. 3.13I). In 5xFAD lacking endogenous ADAMTS4, extremely few $A\beta_{4\text{-}x}$-positive threads were seen in the grey matter of the spinal cord (Fig. 3.13D,E). On the other hand, thread-like structures positive for the full-length Aβ peptide were still present and appeared comparable to 5xFAD mice (Fig. 3.13F). In the white matter, no threads could be observed in 5xFAD with an ADAMTS4$^{-/-}$ background (Fig. 3.13J-L).

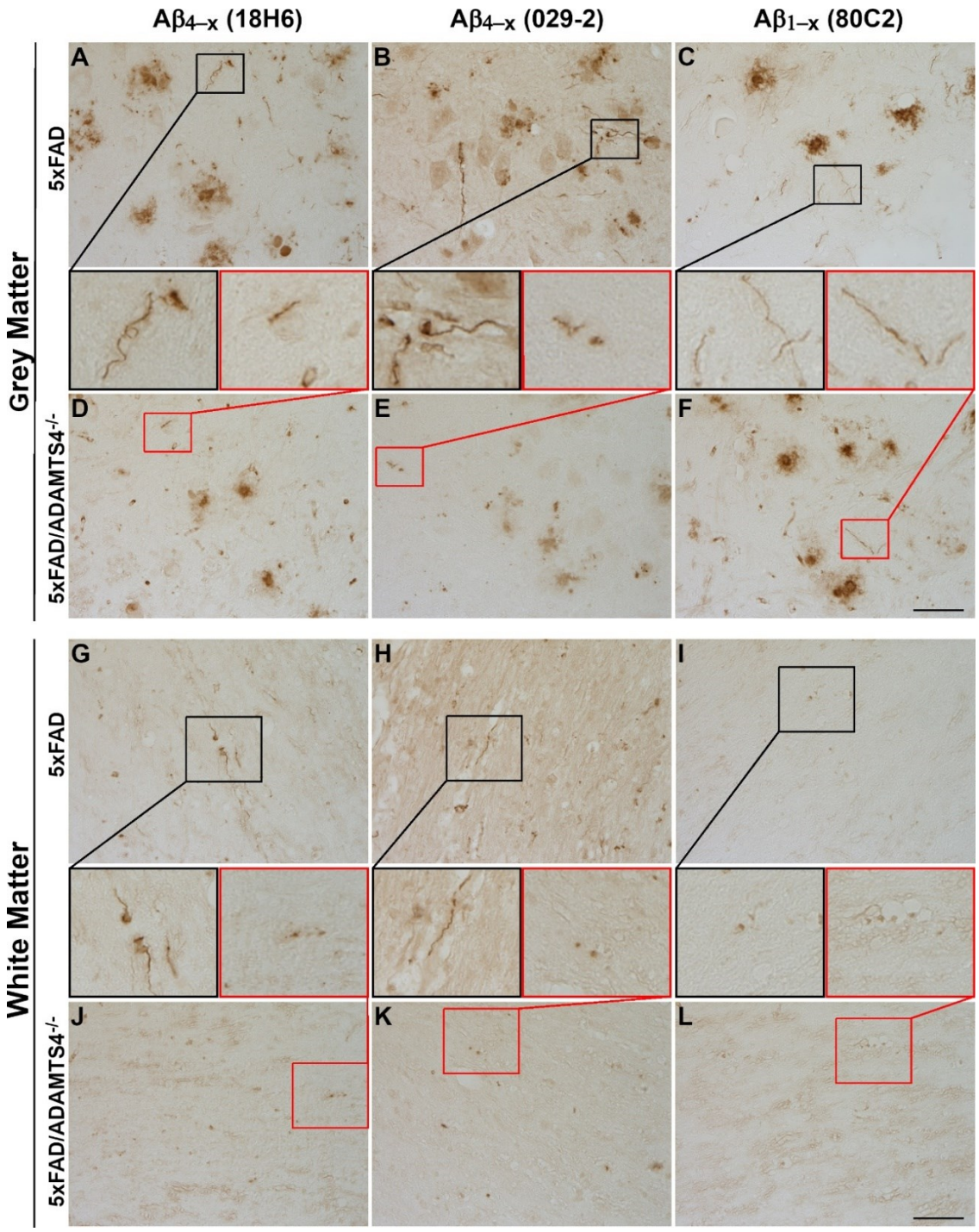

Fig. 3.13 Thread-like structure in grey and white matter of cervical spinal cord of 9-month-old 5xFAD/ADAMTS4$^{-/-}$ and 5xFAD mice.

Cervical spinal cord paraffin sections from 9-month-old female 5xFAD (A-C, G-I) and 5xFAD/ADAMTS4$^{-/-}$ (D-F, J-L) were stained with 18H6 (A,D,G,J), 029-2 (B,E,H,K), and 80C2 (C,F,I,L) antibodies. Aβ$_{4\text{-}x}$-positive threads were observed in grey matter and white matter of 5xFAD but little to none in 5xFAD/ADAMTS4$^{-/-}$ mice. Aβ$_{1\text{-}x}$-positive threads were individuated in the grey matter of both 5xFAD and 5xFAD/ADAMTS4$^{-/-}$ mice while no threads positive for the full-length Aβ peptides could be observed in the white matter of neither genotypes. Scale bar: 33 μm.

3.2.2.3 Unaltered mRNA expression of oligodendrocyte and myelin markers

The metalloprotease ADAMTS4 is exclusively expressed in oligodendrocytes in the adult murine brain (Walter et al. 2019), and we observed that the lack of this metalloprotease ameliorated motor deficits in the 5xFAD mouse model of AD. We therefore questioned whether an altered mRNA expression of oligodendrocyte and myelin markers was present in the spinal cord of 5xFAD mice and if the lack of ADAMTS4 might have an impact on this expression. Quantitative Real-Time PCR was performed on spinal cord mRNA extracted from 9-month-old mice. WT and ADAMTS4$^{-/-}$ animals were included as controls. No significant alteration in mRNA expression of the oligodendrocyte marker CNP, nor of the myelin markers Plp1 and MBP, was observed in 5xFAD mice compared to WT littermates (Fig. 3.14). Similarly, the lack of ADAMTS4$^{-/-}$ did not have any effect in 5xFAD mice, as no significant differences were found between 5xFAD and 5xFAD/ADAMTS4$^{-/-}$ animals.

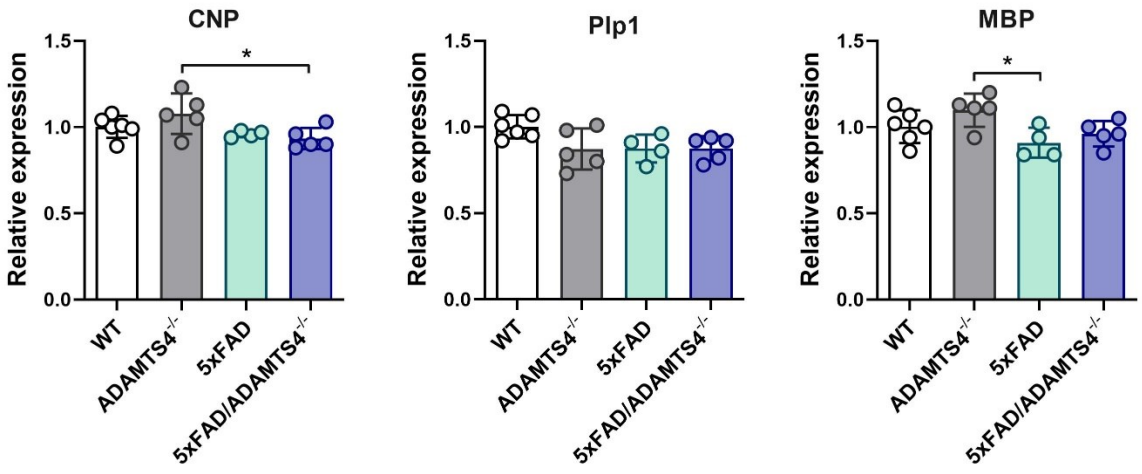

Fig. 3.14 Spinal cord RNA expression of oligodendrocyte and myelin markers in 5xFAD/ADAMTS4-/- mice, transgenic and WT controls.
qRT-PCR of spinal cord mRNA extracts from 9-month-old female WT, ADAMTS4$^{-/-}$, 5xFAD, and 5xFAD/ADAMTS4$^{-/-}$ mice (n=4-6) showed no alteration of oligodendrocyte (CNP) and myelin (Plp1, MBP) markers expression between 5xFAD and 5xFAD/ADAMTS4$^{-/-}$ mice. All data are given as means ± SD. One-way ANOVA followed by Bonferroni's multiple comparison test: *p<0.05.

3.3 PROJECT III: *In-vivo* relationship of Amyloid-β plaques and Aβ$_{4-x}$ peptides

A recent study focused on the role of oligomers and extracellular plaques in AD patients and raised the hypothesis of a linkage between the two as a key pathophysiological event underlying dementia of the Alzheimer type (Esparza et al. 2013), finding that the amount of plaque load did not differ between cognitively normal individuals and AD patients and the AD group presented with higher oligomer levels. To understand the relationship between extracellular plaques and Aβ$_{4-42}$ peptides, we crossed the classical AD model 5xFAD, harboring Aβ plaques, with the Tg4-42^{hom} line expressing exclusively Aβ$_{4-42}$ peptides. The resulting FAD/Tg4-42^{hom} line was assessed under a behavioral and pathological point of view.

3.3.1 Transgene expression and bodyweight of FAD/Tg4-42^{hom} mice

To exclude an altered transgene expression level after the crossing of the two parental lines, mRNA levels of human APP gene and Aβ$_{4-42}$ transgene were assessed at 6 months of age in the hippocampus of the filial line compared to the 5xFAD and the Tg4-42^{hom} parental lines, respectively (Fig. 3.15A,B). The analyses revealed no significant differences in expression of both transgenes. Additionally, bodyweights were measured and compared among the different genotypes at the two time-points (Fig. 3.15C). At 3 months, the bigenic line FAD/Tg4-42^{hom} presented with a significantly reduced bodyweight compared to WT ($p<0.05$) and Tg4-42^{hom} ($p<0.01$) lines, while the two parental lines weighed comparably to the WT group. At 6 months of age, all three transgenic lines displayed comparable bodyweights being all significantly reduced when compared to WT littermates.

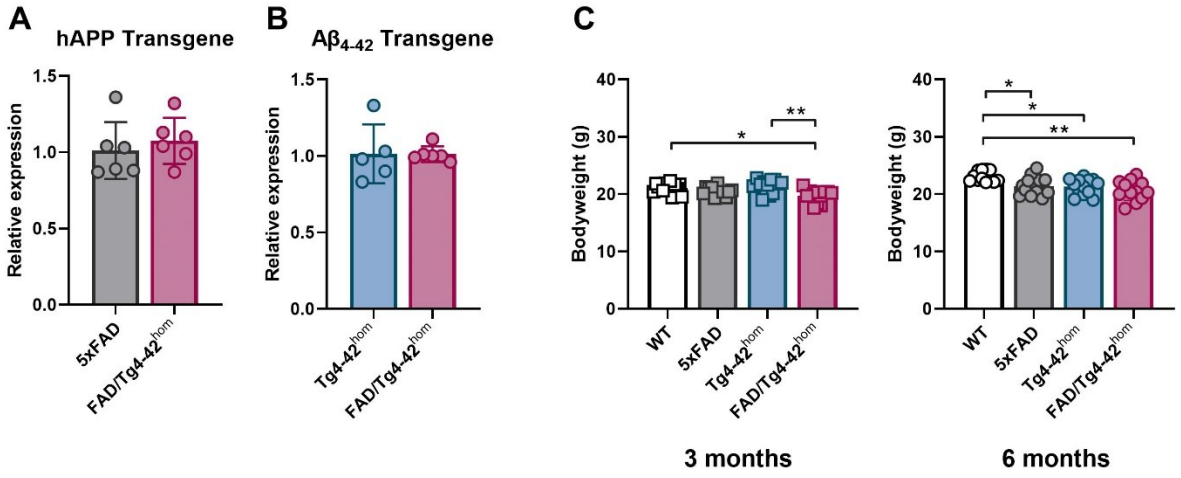

Fig. 3.15 Transgene expression and bodyweight of FAD/Tg4-42^{hom} line.
Hippocampal mRNA from 6-month-old female Tg4-42^{hom}, 5xFAD and FAD/ Tg4-42^{hom} (n=5-6) were used to measure the expression of human APP (hAPP) (A) and Aβ$_{4-42}$ (B) transgenes. No differences were found between the bigenic FAD/Tg4-42^{hom} and the parental lines. (C) Bodyweight comparison (n=12-14) at 3 months showed a significantly decrease in FAD/ Tg4-42^{hom} compared to WT and Tg4-42^{hom} littermates. At 6 months of age, the three transgenic lines showed comparable bodyweights, and all significantly reduced compared to WT animals. All data are given as means ± SD. (A,B) Unpaired t-test. (C) One-way ANOVA followed by Bonferroni's multiple comparison test: *p<0.05, **p<0.01, ***p<0.001.

3.3.2 Part I: Assessment of motor behavior and spinal cord analysis in FAD/Tg4-42^{hom} mice

3.3.2.1 Aggravation of motor phenotype in FAD/Tg4-42^{hom} mice

The accelerating rotarod, the inverted grid and the balance beam tasks were performed to assess the motor phenotype at 3 and 6 months. As shown in PROJECT II- part II, no motor deficits were observed in 3-month-old 5xFAD mice (Fig. 3.16A-C). Contrary, the Tg4-42^{hom} line displayed a significantly reduced latency to fall in the rotarod task compared to WT ($p<0.01$) and 5xFAD ($p<0.001$) already at 3 months of age (Fig. 3.16A), but no altered latencies to fall were observed in the inverted grid and balance beam tests (Fig. 3.16B,C). A comparable behavioral pattern was observed in a previous study (Wagner et al. 2019). In the accelerating rotarod tasks, the FAD/Tg4-42^{hom} line presented with a latency to fall comparable to Tg4-42^{hom} littermates at this time point (Fig. 3.16A), being also significantly decreased compared to the 5xFAD parental line ($p<0.01$).

Interestingly, an aggravation of the motor phenotype was observed in young FAD/Tg4-42^{hom} mice in the inverted grid task (Fig. 3.16B), as shown by a significantly reduced latency to fall compared to WT and the two parental lines ($p<0.05$). On the other hand, no alterations were observed in the balance beam task at this time point (Fig. 3.16C). At 6 months of age, 5xFAD mice still presented with an unaltered motor phenotype (Fig. 3.16D-F) compared to WT littermates. As already published (Stazi and Wirths 2021), 6-month-old Tg4-42^{hom} animals displayed motor deficits in the accelerating rotarod task ($p<0.001$) (Fig. 3.16D) while no changes were observed in the inverted grid task (Fig. 3.16E). Motor deficits in the balance beam task have also been reported in 6-month-old Tg4-42^{hom} mice. In our cohort a reduced latency in the balance beam was observed, which, however, did not reach statistical significance (Fig. 3.16F). At 6 months of age, the motor phenotype was clearly aggravated in 5xFAD mice co-expressing the Aβ_{4-42} transgene. The latencies to fall in both the inverted grid and balance beam tasks were significantly decreased in the FAD/Tg4-42^{hom} line when compared to WT littermates and both the parental lines ($p<0.001$) (Fig. 3.16E,F). Motor deficits were also observed in the accelerating rotarod task compared to WT and 5xFAD groups ($p<0.001$). In this test, the filial line displayed a comparable profile to the Tg4-42^{hom} group during the first day of testing (trials 1-4), while a further reduction in latency was observed during the second day (trials 5-8), which, however, did not reach statistical significance (Fig. 3.16D).

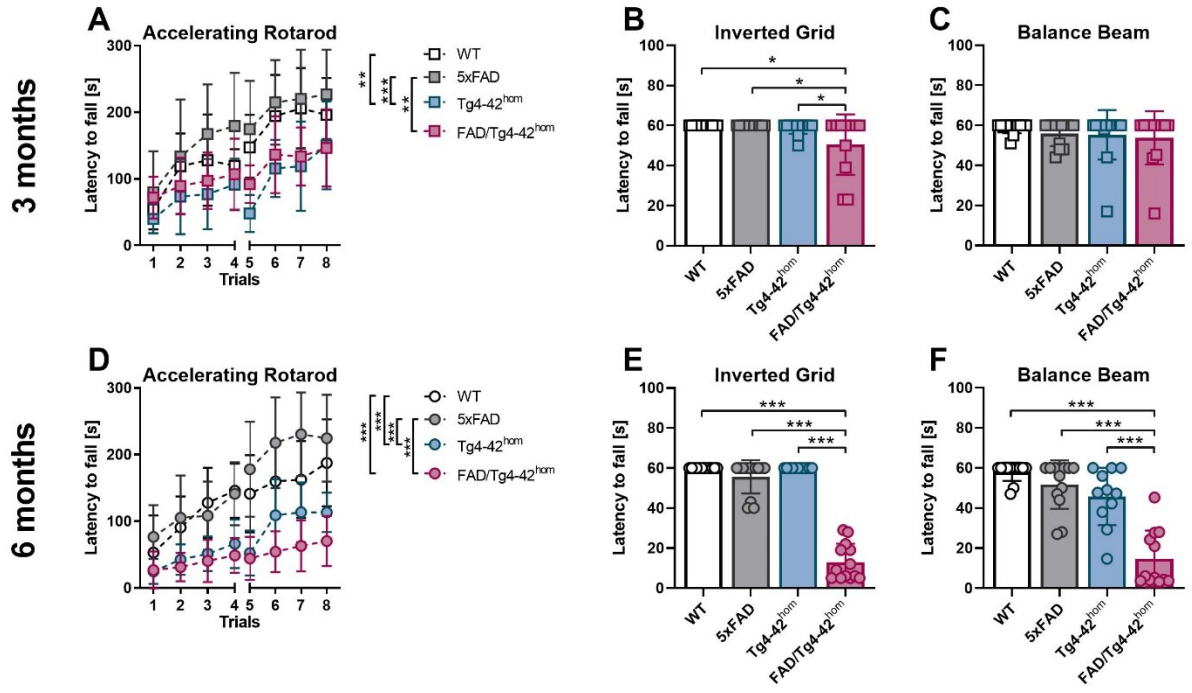

Fig. 3.16 Motor assessment of 3- and 6-month-old FAD/Tg4-42^{hom} mice, transgenic and WT controls. Female WT, 5xFAD, Tg4-42^{hom}, and FAD/Tg4-42^{hom} mice (n=10-13) were tested at 3 (A-C) and 6 (D-F) months in the accelerating rotarod (A,D), inverted grid (B,E), and balance beam (C,F) tasks. Tg4-42^{hom} and FAD/Tg4-42^{hom} mice presented motor deficits in the accelerating rotarod already at 3 months with a further aggravation at 6 months. Young FAD/Tg4-42^{hom} mice displayed motor deficits in the inverted grid task compared to WT animals and the parental lines. These deficits worsened at 6 months of age. While no alterations in latency to fall were observed among the transgenic lines at the 3 months' time point in the balance beam task, aged FAD/Tg4-42^{hom} mice presented with altered motor phenotype in the task. All data are given as means ± SD. (A,D) Two-way ANOVA RM followed by Bonferroni's multiple comparison test, (B,C,E,F) One-way ANOVA followed by Bonferroni's multiple comparison test: *p<0.05, **p<0.01,***p<0.001.

3.3.2.2 Increased loss of motoneurons in the FAD/Tg4-42^{hom} mouse model of AD

Given the clear aggravation of motor behavior in 5xFAD mice co-expressing the Aβ$_{4-42}$ transgene, an analysis of the motoneurons (MNs) was carried out in cervical spinal cord paraffin samples in 3- and 6-month-old mice (Fig. 3.17). Choline acetyltransferase (ChAT) was used as marker to identify MNs, which locate in the gray matter of the ventral horns. Additionally, α- and γ-MNs were differentiated through NeuN staining and size (Friese et al. 2009, Powis and Gillingwater 2016, Lance-Jones 1982). α-MNs are characterized by

immunoreactivity to both ChAT and NeuN and present an average cell body diameter above 20 μm (Fig. 3.17A, upper panel, arrowhead). On the other hand, γ-MNs show strong ChAT immunoreactivity but no NeuN labelling and have smaller cell bodies (Fig. 3.17, upper panel, asterisks). From a functional point of view, α-MNs are responsible for force generation as they drive muscle contraction by innervation of extrafusal skeletal muscle while γ-MNs innervate intrafusal fibers modulating the sensitivity of muscle spindles to stretch (Kanning, Kaplan, and Henderson 2010).

Quantification of the total number of MNs (identified as ChAT positive) showed a significant reduction of MNs in the Tg4-42^{hom} line at both 3 and 6 months of age compared to WT littermates ($p<0.05$), while 5xFAD mice presented comparable numbers to the WT group at both time points (Fig 3.17 lower panel,B,E). FAD/Tg4-42^{hom} mice also presented a significantly reduced number of MNs compared to WT mice and the parental line 5xFAD at 3 months ($p<0.01$) and 6 months ($p<0.05$ and $p<0.01$, respectively) in a Kruskal-Wallis test followed by Bonferroni's multiple comparison test. Direct comparison of Tg4-42^{hom} and FAD/Tg4-42^{hom} with a Mann-Whitney test showed that the presence of amyloid plaques in Tg4-42^{hom} led to a further reduction of MNs, with a trend towards significance at 3 months and a significant decrease at 6 months ($p<0.05$) (Fig. 3.17 A lower panel,B,E). These results are in good agreement with the motor behavioral data, which showed no alteration of motor phenotype in 5xFAD mice, while Tg4-42^{hom} displayed motor deficits already at 3 months and an aggravation was observed in FAD/Tg4-42^{hom} animals. Subsequent distinction between α-MNs and γ-MNs unraveled that the loss of MNs was restricted to α-MNs. Quantification of α-MNs presented a comparable pattern to the quantification of total ChAT^{+}-MNs as no changes were observed in the 5xFAD group, while a significant reduction in Tg4-42^{hom} mice compared to WT littermates ($p<0.05$) and in FAD/Tg4-42^{hom} mice compared to WT ($p<0.001$) and 5xFAD ($p<0.05$) mice was quantified at both time points (Fig. 3.17 lower panel,C,F). Also, in the case of α-MNs, a

direct comparison of Tg4-42^{hom} and FAD/Tg4-42^{hom} with a Mann-Whitney test showed that the presence of plaques led to a significant reduction in Tg4-42^{hom} mice ($p<0.01$). On the contrary, no changes in the number of γ-MNs were observed in any transgenic line compared to WT littermates, nor in FAD/Tg4-42^{hom} mice compared to the parental lines (Fig 3.17A lower panel,D,G).

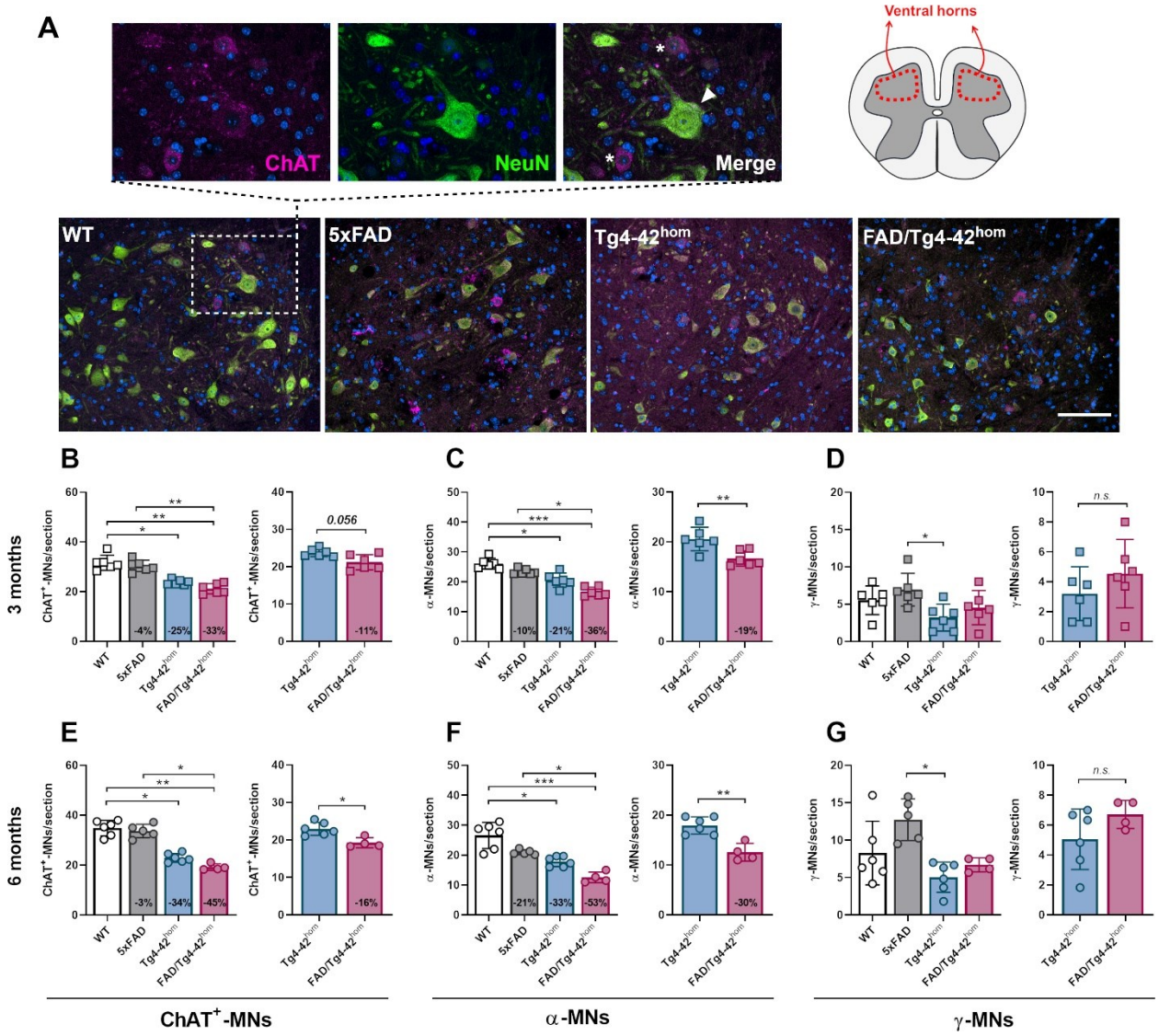

Fig. 3.17 Analysis of MNs in cervical spinal cord in 3- and 6-month-old FAD/Tg4-42^{hom} mice, transgenic and WT controls.

Fluorescent immunohistochemistry to identify and quantify MNs was performed on paraffin spinal cord tissue samples of female WT, 5xFAD, Tg4-42^{hom}, and FAD/Tg4-42^{hom} mice (n=4-6) at 3 and 6 months of age. (A) Example images of staining in the ventral horns at 6 months. ChAT antibody (pink) was used to identify MNs, which were additionally divided in α-MNs (arrowhead) and γ-MNs (asterisks) based on NeuN

immunoreactivity (green) and size. DAPI was used for counterstaining. (B,E) A significant reduction of ChAT$^+$-MNs was observed at 3 and 6 months in Tg4-42^{hom} and FAD/Tg4-42^{hom} mice compared to WT littermates with FAD/Tg4-42^{hom} presenting a significant reduction also compared to the 5xFAD parental line. A direct comparison between Tg4-42^{hom} and FAD/Tg4-42^{hom} mice via an unpaired t-test showed a significant decline in MNs number in the FAD/Tg4-42^{hom} group at 6 months. The loss of MNs is due to loss of α-MNs specifically, as quantification of this subtype revealed a reduction comparable to total ChAT$^+$-MNs (C,F), while no changes were observed in γ-MNs numbers (D,G). All data are given as means ± SD. (B-G) Left graph: Kruskal-Wallis test followed by Bonferroni's multiple comparison test, right graph: Mann-Whitney test: *p<0.05, **p<0.01, ***p<0.001. Scale bar: 100 μm.

3.3.2.3 Decreased spinal cord Aβ accumulation in FAD/Tg4-42^{hom} mice

To assess amyloid pathology in the spinal cord, an electrochemiluminescent assay was performed to measure Aβ concentrations in SDS-soluble protein samples of 5xFAD and FAD/Tg4-42^{hom} mice at 3 and 6 months. At 3 months of age, no changes in total Aβ were observed in the FAD/Tg4-42^{hom} group (Fig. 3.18A). Quantification of Aβ$_{1-x}$ and Aβ$_{4-x}$ variants also showed no alteration at this time point (Fig. 3.18B,C). As expected, Aβ$_{1-x}$ variant comprised the majority of Aβ peptides in 5xFAD and in the derived FAD/Tg4-42^{hom} lines due to the presence of the APP Swedish mutation, while Aβ$_{4-x}$ constituted a minor portion (Wirths et al. 2017, Richard et al. 2015). At 6 months of age a significant decrease in total Aβ could be observed in FAD/Tg4-42^{hom} mice ($p<0.01$) (Fig. 3.18D). The reduction appeared to involve both of the analyzed Aβ variants as the FAD/Tg4-42^{hom} group showed significantly decreased Aβ$_{1-x}$ ($p<0.01$) and Aβ$_{4-x}$ ($p<0.05$) compared to the 5xFAD parental line (Fig. 3.18E,F). Overall, Aβ protein levels increased over time in both lines. The amount of Aβ peptide measure in the Tg4-42^{hom} line was always minimal compared to 5xFAD and FAD/Tg4-42^{hom} mice, which is correlated to the lack of extracellular amyloid deposits in this line.

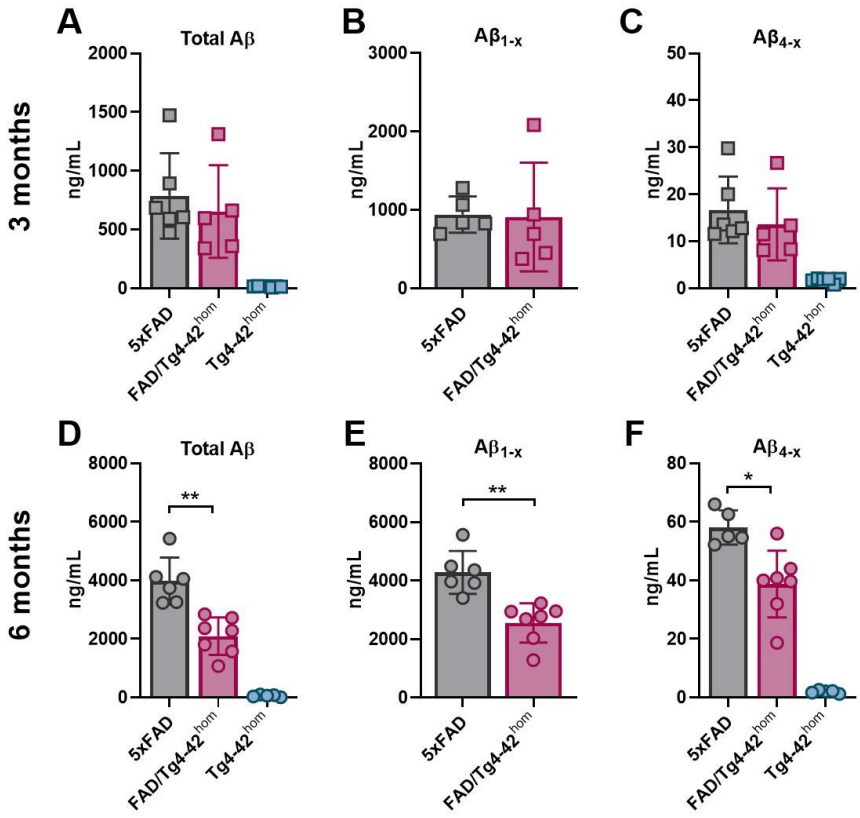

Fig. 3.18 Aβ concentrations in 5xFAD, FAD/Tg4-42^{hom}, and Tg4-42^{hom} spinal cord SDS-soluble protein samples at 3 and 6 months.
Total Aβ (A,D), Aβ$_{1-x}$ (B,E), and Aβ$_{4-x}$ (C,F) concentrations were measure with an electrochemiluminescence assay in SDS spinal cord protein samples of female 5xFAD and FAD/Tg4-42^{hom} mice (n=5-7) at 3 (A-C) and 6 (D-F) months of age. No significant differences were observed between the two groups at the 3 months' time point, while total Aβ, Aβ$_{1-x}$, and Aβ$_{4-x}$ were found significantly reduced in FAD/Tg4-42^{hom} animals compared to 5xFAD littermates at 6 months. All data are given as means ± SD. Mann-Whitney test: *p<0.05, **p<0.01.

These finding were confirmed also through fluorescent immunohistochemistry analysis in the gray matter of spinal cord tissue samples. Immunostaining with the 24311 pan-Aβ antibody showed abundant amyloid plaque pathology in the 5xFAD mouse model, while the Tg4-42^{hom} line presented with few intraneuronal accumulation of the Aβ peptide (Fig. 3.19). Indeed, FAD/Tg4-42^{hom} mice presented a reduced total-Aβ load compared to 5xFAD littermates, with a trend towards significance at 3 months (Fig. 3.19A) and a significant decrease (p<0.05) at 6 months (Fig. 3.19B). Amyloid pathology in 5xFAD mice

was predominantly present as extracellular accumulation in plaques, with very little accumulation in motoneurons in the ventral horns of the spinal cord (Fig. 3.19C, red asterisks). Tg4-42^{hom} mice showed, on the other hand, intraneuronal aggregation of Aβ$_{4-42}$ peptides in some motoneurons without appreciable extracellular accumulation (Fig. 3.19E). FAD/Tg4-42^{hom} mice displayed an apparently increased number of Aβ-positive motoneurons compared to aged-matched Tg4-42^{hom} mice, but while the latter showed clear intracellular aggregation, FAD/Tg4-42^{hom} mice presented with a dot-like staining patter at three months of age (Fig. 3.19D).

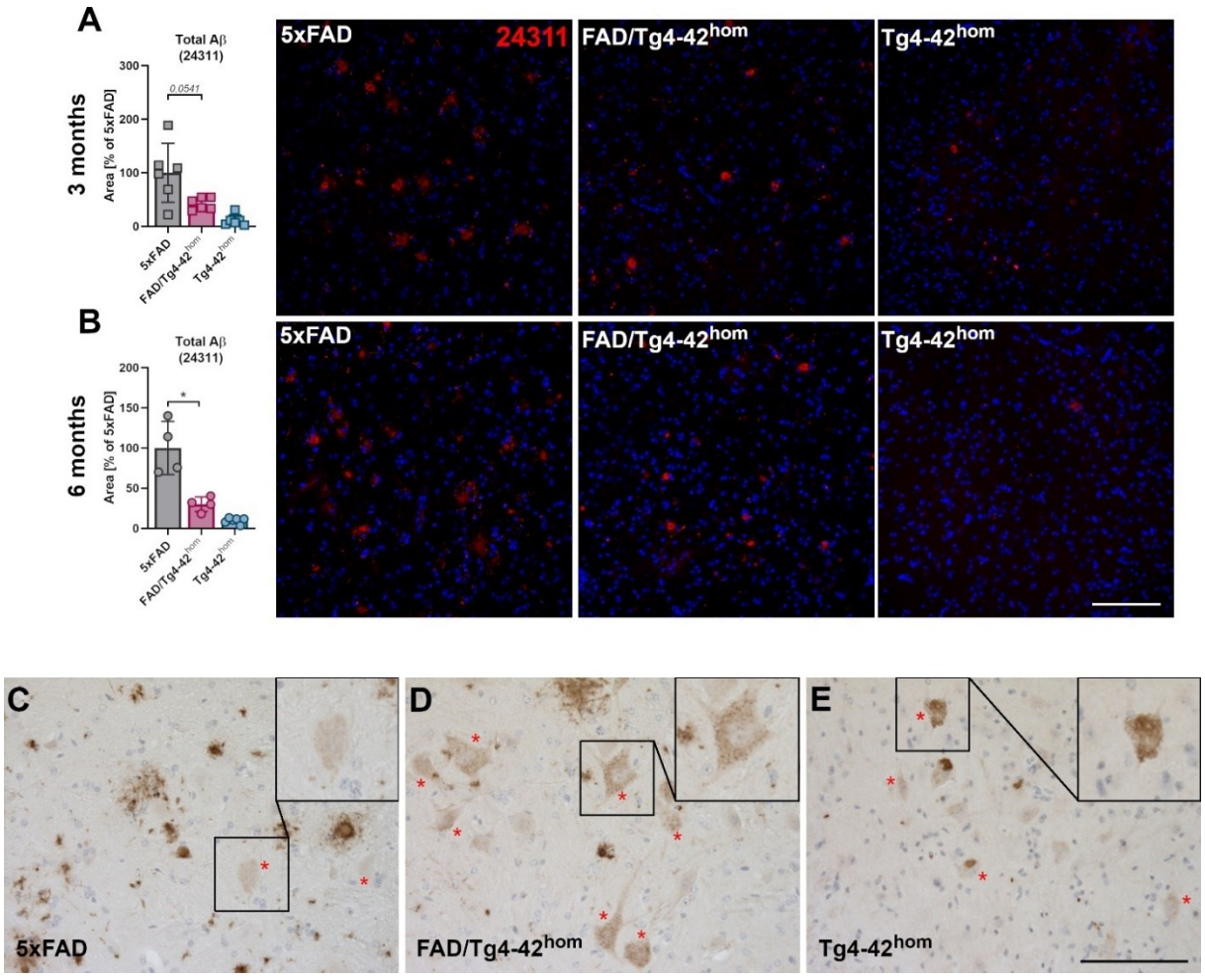

Fig. 3.19 Spinal cord immunohistochemical staining and load analyses of total Aβ in 3- and 6-month-old FAD/Tg4-42^{hom} mice and transgenic controls.

Cervical spinal cord paraffin sections from 3- and 6-month-old female 5xFAD, FAD/Tg4-42^{hom} and Tg4-42^{hom} mice (n=4-6) were stained with the 24311 pan-Aβ antibody. Load analyses of fluorescent immunostaining revealed a tendency towards reduction at 3 months (A) and a significant decrease at 6

months (B) in FAD/Tg4-42^{hom} mice compared to 5xFAD littermates. (C-E) Detail images of Aβ accumulation in motoneurons at 3 months of age (red asterisks). All data are given as means ± SD. Mann-Whitney test: *p<0.01. Scale bars: 100 μm.

3.3.3 Part II: Assessment of cognitive phenotype and analyses of hippocampal pathology

After the analysis of motor deficits and the loss of MNs in the spinal cord of the FAD/Tg4-42^{hom} mice, we shifted the focus towards cognitive performances. The Tg4-42^{hom} mouse model of AD presents recognition memory and spatial memory deficits at 6 months with concomitant age-dependent loss of CA1 pyramidal neuron in the hippocampus (Antonios et al. 2015). We questioned whether the presence of amyloid plaques might alter cognitive behavior and influence the neuron loss in Tg4-42^{hom} mice and if plaque pathology would be altered in the hippocampus of 5xFAD mice also expressing the Aβ$_{4-42}$ peptide.

3.3.3.1 Amyloid plaques do not aggravate memory deficits in Tg4-42^{hom} mice

Learning and memory of FAD/Tg4-42^{hom} mice were tested at 3 and 6 months with the Novel Object Recognition (NOR) and the Morris Water Maze (MWM) tasks. Recognition memory was assessed with the NOR test (Fig. 3.20). 24h after a habituation trial, the mice performed a training trial (Day 1) in which they were exposed to two identical objects. WT controls and all the transgenic lines equally explored the two objects during the 5 minutes trial, showing no preference, at either 3 (Fig. 3.20A) or 6 (Fig. 3.20E) months of age. During the test trial (Day 2), performed 24h after the training trial, one of the identical objects was replaced with a new object. Exploration times of the familiar object and the novel object were recorded and compared within each group. At 3 months, the three transgenic lines and WT group showed intact recognition memory, displaying a significant preference for the novel object (Fig. 3.20B). The genotypes were compared using the discrimination index (DI), a measure of the preference of the mice towards the novel object. No significant differences were observed in the DIs at this time point (Fig.

3.20C). As expected, at 6 months of age the Tg4-42^{hom} group displayed recognition memory deficits (Stazi and Wirths 2021). During the test trial, Tg4-42^{hom} mice did not differentiate between the novel and the familiar object exploring them an equal amount of time (Fig. 3.20F). Analysis of the DIs confirmed the lack of object preference in the Tg4-42^{hom} group as the value was close to zero (Fig. 3.20G). However, no significant differences could be reported when comparing the DIs due to the high variability of the data. Surprisingly, a rescue of recognition memory was observed in 6-month-old FAD/Tg4-42^{hom} mice. Comparably to 5xFAD and WT, they preferentially explored the novel object, thus showing no recognition memory deficits at this time point (Fig. 3.20F). Total exploration times during the second day of the task were compared to exclude an eventual influence of exploration on the outcome of the task. No differences between the genotypes could be observed at either age (Fig. 3.20D,H).

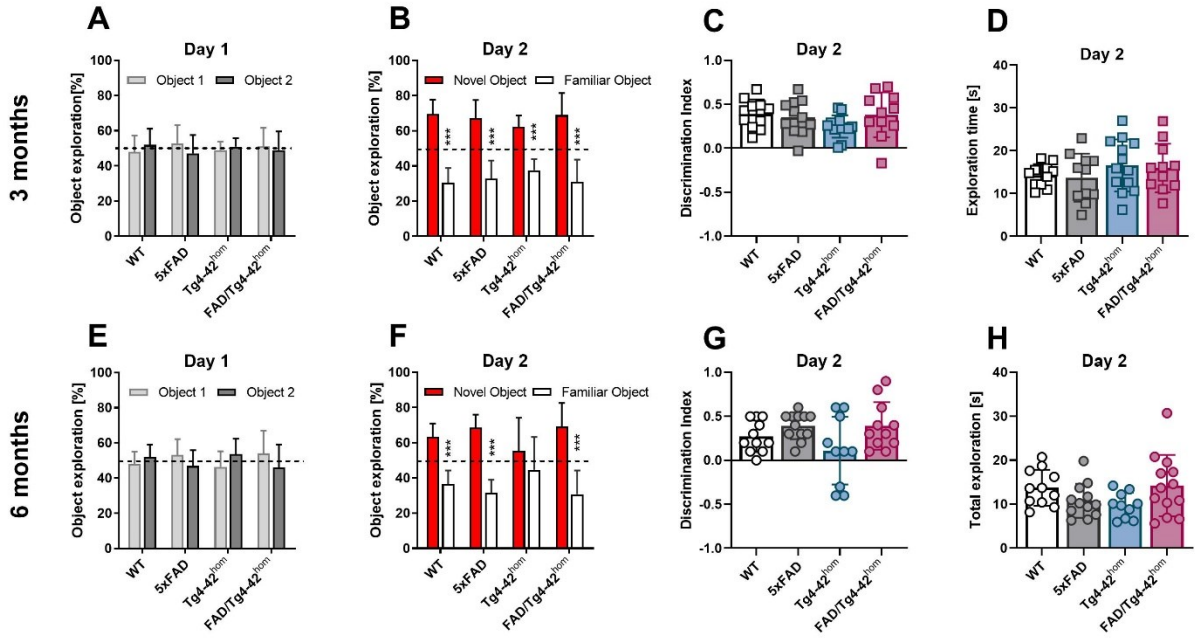

Fig. 3.20 Novel object recognition task in 3- and 6-month-old FAD/Tg4-42^{hom} mice, transgenic and WT controls.

Female WT, 5xFAD, Tg4-42^{hom}, and FAD/Tg4-42^{hom} mice (n=10-14) were tested at 3 (A-D) and 6 (E-H) months. Training trial on day 1 showed no difference in exploration between the two identical objects in all groups at the considered time points (A,E). No recognition memory deficits were observed at 3 months

for WT and the three transgenic lines (B,F), as they all significantly explored more the novel object compared to the familiar one. At 6 months Tg4-42^{hom} mice displayed recognition memory deficits, equally exploring the novel and familiar object on the test trial on day 2, while FAD/Tg4-42^{hom} mice showed a clear preference towards the novel object (F). Total exploration time on the test trial on day 2 was measured and no differences were observed (D,H). All data are given as means ± SD. (A,B,E,F) Black line represents 50%, Two-way ANOVA followed by Bonferroni's multiple comparison test, (C,D,G,H) One-way ANOVA followed by Bonferroni's multiple comparison test: ***$p<0.001$.

The MWM test was performed to assess spatial memory. At first, 3 days of cue training allowed for the detection of possible sensory and motor deficits in this test. During this phase, the platform was tagged with a visible flag and only distal visual cues were present. The average escape latency and the average speed of four trial of max 60 seconds were measured for each day. At 3 months, both WT and the three transgenic lines displayed an expected time-dependent reduction of latency to reach the platform and presented no significant differences between the groups (Fig. 3.21A). At this time point, significant differences were recorded in the average speed among the different lines (Fig. 3.21B). WT and FAD/Tg4-42^{hom} mice swam comparably and significantly slower than 5xFAD and Tg4-42^{hom} mice ($p<0.001$). WT, 5xFAD, and Tg4-42^{hom} mice showed a time-dependent reduction of the time necessary to reach the visible platform also at the 6-months' time point (Fig. 3.21C). This reduction was, on the other hand, not observed in the FAD/Tg4-42^{hom}, which took a significantly increased time to reach the platform during the 60s trials compared to both WT mice ($p<0.001$) and the two parental lines ($p<0.01$). The different behavior observed in FAD/Tg4-42^{hom} was also accompanied by a significantly reduced average speed compared to the other groups (WT and Tg4-42^{hom}: $p<0.01$, 5xFAD: $p<0.05$) (Fig. 3.21D), which might be attributed to the observed motor deficits in this line. During the 5 days of acquisition training, the platform was no longer visible and additional proximal visual cues were added. At 3 months of age, both 5xFAD as well as FAD/Tg4-42^{hom} mice displayed a significantly increased average escape latency compared to WT ($p<0.001$), while no alterations were found in Tg4-42^{hom} animals, as already published (Antonios et al. 2015) (Fig 3.21E). FAD/Tg4-42^{hom} animals also took

significantly more time to reach the hidden platform compared to the Tg4-42^{hom} line ($p<0.05$). During the acquisition training, young WT mice swam significantly slower than 5xFAD ($p<0.001$) and Tg4-42^{hom} ($p<0.05$) mice, respectively (Fig 3.21F). At 6 months of age, Tg4-42^{hom} mice displayed spatial learning deficits compared to WT littermates, showing a significantly increased escape latency ($p<0.001$) (Fig 3.21G). A comparable increase was observed in FAD/Tg4-42^{hom} mice as well, which behaved significantly different from WT ($p<0.001$) and 5xFAD ($p<0.001$) littermates, that presented no alterations. No changes in average speed were detected at this time point (Fig 3.21H).

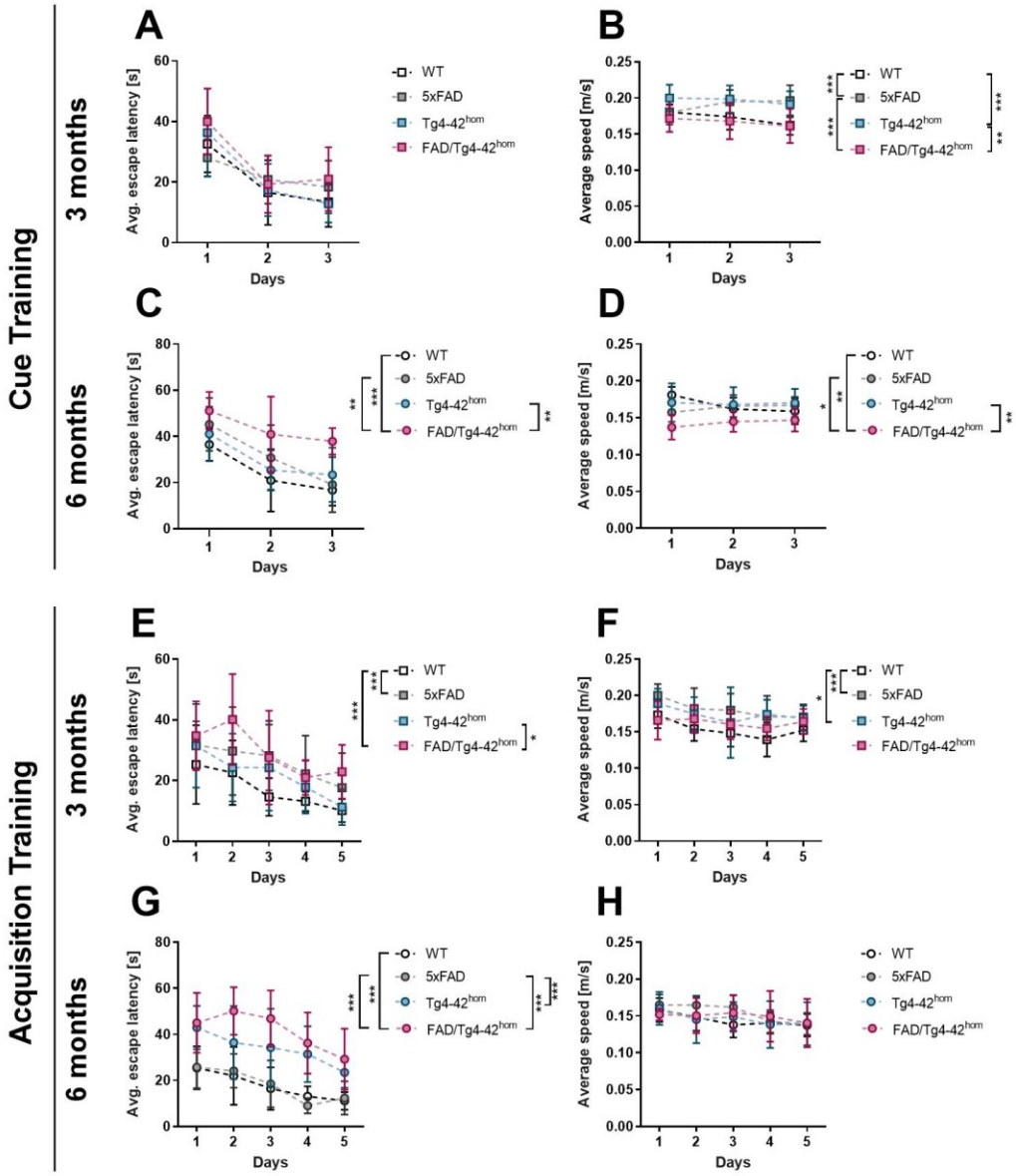

Fig. 3.21 Morris Water Maze task: cue and acquisition training in 3- and 6-month-old FAD/Tg4-42^{hom} mice, transgenic and WT controls.

Female WT, 5xFAD, Tg4-42^{hom}, and FAD/Tg4-42^{hom} mice (n=10-14) were tested at 3 (A,B,E,F) and 6 (C,D,G,H) months. During cue training (A-D) increased escape latencies were measured in aged Tg4-42^{hom} and FAD/Tg4-42^{hom} mice, with no changes in the younger groups. At this phase, young WT and FAD/Tg4-42^{hom} mice swam significantly slower than 5xFAD and Tg4-42^{hom} littermates, while at 6 months only FAD/Tg4-42^{hom} groups displayed a reduced speed. During the acquisition training 5xFAD and FAD/Tg4-42^{hom} mice showed an increased escape latency at 3 months compared to WT mice. At 6 months a clear spatial learning deficits could be observed in bot Tg4-42^{hom} and FAD/Tg4-42^{hom} mice. While no changes in speed were recorded at 6 months during the acquisition training, 3-month-old WT swam significantly slower than the 5xFAD and Tg4-42^{hom} groups. All data are given as means ± SD. Two-way ANOVA repeated measure followed by Bonferroni's multiple comparison test: *p<0.05, **p<0.01, ***p<0.001.

A single-trial probe test, during which the platform was removed, was performed 24h after the end of the acquisition training to test for spatial memory impairments. The time spent in each quadrant, the time spent in the platform zone, and the average speed were recorded. At 3 months, all analyzed groups showed no obvious spatial memory deficits as they spent significantly more time swimming in the target compared to the other quadrants (Fig. 3.22A). At 6 months, both WT and 5xFAD animals showed no spatial memory deficits (Fig. 3.22B). As expected (Antonios et al. 2015, Hüttenrauch et al. 2016), Tg4-42^{hom} mice explored the four quadrants for an equal amount of time, indicating the presence of a memory deficit at this time point. A spatial memory impairment could also be observed in FAD/Tg4-42^{hom} mice, as they failed to remember the location of the target quadrant. At both time points, no alteration of the average speeds were detected in the probe trial (Fig. 3.22A,B). A direct comparison of the four different lines' performances was achieved by confronting the times and entries in the target quadrant and the platform zone. In young animals, no significant differences were observed in either the time and entries of the target quadrant (Fig. 3.22C,D) or the platform zone (Fig. 3.22G,H). At 6 months, as anticipated by the inability to remember the position of target quadrant, Tg4-42^{hom} and FAD/Tg4-42^{hom} mice displayed a reduced time spent swimming in the target quadrant compared to WT (FAD/Tg4-42^{hom}: $p<0.05$) and 5xFAD littermates ($p<0.001$) (Fig. 3.22E). The two lines also showed decreased numbers of entries into the target quadrant, reaching statistical significance compared to the 5xFAD group (Tg4-42^{hom}: $p<0.05$, FAD/Tg4-42^{hom}: $p<0.001$) (Fig. 3.22F). Analyses of the time and entries in the platform zone further confirmed the observed memory deficits. Indeed, both Tg4-42^{hom} and FAD/Tg4-42^{hom} mice spent significantly less time in the platform zone compared to WT ($p<0.01$) and 5xFAD ($p<0.05$) animals (Fig. 3.22I) as well as showing less crosses of the platform area (Fig. 3.22J).

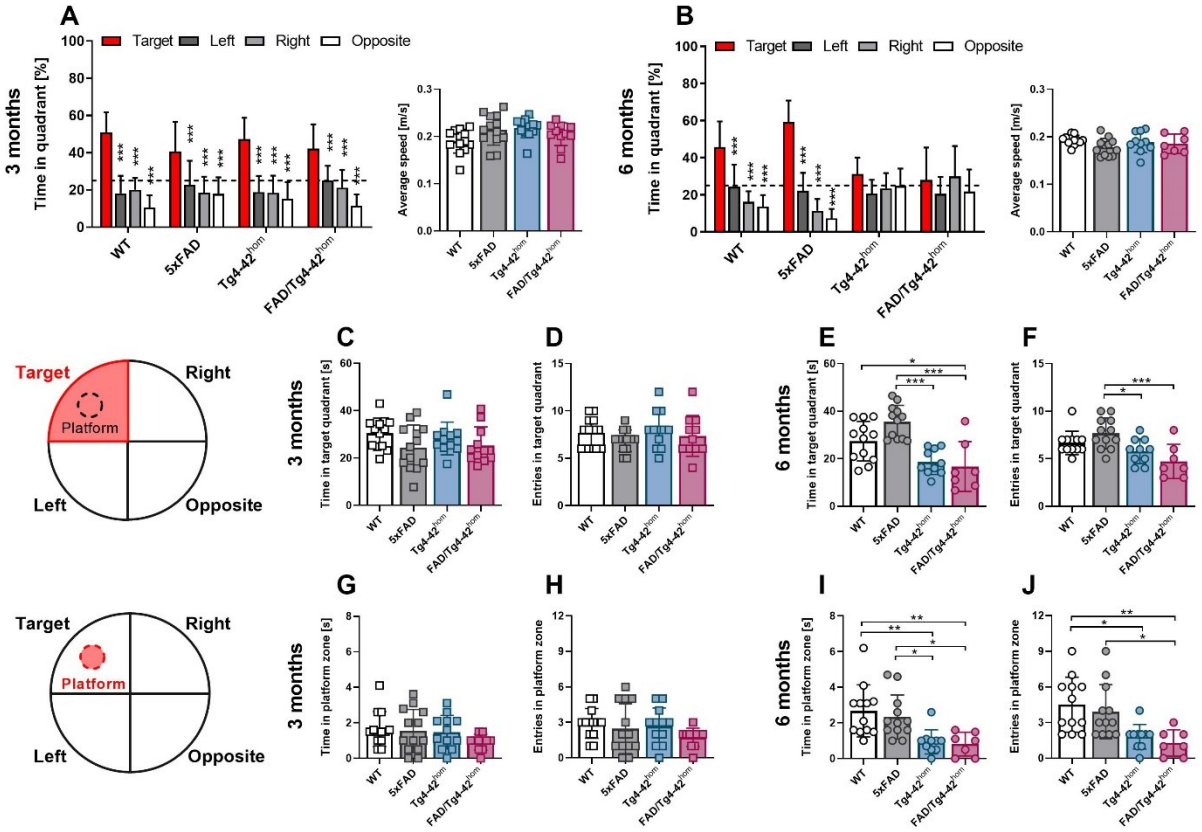

Fig. 3.22 Morris Water Maze task: probe trial in 3- and 6-month-old FAD/Tg4-42^{hom} mice, transgenic and WT controls.

Female WT, 5xFAD, Tg4-42^{hom}, and FAD/Tg4-42^{hom} mice (n=10-14) were tested at 3 (A,C,D,G,H) and 6 (B,E,F,I,J) months. At 3 months, no spatial memory deficits were observed in any group (A), while at 6 months a deficit was clearly present in Tg4-42^{hom} and FAD/Tg4-42^{hom} mice (B). Comparison of time and entries in target quadrant and platform zone showed no differences at 3 months (C,D,G,H). At 6 months a significant reduction was observed in Tg4-42^{hom} and FAD/Tg4-42^{hom} animals (E,F,I,J). All data are given as means ± SD. Two-way ANOVA followed by Bonferroni's multiple comparison test: *p<0.05, **p<0.01, ***p<0.001.

3.3.3.2 Amyloid plaques do not worsen hippocampal CA1 neuron loss in Tg4-42^{hom} mice.

Neuron loss in the CA1 region of the hippocampus is observed in a time- and genotype-dependent manner in the Tg4-42 line, and it is associated with the behavioral deficits observed in the NOR and MWM behavioral tasks (Antonios et al. 2015, Bouter et al. 2013, Hüttenrauch et al. 2016, Stazi and Wirths 2021). Hematoxylin-stained distal and proximal CA1 pyramidal neurons were counted to understand whether the presence of amyloid plaques might have an impact on neuron loss in the Tg4-42^{hom} mouse model (Fig. 3.23). Neuron loss could be detected already in young animals (Fig. 3.23A), as both Tg4-42^{hom} and FAD/Tg4-42^{hom} mice displayed ~ 30% reduction in the distal and ~ 20% reduction in the proximal part of CA1 compared to WT littermates, a loss being significant compared to both WT and 5xFAD animals (distal CA1: $p<0.001$, proximal CA1: $p<0.05$) (Fig. 3.23B,C). As expected, the neuron loss in the Tg4-42^{hom} mice showed an age-dependent aggravation, reaching ~ -60% in the distal CA1 and ~ -45% in proximal CA1 compared to the WT group. Confirming recent findings, the neuron loss was more prominent towards the distal region (Stazi and Wirths 2021). While FAD/Tg4-42^{hom} mice showed a comparable loss in proximal pyramidal neurons (Fig. 3.23F), an ameliorated loss could be observed in the distal part (Fig. 3.23C) as the filial line presented a significant increase of ~30% compared to Tg4-42^{hom} littermates ($p<0.05$) (Fig. 3.24E). At both time points, no loss of CA1 pyramidal neurons was observed in the 5xFAD line, confirming previous findings (Jawhar et al. 2012).

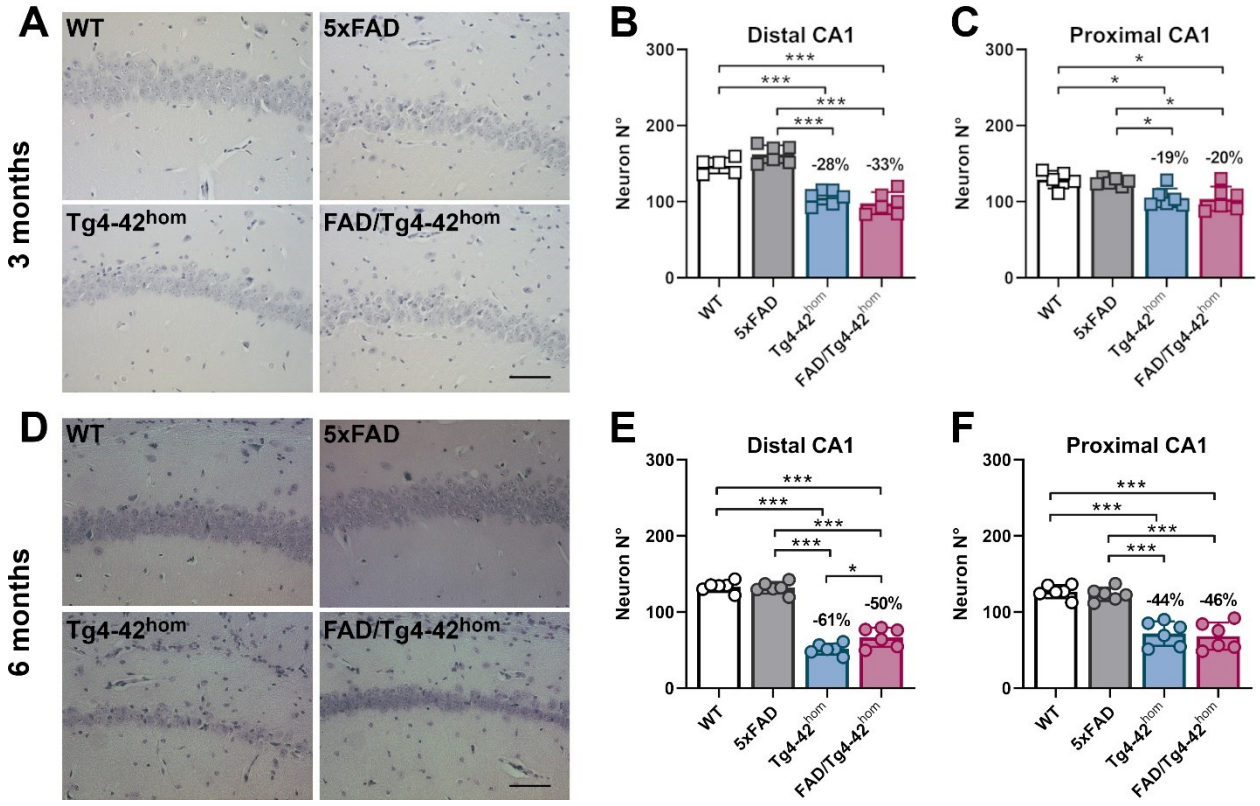

Fig. 3.23 Distal and Proximal CA1 neuron loss in 3- and 6-month-old FAD/Tg4-42^{hom} mice, transgenic and WT controls.

Sagittal paraffin brain sections (n=3 per animal) from female WT, 5xFAD, Tg4-42^{hom}, and FAD/Tg4-42^{hom} mice (n=5-6) were stained with hematoxylin. Pictures were taken from the distal and proximal part of the hippocampal CA1 pyramidal layer at 400x magnification. (A,C) Example images of distal CA1 pyramidal layer at 3 (A) and 6 (C) months. Tg4-42^{hom} and FAD/Tg4-42^{hom} mice displayed a comparable neuron loss at 3 months in both distal and proximal CA1 (B,C). In aged Tg4-42^{hom} and FAD/Tg4-42^{hom} mice, comparable loss was observed in the proximal region (E), while the bigenic line displayed a significant increase in distal pyramidal neuron compared to Tg4-42^{hom} animal. All data are given as means ± SD. One-way ANOVA followed by Bonferroni's multiple comparison test: *p<0.05, **p<0.01, ***p<0.001. (A,C,E) Scale bar: 50 µm.

Young Tg4-42^{hom} and FAD/Tg4-42^{hom} mice presented with a comparably significant reduction of CA1 and pyramidal layer area when contrasted to WT and 5xFAD littermates (Fig. 3.24B,C). At 6 months, the Tg4-42^{hom} consistently displayed a reduced CA1 and pyramidal layer area compared to WT and 5xFAD mice (Fig. 3.24A,D,E). On the other hand, FAD/Tg4-42^{hom} mice showed no difference in CA1 area compared to WT and a significant reduction compared to 5xFAD at this time point (Fig. 3.24D). Quantification of the pyramidal layer area in aged mice showed a significant increase in FAD/Tg4-42^{hom}

mice compared to Tg4-42^{hom} littermates ($p<0.05$), though both lines having a significantly reduced area compared to WT and 5xFAD mice ($p<0.001$) (Fig. 3.24E).

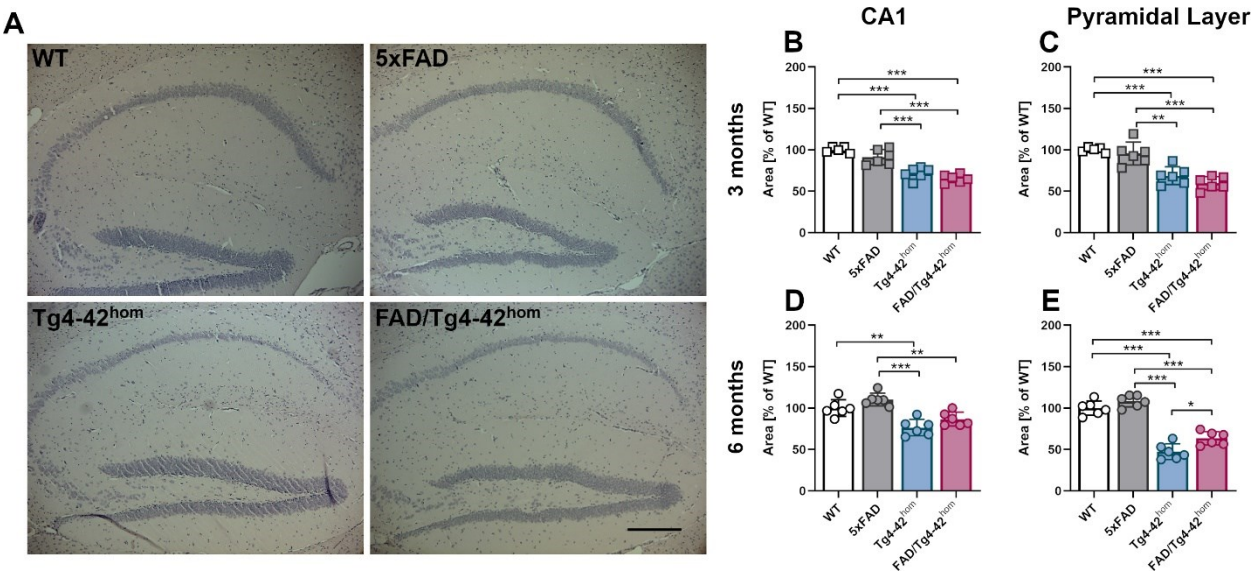

Fig. 3.24 CA1 and pyramidal layer area of 3- and 6-month-old FAD/Tg4-42^{hom} mice, transgenic and WT controls.

Sagittal paraffin brain sections (n=3 per animal) from female WT, 5xFAD, Tg4-42^{hom}, and FAD/Tg4-42^{hom} mice (n=5-6) were stained with hematoxylin. Pictures of the hippocampus were taken at 100x magnification. (A) Example images at 6 months. Young Tg4-42^{hom} and FAD/Tg4-42^{hom} mice displayed a comparable reduction of CA1 and pyramidal layer areas. (B,C). At 6 months, FAD/Tg4-42^{hom} animals showed an increase pyramidal layer area compared to Tg4-42^{hom} littermates (E). All data are given as means ± SD. One-way ANOVA followed by Bonferroni's multiple comparison test: *$p<0.05$, **$p<0.01$, ***$p<0.001$. (A,C,E) Scale bar: 200 µm.

3.3.3.3 Hippocampal amyloid pathology in FAD/Tg4-42^{hom} mice

Amyloid pathology was analyzed and compared between 5xFAD and FAD/Tg4-42^{hom} mice at the considered time points. Sagittal paraffin brain sections were stained with antibodies detecting total Aβ (24311), Aβ$_{1-x}$ (82E1), Aβ$_{4-x}$ (18H6), and microglia cells (Iba1). Amyloid load was measured in the CA1 and DG areas of the hippocampus. The pyramidal neuron layer of the CA1 was omitted from the analysis to exclude the Aβ$_{4-x}$ immunoreactivity originating from the Tg4-42^{hom} background in the FAD/Tg4-42^{hom} line. Analysis of total Aβ with the 24311 antibody revealed no significance difference in CA1 and DG between 5xFAD and FAD/Tg4-42^{hom} mice at either 3 or 6 months (Fig. 3.25B,C,E,F). The majority of amyloid plaques were observed in the DG region while little immunoreactivity was observed in the CA1 (Fig 3.25A,D). Analysis of the microglia marker Iba1 also showed no significant difference in inflammatory response between these two lines (Fig 3.25G,J). Immunoreactivity was indeed comparable among the genotypes at the considered ages in both CA1 (Fig 3.25H,I) and DG regions (Fig 3.25K,L). As microglia cells cluster around amyloid plaques, the absence of changes in inflammation could be correlated to the absence of change in total amyloid plaques. Subsequently, Aβ$_{1-x}$ and Aβ$_{4-x}$ specifically were analyzed with variant-specific antibodies. Aβ starting at position 1 represents the majority of Aβ peptides in 5xFAD mice due to the Swedish mutation present on the overexpressed APP gene. No differences in Aβ$_{1-x}$ were found between the two genotypes at the time points considered in this study (Fig 3.26A-F). We could observe an increased amount of Aβ load with aging in both regions, consistent with an increased amyloid pathology over time in the 5xFAD line. Aβ$_{4-x}$ peptides comprises only for a small part of the overall Aβ pathology in 5xFAD mice, and very little immunoreactivity could be observed in the hippocampus (Fig 3.26G,J). FAD/Tg4-42^{hom} mice presented with a comparable Aβ$_{4-x}$ immunoreactivity in the two hippocampal regions at both 3 (Fig 3.26H,K) and 6 (Fig 3.26I,L) months.

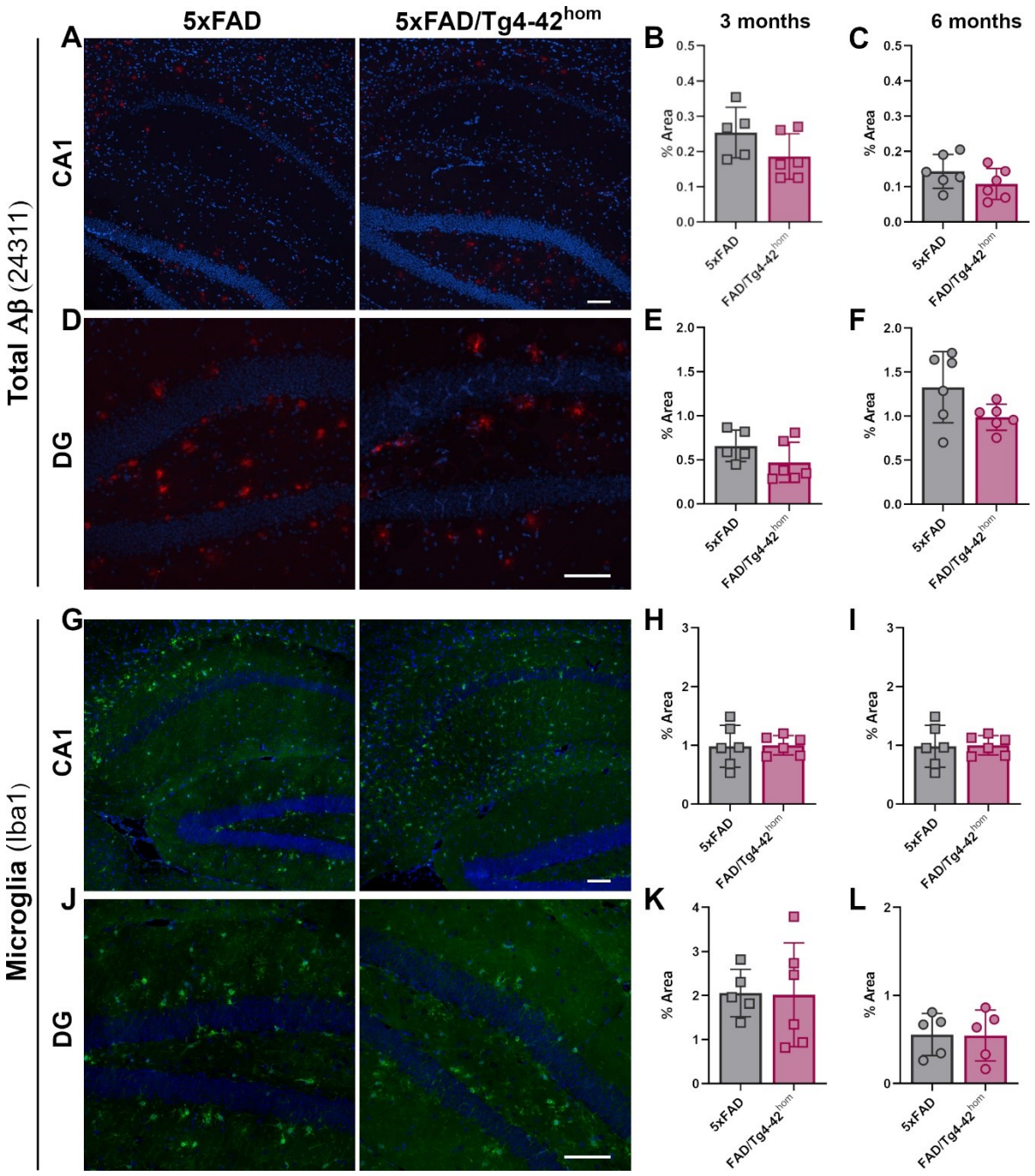

Fig. 3.25 Total Aβ and microglia immunoreactivity in 3- and 6-month-old FAD/Tg4-42^{hom} and 5xFAD mice.

Sagittal brain paraffin sections from 3- and 6-month-old female 5xFAD and FAD/Tg4-42hom mice (n=5-6) were stained with the 24311 pan-Aβ antibody (A,D) and Iba1 microglia marker (G,J). 100X and 200X magnification images were taken from the CA1 (A,G) and DG (D,J) region, respectively. Example images of total Aβ are from 6 months while of Iba1 are from 3 months animals. Load analysis revealed no changes in total Aβ or microglia immunoreactivity at either time points for both hippocampal regions (B,C,E,F,H,I,K,L). All data are given as means ± SD. Unpaired t-test. Scale bar: 100 μm.

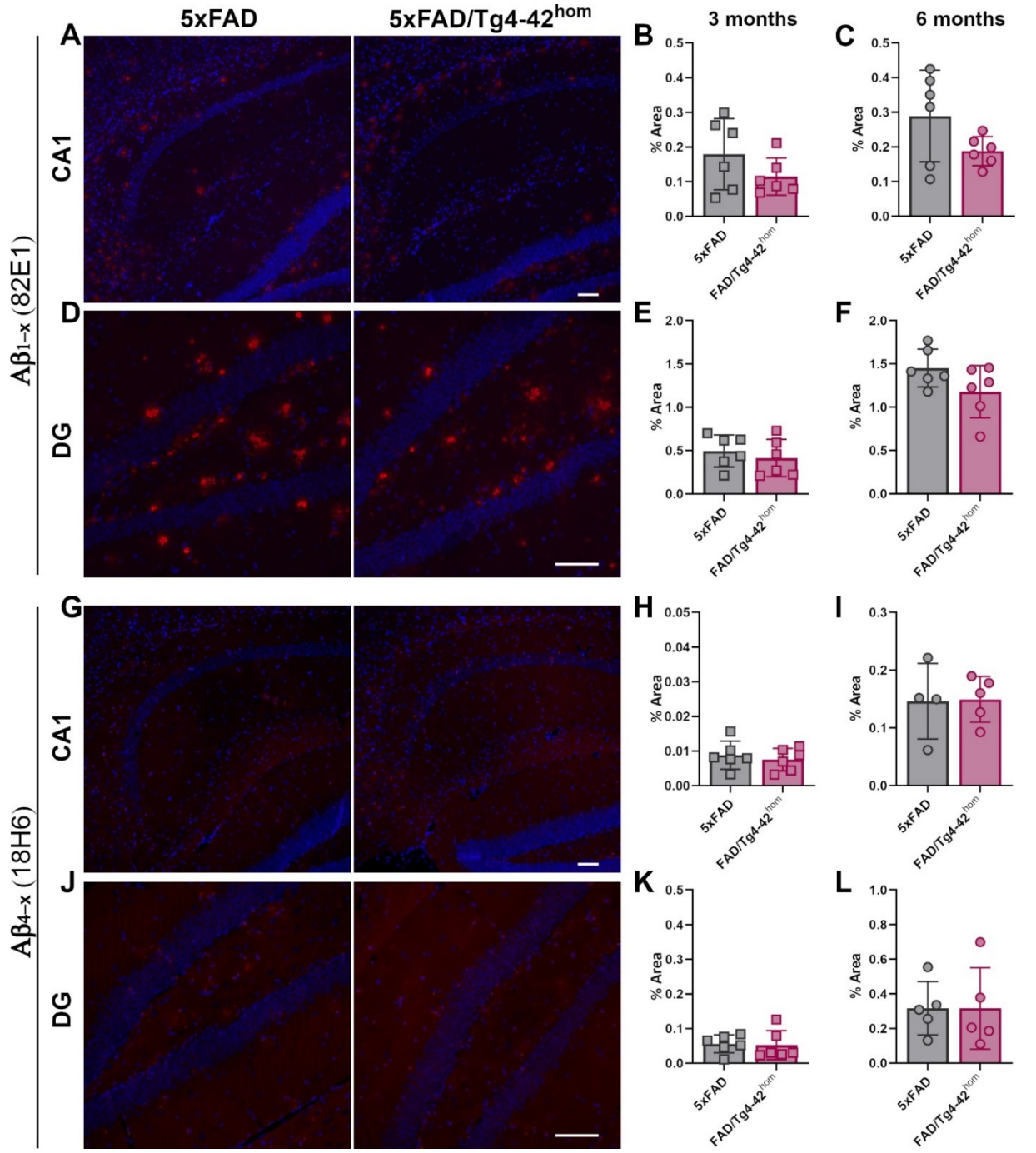

Fig. 3.26 Aβ$_{1-x}$ and Aβ$_{4-x}$ immunoreactivity in 3- and 6-month-old FAD/Tg4-42^{hom} mice, transgenic and WT controls.

Sagittal brain paraffin sections from 3- and 6-month-old female 5xFAD and FAD/Tg4-42^{hom} mice (n=5-6) were stained with the Aβ$_{1-x}$ (82E1) (A,D) and Aβ$_{4-x}$ (18H6) (G,J) specific antibodies. 100X and 200X magnification images were taken from the CA1 (A,G) and DG (D,J) region, respectively. Example images of Aβ$_{1-x}$ are from 6 months while of Aβ$_{4-x}$ are from 3-month-old animals. Load analysis revealed no changes in Aβ$_{1-x}$ or Aβ$_{4-x}$ immunoreactivity at either time points for both hippocampal regions (B,C,E,F,H,I,K,L). All data are given as means ± SD. Unpaired t-test. Scale bar: 100 μm.

Given the changes in distal CA1 neuron numbers and behavioral performances in 6-month-old FAD/Tg4-42^{hom} mice, Aβ concentrations were analyzed in the entire hippocampus with an electrochemiluminescent assay to obtain comprehensive information that could have been missed with the immunohistochemical analyses (Fig. 3.27). TBS- and SDS-soluble protein fractions were extracted from frozen hippocampal tissues and total Aβ, Aβ$_{1-x}$, and Aβ$_{4-x}$ peptides were compared between 5xFAD and FAD/Tg4-42^{hom}. Total Aβ concentration in the hippocampus was found comparable between 5xFAD and FAD/Tg4-42^{hom} mice, both in the SDS-soluble (Fig. 3.27A) and TBS-soluble (Fig. 3.27D) fractions, in line with the immunohistochemical data (Fig. 3.27A,C,F). Similarly, no changes were detected in Aβ$_{1-x}$ concentrations among the two genotypes for both fractions (Fig. 3.27B,E). As expected (Walter et al. 2019), Aβ$_{4-x}$ represented a minor fraction of the Aβ species in the 5xFAD line. In the SDS fraction of FAD/Tg4-42^{hom} mice, Aβ$_{4-x}$ was found to be significantly increased compared to 5xFAD littermates (Fig. 3.27C), an increase not ascribable to the transgene peptide expressed from the Tg4-42^{hom} line as samples from this line showed no detectable Aβ$_{4-x}$ in this analysis, due to below-detection-limit concentrations. No changes in Aβ$_{4-x}$ were found in the TBS-soluble fraction (Fig. 3.27F).

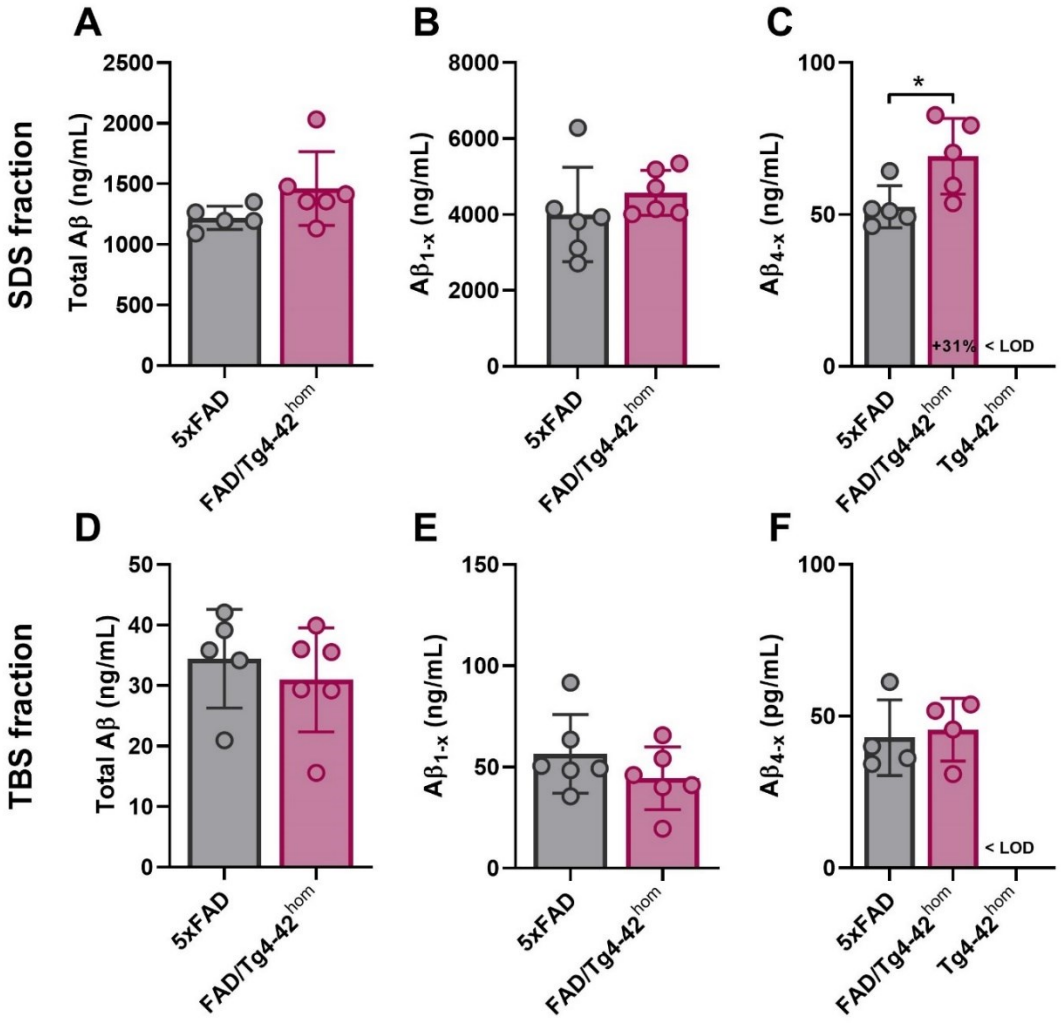

Fig. 3.27 Electrochemiluminescence measurements of hippocampal Aβ protein levels in 6-month-old FAD/Tg4-42^{hom} mice and transgenic controls.
Total Aβ (A,D), Aβ$_{1-x}$ (B,E), and Aβ$_{4-x}$ (C,F) concentrations were measured with an electrochemiluminescence assay in SDS- (A-C) and TBS- (D-F) soluble fraction from hippocampal samples of female 5xFAD and FAD/Tg4-42^{hom} mice (n=5-6) at 6 months of age. No significant differences were observed between the two groups in total Aβ (A,D) or Aβ$_{1-x}$ (B,E) concentrations. Aβ$_{4-x}$ levels were found significantly increased in FAD/Tg4-42^{hom} animals compared to 5xFAD littermates in the SDS-soluble fraction (C), while no changes were observed in the TBS-soluble fraction (F). Aβ$_{4-x}$ concentration were below detection limit (LOD) in the Tg4-42^{hom} line (C,F). All data are given as means ± SD. Mann-Whitney: *p<0.05.

To check if Aβ$_{4-x}$ pathology in the pyramidal neuron layer of Tg4-42^{hom} animals changed with the presence of extracellular amyloid plaques, DAB immunostainings were performed on 3- and 6-month-old Tg4-42^{hom} mice and compared to FAD/Tg4-42^{hom}

littermates (Fig. 3.28). The load analysis was performed delimiting the pyramidal layer exclusively, to avoid interference of the extracellular deposits in the FAD/Tg4-42^{hom} line. No alteration in Aβ$_{4-x}$ immunoreactivity was observed at 3 months (Fig. 3.28A,B), while in aged FAD/Tg4-42^{hom} mice a significant increase in Aβ$_{4-x}$ load was found in the pyramidal layer of the CA1 (Fig. 3.28C,D).

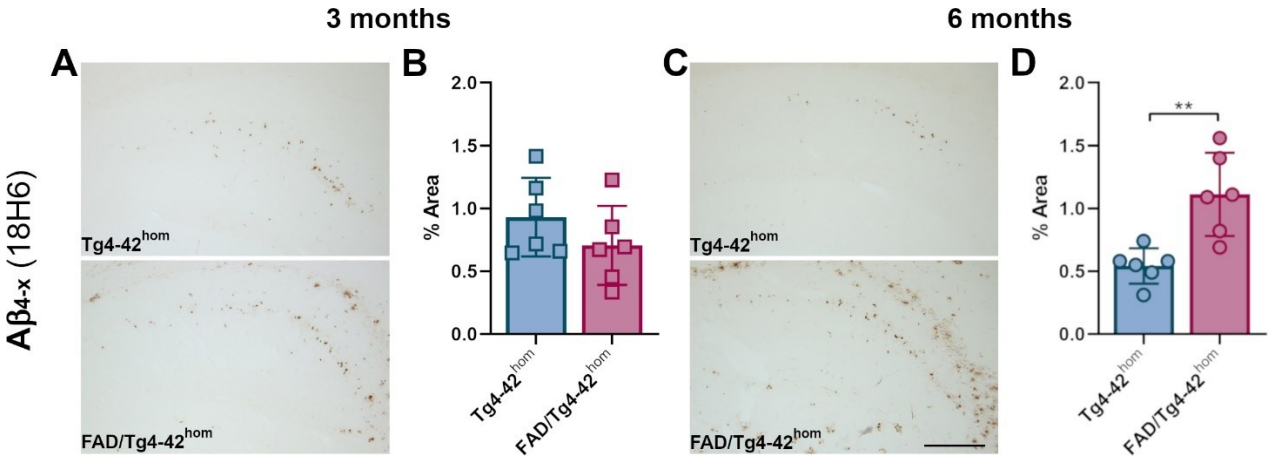

Fig. 3.28 Aβ$_{4-x}$ immunoreactivity in CA1 pyramidal layer of 3- and 6-month-old FAD/Tg4-42^{hom} and Tg4-42^{hom} mice.

Sagittal brain sections of 3- (A,B) and 6- (C,D) month-old Tg4-42^{hom} and FAD/Tg4-42^{hom} were stained with 18H6 (Aβ$_{4-x}$) antibody. 100x magnification images were taken of 3 section/animal. At 3 months no changes in Aβ$_{4-x}$ were observed (B), while FAD/Tg4-42^{hom} displayed a significant increase (D). All data are given as means ± SD. Unpaired t-test: *p<0.05. Scale bar: 200 μm.

3.4 PROJECT IV: *In-vivo* relationship of Aβ$_{4-x}$ peptides and protein tau

Several studies showed that tau is essential for Aβ toxicity in AD (Rapoport et al. 2002, Roberson et al. 2007) and in mice co-expressing APP and tau an aggravation of tau pathology and behavioral decline were reported (Hurtado et al. 2010, Saul et al. 2013b, Stancu et al. 2014a). In these bigenic lines, usually no alteration of amyloid pathology is observed, putting Aβ upstream of tau, which then acts as a mediator of the toxicity (Bloom 2014, Stancu et al. 2014b). The influence of specific Aβ variants on tau pathology is however unclear at present. In this project the Tg4-42 mouse model of AD, expressing exclusively Aβ$_{4-42}$ peptides, was crossed with a classical tau mouse model, MAPT (PS19), expressing mutant P310S human microtubule-associated protein tau (MAPT), with the aim to understand the relationship between Aβ peptides starting at position 4 and protein tau in the context of AD (Zampar and Wirths 2021).

3.4.1 Transgene expression and bodyweight of MAPT/Tg4-42^{hom} mice

To exclude an altered transgene expression level after the crossing of the two parental lines, mRNA levels of Aβ$_{4-42}$ transgene and human MAPT gene were assessed in the bigenic line. RNA was extracted from the hippocampus and the expression of the Aβ$_{4-42}$ and human MAPT transgenes was analyzed in comparison to the Tg4-42^{hom} or MAPT single transgenic lines, respectively (Fig. 3.29A,B). No significant differences were detected in expression for both transgenes at all three considered time points. Additionally, bodyweight was measured and compared among the different genotypes (Fig 3.29C). MAPT and MAPT/Tg4-42^{hom} mice displayed a significantly reduced weight compared to WT at 9 months ($p<0.05$ and $p<0.001$ respectively), but at all considered ages, no difference between the bigenic MAPT/Tg4-42^{hom} line and the MAPT and Tg4-42^{hom} parental lines was obvious.

Data partly published in (Zampar and Wirths 2021)

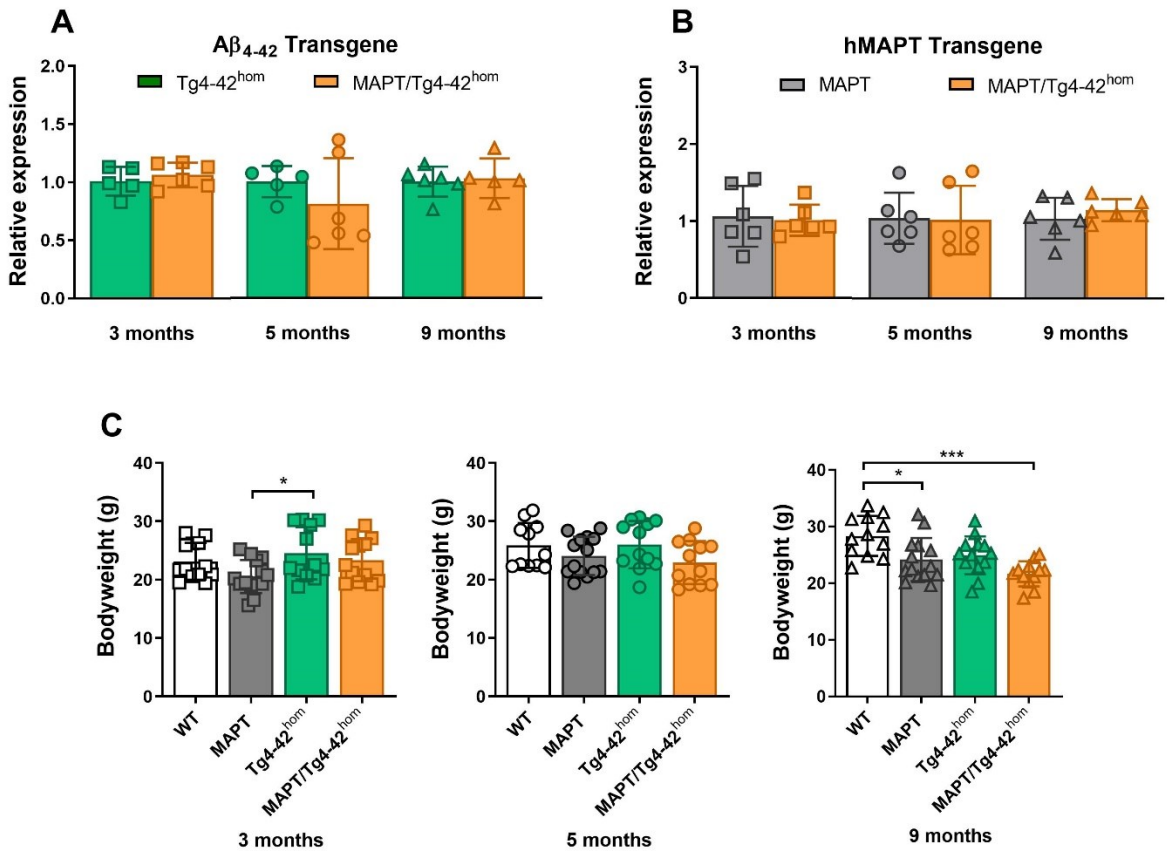

Fig. 3.29 Transgenes expression and bodyweight of MAPT/Tg4-42^{hom} line.
Hippocampal RNA from female and male 3-, 5-, and 9-month-old Tg4-42^{hom}, MAPT and MAPT/ Tg4-42^{hom} (n=5-6) was used to measure the expression of Aβ$_{4-42}$ (A) and human MAPT (hMAPT) (B) transgenes. No differences were found between the bigenic MAPT/Tg4-42^{hom} and the parental lines. (C) Bodyweight comparison (n=12-14) at the different ages showed no differences between the bigenic and parental lines. At 9 months of age, both MAPT and MAPT/Tg4-42^{hom} mice displayed significantly reduced bodyweight compared to WT animals. All data are given as means ± SD. (A,B) Unpaired t-test. (C) One-way ANOVA followed by Bonferroni's multiple comparison test: *p<0.05, ***p<0.001.

3.4.2 Behavioral assessment of MAPT/Tg4-42^{hom} mice

Mice underwent a battery of behavioral tests to assess motor performances and learning- and memory-related behaviors. The accelerating rotarod, balance beam, and inverted grid tasks were used to investigate and compare the locomotor activity at 3, 5, and 9 months in female and male WT, MAPT, Tg4-42^{hom}, and MAPT/Tg4-42^{hom} mice. Already at 3 months of age, Tg4-42^{hom} displayed a reduced latency to fall in the accelerating rotarod test compared to WT (p<0.05) and MAPT (p<0.001), which on the other hand

Data partly published in (Zampar and Wirths 2021)

performed comparably to WT littermates (Fig 3.30A). At this time point, MAPT/Tg4-42^{hom} mice presented a latency curve overlapping to the one of Tg4-42^{hom} mice, which was however significantly different only to MAPT animals ($p<0.01$). The motor performances of Tg4-42^{hom} and MAPT/Tg4-42^{hom} mice remained comparable in this task at 5 months (Fig 3.30D), displaying a significantly reduced latency only compared to MAPT mice ($p<0.01$ and $p<0.05$, respectively), probably due to a reduce WT littermates' performance. At 9 months of age, an aggravation of the motor deficits in the accelerating rotarod became evident in both Tg4-42^{hom} and MAPT/Tg4-42^{hom} mice compared to WT and MAPT lines ($p<0.001$) (Fig. 3.30G). At all three considered time points, a significant difference between Tg4-42^{hom} and MAPT/Tg4-42^{hom} lines was never observed in this task, suggesting that the co-expression of A$\beta_{4\text{-}42}$ and mutated tau protein did not affect the motor abilities addressed in the accelerating rotarod task. In the balance beam task, used to assess balance and fine motor coordination, no differences between the groups were observed in young animals (Fig. 3.30B). At 5 months, the MAPT/Tg4-42^{hom} line had a significantly reduced latency to fall compared to WT, MAPT, and Tg4-42^{hom} animals ($p<0.001$). At this age, no motor deficits were detected in the parental MAPT and Tg4-42^{hom} lines (Fig. 3.30E). At 9 months, Tg4-42^{hom} mice showed a clear motor deficit in the balance beam task compared to WT and MAPT mice ($p<0.001$), with a significantly reduced latency to fall, which was comparable to and not significantly different from the MAPT/Tg4-42^{hom} line (Fig. 3.30H). The findings observed in the balance beam test indicate that mice expressing both A$\beta_{4\text{-}42}$ and mutant tau P301S protein might present reduced motor performances regarding balance and fine motor skills at an earlier time point. At older ages, the motor deficits are comparable to mice only expressing A$\beta_{4\text{-}42}$. In the inverted grid task, differences were observed at neither time point nor in any of the analyzed lines (Fig. 3.30C,F,I).

Data partly published in (Zampar and Wirths 2021)

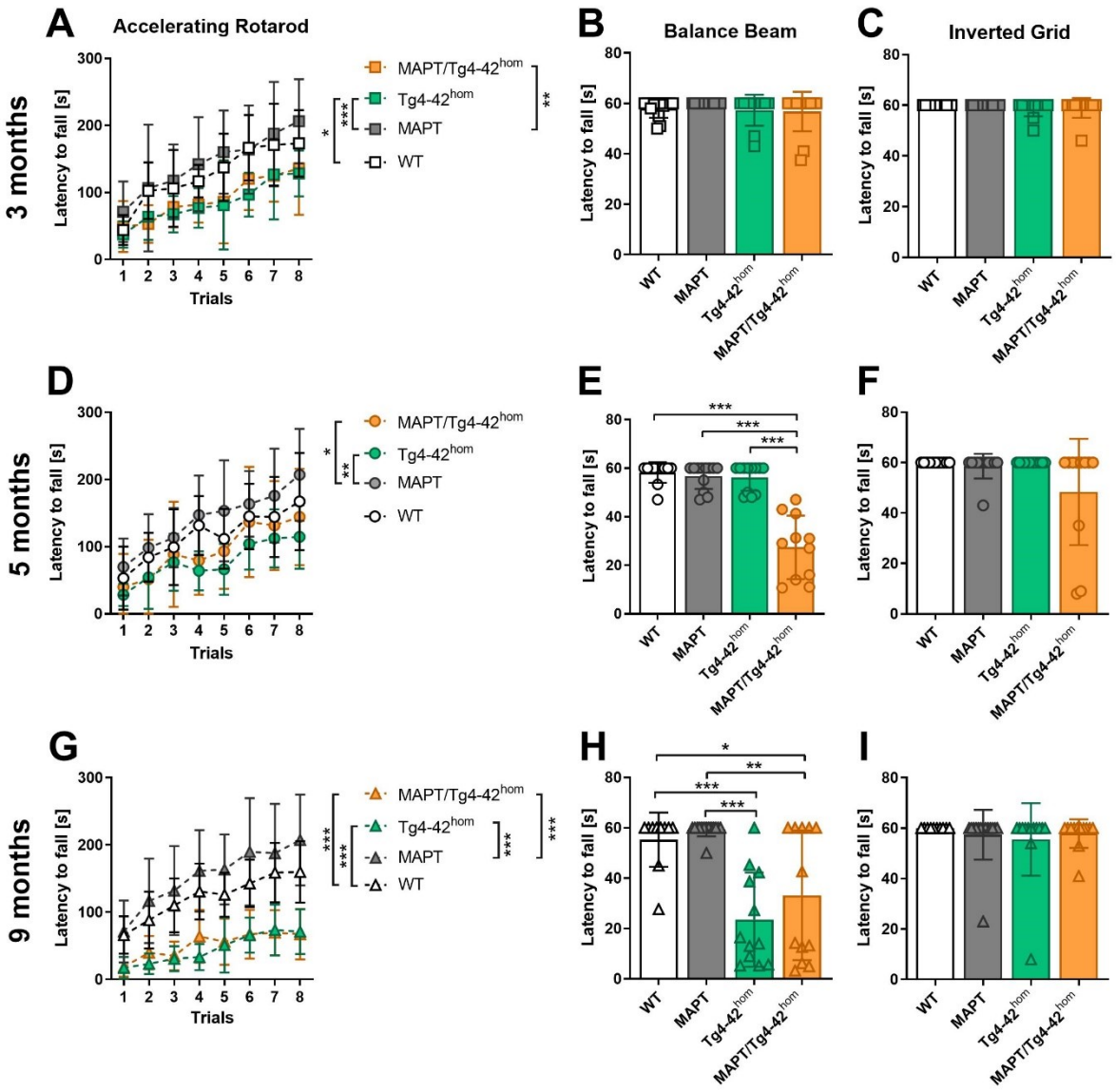

Fig. 3.30 Motor assessment of 3-, 5-, and 9-month-old MAPT/Tg4-42^{hom} mice, transgenic and WT controls. Female and male WT, MAPT, Tg4-42^{hom}, and MAPT/Tg4-42^{hom} mice (n=10-14) were tested at 3 (A-C), 5 (D-F) and 9 (G-I) months in the accelerating rotarod (A,D,G), balance beam (B,E,H) and inverted grid (C,F,I) tasks. Tg4-42^{hom} and MAPT/Tg4-42^{hom} mice presented motor deficits in the accelerating rotarod starting at 3 months and aggravating over time. In the balance beam task, MAPT/Tg4-42^{hom} displayed a reduced latency to fall at 5 months compared to WT, MAPT and Tg4-42^{hom}, a deficit that became evident also in the Tg4-42^{hom} line at 9 months of age. No significant differences were detected in the inverted grid test for all the considered ages. In this motor behavioral battery, the MAPT line did not show any motor deficits at the three considered time points compared to WT controls. All data are given as means ± SD. (A,D,G) Two-way ANOVA RM followed by Bonferroni's multiple comparison test, (B,C,E,F,H,I) One-way ANOVA followed by Bonferroni's multiple comparison test: *p<0.05, **p<0.01,***p<0.001.

Data partly published in (Zampar and Wirths 2021)

The MAPT line did not show any motor deficit in the performed tasks, even the aged group. Overall, the results of the motor assessment did not point towards a clear aggravation of the motor phenotype when $A\beta_{4-42}$ and protein tau are co-expressed.

The open field (OF) task was performed to address both general motor performances and anxiety-like behavior. No differences in average speed were found among the young groups (Fig. 3.31A). At 5 months, none of the transgenic lines performed significantly different from the WT control group but a significant increase in speed was observed in Tg4-42^{hom} mice compared to the MAPT line ($p<0.05$) (Fig 3.31B). Aged Tg4-42^{hom}, on the other hand, moved significantly less compared to MAPT and MAPT/Tg4-42^{hom} mice ($p<0.05$) (Fig 3.31C) but did not behave significantly different from the WT group. None of these motor-activity alterations observed in mice expressing $A\beta_{4-42}$ were found in the MAPT/Tg4-42^{hom}, which performed comparably to the WT and MAPT groups at all given time points but with a greater variability in the analyzed parameters. As observed in the above-described motor tasks, an aggravation was also not observed in the OF test in the bigenic line. Time spent in the center of the OF arena was used as a measure of anxiety-like behavior in mice. At 3 and 5 months of age, Tg4-42^{hom} mice displayed an increased time spent in the center of the arena compared to WT mice ($p<0.01$), indicating a decreased anxiety-like behavior. The increase in center time was significantly different also compared to the MAPT/Tg4-42^{hom} group at 3 ($p<0.05$) and 5 ($p<0.01$) months, which on the other hand explored the center of the arena comparably to WT and MAPT mice at both time points (Fig. 3.31D,E). At 9 months, MAPT, Tg4-42^{hom} and MAPT/Tg4-42^{hom} mice displayed an increase of time spent in the center. A statistically significant difference was measured only between Tg4-42^{hom} and WT animals ($p<0.05$) (Fig. 3.31F), while no difference was detected between Tg4-42^{hom} and MAPT/Tg4-42^{hom} lines at this time point.

Data partly published in (Zampar and Wirths 2021)

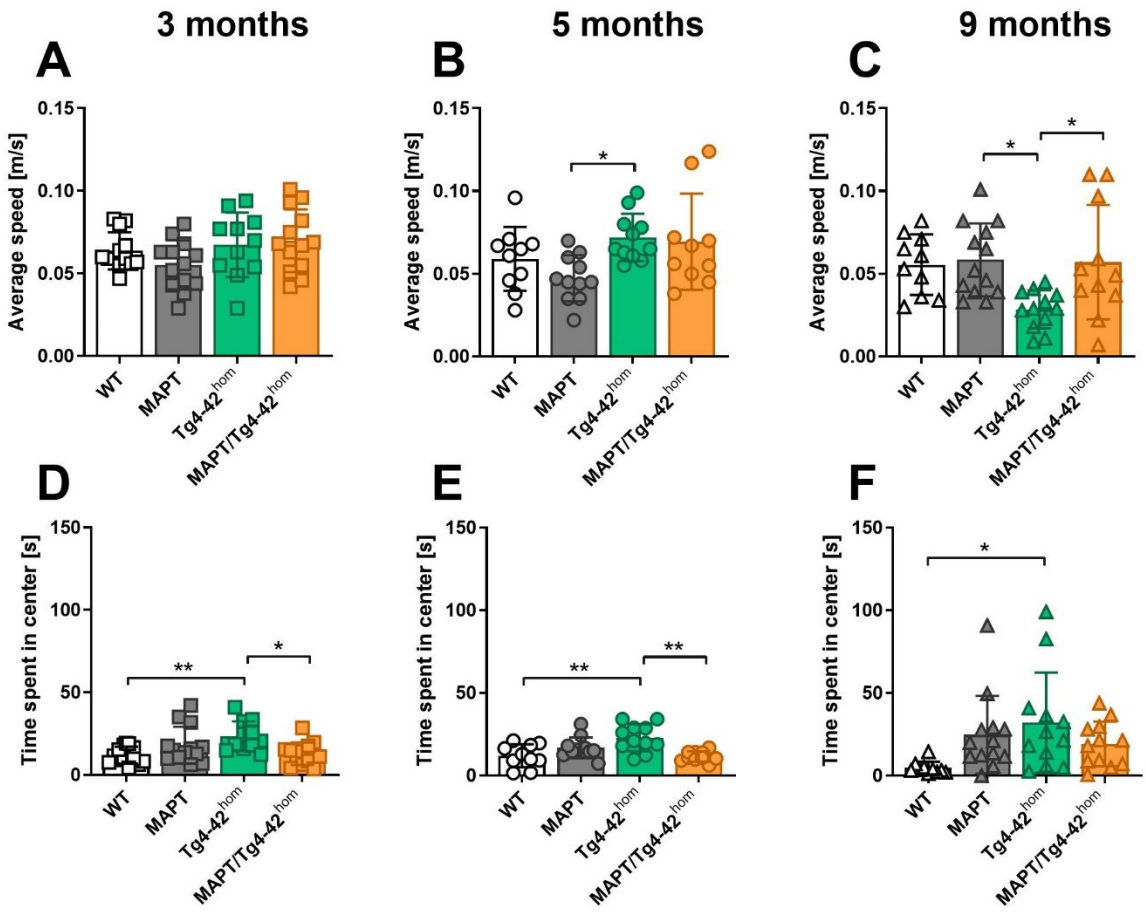

Fig. 3.31 Open field task in 3-, 5-, and 9-month-old MAPT/Tg4-42^{hom} mice, transgenic and WT controls. Female and male WT, MAPT, Tg4-42^{hom} and MAPT/Tg4-42^{hom} mice (n=10-14) were tested at 3 (A,D), 5 (B,E) and 9 (C,F) months. No differences in average speed were found at 3 months between the groups (A), and only a significant difference between MAPT and Tg4-42^{hom} at 5 months (B). 9-month-old Tg4-42^{hom} presented a reduced average speed compared to MAPT and MAPT/Tg4-42^{hom} mice (C). Starting already at 3 months, the Tg4-42^{hom} line presented an increase time spent in center of the arena compared to WT and MAPT/Tg4-42^{hom} mice (D), a finding observed also at the 5-month time point (E). Older MAPT, Tg4-42^{hom} and MAPT/Tg4-42^{hom} mice displayed an increased center time, but with significant difference only between WT and Tg4-42^{hom} mice (F). All data are given as means ± SD. One-way ANOVA followed by Bonferroni's multiple comparison test: *p<0.05, **p<0.01.

Data partly published in (Zampar and Wirths 2021)

Anxiety-like behavior was assessed also in the elevated plus maze (EPM) task, as a measure of time spent in the open arm of the maze. Contrary to the findings in the OF test, no alteration in anxiety-like behavior was observed in young Tg4-42^{hom} (Fig. 3.32A). At 5 months of age, Tg4-42^{hom} and MAPT/Tg4-42^{hom} mice displayed a significant increase in time spent in open arms compared to WT ($p<0.01$ and $p<0.001$, respectively) and MAPT ($p<0.01$ and $p<0.01$, respectively) mice (Fig. 3.32C). At 9 months, the significantly reduced anxiety-like behavior was again observed in the Tg4-42^{hom} and MAPT/Tg4-42^{hom} line compared to WT animals ($p<0.05$ and $p<0.001$, respectively) (Fig. 3.32E). Aged MAPT mice also presented an increased time spent in open arms but due to high variability, the increase did not reach statistical significance compared to WT littermates. Analysis of the arm entries as a measure for different exploration activity between the groups revealed no critical differences at the three considered time points (Fig. 3.32B,D,F). In the EPM, no differences were detected in anxiety-like behavior between Tg4-42^{hom} and MAPT/Tg4-42^{hom} mice in any of the age groups.

Learning and memory was analyzed through the cross maze, novel object recognition (NOR) and Morris Water Maze (MWM) tasks. In the cross maze, which assesses working memory, no significant differences were observed in the alternation rates between the groups at 3 and 5 months of age (Fig. 3.32G,I). In aged animals, MAPT mice displayed a significant reduced alternation rate compared to WT littermates ($p<0.01$) (Fig. 3.32K), indicating working memory deficits in this line. This deficit was also observed in MAPT mice co-expressing Aβ_{4-42} when compared to WT ($p<0.001$), as well as to Tg4-42^{hom} mice ($p<0.01$) that, on the other hand, did not present working memory deficits in this task.

Data partly published in (Zampar and Wirths 2021)

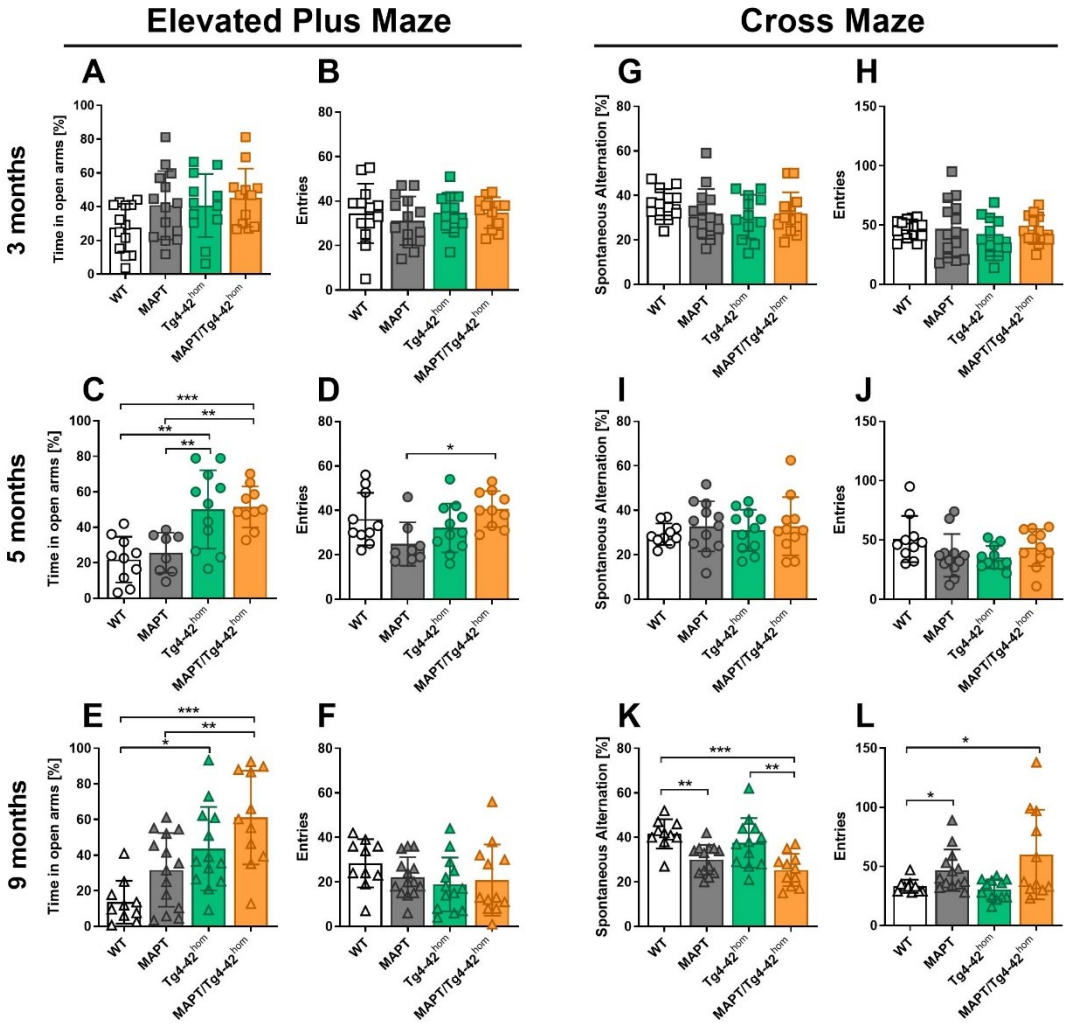

Fig. 3.32 Elevated plus maze and cross maze tasks in 3-, 5-, and 9-month-old MAPT/Tg4-42^{hom} mice, transgenic and WT controls.

Female and male WT, MAPT, Tg4-42^{hom}, and MAPT/Tg4-42^{hom} mice (n=10-14) were tested at 3 (A,B,G,H), 5 (C,D,I,J) and 9 (E,F,K,L) months in the elevated plus maze (A-F) and cross maze (G-L) tasks. No alteration in time spent in open arms and arm entries were detected between the young groups (A,B). At 5 months, both Tg4-42^{hom} and MAPT/Tg4-42^{hom} mice displayed a significantly increased time in open arms compared to WT and MAPT animals, and a significant increase in arm entries between MAPT and MAPT/Tg4-42^{hom} mice (C,D). In aged animals, Tg4-42^{hom} and MAPT/Tg4-42^{hom} mice still displayed a significantly increased time in open arms compared to WT, while as an increase in time was present in the MAPT line, a significant difference was found between MAPT and MAPT/Tg4-42^{hom} mice only (E). No differences in arm entries were detected at this time point (F). No differences in working memory, measured as alternation rate in the cross maze tests, as well as differences in arm entries were found at 3 and 5 months (G-J), while in aged animals, a reduced alternation rate was observed in MAPT and MAPT/Tg4-42^{hom} mice compared to WT littermates (K), accompanied by an increase in arm entries (L). All data are given as means ± SD. One-way ANOVA followed by Bonferroni's multiple comparison test: *p<0.05, **p<0.01, ***p<0.001.

Data partly published in (Zampar and Wirths 2021)

In contrast to the two earlier time points, differences in arm entries were observed at 9 months of age, with an increased exploration for MAPT and MAPT/Tg4-42^{hom} mice compared to WT animals ($p<0.05$) (Fig. 3.32L). Recognition memory was assessed with the NOR test. The OF test was used as habituation phase and 24h later, on the first day of the NOR task, the mice performed a training trial in which they were exposed to two identical objects. Exploration times of the two objects were recorded and compared. At the three analyzed time points, no preference was observed between the two identical objects, with all mice exploring them a comparable amount of time (Fig. 3.33A,E,I). On the second day of the NOR task, 24h after the training trial, the test trial was performed. One of the identical objects was replaced with a novel object and the exploration times between the novel and familiar objects were compared. At 3 and 5 months of age, WT and the three transgenic lines spent significantly more time exploring the novel object compared to the familiar one (Fig. 3.33B,F), which indicates an intact recognition memory. The discrimination index (DI), a measure of the preference of the mice toward the novel object, was used to discern differences among the genotypes. At 3 months, a significant difference in DI was found between WT and Tg4-42^{hom} mice ($p<0.05$), which was likely due to the small variability within the values inside each group (Fig. 3.33C). Both lines, in fact, displayed positive DI values (~0.5 in WT and ~0.3 in Tg4-42^{hom} group), indicating the preference for the novel object in the NOR test and excluding the presence of a recognition memory deficit in the Tg4-42^{hom} line at this time point. At 5 months, no significant differences were found in DIs between the groups (Fig. 3.33G). Analysis of total exploration time on the test trail day showed no differences in the total time spent exploring the objects at either 3 and 5 months between the genotypes (Fig. 3.33D,H), excluding an eventual influence of exploration on the outcome of the task.

Data partly published in (Zampar and Wirths 2021)

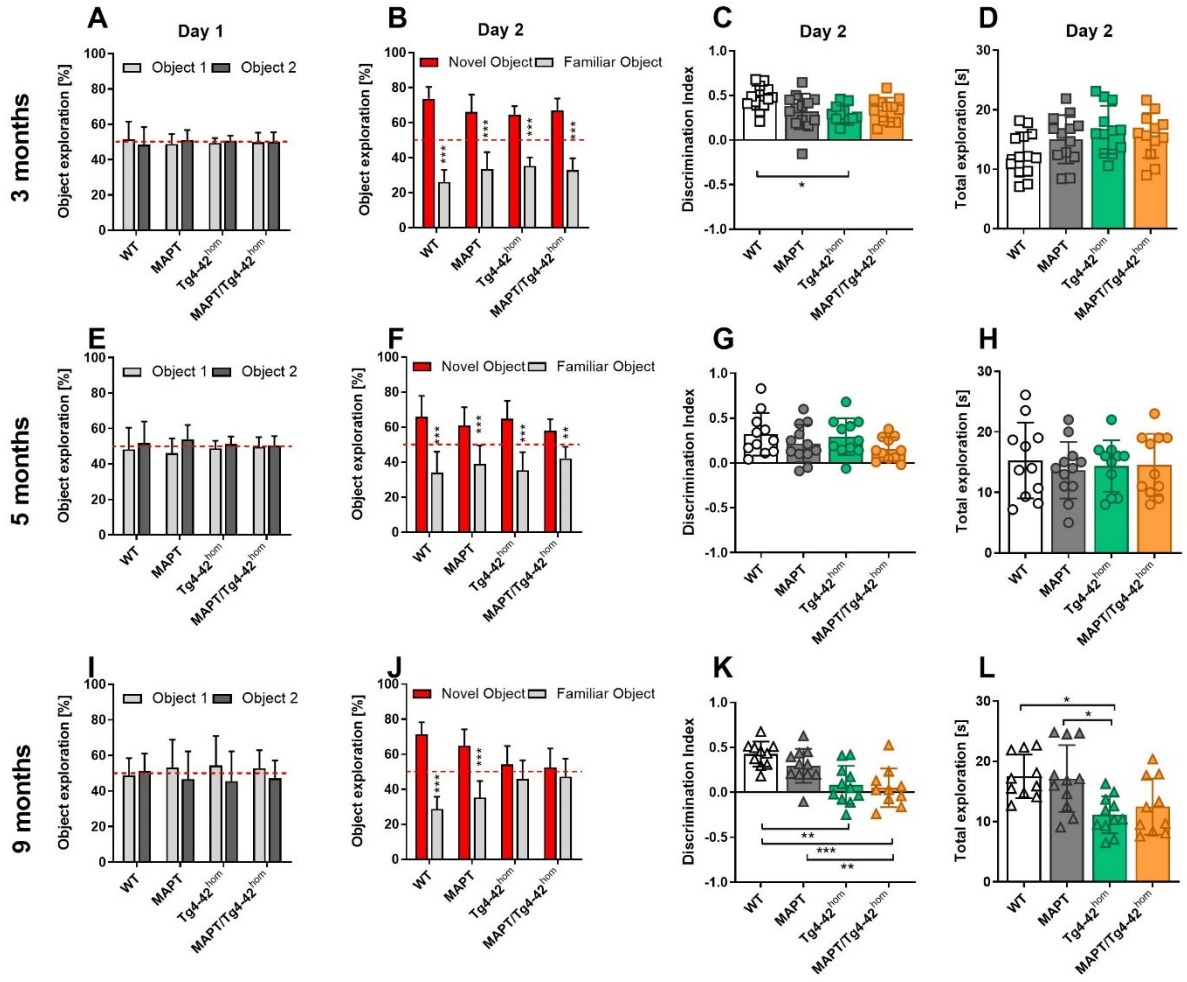

Fig. 3.33 Novel object recognition task in 3-, 5-, and 9-month-old MAPT/Tg4-42^{hom} mice, transgenic and WT controls.

Female and male WT, MAPT, Tg4-42^{hom}, and MAPT/Tg4-42^{hom} mice (n=10-14) were tested at 3 (A-D), 5 (E-H), and 9 (I-L) months. The training trial on day 1 showed no difference in exploration between the two identical objects in all groups at the considered time points (A,E,I). No recognition memory deficits were observed at 3 and 5 months for WT and the three transgenic lines (B,F), as they all significantly explored more the novel object compared to the familiar one. At 9 months both Tg4-42^{hom} and MAPT/Tg4-42^{hom} mice displayed recognition memory deficits, equally exploring the novel and familiar object on the test trial on day 2 (J). Discrimination index was further used as a parameter to compare the performances between the analyzed lines, showing a clear deficit in recognition memory in old Tg4-42^{hom} and MAPT/Tg4-42^{hom} mice compared to WT and MAPT mice (C,G,K). Total exploration time on the test trial on day 2 was measured and, while no differences were observed in 3- and 5-month-old animals (D,H), aged Tg4-42^{hom} animals explored significantly less than WT and MAPT mice (L). All data are given as means ± SD. (A,B,E,F,I,J) red line represents 50%, Two-way ANOVA followed by Bonferroni's multiple comparison test, (C,D,G,H,J,L) One-way ANOVA followed by Bonferroni's multiple comparison test: *p<0.05, **p<0.01, ***p<0.001.

Data partly published in (Zampar and Wirths 2021)

At 9 months, Tg4-42^{hom} mice displayed a clear deficits in the NOR task, as no significant difference was observed in the exploration between novel and familiar object (Fig. 3.33J), which is in line with previous findings showing a memory deficit in the NOR tasks in Tg4-42^{hom} mice starting at 6 months of age (Stazi and Wirths 2021). Similarly, MAPT/Tg4-42^{hom} mice did not show any preference toward the novel object, which they explored a comparable amount of time to the familiar one. On the other hand, aged WT and MAPT mice did not present any recognition memory deficit. A comparison of the DIs confirmed these observations. While WT and MAPT animals showing positive indexes, Tg4-42^{hom} and MAPT/Tg4-42^{hom} presented with DIs were close to a zero value, indicating no preference between the novel and familiar objects (Fig. 3.33K). A significant reduction in DIs was found in Tg4-42^{hom} compared WT animals ($p<0.01$) and in MAPT/Tg4-42^{hom} compared to WT ($p<0.001$) and to MAPT mice ($p<0.01$). In aged mice, a significant reduction in total exploration time was observed in Tg4-42^{hom} compared to WT and MAPT mice ($p<0.05$) (Fig. 3.33L).

Lastly, spatial memory was assessed in the MWM test. The presence of sensory and motor deficits in this test was checked during the first 3 days of cue training. At 3 and 5months, WT and transgenic lines displayed a progressively reduced escape latency. In young mice, MAPT/Tg4-42^{hom} showed a slight but significant increase in escape latency compared to Tg4-42^{hom} mice ($p<0.05$), and at 5 months the time to reach the visible platform was significantly increased in comparison to WT ($p<0.01$) and MAPT ($p<0.001$) animals (Fig. 3.34A,B). In aged animals, the expected reduction in escape latency over time was observed in the WT, MAPT and Tg4-42^{hom} groups (Fig. 3.34C), although significant increases in latencies were observed in MAPT and Tg4-42^{hom} mice compared to WT ($p<0.05$ and $p<0.01$, respectively).

Data partly published in (Zampar and Wirths 2021)

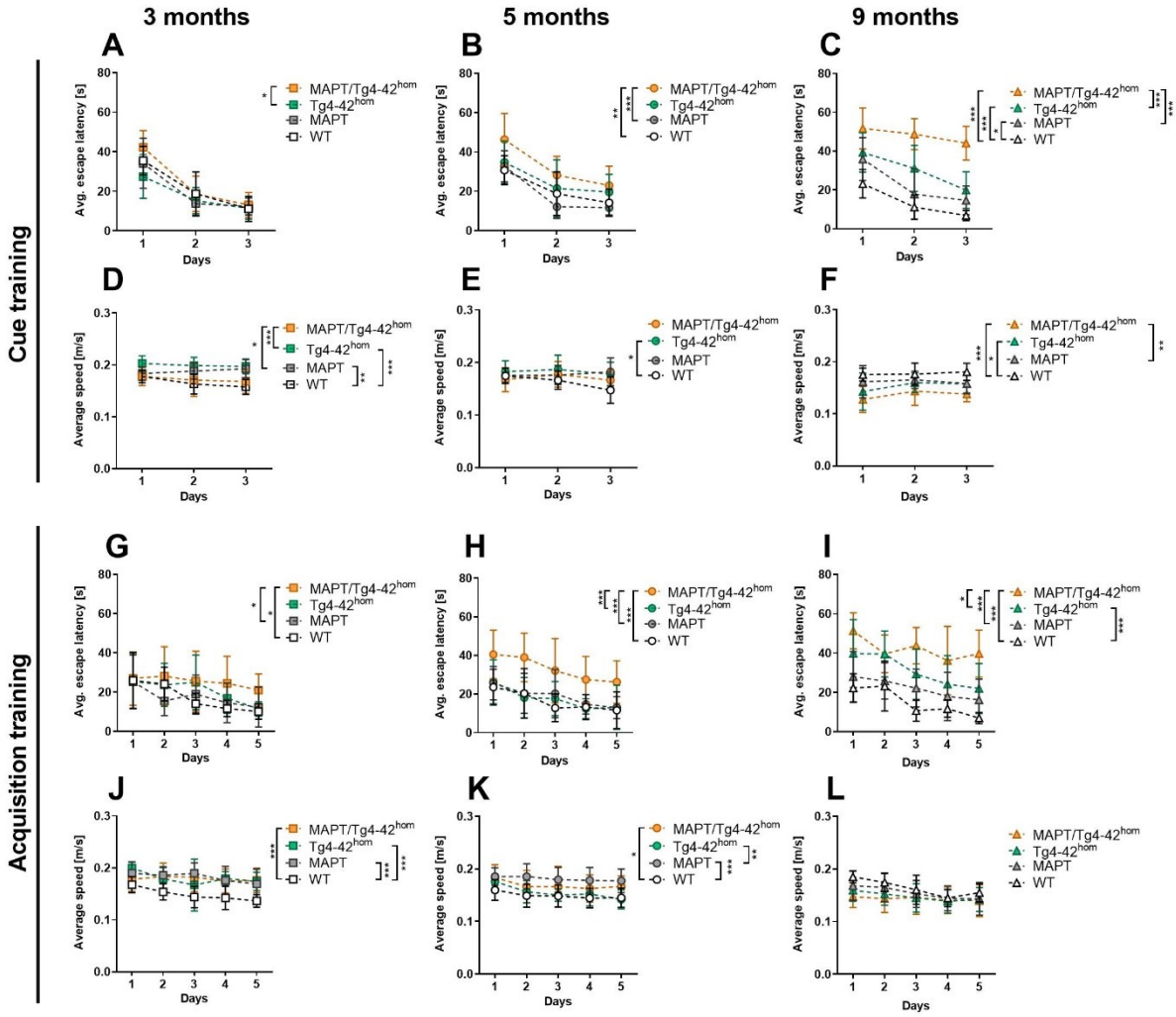

Fig. 3.34 Cue and acquisition trainings of Morris Water Maze task in 3-, 5- and 9-month-old MAPT/Tg4-42^{hom} mice, transgenic and WT controls.

Female and male WT, MAPT, Tg4-42^{hom} and MAPT/Tg4-42^{hom} mice (n=10-14) were tested at 3 (A,D,G,J), 5 (B,E,H,K) and 9 (C,F,I,L) months. Cue training (A-F) was performed during the first 3 days. Increased escape latency was observed in MAPT/Tg4-42^{hom} mice compared to Tg4-42^{hom} in young animals (A) as well as at the intermediate time point compared to WT and MAPT mice (B). In the aged group, all the transgenic lines displayed a significantly increased escape latency compared to WT, and MAPT/Tg4-42^{hom} mice performed worse than MAPT animals (C). Differences in average swimming speed between the groups were found at the three time points during the cue training (D-F). Spatial learning deficits were found in MAPT/Tg4-42^{hom} mice at 3, 5 and 9 months (G,H,I), as well as in aged Tg4-42^{hom} animals. WT mice were found to swim significantly slower compared to the transgenic lines at 3 months (J), a finding partially observed also in the intermediate time point (K). No differences in speed were found in aged animals (L). All data are given as means ± SD. Two-way ANOVA RM followed by Bonferroni's multiple comparison test: *p<0.05, **p<0.01, ***p<0.001.

Data partly published in (Zampar and Wirths 2021)

Aged MAPT/Tg4-42^{hom} animals performed poorly, with almost no decrease over time in escape latency, which significantly differed from WT, MAPT, and Tg4-42^{hom} mice ($p<0.001$). In terms of motor performance, WT and MAPT/Tg4-42^{hom} mice displayed comparable average speeds at 3 months, even though they were significantly slower than MAPT ($p<0.01$ and $p<0.05$, respectively) and Tg4-42^{hom} animals ($p<0.001$ and $p<0.01$, respectively) (Fig. 3.34D). At the intermediate time point, the only difference in speed was observed in Tg4-42^{hom} mice, swimming significantly faster than WT mice ($p<0.05$) (Fig. 3.34E). At 9 months, Tg4-42^{hom} and MAPT/Tg4-42^{hom} displayed significantly reduced swimming speeds compared to WT ($p<0.05$ and $p<0.001$, respectively), as well as the bigenic line compared to MAPT mice ($p<0.01$) (Fig 3.34F). During the 5 days of acquisition training, young MAPT/Tg4-42^{hom} mice showed a spatial learning deficit compared to WT and MAPT, with a significantly increased average escape latency ($p<0.05$) (Fig. 3.34G). This deficit became more obvious at 5 months, when the co-expressing A$\beta_{4\text{-}42}$ and mutant human tau line caused a significant increase in the time to find the hidden platform in MAPT/Tg4-42^{hom} mice compared to WT and both parental transgenic lines ($p<0.001$) (Fig 3.34H). As expected, at 9 months the Tg4-42^{hom} line displayed a spatial learning deficit compared to WT littermates ($p<0.05$) (Fig. 3.34I), as a progressive increase in escape latency with aging was previously shown in Tg4-42^{hom} mice (Antonios et al. 2015). During the acquisition training, young WT mice swam significantly slower compared to the transgenic lines ($p<0.001$) (Fig. 3.34J), a reduction partially observed also in 5-month-old WT when compared to MAPT mice ($p<0.001$) and the bigenic line ($p<0.05$) (Fig. 3.34K). At this time point, Tg4-42^{hom} mice presented with significantly slower swimming speed than MAPT mice ($p<0.01$), while in the older mice no significant differences were detected between the groups during the acquisition training (Fig. 3.34L). 24h after the last day of acquisition training, spatial reference memory deficits were assessed in a single probe trial, during which the hidden platform was removed, and the time spent swimming in the different quadrants was recorded.

Data partly published in (Zampar and Wirths 2021)

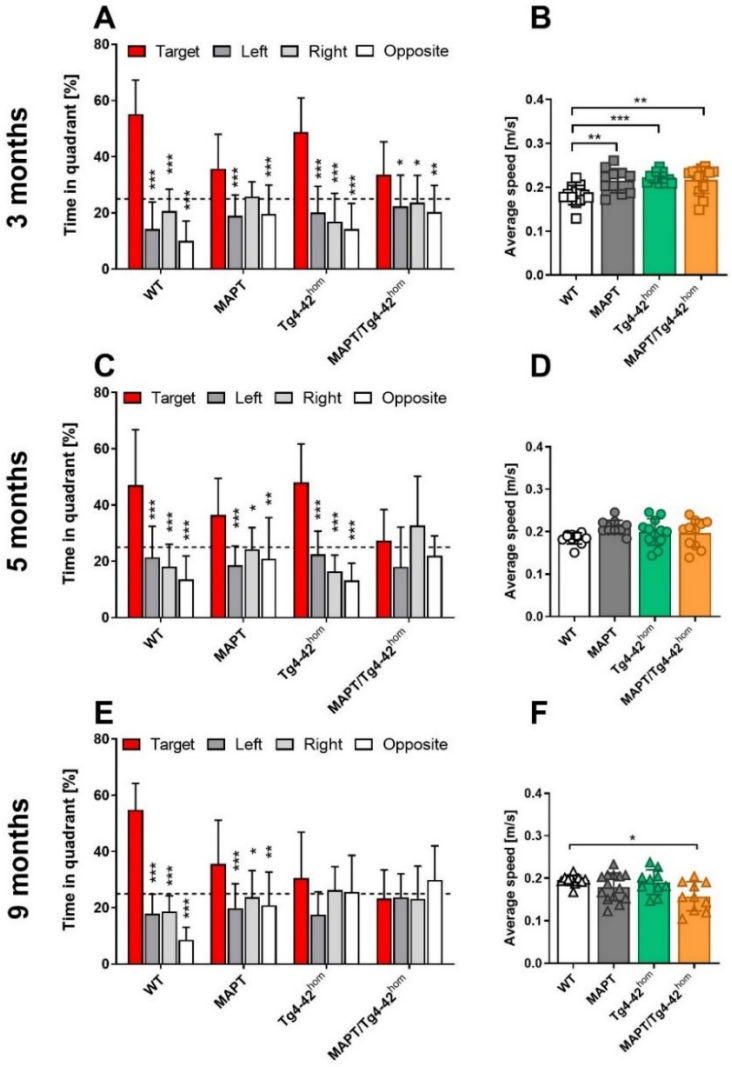

Fig. 3.35 Probe trial of MWM task in 3-, 5-, and 9-month-old MAPT/Tg4-42^{hom} mice, transgenic and WT controls.

Female and male WT, MAPT, Tg4-42^{hom} and MAPT/Tg4-42^{hom} mice (n=10-14) were tested at 3 (A,B), 5 (C,D) and 9 (E,F) months. At 3 months, no deficits in spatial reference memory were observed, as all the groups spent significantly more time swimming in the target quadrant (A). At 5 months, MAPT/Tg4-42^{hom} mice did not show a preference for the target quadrant, in contrast to WT and the two parental transgenic lines (C), indicating the development of a spatial memory deficits. As expected, aged Tg4-42^{hom} mice displayed a severe spatial reference memory deficit, still observed also in the bigenic line (E). Young WT mice swam significantly slower than the transgenic lines during the probe trial in the earl time point (B), while no differences in speed were found at 5 months (C). In contrast, aged MAPT/Tg4-42^{hom} presented with a significantly reduced speed compared to WT littermates (F). All data are given as means ± SD. (A,C,E) black line represents 25%, Two-way ANOVA followed by Bonferroni's multiple comparison test, (B,D,F) One-way ANOVA followed by Bonferroni's multiple comparison test: *p<0.05, **p<0.01, ***p<0.001.

Data partly published in (Zampar and Wirths 2021)

In young mice, each group showed a significant preference towards the target quadrant, indicative of a lack of spatial reference memory deficits (Fig. 3.35A). All the three young transgenic lines swam significantly faster than the WT control group ($p<0.001$) (Fig. 3.35B). At 5 months, no deficit was observed in WT nor in the two parental transgenic lines, but mice co-expressing $A\beta_{4\text{-}42}$ and transgenic tau performed poorer, showing no preference for the target compared to the other quadrants (Fig. 3.35C). As suggested already by the observed spatial learning deficits during the acquisition training, the absence of preference might indicate spatial memory deficits in this line at this age and an aggravation compared to the two parental lines. No differences in average speed were found at the intermediate time point (Fig. 3.35D). As expected, and anticipated by the findings of the acquisition training, aged Tg4-42^{hom} mice displayed severe spatial reference memory deficits, which were also maintained in the bigenic line (Fig. 3.35E). At 9 months a significant decrease in average speed was observed in MAPT/Tg4-42^{hom} mice compared to WT littermates ($p<0.05$) (Fig. 3.35F), indicating that potential motor alterations might have influenced the outcome of the probe trial.

To compare the performances among the different lines during the probe trial, additional parameters were extracted from the existing recordings. Time spent in the target quadrant, a measure of target preference, was compared between the groups at the different time points. At 3 months, MAPT mice showed a significantly decreased time in target quadrant compared to WT ($p<0.01$) littermates (Fig. 3.36A). The bigenic line also showed a significant reduction compared to WT ($p<0.001$) and Tg4-42^{hom} ($p<0.05$) mice, indicating a poorer performance already at young age. This reduction, together with the increased latency in the acquisition training, suggests the development of spatial learning deficit in MAPT/Tg4-42^{hom} mice already at 3 months of age.

Data partly published in (Zampar and Wirths 2021)

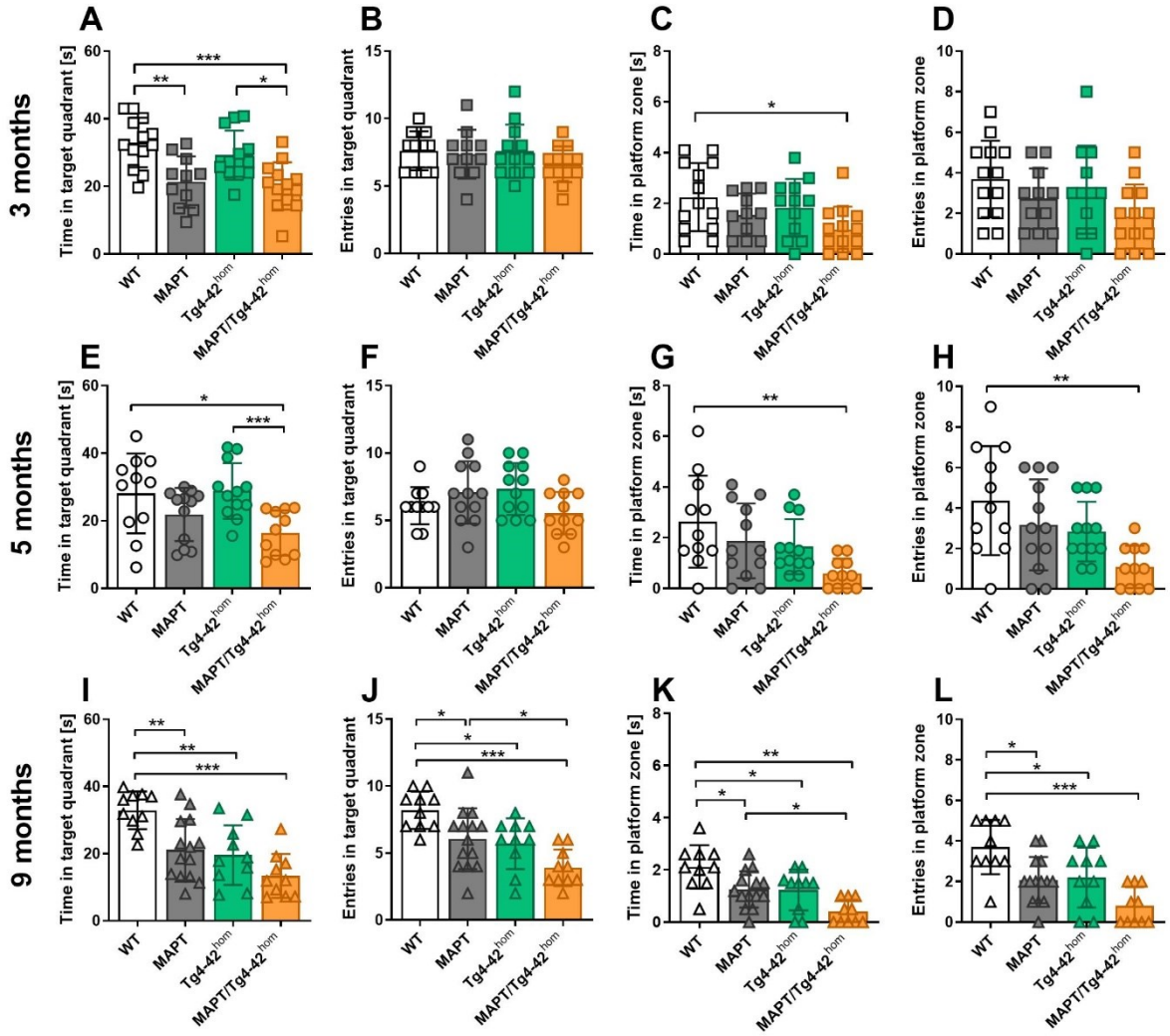

Fig. 3.36 Times and entries in target quadrant and platform zone during the probe trial of MWM task in 3-, 5-, and 9-month-old MAPT/Tg4-42^{hom} mice, transgenic and WT controls.

Female and male WT, MAPT, Tg4-42^{hom} and MAPT/Tg4-42^{hom} mice (n=10-14) were tested at 3 (A-D), 5 (E-H), and 9 (I-L) months. A significant reduction in time spent in the target quadrant was observed in MAPT/Tg4-42^{hom} mice at 3 (A) and 5 (E) months compared to Tg4-42^{hom} mice and WT controls, a reduction observed in all the three transgenic lines at 9 months (I), accompanied by a reduced number of entries in the quadrant (J). No differences of entries in the target quadrant were observed at the earlier time points (B,F). MAPT/Tg4-42^{hom} mice, moreover, presented a reduced exploration of the platform zone compared to WT controls at 3 (C) and 5 months (G), while in aged animals a significant reduction was observed in all the transgenic lines, even though the bigenic mice performed worst (K). Altered entries in the platform zone were registered in MAPT/Tg4-42^{hom} at the intermediate time point (H), an alteration that was later found in the three transgenic lines at 9 months (L). All data are given as means ± SD. One-way ANOVA followed by Bonferroni's multiple comparison test: *p<0.05, **p<0.01, ***p<0.001.

Data partly published in (Zampar and Wirths 2021)

At 5 months, as already suggested from the lack of preference towards the target quadrant, MAPT/Tg4-42^{hom} mice spent significantly less time in the target quadrant compared to WT ($p<0.05$) and Tg4-42^{hom} ($p<0.001$) mice, while the two parental transgenic lines did not display any significant difference compared to WT controls (Fig. 3.36E). In aged animals, where spatial memory deficits were prominent in both Tg4-42^{hom} and MAPT/Tg4-42^{hom}, an expected significant reduction in time spent in target quadrant was observed compared to WT ($p<0.01$ and $p<0.001$, respectively) (Fig. 3.36I). At this time point, the MAPT line displayed a significant reduction as well ($p<0.01$). No alteration in entries in the target quadrant were observed at the young and intermediate time points (Fig. 3.36B,F), while aged transgenic mice entered the target quadrant significantly less frequently than the WT line (Fig. 3.36J). MAPT/Tg4-42^{hom} animals displayed, at this time point, the least number of entries among the transgenic line, showing a significant difference also compared to the MAPT parental line ($p<0.05$). The time spent in the actual platform zone could be considered a measure of fine spatial memory. Mice expressing both A$\beta_{4\text{-}42}$ and mutant human protein tau performed significantly worse than WT controls ($p<0.05$) already at 3 months in this parameter (Fig. 3.36C). This difference increased at 5 months ($p<0.01$) (Fig. 3.36G) and was accompanied by a significant reduction of entries in the platform zone (Fig 3.36H). Such differences were not observed in the two parental transgenic lines. In aged animals, a reduction of time spent and entries in the platform zone was found in all the transgenic lines (Fig. 3.36K,L), with MAPT/Tg4-42^{hom} animals presenting the most pronounced reduction.

Data partly published in (Zampar and Wirths 2021)

3.4.3 CA1 pyramidal neuron loss MAPT/Tg4-42^{hom} mice

To understand whether the cognitive phenotype observed in the MAPT/Tg4-42^{hom} line could be caused by an increased and differential neuron loss, the number of pyramidal neurons of the CA1 region of the hippocampus was compared between the lines at the three considered time points. Sagittal paraffin sections were stained with hematoxylin and neurons, sub-classified into the distal and proximal part of the CA1 pyramidal layer, were counted. The distal and proximal part of the hippocampus were associated with differential types of memory, with the distal part being specifically involved with non-spatial memory and the proximal part being more important for spatial-related memory (Masurkar 2018). The expected time-dependent neuron loss was observed in the Tg4-42^{hom} line, and was more severe towards the distal part of the CA1 pyramidal layer (Stazi and Wirths 2021), while MAPT mice showed no pyramidal neuron loss in the hippocampus at the considered time points (Fig. 3.37A-F). As evident in the Tg4-42^{hom} parental line, mice co-expressing A$\beta_{4\text{-}42}$ and P301S protein tau also presented a time-dependent neuron loss. A significant reduction in distal CA1 pyramidal neurons at 3 months (Fig. 3.37B) but aside from this finding, the bigenic line showed a similar neuron loss as Tg4-42^{hom} in both the distal and proximal CA1, thus indicating no aggravation due to the co-expression of mutated human protein tau.

Data partly published in (Zampar and Wirths 2021)

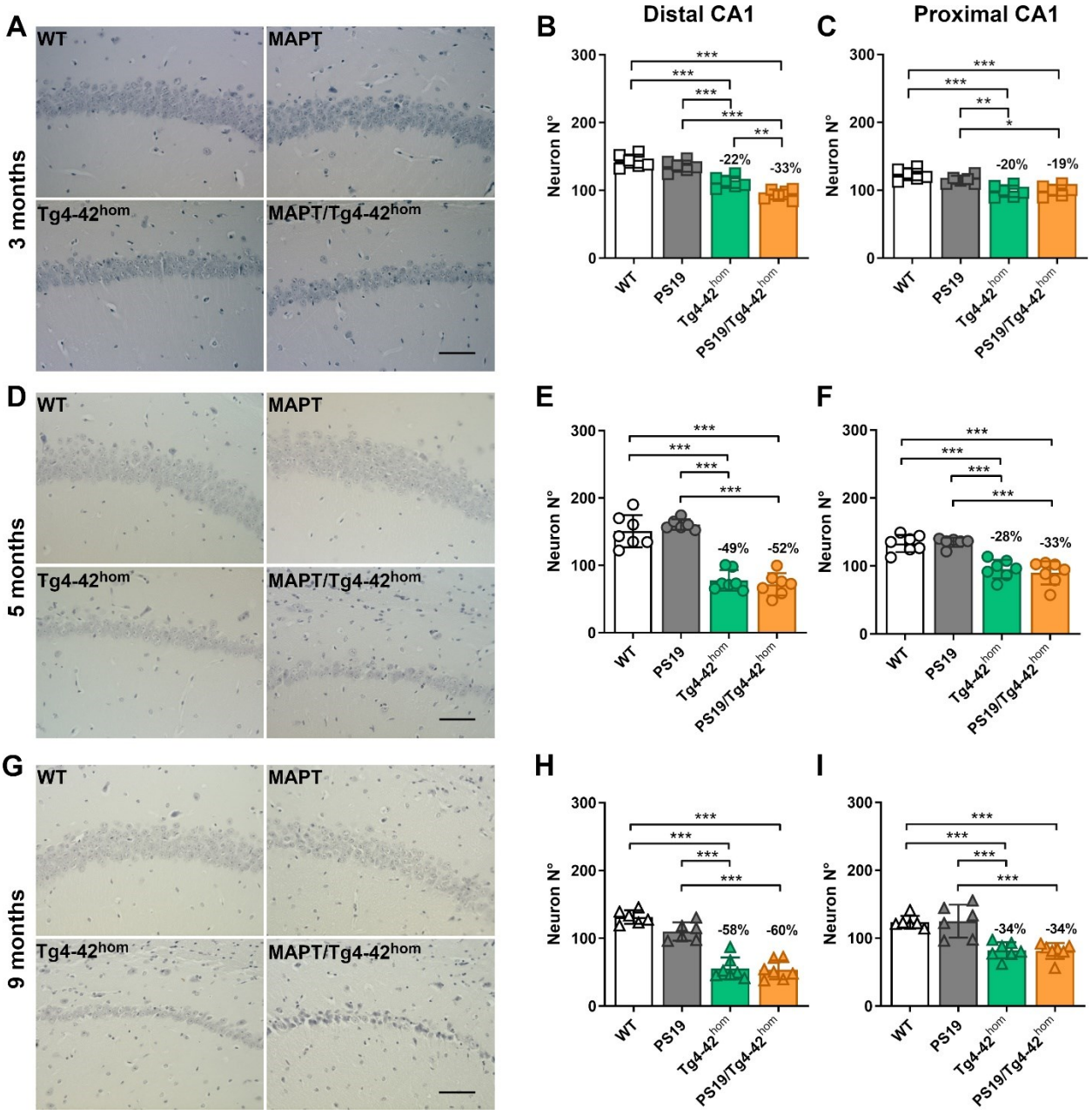

Fig. 3.37 Distal and proximal CA1 pyramidal neuron loss in 3-, 5-, and 9-month-old MAPT/Tg4-42^{hom} mice, transgenic and WT controls.

Sagittal paraffin brain sections (n=3 per animal) from female and male WT, MAPT, Tg4-42^{hom}, and MAPT/Tg4-42^{hom} mice (n=6-7) were stained with hematoxylin. Pictures were taken from the distal and proximal part of the hippocampal CA1 pyramidal layer at 400x magnification. (A,D,G) Example images of distal CA1 pyramidal layer at 3 (A), 5 (D) and 9 (G) months. Tg4-42^{hom} and MAPT/Tg4-42^{hom} mice displayed a comparable neuron loss at 5 and 9 months in both distal and proximal CA1 (D-G). In young MAPT/Tg4-42^{hom} mice, a significant reduction in neuron numbers was observed compared to Tg4-42^{hom} in the distal, but not in the proximal, CA1 region (B). All data are given as means ± SD. One-way ANOVA followed by Bonferroni's multiple comparison test: *p<0.05, **p<0.01, ***p<0.001. (A,C,E) Scale bar: 50 µm.

Data partly published in (Zampar and Wirths 2021)

3.4.4 Hippocampal Aβ and tau pathology in MAPT/Tg4-42^{hom} mice

Fluorescent double staining was performed to investigate whether Aβ$_{4-42}$ and mutant human tau co-localize within neurons in the bigenic line. Pyramidal neurons in the CA1 region of the hippocampus were analyzed as the main brain region expressing the Aβ transgene in Tg4-42^{hom} mice (Fig. 3.38). No major co-localization was observed in the MAPT/Tg4-42^{hom} line.

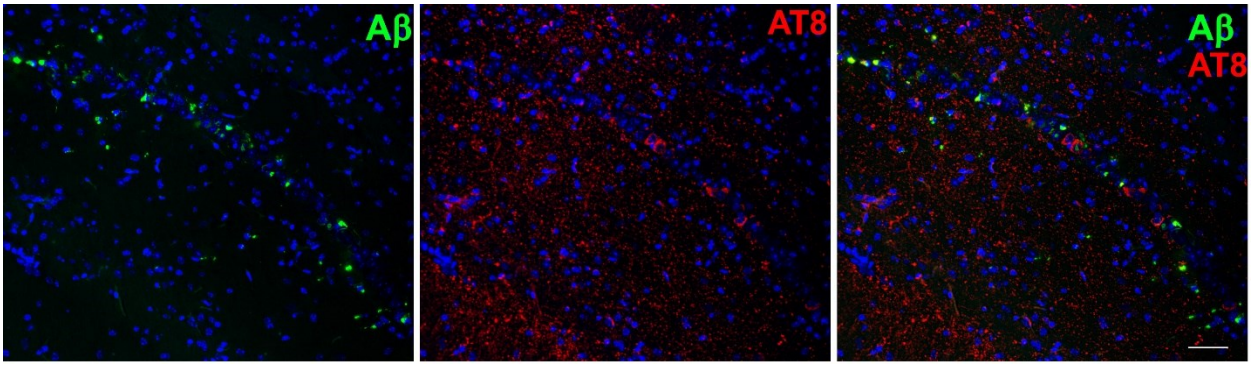

Fig. 3.38 Fluorescent staining of Aβ$_{4-42}$ and tau protein co-localization in MAPT/Tg4-42^{hom} mice.
Example images of hippocampal CA1 pyramidal layer from a 3 months MAPT/Tg4-42^{hom} mouse, taken with 200x magnification. Fluorescent staining was performed with the 24311 antibody to detect Aβ$_{4-42}$ (green) and AT8, binding to phosphorylated protein tau (red). DAPI nuclei counterstaining is present in all three images (blue). Scale bar: 100 μm

Next, to determine whether tau expression influences Aβ pathology, sagittal paraffin brain sections were immunohistochemically stained with the pan-Aβ antibody 24311. Quantification of Aβ load was performed in the pyramidal layer of the CA1 region of the hippocampus in Tg4-42^{hom} and MAPT/Tg4-42^{hom} mice at the three considered time points (Fig. 3.39). Intraneuronal accumulation was detectable with no significant difference in immunoreactivity between the two lines at any age.

Data partly published in (Zampar and Wirths 2021)

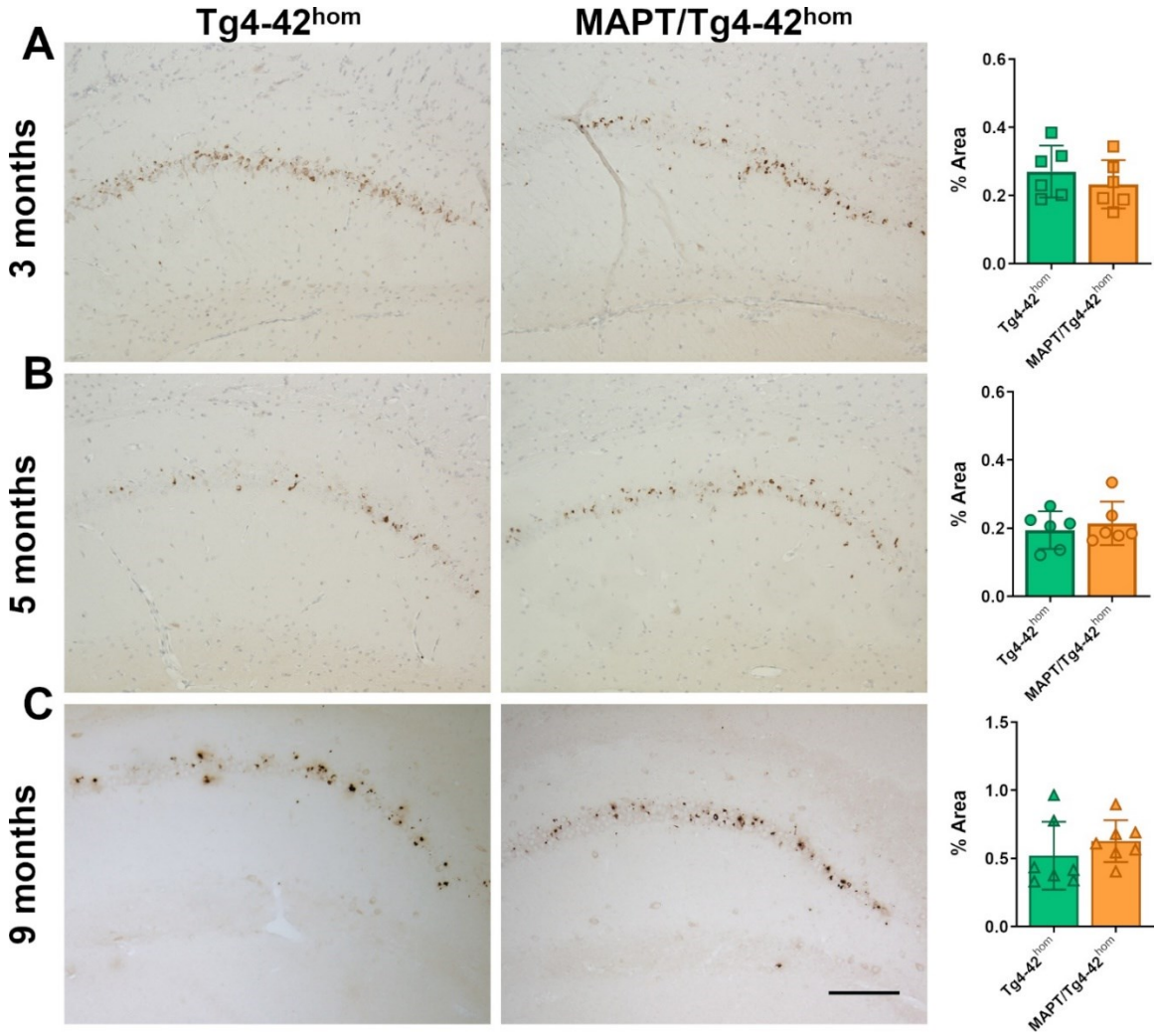

Fig. 3.39 Aβ4-42 CA1 immunohistochemical staining and load analysis in 3-, 5-, and 9-month-old MAPT/Tg4-42hom and Tg4-42hom mice.
DAB staining and load analysis of Aβ were performed in the CA1 region of the hippocampus at 3 (A), 5 (B), and 9 (C) months in female and male Tg4-42hom and MAPT/Tg4-42hom mice (n=6-7). 3 sagittal paraffin brain sections per animal were stained using the pan-Aβ antibody 24311 and images taken 100x magnification for load quantification analysis. No difference in % Area covered were found between the two lines at any considered time point. All data are given as means ± SD. Unpaired t-test. Scale bar: 100 μm.

Subsequently, tau pathology was analyzed in MAPT and MAPT/Tg4-42hom mice to assess if Aβ4-42 might aggravate tau pathology. Load analysis of staining performed with the AT8 antibody, recognizing two phosphorylated tau epitopes (pS202/pT205), revealed no significant differences in CA1 tau pathology between MAPT and MAPT/Tg4-42hom, but for a tendency towards significance at 3 months (p=0.0573) (Fig. 3.40A). At 3 and 5 months

Data partly published in (Zampar and Wirths 2021)

of age, phosphorylated tau immunoreactivity presented mostly as a diffuse staining with very few intracellular accumulations, mostly seen in the bigenic line (Fig. 3.40A,B). At 9 months, neurons accumulating hyperphosphorylated tau were detected in both MAPT and MAPT/Tg4-42^{hom} mice (Fig. 3.40C).

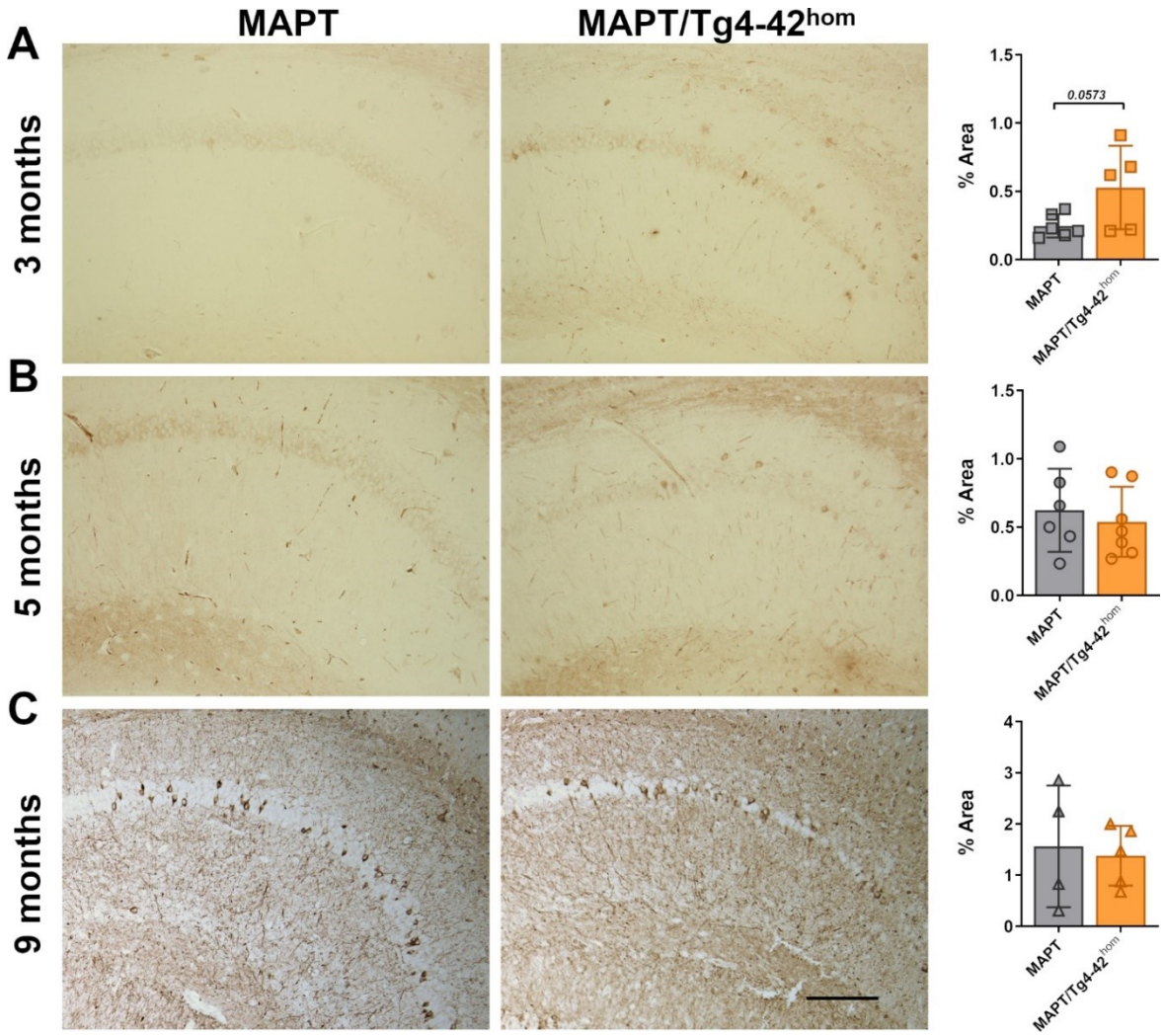

Fig. 3.40 Phosphorylated tau CA1 immunohistochemical staining and load analysis in 3-, 5-, and 9-month-old MAPT/Tg4-42^{hom} and MAPT mice.
DAB staining and load analysis of Aβ were performed in the CA1 region of the hippocampus at 3 (A), 5 (B) and 9 (C) months in female and male MAPT and MAPT/Tg4-42^{hom} mice (n=4-6). 3 sagittal paraffin brain sections per animal were stained using the tau antibody AT8 () and images were taken with 100x magnification for load quantification analysis. A trend towards significance increased in % Area covered was found in MAPT/Tg4-42^{hom} mice compared to MAPT littermates (A), while no significant differences were observed in the two later time points (B,C). All data are given as means ± SD. Unpaired t-test. Scale bar: 100 μm.

Data partly published in (Zampar and Wirths 2021)

4 DISCUSSION

4.1 PROJECT I: Assessment of N-terminal heterogeneity of parenchymal and vascular amyloid-β deposits in autopsied Alzheimer's disease brains.

4.1.1 Determination of antibodies selectivity by capillary isoelectric focusing immunoassay

Mass spectrometry analyses have allowed for the identification of a variety of N- and C-terminal truncated Aβ peptides in human brains and showed that N-truncated Aβ peptides account for the majority of Aβ species in AD brains (Moore et al. 2012, Portelius et al. 2010, Wildburger et al. 2017). This analytical technique, however, cannot provide the precise spatial localization and distribution of peptides in the way immunohistochemical staining would. The success of immunohistochemistry relies nevertheless on an accurate characterization of antibody selectivity and sensitivity. Before employing the set of antibodies used in this project to profile different Aβ N-termini immunostaining in autopsied brain samples from sporadic AD cases and non-demented control cases (NDC), the antibodies selectivity was determined by capillary isoelectric focusing immunoassays (CIEF-immunoassays). The selectivity was tested using a variety of Aβ peptide variants, comprising N-terminally elongated ($Aβ_{-3–40}$), full-length ($Aβ_{1–40}$), as well as N-terminally truncated ($Aβ_{2–40}$, $Aβ_{3–40}$, $Aβ_{pE3-40}$, $Aβ_{4–40}$, $Aβ_{5–40}$, $Aβ_{11–40}$) peptides. The 24311 antibody, considered a pan-Aβ antibody showing a preference towards $Aβ_{4-x}$ peptides (Saul et al. 2013b), interestingly detected all the employed Aβ species but for the N-elongated $Aβ_{-3–40}$ variant ($APP_{669–711}$) (Fig. 3.1). This proteolytic fragment of APP was so far not found in appreciable amounts in amyloid plaques and its relevance for AD pathology is yet to be determined (Klafki et al. 2020). The selectivity of antibodies specifically directed towards full-length (80C2 and 82E1) and N-terminally truncated peptides starting at position 4 (18H6) was here furthermore

confirmed (Walter et al. 2019, Cabrera et al. 2018) (Fig. 3.1). The selectivity of the other antibodies used, 029-2 and pAb77, binding to $A\beta_{4–40}$ and $A\beta_{2–40}$ respectively, was previously assessed through comparable analyses (Wirths et al. 2017, Savastano et al. 2016). The set of synthetic Aβ peptides used for the main CIEF analyses ends at position 40, rather than at position 42, because of the increased aggregation propensity of the latter (Jarrett, Berger, and Lansbury 1993) that could negatively interfere with the technique. $A\beta_{42}$ peptides are however considered more toxic than $A\beta_{40}$ precisely in virtue of this propensity. They also differ from $A\beta_{40}$ peptides for their N-terminus conformation (Sgourakis et al. 2007), which could affect the binding ability of the employed antibodies. This was not observed for 80C2 and 18H6, which maintained the expected selectivity in a CIEF analysis also with a set of $A\beta_{42}$-ending peptides (Fig. 3.2).

4.1.2 Heterogeneity of N-terminal Aβ peptide immunoreactivity in human brains

In good agreement with the Braak stages and amyloid scores assigned to the cortical brain samples during pathological assessment (Table 3.1), all AD and DS cases and four out of ten NDC cases showed abundant parenchymal plaque staining with the pan-Aβ and $A\beta_{42}$ antibodies (Fig 3.3). An expected heterogeneity was observed when applying antibodies detecting the full length and $A\beta_{4–x}$ and $A\beta_{2–x}$ peptides. While the two antibodies detecting the phenylalanine at position 4 of the Aβ sequence (029-2 and 18H6) showed a comparable plaque staining profile, differences between 80C2 and 82E1 (targeting $A\beta_{1–x}$) were observed: 82E1 showed a more widespread pattern of extracellular deposits compared to 80C2, which on the other hand displayed a weaker neuritic plaques staining (Fig 3.3, 3.4). Since these two antibodies showed a concordant profile in terms of selectivity in the CIEF assays, such differences could be attributed to antibody detection sensitivities or Aβ peptide conformation that could additionally impact the binding. Both antibodies detecting $A\beta_{4–x}$ peptides did stain amyloid plaque cores, but the 18H6 antibody presented with a more abundant pattern. Vascular deposits were analyzed

distinguishing between parenchymal and meningeal cerebral amyloid angiopathy (CAA). Again, staining with pan-Aβ and $A\beta_{42}$ antibodies confirmed the neuropathological assessment, with three AD cases presenting no evidence of CAA. A heterogeneous staining pattern could be detected also in term of vascular deposits. Several studies found $A\beta_{1\text{-}40}$ and $A\beta_{1\text{-}42}$ peptides to be the primary components of CAA pathology (Haglund et al. 2006), but also N-terminally truncated variants of the peptides ($A\beta_{2\text{-}x}$, $A\beta_{pE3\text{-}x}$, $A\beta_{4\text{-}x}$) were observed in vascular deposits (Savastano et al. 2016, Wirths et al. 2017, Gerth et al. 2018). Interestingly, differences in vascular deposition were observed between the full-length and N-truncated $A\beta_{4\text{–}x}$ peptides in the present study. Generally, deposition of full-length Aβ was more often and more intensely observed than of $A\beta_{4\text{–}x}$ peptides. Comparing parenchymal and meningeal CAA pathology in our sample set, $A\beta_{1\text{–}x}$ staining appeared to be more prominent in meningeal vessels, with $A\beta_{4\text{–}x}$ peptides being relatively more abundant in parenchymal vessels (Fig. 3.3, 3.5). While all AD patients with severe CAA pathology showed abundant accumulation of both $A\beta_{1\text{–}x}$ and $A\beta_{4\text{–}x}$ peptides, almost all cases with claimed mild CAA pathology showed $A\beta_{1\text{–}x}$ staining but little to no $A\beta_{4\text{–}x}$ vascular deposits. Confirming previous observation, $A\beta_{2\text{–}x}$ staining pattern with the pAb77 antibody displayed an abundant vascular immunoreactivity and a lower reactivity against amyloid plaques, detecting primarily the dense plaque cores (Savastano et al. 2016). On the other hand, NDC cases showed no vascular immunoreactivity. Two DS cases were included as controls and displayed abundant parenchymal plaques and CAA staining with all the employed antibodies (Fig 3.3, 3.6). Possessing an extra copy of chromosome 21, which includes the *APP* gene, people with Down syndrome are at greater risk of developing AD pathology (Hartley et al. 2015). A critical aspect of neuropathological analysis is the integrity of protein and nucleic acid in the collected samples. The short average PMI of the samples used in this study (< 5h for AD cases, < 9h for NDC cases) assures that the possible occurrence of protein denaturation might have only a limited impact. Studies on the effect of PMI on samples

integrity showed that immunostaining profiles of several proteins remained unchanged even with PMI > 50h (Blair et al. 2016) and that the relative abundance of N-truncated Aβ peptides was not correlated with the PMI in human brain samples (Wildburger et al. 2017).

4.1.3 Conclusions of PROJECT I

Based on the results of the present study:

- Proper antibody characterization in term of selectivity and specificity is fundamental to perform reliable immunohistochemical analyses. Antibody sensitivity and protein conformation might play additional important roles.
- Heterogeneity of N-terminal Aβ peptides could be demonstrated in both parenchymal plaques and parenchymal and meningeal vascular deposits in AD, NDC, and DS cases.
- Abundant and comparable immunoreactivity of full-length Aβ and N-truncated $A\beta_{4\text{-}x}$ peptides was observed in terms of parenchymal plaques. While staining of $A\beta_{1\text{-}x}$ displayed both widespread and neuritic plaques, antibodies targeting $A\beta_{4\text{-}x}$ variants primarily stained the plaque cores.
- Vascular deposition of $A\beta_{1\text{-}x}$ was generally more prominent than of $A\beta_{4\text{-}x}$. The antibodies detecting $A\beta_{1\text{-}x}$ peptides stained meningeal vessels more abundantly while $A\beta_{4\text{-}x}$ accumulation appeared to be relatively more abundant in parenchymal than meningeal vessels.
- AD patients with mild CAA pathology in the present study showed $A\beta_{1\text{–}x}$ staining but little to no $A\beta_{4\text{–}x}$ parenchymal and meningeal vascular deposits.

4.2 PROJECT II: *In-vitro* and *in-vivo* activity of enzymes involved in the digestion and generation of Aβ$_{4-x}$ peptides: an outlook on Neprilysin and ADAMTS4

As supported by afore-mentioned studies and by the results of project I, N-truncated Aβ peptides account for the majority of Aβ species in AD brains (Portelius et al. 2010, Wildburger et al. 2017). Alongside Aβ$_{pE3-x}$, Aβ$_{4-x}$ peptides were reported to be the most prominent species among the N-terminally truncated variants (Portelius et al. 2010, Moore et al. 2012). The aggregation propensity of Aβ$_{4-42}$ peptides was found comparable or exceeding the one of full length peptides, forming oligomers and stable aggregates, in several *in-vitro* studies (Cabrera et al. 2018, Wirths et al. 2017, Bouter et al. 2013). Due to these characteristics, Aβ$_{4-42}$ peptides possess a toxicity comparable to full-length Aβ$_{1-42}$ or Aβ$_{pE3-42}$ in *in-vitro* assays, and *in-vivo* intracerebral injection of the peptide led to spatial working deficits in wild type mice (Bouter et al. 2013). Given the abundance and toxicity of the N-truncated Aβ variants, it is vital to understand how these peptides are generated and degraded. Alterations in Aβ catabolism mechanisms are believed to contribute to Aβ deposition in AD, especially in sporadic cases (Tarasoff-Conway et al. 2015). Among the known Aβ-degrading enzymes, neprilysin (NEP) is one of the most studied (Carson and Turner 2002). A recent meta-analysis points toward the direction of reduced NEP mRNA levels and enzymatic activity in AD patients (Zhang et al. 2017). In the first part of this project, we questioned whether NEP would be able to digest Aβ$_{4-42}$ peptides *in-vitro,* and *in-vivo* using the Tg4-42^{het} mouse model of AD when lacking endogenous NEP. Several proteases have been linked with the generation of N-truncated Aβ peptides [reviewed in (Wirths and Zampar 2019)] and recent findings identified the metalloprotease ADAMTS4 as being able to generate Aβ$_{4-x}$ both *in-vitro* and *in-vivo* (Walter et al. 2019). When 5xFAD mice were bred on a full ADAMTS4 knockout background, they presented with reduced Aβ$_{4-x}$ levels, especially in white matter structures. ADAMTS4 appears indeed only expressed in oligodendrocytes (Zhang et al. 2014, Walter et al. 2019). In the second part

of PROJECT II, we aimed to further characterize 5xFAD/ADAMTS4$^{-/-}$ mice from a behavioural and pathological point of view.

4.2.1 Part I: *In-vitro* and *in-vivo* degradation of N-terminal truncated Aβ$_{4-42}$ by neprilysin

Several *in-vitro* studies showed that the metalloprotease NEP is able to hydrolyze the full length Aβ$_{1-40}$ and Aβ$_{1-42}$ peptides (Howell, Nalbantoglu, and Crine 1995, Shirotani et al. 2001), but no information about its potential action on N-truncated Aβ$_{4-x}$ peptides was available. We showed that NEP effectively hydrolyzed both synthetic Aβ$_{4-40}$ and Aβ$_{4-42}$ *in-vitro*, producing Aβ fragments that were previously identified by mass spectrometry analysis after digestion of full-length peptides (Fig. 3.7). In our experimental conditions, the peptides ending at position 40 were hydrolyzed in higher amounts compared to the Aβ$_{42}$ counterparts. Our observations confirmed the already reported increased degradation rate of Aβ$_{1-40}$ compared to Aβ$_{1-42}$ (Shirotani et al. 2001). This difference also applied to the Aβ variants starting with phenylalanine at position 4. Moreover, Aβ$_{4-x}$ peptides appeared to be degraded in higher amount than the full-length counterparts, which might be speculatively attributed to an increased hydrolyzation rate or to an increased affinity of NEP towards the N-truncated variants. Interestingly, Shirotani and colleagues reported a higher affinity of NEP to Aβ$_{1-42}$ than to Aβ$_{1-40}$ peptides despite the slower degradation rate. Confirming recent analyses (Mital et al. 2018), the major cleavages of NEP on the Aβ sequence occurred prior to hydrophobic residues (Phe, Tyr, Leu, Ile, and Val), resulting in Aβ$_{4-9}$, Aβ$_{10-17}$, and Aβ$_{20-30}$ as primary degradation products.

Among the N-truncated peptides, Aβ$_{4-42}$ was found to be the major species in *post mortem* brain samples from aged controls, patients with vascular dementia, and AD patients (Lewis et al. 2006). To investigate if Aβ$_{4-42}$ peptides are subjected to NEP hydrolysis *in-vivo*, endogenous NEP was removed in the Tg4-42^{het} mouse model of AD, expressing exclusively Aβ$_{4-42}$ peptides. Tg4-42^{het} mice display intraneuronal accumulation of the Aβ$_{4-}$

$_{42}$ preferentially in the CA1 region of the hippocampus, which is associated with age-dependent neuron loss and behavioral deficits (Bouter et al. 2013). The lack of endogenous NEP led to an increase of Aβ$_{4-42}$ accumulation in CA1 pyramidal neurons in young mice (Fig. 3.8). On the other hand, no difference was observed between aged Tg4-42^{het}/NEP$^{-/-}$ and Tg4-42^{het} mice. Comparing the two time points, an obvious age-dependent decrease in Aβ immunoreactivity could be observed with in both lines. This could be explained by the abundant neuron loss Tg4-42^{het} mice experience at 12 months. The observed increased amyloid pathology in the CA1 pyramidal layer at 3 months was accompanied by an increased neuron loss in Tg4-42^{het}/NEP$^{-/-}$ at 3 months, (Hornung et al. 2019). The impact of NEP on Aβ levels was studied in several APP-overexpressing AD mouse model. When NEP was knocked-out, J9 mice presented with increased hippocampal amyloid plaque deposits (Farris et al. 2007). Significantly increased numbers of extracellular amyloid plaques were found in the brain (dentate gyrus, subiculum) as well as in the spinal cord of 5xFAD/NEP$^{+/-}$ mice, concomitant to an elevation of soluble Aβ$_{42}$ peptide levels (Hüttenrauch et al. 2015). In good agreement, an increased clearance of Aβ peptides was observed after an elevation of NEP levels by viral vector-mediated gene transfer or by transgenic overexpression (Poirier et al. 2006, Iwata et al. 2004, Leissring et al. 2003). Our study shows that NEP is involved in the degradation not only of full-length Aβ peptides, but also N-terminally truncated Aβ$_{4-x}$ variants, making this enzyme an interesting target for possible disease-modifying treatments.

4.2.2 Part II: *In-vivo* role of ADAMTS4 in the generation of Aβ$_{4-x}$ peptides

4.2.2.1 The lack of ADAMTS4 rescues motor deficits in the 5xFAD mouse model of AD, while cognitive performance remains unaltered

Decline of motor functions, which includes bradykinesia, impaired posture/gait, speech/facial expression, and rigidity, have been described in patients suffering from AD (Scarmeas et al. 2004, Pettersson, Olsson, and Wahlund 2005). Motor abilities usually worsen in time and are associated with increased cognitive decline, caretaking costs, and

eventually mortality (Scarmeas et al. 2005). Changes in motor performances can be observed also preclinically and, interestingly, impaired motor function in people with mild cognitive impairments (MCI) could be associated with the risk of later developing AD (Buchman and Bennett 2011, Aggarwal et al. 2006), which underlies the importance of such deficits in the context of this disease. Alteration of motor performances have been described in several mouse model of AD (Lalonde et al. 2002, Lalonde et al. 2003, Wirths and Bayer 2008, Seo et al. 2010, Jawhar et al. 2012, Wagner et al. 2019). The 5xFAD mouse model is characterized by an age-dependent accumulation of amyloid plaques in the brain and spinal cord, and the development of behavioral deficits (Jawhar et al. 2012, O'Leary et al. 2020, Chu et al. 2017). Starting at 9 months of age, motor deficits can be observed in behavioral tests, such as the balanced beam and string suspension tasks (Jawhar et al. 2012, O'Leary et al. 2020). By generating 5xFAD on a ADAMTS4$^{-/-}$ background, the formation of A$\beta_{4\text{-}x}$ by this specific metalloprotease in oligodendrocytes was inhibited (Walter et al. 2019). In our study, the lack ADAMTS4$^{-/-}$ led to a rescue of motor deficits in the balance beam and inverted grid tasks in aged 5xFAD mice (Fig. 3.9). At this time point, impairments in the rotarod task were generally observed in the 5XFAD line (O'Leary et al. 2020, Peters et al. 2013). In our mice cohort, no obvious deficits were observed compared to WT littermates but 5xFAD/ADAMTS4$^{-/-}$ mice performed significantly better than 5xFAD. ADAMTS4$^{-/-}$ mice showed no altered motor abilities in the mentioned tasks at either 3 or 9 months of age, which appears to contrast a previous study reporting reduced motor performances in mice lacking ADAMTS4 already at 8 weeks of age (Pruvost et al. 2017). It must be noted that most of the behavioral tasks employed in Provost's study, such as actimetry, Open Field (OF), and CatWalk, addressed global spontaneous locomotor activity, while balance, agility, and grip capacity, which remained unaltered in our analyses, were not fully explored. Interestingly, in good agreement with Provost's results, a reduced average speed and average distance travelled were observed in young ADAMTS4$^{-/-}$ mice in the OF task (Fig.

3.10). This phenotype was even more pronounced in 5xFAD/ADAMTS4$^{-/-}$ at 3 months and accompanied by increased immobility in the arena, an observation that persisted also in aged animals. On the other hand, aged ADAMTS4$^{-/-}$ behaved comparably to WT controls. The interpretation of the locomotor parameters in 9-month-old 5xFAD/ADAMTS4$^{-/-}$ mice is additionally complicated by the fact that also 5xFAD mice showed decreased speed and distance travelled at this point. Since the motor assessment in the balance beam and inverted grid tasks at 9 months showed an improvement of motor performances in 5xFAD lacking endogenous ADAMTS4 (Fig 3.9), the reduced locomotor parameters in the OF might be partially explained by the lowered exploratory activity of the mice in the arena.

Alongside with cognitive decline and motor impairments, patients with AD display a wide range of psychological symptoms. Social withdrawal and depression, but also disinhibited behavior, inappropriate euphoria, and changes in anxiety have been reported (Ferretti et al. 2001, Chung and Cummings 2000, Hart et al. 2003). The time spent in the center of the OF arena is used as an indicator of anxiety-like phenotypes in mice. In our study, aged 5xFAD mice showed reduced anxiety-like behavior in the OF task, which confirms some studies (Braun and Feinstein 2019) but contrasts others (Jawhar et al. 2012, O'Leary et al. 2020). 5xFAD/ADAMTS4$^{-/-}$ mice showed, on the other hand, a time span spent in the center comparable to WT and ADAMTS4$^{-/-}$ mice (Fig. 3.10). It was significantly reduced compared to the 5xFAD parental line, which could argue for a rescue of the decreased anxiety-like behavior in the AD transgenic line. The reduced speeds observed in the AD lines and increased immobility of 5xFAD/ADAMTS4$^{-/-}$ mice in this task make drawing conclusions difficult. Anxiety-like behavior in the EPM has been far more characterized in the 5xFAD line. Several groups indeed reported an increased time spent in open arms in aged (6-12 months) 5xFAD animals (Jawhar et al. 2012, Hüttenrauch et al. 2017, Schneider et al. 2014, 2015). In this task, no difference was

found after ADAMTS4 was knocked-out in aged 5xFAD mice, as both the mouse lines showed a decreased anxiety-like phenotype (Fig. 3.11). This observation might support the idea that the reduced time spent in the center of the OF in 5xFAD/ADAMTS4$^{-/-}$ mice was due to the general decreased exploration of the arena, as indicated by the increased immobility time, and that the lack of endogenous ADAMTS4 does not have consequences on the anxiety-like behavior in 5xFAD at this time point.

From a cognitive point of view, 5xFAD mice show working memory deficits when tested in Y-Maze or Cross Maze paradigms starting around 6 months of age (Jawhar et al. 2012, Oakley et al. 2006, Devi and Ohno 2016, Hüttenrauch et al. 2017). We challenged our mice in the Cross Maze task since it allows for a more sensitive detection of working memory impairments due to its increased complexity compared to the Y-Maze task. We observed no rescue of the obvious working memory deficits in 5xFAD lacking endogenous ADAMTS4 at 9 months (Fig. 3.11).

Numerous studies have investigated how lack of enzymes involved in the formation of specific Aβ peptides influences the behavioral performances of 5xFAD mice. A reduction of BACE1, the principal enzyme involved in the generation of full length Aβ peptides in the amyloidogenic processing of APP, by hemizygous knockout, led to a rescue of memory impairments in the Y-Maze (Devi and Ohno 2010, Kimura, Devi, and Ohno 2010) and of hippocampal-dependent deficits in the contextual fear conditioning test at 6 months (Kimura, Devi, and Ohno 2010). Similarly, full deletion of BACE1 was able to rescue working memory deficits in 15-18 month-old 5xFAD (Ohno et al. 2007) and temporal memory deficits observed in the fear conditioning and Morris Water Maze tasks at 6 months of age (Ohno et al. 2006). On the same trend, 6-month-old 5xFAD mice lacking glutaminyl cyclase, the enzyme responsible for the formation of another N-terminally truncated peptide, $A\beta_{pE3\text{-}x}$, presented with significantly improved performances in the Cross Maze task compared to 5xFAD littermates (Jawhar et al. 2011). It must be noted

that in the above-mentioned studies motor performances were almost never assessed. We showed that removal of Aβ4-x formation by ADAMTS4 caused no amelioration of working memory impairments nor anxiety-like behavior in the 5xFAD line, but a clear improvement of the motor deficits in the aged group. The selective expression of the metalloprotease in oligodendrocytes could be one of the reasons why the main effects of the ADAMTS4 knockout background were observed only on motor performances. Additionally, although Aβ4-x peptides can be found in the 5xFAD mouse model, they account only for a minor Aβ portion as the Swedish mutation on the overexpressed *APP* gene results in an over production of Aβ1-x peptides (Wirths et al. 2017). Since deletion of ADAMTS4 does not completely prevent the formation of Aβ4-x peptides, the N-truncated variant in 5xFAD must be generated also by other sources than the enzymatic activity of ADAMTS4. The removal of this cell-type specific Aβ4-x pool is likely not enough to change the robust behavioral deficits in this AD line.

4.2.2.2 Reduced Aβ4-x pathology in the spinal cord of 5xFAD/ADAMTS4$^{-/-}$ mice

The lack of ADAMTS4 led to a rescue of motor deficits in 9-month-old 5xFAD mice. Thus, we specifically analyzed the spinal cord amyloid pathology of 5xFAD mice possessing or lacking the endogenous metalloprotease. The 5xFAD mouse model of AD shows an age-dependent accumulation of β-amyloid in the spinal cord, with plaques present mostly, but not exclusively, in the grey matter (Jawhar et al. 2012, Chu et al. 2017). An ADAMTS4$^{-/-}$ background was previously linked to a significant reduction of Aβ4-40 peptides in whole-brain SDS protein lysates of 12-month-old 5xFAD mice, as well as decreased whole-brain Aβ4-x immunoreactivity (Walter et al. 2019). On the same trend, we observed a significantly reduced immunoreactivity of Aβ4-x peptides in the grey matter of cervical spinal cord tissues of 5xFAD mice lacking ADAMTS4 (Fig. 3.12). The expression of full-length Aβ peptides appeared to be unaltered, in line with the previous *in-vivo* and cell culture findings (Walter et al. 2019).

Walter and colleagues described an ADAMTS4-dependent pool of $A\beta_{4\text{-}x}$ peptides in the white matter fiber tracts and in cortical neuronal processes due to the exclusive expression of the metalloprotease in oligodendrocytes. At the spinal cord level, abnormalities in myelin structures associated with increased axonal swellings and axonal spheroids were previously reported in 5xFAD mice (Jawhar et al. 2012, Chu et al. 2017). Several studies showed the presence of white matter abnormalities and oligodendrocyte dysfunction in AD patients (De Strooper and Karran 2016, Brun and Englund 1986, Nasrabady et al. 2018) but the etiology of such lesions is still unknown. In the work of Chu and coworkers, a microscopic examination of the spinal cord tissue of 5xFAD mice revealed the presence of $A\beta_{42}$-positive thread-like structures in both the white and grey matter (Chu et al. 2017). In the white matter, these Aβ threads located in the peri-axonal space, occasionally penetrating the myelin sheath. Interestingly, the Aβ threads supposedly preceded plaque formation and axonal neurodegeneration but appeared later in the axonal spheroid swellings of aged 5xFAD mice, pointing towards their involvement with the development of axonopathy in the spinal cord. We could visualize Aβ thread-like structures in spinal cord via both full-length and $A\beta_{4\text{-}x}$ immunohistochemical staining (Fig.3.13). In our sample set, only $A\beta_{4\text{-}x}$-positive threads could be observed in the white matter of aged 5xFAD mice, while these structures were constituted of both $A\beta_{4\text{-}x}$ and $A\beta_{1\text{-}x}$ variants in the grey matter. In this region, the amyloid threads were strongly positive to $A\beta_{4\text{-}x}$ staining while $A\beta_{1\text{-}x}$ immunoreactivity resulted in weaker and fewer structures. On an ADAMTS4$^{-/-}$ background, few to no $A\beta_{4\text{-}x}$ threads could be observed both in the grey and white matter, while $A\beta_{1\text{-}x}$ threads were still present in the grey matter to the same extent as in 5xFAD controls. The observations in the white matter were particularly interesting. While a reduction of $A\beta_{4\text{-}x}$ immunoreactivity due to the lack of ADAMTS4 was not surprising, it appeared that only $A\beta_{4\text{-}x}$ threads were present in the white matter and that their generation was dependent on ADAMTS4 activity. The rescue of motor deficits observed in aged 5xFAD/ADAMTS4^{-}

$^{/-}$ mice, together with the exclusive expression of the metalloprotease in oligodendrocytes and the observation that possibly only Aβ$_{4-x}$ threads were present in the white matter, might indicate that Aβ$_{4-x}$ peptides specifically contribute to demyelination and white matter damage in this mouse model. We observed no alteration of mRNA expression of oligodendrocytes and myelin markers in 5xFAD and 5xFAD/ADAMTS4$^{-/-}$ mice (Fig. 3.14) compared to controls. However, given the myelin and axonal abnormalities in aged 5xFAD mice, analysis on the protein level would be a crucial next step to further investigate the effects of the lack of ADAMTS4 and the related Aβ$_{4-x}$ peptide variant on axonal and myelin pathology.

4.2.3 Conclusions of PROJECT II

4.2.3.1 Conclusions of Part I - *In-vitro* and *in-vivo* degradation of N-terminal truncated Aβ$_{4-42}$ by neprilysin

Based on the results of the present study:

- Aβ$_{4-x}$ peptides are subjected to degradation by recombinant neprilysin *in-vitro*.
- Recombinant neprilysin degrades Aβ$_{4-x}$ peptides more efficiently than full-length Aβ$_{1-x}$ peptides *in-vitro*.
- *In-vivo*, the lack of endogenous neprilysin led to a significant increase of Aβ$_{4-42}$ peptides in the Tg4-42^{het} mouse model of AD at a young age.

4.2.3.2 Conclusions of Part II - *In-vivo* role of ADAMTS4 in the generation of Aβ$_{4-x}$ peptides

Based on the results of the present study:

- The lack of endogenous metalloprotease ADAMTS4 led to the rescue of motor deficits in aged 5xFAD mice.
- Cognition deficits in the Cross Maze task were not altered by the absence of endogenous ADAMTS4 in aged 5xFAD mice.

- ADAMTS4$^{-/-}$ background was responsible for a significant reduction of Aβ$_{4-x}$ immunoreactivity in the grey matter of spinal cord in aged 5xFAD mice.
- Aβ thread-like structures in the spinal cord are composed of both Aβ$_{1-x}$ and Aβ$_{4-x}$ in the grey matter, while only Aβ$_{4-x}$-positive threads could be observed in the white matter.
- Aβ$_{4-x}$ threads were greatly reduced in the gray matter and apparently absent in the white matter of 5xFAD/ADAMTS4$^{-/-}$ mice.

4.3 PROJECT III: *In-vivo* relationship of Amyloid-β plaques and Aβ$_{4-x}$ peptides

The most prominent pathological hallmark of AD is the brain deposition of Aβ in the form of extracellular amyloid plaques. The central role of fibrillary Aβ plaques, proposed by the classical amyloid cascade hypothesis, has been questioned as the amount and localization of these deposits do not correlate well with disease state, and about 40% of non-demented individuals meet criteria for a neuropathological diagnosis of AD to a certain degree (Hulette et al. 1998, Price and Morris 1999). Recent studies employing *in-vivo* imaging techniques indeed demonstrated that the plaque deposition in non-demented patients is equivalent to those of AD patients, with amyloid burden even reaching a plateau despite of the ongoing cognitive decline (Aizenstein et al. 2008). Additionally, several clinical trials aiming to a reduction of amyloid burden failed because the primary endpoints were not met (Harrison and Owen 2016, Zampar and Wirths 2020). These considerations led to an adjustment of the amyloid hypothesis, putting the emphasis on soluble Aβ oligomers. Soluble oligomeric forms of Aβ have been described in *post mortem* tissues from AD patients (Roher et al. 1996, Shankar et al. 2008, Esparza et al. 2013) and have been found to better correlate with the risk and severity of the disease than insoluble amyloid plaques (McLean et al. 1999, Wang et al. 1999, Esparza et al. 2013). Therefore, it has been proposed that soluble Aβ oligomers, rather than

insoluble fibrillar Aβ deposits, may be the crucial players in AD etiology. Several *in-vitro* (Selkoe 2008, Lambert et al. 1998, Wang et al. 2002, Dahlgren et al. 2002) and *in-vivo* (Walsh et al. 2002, Cleary et al. 2005, Lesne et al. 2006, Shankar et al. 2008) studies support the hypothesis of fibrillary Aβ being less harmful in contrast to soluble oligomeric Aβ forms causing direct adverse effects. Several groups have addressed the relationship between insoluble amyloid plaques and soluble Aβ oligomers and it is still open for debate. It has been hypothesized that plaques may serve as reservoirs, sequestering toxic Aβ oligomers thus preventing their toxicity at initial stages of the pathology. However, with the progression of the disease and saturation of the reservoirs, they start to release the soluble Aβ aggregates, now free to bind to other targets accomplishing their detrimental effects (Brody et al. 2017, Maggio et al. 1992). The findings of Koffie and coworkers, who analyzed synaptic loss as a function of distance from amyloid plaques with array tomography, support the idea of amyloid plaques acting as reservoirs of toxic soluble Aβ species. In both AD transgenic mice and human AD brains, synaptic density decreased progressively around plaques, returning close to normal values beyond 50 μm of distance (Koffie et al. 2009, Koffie et al. 2012). Esparza and coworkers further tested this hypothesis by measuring the binding abilities of amyloid plaques in human unfixed frozen brain sections. Amyloid plaques were indeed found to be able to bind synthetic $A\beta_{1-42}$ peptides, although comparably between AD patients and high-pathology controls (Esparza et al. 2018). As already mentioned, $A\beta_{4-42}$ is one of the most abundant N-terminally truncated Aβ species, showing comparable toxicity to full-length $A\beta_{1-42}$ peptides (Portelius et al. 2010, Wildburger et al. 2017, Cabrera et al. 2018, Bouter et al. 2013). To understand the relationship between insoluble extracellular amyloid deposits and soluble $A\beta_{4-42}$ oligomers *in-vivo*, we crossed the classical AD model 5xFAD, harboring Aβ plaques from an early age, with the Tg4-42^{hom} line, expressing exclusively soluble $A\beta_{4-42}$ oligomers without developing extracellular amyloid plaques. The resulting FAD/Tg4-

42^{hom} line was challenged in a behavioral battery at 3 and 6 months of age, after which neuropathology was analyzed in the spinal cord and hippocampus.

4.3.1 Part I: Assessment of motor behavior and spinal cord analysis of FAD/Tg4-42^{hom} mice

4.3.1.1 Increased motor deficits in FAD/Tg4-42^{hom} mice

As discussed in PROJECT II - Part II, motor impairments are widely common in AD. They predict cognitive and functional decline and are associated with poorer outcomes (Scarmeas et al. 2004, Scarmeas et al. 2005). The two parental mouse lines used in this project, 5xFAD and Tg4-42^{hom}, have been reported to develop motor deficits on a different time-line: 5xFAD mice showed robust impairments around 9 months of age (Jawhar et al. 2012), while decreased performances could be detected in the Tg4-42^{hom} line already at 6 months (Wagner et al. 2019, Stazi and Wirths 2021). The accelerating rotarod, balance beam, and inverted grid tasks revealed a further age-dependent decline of motor coordination, strength, and balance in the FAD/Tg4-42^{hom} line compared to Tg4-42^{hom} littermates (Fig. 3.16). Although the expression of transgenic $A\beta_{4\text{-}42}$ in Tg4-42^{hom} mice caused deficits in the accelerating rotarod and balance beam at 6 months, the co-overexpression of APP and PSEN1, resulting in abundant extracellular amyloid pathology, aggravated the phenotype. Motor deficits were observed in the inverted grid tasks, a test in which no deficits were present in the parental transgenic lines, already at 3 months in FAD/Tg4-42^{hom} mice. Alongside $A\beta_{4\text{-}42}$, another N-truncated variant, $A\beta_{pE3\text{-}42}$, has been linked to the development of motor deficits in mouse models of AD (Alexandru et al. 2011, Wittnam et al. 2012, Meissner, Bouter, and Bayer 2015). In a similar experiment, Wittnam and colleagues showed that the expression of $A\beta_{pE3\text{-}42}$ in 5xFAD mice resulted in poorer performances in the balance beam task at a time point when neither of the parental transgenic lines displayed motor deficits (Wittnam et al. 2012). The two mentioned N-truncated Aβ peptides appear to be key contributors to the generation of motor impairments in the generated mouse lines. Indeed, the co-expression of $A\beta_{pE3\text{-}42}$ and $A\beta_{4\text{-}}$

42 caused a further motor decline in a mouse model of AD, and was associated with increased accumulation of Aβ in the motor neurons of the spinal cord (Lopez-Noguerola et al. 2018a).

4.3.1.2 Decreased motoneurons and general amyloid pathology in the spinal cord of FAD/Tg4-42^{hom} mice

Given the clear aggravation of motor performances of FAD/Tg4-42^{hom} mice, pathology in spinal cord tissues was analyzed. Despite the abundant age-dependent accumulation of amyloid plaques in the spinal cord (Jawhar et al. 2012, Chu et al. 2017), no loss of motoneurons (MNs) can be detected at 7 months in the 5xFAD line (Chu et al. 2017) and general loss of neurons in the spinal cord was observed only after 8 months of age (Li et al. 2013). Motor impairments in the Tg4-42^{hom} have been previously associated with intracellular accumulation of Aβ$_{4-42}$ in motoneurons (Lopez-Noguerola et al. 2018b), but the potential loss of neurons in the spinal cord has so far not been studied. We thus measured the number of motoneurons (ChAT^{+}) in the cervical spinal cord of the different transgenic lines (Fig. 3.17). We found an age-dependent loss of motoneurons in the Tg4-42^{hom} line which started already at 3 months, while, as expected, no significant loss could be observed in age-matched 5xFAD mice. The spinal cord neurodegeneration could relate to the motor deficits observed in the Tg4-42^{hom} line. When a motoneuron loss of 25% occurred at 3 months, Tg4-42^{hom} mice also presented with deficits in the accelerating rotarod task. At 6 months, the motor deficits were more pronounced, together with an increased percentage of lost motoneurons. Supporting the aggravated impairments in the motor tasks, FAD/Tg4-42^{hom} mice presented with a further motoneurons loss compared to the already existing degenerative phenotype of the Tg4-42^{hom} line. Further discrimination between α-MNs and γ-MNs revealed that the loss can be entirely attributed to the α-MNs pool, as γ-MNs numbers did not changed among genotypes or ages. The loss of this specific subset also fits with the specific motor decline we observed in the mouse models. From a functional point of view, α-MNs are responsible for force

generation as they drive muscle contraction by innervation of extrafusal skeletal muscle while γ-MNs innervates intrafusal fibers modulating the sensitivity of muscle spindles to stretch (Kanning, Kaplan, and Henderson 2010). Interestingly, α-MNs susceptibility could be a feature of MNs disease, as selective degeneration of α-MNs with concomitant sparing of γ-MNs was observed in several mouse models of amyotrophic lateral sclerosis and spinal muscular atrophy (Lalancette-Hebert et al. 2016, Powis and Gillingwater 2016). It is tempting to speculate that the increased loss of α-MNs in the FAD/Tg4-42^{hom} line is the result of an additive effect originating from the two parental transgenic lines. Indeed, the percentage of α-MNs lost in the filial line is approximately the sum of the ones of 5xFAD and Tg4-42^{hom} mice at both time points. This, however, does not reflect the results of the motor behavior assessment where the impairments observed in the FAD/Tg4-42^{hom} were clearly not the result of an additive effect.

Since in the FAD/Tg4-42^{hom} line Aβ$_{4-42}$ peptides are added to the already abundant amyloid pathology present in the 5xFAD mouse model of AD and given the increased motor deficits and MNs loss in the filial line, an increased amyloid pathology in the spinal cord of FAD/Tg4-42^{hom} mice could have been expected. Surprisingly, not only we observed no exacerbation of amyloid pathology in the spinal cord, but we detected a general decrease of Aβ concentrations in the SDS-soluble protein fraction in the spinal cord of 6-month-old FAD/Tg4-42^{hom} compared to 5xFAD mice (Fig. 3.18). Full-length Aβ$_{1-x}$ and N-terminally truncated Aβ$_{4-x}$ peptides were affected indiscriminately, suggesting an overall decreased production of Aβ peptides in FAD/Tg4-42^{hom} mice. This might be attributed to the reduced number of MNs, which contributes to the generation of Aβ peptides. Quantification showed indeed an ~30% and ~40% reduction of total ChAT^{+}-MNs in FAD/Tg4-42^{hom} at 3 and 6 months, respectively (Fig 3.18). Analysis of immunohistochemical staining confirmed the significant decrease of Aβ pathology in the FAD/Tg4-42^{hom} line (Fig. 3.19). In the Tg4-42^{hom} line, the accumulation of Aβ$_{4-42}$ peptides

takes place in few motoneurons at a spinal cord level (Lopez-Noguerola et al. 2018b). The concentration of Aβ peptides was understandably lower in the spinal cord of Tg4-42^{hom} than in that of 5xFAD mice, which in contrast present robust extracellular amyloid pathology. While observing the expected age-related increase of Aβ$_{1\text{-}x}$ and Aβ$_{4\text{-}x}$ levels in both 5xFAD and FAD/Tg4-42^{hom} mice, N-terminally truncated Aβ peptides represented only a minor fraction of the total amount of Aβ. The concentration of Aβ$_{4\text{-}x}$ peptides in SDS-soluble fractions of the spinal cord were approximately 55-fold and 65-fold lower than full-length peptides at 3 and 6 months, respectively, which is in line with previous observations detecting a 75-fold ratio of Aβ$_{1–40}$/Aβ$_{4–40}$ in whole brain protein extracts of 5- and 12-month-old 5xFAD mice (Wirths et al. 2017, Walter et al. 2019). Focusing on intracellular amyloid accumulation in MNs, FAD/Tg4-42^{hom} mice showed an apparent increased number of Aβ-positive MNs compared to Tg4-42^{hom} littermates, although presenting with dot-like staining profiles compared to the clear aggregation in the latter line (Fig. 3.19). A similar increase was reported by Wittnam and co-workers in 5xFAD mice co-expressing Aβ$_{pE3\text{-}42}$ (Wittnam et al. 2012).

The reduced α-MNs numbers and apparent increase of intraneuronal Aβ in FAD/Tg4-42^{hom} could explain the reported motor deficits, despite the general decrease of extracellular amyloid pathology. However, it is important to remember that motor performances involve the coordination of other brain structures not analyzed here, such as motor cortex, cerebellum, or basal ganglia (Lalonde and Strazielle 2007). Alteration of pathology in these regions could also contribute to the motor deficits in the FAD/Tg4-42^{hom} line.

4.3.2 Part II: Assessment of cognitive phenotype and analyses of hippocampal pathology

4.3.2.1 Abundant extracellular amyloid pathology does not increase memory deficits nor hippocampal CA1 neurodegeneration of Tg4-42^{hom} mice

Neuron loss is a key feature in in the pathogenesis of AD (Coleman and Flood 1987, Hof, Cox, and Morrison 1990). Loss of neurons in the CA1 region of the hippocampus appears to be particularly correlated with the severity of memory deficits in AD patients (Simic et al. 1997, West et al. 1994). In rodent models of AD, hippocampal neuron loss has been associated with the development of memory deficits analyzed in the behavioral assessment of this study. Damage limited to the hippocampus was sufficient to cause recognition memory deficits, tested in the NOR task in rodents, non-human primates, and memory-impaired patients (Broadbent et al. 2010, Squire, Wixted, and Clark 2007). Spatial memory deficits evident in the MWM task are also related to changes in hippocampal circuitry (Morris 1984). The Tg4-42^{hom} line displays an age-dependent neuron loss in the CA1 region of the hippocampus, losing approximately 50% of pyramidal neurons at 6 months of age, with the development of behavioral deficits in MWM and NOR tasks (Antonios et al. 2015, Stazi and Wirths 2021). A loss of 50% of CA1 pyramidal neurons appeared to be critical for the development of cognitive deficits in this line and even small changes in neuron number could influence the behavioral phenotype. In the work of Antonios and colleagues, a 50% neuron loss at 6 months of age was indeed accompanied by clear spatial memory deficits in the MWM task, while 5-month-old mice, presenting with 43% of CA1 pyramidal neuron loss, showed only mild spatial learning deficits and intact spatial recognition memory (Antonios et al. 2015). Likewise, an increment between 10-20% resulted in restored spatial and recognition memory in Tg4-42^{hom} at 6 months (Stazi and Wirths 2021). In the present study, we observed the expected recognition and spatial memory deficits in 6-month-old Tg4-42^{hom} mice when tested in the MWM and NOR tasks (Fig. 3.20, 3.21, 3.22), accompanied by the

age-dependent loss of CA1 pyramidal neurons (Fig. 3.23). Different regions of the CA1 pyramidal layer have been correlated with the development of specific memory delays: the distal CA1 is linked to non-spatial memory while the proximal part with spatial memory formation (Masurkar 2018). A differentiated analysis of these two regions showed that Tg4-42^{hom} mice presented with robust neuron loss in both regions. A more remarkable neurodegeneration could be detected towards the distal part, starting already at a young age and worsening with time (Fig. 3.23). On the other hand, 5xFAD mice presented with intact cognition in both tests (Fig. 3.20, 3.21, 3.22), showing unaltered CA1 pyramidal neuron numbers compared to controls (Fig. 3.23). Previous studies also reported no loss of hippocampal neuron in this line, even at 12 months of age (Jawhar et al. 2012). Upon crossing of 5xFAD and Tg4-42^{hom} lines, no further aggravation of spatial learning and memory deficits was detected in the FAD/Tg4-42^{hom} line as they performed comparably to Tg4-42^{hom} littermates at both time points (Fig. 3.21, 3.22). Interestingly, recognition memory deficits in Tg4-42^{hom} mice appeared to be rescued after the crossing with 5xFAD mice (Fig. 3.20). The concomitant changes in neuron loss at 6 months in the distal and proximal pyramidal layer of FAD/Tg4-42^{hom} mice nicely support the outcomes of the cognitive tasks. FAD/Tg4-42^{hom} mice displayed an increased neuron numbers compared to Tg4-42^{hom} mice in the distal portion of the pyramidal layer. As this region is more associated with non-spatial memory, it could be linked with the lack of recognition memory deficits of the bigenic line in the NOR task. On the other hand, the comparable loss in the proximal CA1 region, mainly associated with spatial memory, might correlate with the deficits found in MWM test for both lines. The amyloid pathology deriving from the 5xFAD background had no effects on spatial impairments of Tg4-42^{hom} mice, and even a rescue of recognition memory deficits and distal CA1 neuron loss was observed. Neuron loss in transgenic AD mouse models has been associated with intracellular Aβ accumulation (Wirths and Zampar 2020). In the 5XFAD mouse model, loss of neurons has been reported in cortical layer 5 at 9 and 12 months of age but none in the CA1 region

at any studied age. Interestingly, neuron loss in the fifth cortical layer correlates with intraneuronal $A\beta_{x-42}$ accumulation and, on the same line, no intracellular accumulation of Aβ could be observed in the hippocampus (Jawhar et al. 2012, Shao et al. 2011, Eimer and Vassar 2013). In the Tg4-42^{hom} line, neuron loss is attributed to the predominant intracellular expression and accumulation of $A\beta_{4-42}$ in CA1 pyramidal neurons (Bouter et al. 2013). This might explain our observations, supporting the fact that the abundant extracellular amyloid deposition alone had no influence on neurodegeneration in FAD/Tg4-42^{hom} mice. In good agreement, Lopez-Noguerola and colleagues showed that increased intraneuronal Aβ accumulation in TBA42 mice, resulting from the co-expression of the N-terminally truncated $A\beta_{4-42}$ and $A\beta_{pE3-42}$, led to an increased loss of CA1 pyramidal neurons at 5-6 months (Lopez-Noguerola et al. 2018b).

As a consequence of neurodegeneration, brain atrophy is observed in people suffering from AD and is considered one of the most prominent pathological features of the disease (Jack et al. 2005). Several studies in rodent models correlated hippocampal volume with spatial memory (Moser et al. 1995, Broadbent, Squire, and Clark 2004). While the area of CA1 region of the hippocampus was found comparably reduced in Tg4-42^{hom} and FAD/Tg4-42^{hom} mice, the area of the pyramidal layer was significantly increased in 6-month-old FAD/Tg4-42^{hom}, concomitant with the reduced neuron loss and rescue of recognition memory deficits (Fig. 3.24).

4.3.2.2 Hippocampal amyloid pathology in FAD/Tg4-42^{hom} mice

As already mentioned, soluble oligomeric forms of Aβ and insoluble amyloid plaques might contribute differently to the etiology of AD, with the first better correlating with the severity of the disease (McLean et al. 1999, Wang et al. 1999, Esparza et al. 2013). Different *in-vivo* studies support this differential role (Walsh et al. 2002, Cleary et al. 2005, Lesne et al. 2006, Shankar et al. 2008). Shankar and colleagues reported that soluble Aβ oligomers extracted from the temporal and frontal cortices of AD brains caused inhibition

of long-term potentiation (LTP) and enhancement of long-term depression (LTD). This resulted in impaired learning and memory behavior in wild type rats, however no such effects were seen when insoluble amyloid cores were injected (Shankar et al. 2008). Interestingly, the solubilization of these plaque cores into soluble Aβ dimers led to the above-mentioned negative effects. Additionally, the specific accumulation of Aβ in the extracellular space or intracellular compartments might have a different impact on the pathology. In several AD mouse models, neurodegeneration was indeed correlated with the presence of intraneuronal Aβ accumulation, while extracellular amyloid plaques appeared to be little involved with the loss of neurons (Wirths and Zampar 2020). Given the peculiar contribution of insoluble extracellular Aβ plaques and soluble intraneuronal Aβ on neurodegeneration and development of cognitive deficits, hippocampal amyloid pathology of FAD/Tg4-42^{hom} mice was analyzed and compared to 5xFAD and Tg4-42^{hom} littermates. Tg4-42^{hom} mice accumulate intracellular soluble Aβ$_{4-42}$ peptides in hippocampal CA1 pyramidal neurons, developing age-dependent neuron loss and cognitive deficits (Bouter et al. 2013, Antonios et al. 2013). The 5xFAD line, on the other hand, shows no intracellular Aβ accumulation in the CA1 region of the hippocampus but only extracellular deposition in plaques, which results in no neuron loss in this brain region (Jawhar et al. 2012). No changes in extracellular hippocampal amyloid pathology were observed in young nor aged FAD/Tg4-42^{hom} mice compared to 5xFAD littermates (Fig. 3.25), as the load of both full-length and Aβ$_{4-x}$ peptides remained unaffected (Fig. 3.26). In good agreement with the unchanged extracellular amyloid pathology, no changes in the neuroinflammatory response were observed (Fig. 3.25). Although immunohistochemical analysis can give important information on protein localization, the possibility of characterizing the protein of interest only in restricted spatial depth and only with semiquantitative measures is a limitation of the technique. To further address possible changes at the time-point when a rescue of recognition memory deficits and neuron loss were observed in FAD/Tg4-42^{hom} mice, Aβ concentrations were measured in

the total hippocampus distinguishing between soluble (TBS) and insoluble (SDS) fractions (Fig. 3.27). Total Aβ and full-length $A\beta_{1-x}$ levels were comparable between 5xFAD and FAD/Tg4-42^{hom} mice, while insoluble $A\beta_{4-x}$ concentrations were significantly increased in the bigenic line. This could not be attributed to the mere addition of $A\beta_{4-42}$ coming from the Tg4-42^{hom} background as the N-truncated peptide levels in the latter line were below detection limits in this analysis. Considering the increased neuron numbers and rescue of cognitive deficits in FAD/Tg4-42^{hom} mice at 6 months of age, these results are in line with possible buffering properties of insoluble amyloid plaques, capturing the toxic soluble $A\beta_{4-42}$ and sequestering them from their perpetuating damage. Unfortunately, this hypothesis could not be supported by measuring an alleged corresponding reduction of TBS-soluble $A\beta_{4-42}$ peptides in FAD/Tg4-42^{hom} mice compared to Tg4-42^{hom} littermates. Because the accumulation of $A\beta_{4-42}$ in Tg4-42^{hom} mice occurs predominantly in the CA1 pyramidal layer, soluble $A\beta_{4-42}$ levels could not be measured in this line when analyzing the entire hippocampus as the amounts were below the detection limit of the assay. Additionally, 5xFAD mice showed small amounts (<50 pg/mL) of soluble $A\beta_{4-x}$ in the hippocampus, which would obscure any measurements of intraneuronal $A\beta_{4-42}$ in the FAD/Tg4-42^{hom}, even if they were possible. Analysis of intracellular Aβ accumulation by means of immunohistochemistry in the CA1 pyramidal neurons showed a significant increase of $A\beta_{4-x}$ in immunoreactivity in aged FAD/Tg4-42^{hom} mice compared to Tg4-42^{hom} littermates (Fig. 3.28), which appears to be in contrast with the hypothetical buffering capacity of insoluble extracellular plaques in our scenario. It could be speculated that the higher immunoreactivity could be related to the increased area of the pyramidal layer (Fig. 3.24) and the number of Aβ-producing neurons in the distal CA1 (Fig. 3.23) of FAD/Tg4-42^{hom} mice. The decreased loss of distal CA1 pyramidal neurons (Fig. 3.20) and rescue of recognition memory deficits (Fig. 3.23) in the bigenic line at this specific time-point indeed support the above-mentioned hypothesis. As observed in the spinal cord tissues, $A\beta_{4-x}$ peptides comprise only for a

fraction of Aβ peptides in the 5xFAD mouse model. In the hippocampus, the N-truncated peptide concentrations were 80-fold less than full-length peptides in the SDS-soluble fraction, which is in line with previous results (Wirths et al. 2017, Walter et al. 2019). In the TBS-soluble fraction, the ratio was even lower, with 130-fold decreased amount of $A\beta_{4\text{-}x}$ to $A\beta_{1\text{-}x}$ at 6 months.

The changes in amyloid pathology in FAD/Tg4-42^{hom} mice are difficult to interpret. In summary, $A\beta_{1\text{-}x}$ pathology was generally never affected at neither 3 nor 6 months when $A\beta_{4\text{-}x}$ was co-expressed in 5xFAD mice. While semiquantitative analysis of extracellular amyloid deposition in the CA1 and DG by means of immunohistochemistry showed no difference in $A\beta_{4\text{-}x}$ pathology between 5xFAD and FAD/Tg4-42^{hom} mice, measurements of $A\beta_{4\text{-}x}$ concentrations in the entire hippocampus revealed an increment of insoluble levels in 6-month-old FAD/Tg4-42^{hom} mice. Taking into consideration the improved cognition and neurodegeneration of FAD/Tg4-42^{hom} mice at this time point, this result might support the hypothesis of buffering-properties of insoluble amyloid plaques, sequestering toxic $A\beta_{4\text{-}42}$ peptides in FAD/Tg4-42^{hom} mice. The impossibility to accurately measure the concentration of soluble $A\beta_{4\text{-}42}$ levels in the CA1 region of the hippocampus leaves open the question of whether soluble toxic Aβ oligomers are actually reduced in FAD/Tg4-42^{hom} mice. It is anyway clear that the addition of abundant extracellular amyloid pathology did not have detrimental effects on cognition nor hippocampal neurodegeneration of Tg4-42^{hom} mice at either 3 or 6 months of age.

4.3.3 Conclusions of PROJECT III

4.3.3.1 Conclusions of Part I - Motor phenotype and spinal cord pathology of FAD/Tg4-42^{hom} mice

Based on the results of the present study:

- Co-occurrence of extracellular amyloid pathology and intraneuronal accumulation of $A\beta_{4-42}$ caused aggravation of motor deficits in FAD/Tg4-42^{hom} mice starting at 3 months of age.
- Tg4-42^{hom}, but not 5xFAD mice, showed significant loss of α-MNs in the cervical spinal cord. This loss was increased in FAD/Tg4-42^{hom} mice, which could however be attributed to a cumulative effect.
- FAD/Tg4-42^{hom} presented with reduced extracellular amyloid pathology and both soluble and insoluble Aβ concentration in the spinal cord compared to 5xFAD littermates, which might be caused by the reduced number of Aβ-producing MNs.
- Tg4-42^{hom} and FAD/Tg4-42^{hom} mice both showed clear Aβ accumulation in MNs, with an apparent increase of Aβ-positive MNs in the latter line.
- The aggravated motor phenotype in the FAD/Tg4-42^{hom} line might be caused by the decreased number of α-MNs but cannot relate to extracellular amyloid pathology.

4.3.3.2 Conclusions of Part II - Cognitive phenotype and hippocampal pathology of FAD/Tg4-42^{hom} mice

Based on the results of the present study:

- Extracellular amyloid pathology did not aggravate spatial memory deficits of Tg4-42^{hom} mice and appeared to have a protective effect on recognition memory.
- Increased distal CA1 neuron numbers and increased pyramidal layer area accompanied the rescue of recognition memory deficits in FAD/Tg4-42^{hom} mice.
- No changes in hippocampal extracellular amyloid pathology could be observed in 5xFAD mice after the co-expression of $A\beta_{4-42}$ peptides.
- An increase of insoluble $A\beta_{4-x}$ levels was detected in the hippocampus of FAD/Tg4-42^{hom} mice compared to 5xFAD littermates at 6 months, suggesting a possible

buffering effect of insoluble amyloid plaques on $A\beta_{4\text{-}42}$ oligomers of the Tg4-42^{hom} line.

- Changes of soluble $A\beta_{4\text{-}x}$ levels could technically not be measured. Semiquantitative analysis of CA1 immunoreactivity at 6 months showed increased $A\beta_{4\text{-}x}$ staining in CA1 pyramidal neurons of FAD/Tg4-42^{hom} mice, which could be attributed to the increased number of neurons at this time point.
- Overall, extracellular amyloid pathology had no negative effects on cognition nor hippocampal neurodegeneration in Tg4-42^{hom} mice. The rescue of recognition memory and neurodegeneration, together with the increased amount of insoluble $A\beta_{4\text{-}x}$ levels in FAD/Tg4-42^{hom} mice, support the hypothesis of buffering properties of amyloid plaques.

4.4 PROJECT IV: *In-vivo* relationship of $A\beta_{4\text{-}x}$ peptides and protein tau

Next to extracellular Aβ senile plaques, one of the main neuropathological hallmarks of AD is the intracellular accumulation of hyperphosphorylated tau into neurofibrillary tangles (NFTs) (Grundke-Iqbal et al. 1989). According to the amyloid cascade hypothesis, Aβ is believed to trigger the formation of NFTs and the subsequent neurodegeneration, being upstream in the pathological order of events (Bloom 2014). This hypothesis is supported by observations made in different mouse model of AD co-expressing APP and tau, in which an aggravation of tau pathology and behavioral decline is reported without alterations in amyloid pathology (Hurtado et al. 2010, Saul et al. 2013b, Stancu et al. 2014a). Although the aggravating effects of extracellular Aβ deposits on tau pathology were largely studied, the contribution of soluble Aβ peptides is still much less clear. Soluble Aβ dimers isolated from human AD brain were reported to induce tau hyperphosphorylation in hippocampal neurons when applied at sub-nanomolar concentrations (Jin et al. 2011). On the other hand, *in-vivo* studies in murine models gave conflicting results. While intracerebral injection of $A\beta_{1\text{-}42}$ peptides induced tau

phosphorylation and aggregation in the P301S transgenic tau model (Hu et al. 2014), co-expression of $A\beta_{1-42}$ and transgenic human tau did not lead to an increased tau pathology (Gomes et al. 2019). As already mentioned, N-terminally truncated Aβ peptides account for the majority of Aβ species in AD brains, with $A\beta_{4-42}$ being one of the most abundant and highly toxic (Portelius et al. 2010, Wildburger et al. 2017, Cabrera et al. 2018, Bouter et al. 2013). To understand whether this important N-truncated variant has an impact on the onset or extent of tau pathology, we crossed the Tg4-42^{hom} mouse model of AD, expressing exclusively $A\beta_{4-42}$ peptides, with the MAPT (PS19) mouse model of tauopathy, expressing mutant P301S human microtubule-associated protein tau (MAPT).

4.4.1 Behavioral characterization of MAPT/Tg4-42^{hom} mice

Motor abilities, balance, and strength were assessed with the accelerating rotarod, balance beam, and inverted grid tasks in control and transgenic mice. Several studies showed that the MAPT line did not manifest obvious locomotor impairments compared to age-matched WT mice in the tasks and ages considered here (Mikhail et al. 2015, Takeuchi et al. 2011, Sun et al. 2020). While we concurrently observed no deficits in our study, MAPT mice appeared to perform slightly better than controls in the accelerating rotarod task (Fig. 3.30). A hyperactive phenotype resulting in a non-significant improvement in rotarod performance was previously reported in 6-month-old P301S mice (Takeuchi et al. 2011). Moreover, Sun and coworkers recently reported a ~10% prolonged latency in the accelerating rotarod test for 3.5- to 12-month-old MAPT mice (Sun et al. 2020), a finding that is supported by our data. Clear motor impairments in the rotarod and balance beam tasks have been described in the Tg4-42^{hom} line starting around 6 months of age (Wagner et al. 2019, Stazi and Wirths 2021), accompanied by intracellular Aβ accumulation in motoneurons (Lopez-Noguerola et al. 2018b). Although we observed deficits in the accelerating rotarod already at 3 months of age, Tg4-42^{hom} mice performed comparably to controls in the balance beam and inverted grid tasks at 3 and 5 months,

confirming the previous findings (Fig. 3.30). The co-expression of $A\beta_{4\text{-}42}$ and mutant human tau led to the development of motor deficits in the balance beam task at 5 months but MAPT/Tg4-42^{hom} mice generally did not perform differently than the Tg4-42^{hom} parental line from a motor point of view. Motor performances have been assessed in several AD mouse models co-expressing mutated human APP and tau protein, giving unclear results on whether the concomitant expression could lead to an aggravation of the phenotype. Similar to our observations, Tg2576 mice crossed with P301L tau mice showed an aggravated phenotype on the balance beam task at 7 months of age, but generally did not perform worse than controls or the transgenic parental lines in the accelerating rotarod tasks at 5 and 7 months (Morgan et al. 2008). 3xTg mice, expressing APP_{SWE}, $PS1_{M146V}$, and Tau_{P301L}, displayed no motor deficits in the rotarod or wire suspension tasks at 9 months (Sterniczuk et al. 2010). Stover and coworkers even reported enhanced motor performance on the rotarod, but aggravation in grid suspension task at 6 months (Stover et al. 2015). On the other hand, 5xFADxTg30 mice displayed clear motor impairments in the accelerating rotarod task compared to both controls and the transgenic parental lines starting at 6 months of age (Héraud et al. 2014) and clear motor deficits in the accelerating rotarod tasks could be observed in 12-month-old APP/Tau mice, expressing APP_{SWE} and Tau_{P301L}, compared to controls (Saydoff et al. 2013). Unfortunately, no study on motor function investigated transgenic lines crossed with the P301S line used here. Overall, it appears that although an aggravation was observed in few tasks, no obvious exacerbation of motor pathology is displayed in mice developing both Aβ and tau pathology. Spontaneous locomotor activity in the open field test also points into this direction (Fig. 3.31), with no diminished average speed in the bigenic line at any time point.

Anxiety-like behavior can be assessed through the time mice spend in the center of the open field arena and in the open arms of the elevated plus maze task. Psychological

symptoms have indeed been observed in AD patients (Ferretti et al. 2001, Chung and Cummings 2000, Hart et al. 2003). Several transgenic mouse models of AD display a reduced anxiety-like behavior in these tasks (O'Leary et al. 2018, Jawhar et al. 2012, Stazi and Wirths 2021), which would mimic the disinhibited behavior observed in people suffering from AD. In the open field task, only the Tg4-42^{hom} line displayed significantly reduced anxiety-like behavior, starting already at 3 months (Fig. 3.31). The MAPT line, as reported (Ohia-Nwoko et al. 2014), did not show any alteration in anxiety-like phenotype, even in the aged group, and this observation applied also to the bigenic line studied here. Mice co-expressing A$\beta_{4\text{-}42}$ and mutated human protein tau behave comparably to the parental transgenic lines also in the EPM task, suggesting no general alteration of anxiety like behavior in MAPT/Tg4-42^{hom} mice (Fig. 3.32).

Cognition performances were tested in the Cross Maze, Novel Object Recognition (NOR), and Morris Water Maze (MWM) tasks. The Cross Maze task investigates the presence of working memory deficits and is based on the natural tendency of mice to explore novel environments. Working memory impairments in the Y-maze task, which is based on the same principles as the Cross Maze but with a lower degree of complexity, have been reported in mice expressing the tau P301S mutation from 6-7 months (Van der Jeugd et al. 2016, Vagnozzi, Giannopoulos, and Pratico 2018), and were observed in the present study in the aged group when the Cross Maze task was performed (Fig. 3.32). The Tg4-42^{hom} line, on the other hand, showed no working memory deficits, even in the aged group. The bigenic MAPT/Tg4-42^{hom} line displayed impairments comparable to the MAPT parental line at 9 months, but without further aggravation. Analysis of working memory in other transgenic lines presenting both Aβ and tau pathology gave conflicting results. Working memory impairment has been observed in 7-9 months 3xTg-AD mice compared to WT controls (Duarte et al. 2020), but the lack of the transgenic parental lines in the study prevents the understanding of whether an aggravation compared to mice

exclusively presenting Aβ or tau pathology occurred. On the other hand, Tg2576 mice crossed with the Tau^{P301L}-JNPL3 line showed no deficits at 7-8 months of age (Morgan et al. 2008).

Recognition memory, based on the ability to recognize a previously encountered object as familiar, was assesses in the NOR task. Deficits have been reported in lines overexpressing APP and mutant tau. Indeed, impairments in the NOR task were observed in 3xTg (Filali et al. 2012) and APP/Tau (Saydoff et al. 2013) mice compared to WT controls, but it is worth mentioning that single transgenic Tg2576 mice, expressing the same APP^{SWE} mutation, presented with impairments in the NOR tasks at the same 7 months' time point (Giuliani et al. 2013). In the present study we saw no aggravation of recognition memory in bigenic MAPT/Tg4-42^{hom} mice (Fig. 3.33). An expected impairment in the aged group deriving from the Tg4-42^{hom} line was observed, as this line starts to develop recognition memory deficits at around 6 months of age (Stazi and Wirths 2021).

On the other hand, increased spatial memory deficits in the MWM were detectable in mice co-expressing Aβ$_{4-42}$ and mutated human tau. The Morris Water Maze (MWM) test is one of the most-widely used tasks to study age- and hippocampal-dependent memory deficits in rodents (Morris 1984, Duyckaerts, Potier, and Delatour 2008). As already mentioned, spatial learning and long-term spatial reference memory can be distinguished in this task and assessed during the acquisition training and probe trial, respectively (Vorhees and Williams 2006). Spatial learning deficits during the acquisition training could be spotted in MAPT/Tg4-42^{hom} mice already at 3 months and worsened with time (Fig. 3.34). Aged Tg4-42^{hom}, which usually develop spatial memory deficits around 6 months (Stazi and Wirths 2021, Antonios et al. 2015), and aged MAPT/Tg4-42^{hom} mice both failed to remember the position of the target quadrant, but the bigenic line presented with this inability already at 5 months of age (Fig. 3.35). Analyses of additional parameters supported the observed worsening of spatial memory in mice expressing

both Aβ4-42 and mutated human tau already at a young age (Fig. 3.36). Although both MAPT and Tg4-42hom mice showed deficits in spatial memory at 9 months, the MAPT/Tg4-42hom group performed the worst. The presence of spatial memory deficits in the MAPT line is controversial. Some studies described the development of deficits in the MWM test starting at 5-6 months (Takeuchi et al. 2011, Eckenweber et al. 2020), while in other studies impairments became evident between 10-12 months (Sun et al. 2020, Chalermpalanupap et al. 2018). Considering other mouse models co-expressing amyloid and tau pathology, a worsening of spatial learning deficits were reported also in 6-month-old 5xFAD mice crossed with the MAPT line used in our study, performing a modified version of the MWM task (Stancu et al. 2014a). APP/Tau mice, on the other hand, showed no deficits at 9 months and, while spatial memory impairments could be observed at 16 months, they did not perform differently from the APPSWE parental line (Ribe et al. 2005). Unfortunately, the work of Stancu and colleagues (Stancu et al. 2014a) is, to the best of my knowledge, the only one in which the MAPT (PS19) line was crossed with an AD mouse model to assess the behavior phenotype of the resulting filial line. The other transgenic mouse models co-exhibiting Aβ and tau pathology used different tau transgenic line thus the comparison of the observations should be careful. Additionally, discrepancies among the different studies could be attributed to differences in the transgene promoter, the transgene expression patterns, and levels, age, sex, and genetic background of the animals used and/or variants in the paradigms used. From a behavioral point of view, the effects of the co-expression of transgenes leading to Aβ and tau pathology are unclear. While some observations point towards an aggravated phenotype upon co-expression of the two proteins, an unquestionable worsening of behavior performances cannot be stated. In the present work, the co-expression of specifically Aβ4-42 and mutated human tau did not lead to an aggravation of working memory nor recognition memory, assessed in the cross maze and NOR, respectively. Also, anxiety-like behavior and motor performances appeared generally unaffected. On

the other hand, a worsening of spatial learning and spatial reference memory was observed in the bigenic line, showing reduced performance already at 3 and 5 months, representing time points when the parental lines still performed similarly to WT controls. We can exclude an influence of differential transgene expression on the results given here, as the transgenic lines presented with comparable transgene mRNA levels at all the considered time points (Fig. 3.29).

4.4.2 Increased neuron loss only in distal CA1 of young MAPT/Tg4-42^{hom} mice

As already mentioned, neurodegeneration in the hippocampus has been associated with the development of memory deficits in rodent models. Impairments in the MWM and NOR tasks, assessing spatial and recognition memory, have been connected to loss of CA1 pyramidal neurons (Broadbent et al. 2010, Squire, Wixted, and Clark 2007, Morris 1984). Additionally, the Cross Maze task was found to be sensitive to hippocampal impairments (Lalonde 2002). Since different types of memory were affected differently in the bigenic MAPT/Tg4-42^{hom} line, we have analyzed neuron numbers distinguishing between distal and proximal regions of the CA1 pyramidal layer as they are correlated with the development of specific memory delays: the distal CA1 is associated with non-spatial memory while the proximal part is closer linked to spatial memory formation (Masurkar 2018). The Tg4-42^{hom} line displayed an expected age-dependent loss of both distal and proximal CA1 pyramidal neurons, with a more prominent degeneration in the distal region (Fig. 3.37). Young MAPT/Tg4-42^{hom} mice presented with increased neurodegeneration compared to Tg4-42^{hom} mice in the distal part of the CA1. However, this loss was not accompanied by specific non-spatial memory deficits as they displayed intact working and recognition memory. No significant further aggravation of the neuron loss could be observed in the MAPT/Tg4-42^{hom} in neither distal nor proximal region of the hippocampus at the considered time points. At 5 months MAPT/Tg4-42^{hom} mice possessed reduced albeit not significantly, proximal neuron numbers, concomitant with

the development of spatial reference deficits in the MWM task. The clear deficits observed in the aged group could not be associated with changes in neuron loss as the bigenic line presented comparable numbers to the Tg4-42^{hom} parental line. The lack of a difference at 5 and 9 months could be attributed to the extensive neuron loss characterizing the Tg4-42^{hom} line already at 5 months. Neurodegeneration reaches a plateau after this point, with an additional loss of only 10% of neurons between 5 and 9 months of age. The MAPT line did not show loss of CA1 pyramidal neurons in the aged group, while spatial memory deficits were observed at this time point. Previously, neurodegeneration of the CA3 neurons and reduced DG volume have been described at 8 months in the MAPT line (Yoshiyama et al. 2007, Liu et al. 2019). Indeed, loss of neurons in regions of the hippocampus not analyzed here could be related with the spatial memory cognitive deficits observed in this line and in mice co-expressing Aβ_{4-42} and P301S mutated tau. Contrary to our finding, increased CA1 neurodegeneration was evident in 9-month-old 5xFAD mice crossed with P301S tau transgenic mice in comparison to the parental transgenic 5xFAD or MAPT lines (Saul et al. 2013b). Similarly, a significant loss of hippocampal pyramidal neurons was reported in 5xFADxTg30 mice at the same time point (Héraud et al. 2014). On the same trend, Tg2576 mice crossed with Tau^{VLW}, harboring three tau mutations, presented with reduced pyramidal neuron numbers in the entorhinal cortex at 9 months compared to non-transgenic controls (Ribe et al. 2005). Increased hippocampal neurodegeneration has thus been observed in mutant-APP overexpressing mice when crossed with models of tauopathy, while no general aggravation was observed in our model expressing exclusively Aβ_{4-42} and P301S tau. As mentioned before, this could be related to the extensive neuron loss in the single Tg4-42^{hom} mice. Synapse loss and disrupted synaptic transmission were observed in AD patient and associated to the detrimental effects of both Aβ and tau proteins (Spires-Jones and Hyman 2014). Several studies in rodent models suggest that Aβ and tau indeed

cooperate at synapse level leading to LTP impairments and resulting in behavioral deficits (Shipton et al. 2011, Pickett et al. 2019, Ittner et al. 2010).

4.4.3 Hippocampal Aβ pathology and tau hyperphosphorylation in MAPT/Tg4-42^{hom} mice

According to the classical amyloid cascade hypothesis, accumulation of Aβ is one of the upstream events leading to the formation of NFT and subsequent loss of synapses and neurons (Hardy and Selkoe 2002). Several experimental paradigms have been used to investigate the effects of an excess of Aβ peptide on tau pathology. A five-fold increased number of NFTs could be measured after fibrillary Aβ$_{42}$ peptides were injected into the brains of P301L mutant tau transgenic mice (Gotz et al. 2001). Related findings showed that pre-aggregated Aβ was able to induce fibrillization of tau both *in-vitro* and *in-vivo* (Vasconcelos et al. 2016) and, interestingly, passive immunization against Aβ resulted in reduced tau pathology in the 3xTg mouse model of AD (Oddo et al. 2004). In contrast, mutant tau appears to have no influence on Aβ accumulation. We observed no increase in amyloid pathology in the Tg4-42^{hom} line upon co-expression of mutant tau (Fig. 3.39), which is in good agreement with previous findings. No alteration of Aβ immunoreactivity was detected in PDAPP mice at 8-11 months (Hurtado et al. 2010) or in 5xFAD mice at either 3 or 9 months (Saul et al. 2013b) when crossed with the same P301S tau transgenic line employed in our study. However, increased amyloid pathology was spotted in the Tg2576 line after crossing with a tau transgenic mouse model expressing a triple-mutated tau (Ribe et al. 2005). The so-far-mentioned transgenic lines overexpress human APP and present with robust extracellular amyloid pathology, while the Tg4-42^{hom} line is mostly characterized by intracellular accumulation of the Aβ$_{4-42}$ peptides in CA1 hippocampal pyramidal neurons. A related model, expressing exclusively Aβ$_{1-42}$ peptides without the presence of APP overexpression and formation of extracellular amyloid plaques, is the APP48 mouse model (Abramowski et al. 2012). Like Tg4-42^{hom} mice, APP48 rodents present with intracellular Aβ lesions and hippocampal

neurodegeneration already at 3 months. When crossed with a transgenic line expressing P301S mutated tau (TAU58), no evidence of increased soluble Aβ levels was observed (Gomes et al. 2019), similarly to our findings. The absence of significant increment of phospho-tau pathology after the Aβ expressing line is crossed with a model of tauopathy is another similarity with our study. We indeed observed no significant increase of phosphorylated tau immunoreactivity in MAPT/Tg4-42^{hom} mice when compared to MAPT controls at any of the considered ages (Fig. 3.40), if not for a trend at 3 months. The findings in these two models harboring transgenic Aβ peptides are in striking contrast to the obvious exacerbation of tau pathology reported in several APP-overexpressing mice when crossed with tau transgenic lines (Grueninger et al. 2010, Hurtado et al. 2010, Chabrier et al. 2012, Saul et al. 2013b, Stancu et al. 2014a, Héraud et al. 2014). Focusing on the studies employing the same PS19 tau line used here, 5xFAD/PS19 mice showed increased hyperphosphorylated tau immunoreactivity in the hippocampal CA1 field already at 3 months, which worsens over time (Saul et al. 2013b, Stancu et al. 2014a). Additionally, Stancu and colleagues reported increased tau pathology in the same line in the cortex and entorhinal cortex at 9 months (Stancu et al. 2014a). On the same trend, accelerated neurofibrillary tangle formation was reported in PDAPP/PS19 mice by Hurtado and coworkers (Hurtado et al. 2010). The overexpression of APP could be a critical factor in the exacerbation of phospho-tau pathology in these lines. Takahashi and coworkers reported that intracellular aggregation of phosphorylated tau was induced in cell culture by APP in a dose-dependent fashion (Takahashi et al. 2015). Recent findings additionally suggest that the detrimental effects of oligomeric tau on LTP in wildtype mice might be APP-dependent (Puzzo et al. 2017).

In summary, Aβ$_{4-42}$ peptides did not cause an aggravation of hippocampal tau hyperphosphorylation and NFTs. As tau pathology has been found to nicely relate to neuronal loss (Gomez-Isla et al. 1997, Giannakopoulos et al. 2003) and grey matter

atrophy (Jack et al. 2002, Whitwell et al. 2008) in AD patients, it is no surprise that further neurodegeneration of hippocampal CA1 pyramidal neurons was generally not observed in MAPT/Tg4-42^{hom} mice. Supporting this correlation, when a trend towards significant increase of tau phosphorylation was present in young mice (Fig. 4.41), an enhanced neurodegeneration in distal CA1 could be appreciated (Fig. 3.38). The lack of exacerbated tau pathology and neurodegeneration suggests that the worsening of spatial memory deficits at later time points must be attributed to other types of impairments in mice co-expressing A$\beta_{4\text{-}42}$ and P301S tau. It is possible that the additive singular detrimental effects of A$\beta_{4\text{-}42}$ and tau caused the behavioral deficits in MAPT/Tg4-42^{hom} mice. Since several APP/tau transgenic lines reported aggravated pathology, our study supports an important role of transgenic human APP overexpression and extracellular amyloid plaques for an enhanced formation of neurofibrillary tangles.

4.4.4 Conclusions of PROJECT IV

Based on the results of the present study:

- Co-expression of A$\beta_{4\text{-}42}$ and P301S tau in MAPT/Tg4-42^{hom} mice led to a partial worsening of the motor phenotype at 5 months, while anxiety-like behavior remained unchanged.
- Expression of transgenic tau in Tg4-42^{hom} mice aggravated spatial learning and memory deficits from a young age, while recognition memory was unaffected.
- The observed spatial memory deficits cannot be explained by an increased hippocampal neurodegeneration at 5 and 9 months, as Tg4-42^{hom} and MAPT/Tg4-42^{hom} mice presented with comparable CA1 pyramidal neuron numbers.
- The expression of P301S tau did not alter hippocampal Aβ pathology in Tg4-42^{hom} and, likewise, A$\beta_{4\text{-}42}$ had generally no influence on hippocampal phospho-tau levels.

- The observed deficits could be caused by the additive detrimental effects of $A\beta_{4\text{-}42}$ and transgenic tau, by neuron loss in brain region here not assessed or by other physiological impairments which do not result in neuron loss.
- Our data support an important role of extracellular plaque pathology and APP overexpression in the exacerbation of tau pathology in *in-vivo* models.

5 SUMMARY AND CONCLUSIONS

A heterogeneity of amyloid-β peptides (Aβ) variants have been described in the brains of Alzheimer's disease (AD) patients by means of mass spectrometry. Alongside full-length Aβ peptides, a variety of C-terminally and N-terminally truncated species were identified. N-terminally truncated peptides were the most prominent species with $A\beta_{4\text{-}42}$ being one of the most abundant variants.

In the first project, we confirmed and further characterized the heterogeneity of Aβ with immunohistochemical staining of *post mortem* tissues from AD brains, qualitatively analyzing the spatial localization and distribution of full-length and N-terminally truncated Aβ variants, which would not be possible with classical mass spectrometry techniques. While the heterogeneity of N-truncated peptides could be appreciated in both plaques and vessels in AD and non-demented control cases (NDC), we noticed a possible different distribution pattern between full-length and $A\beta_{4\text{-}x}$ peptides. Parenchymal plaques showed strong immunoreactivity of both $A\beta_{1\text{-}x}$ and $A\beta_{4\text{-}x}$, but while full-length peptides showed a wide-spread and neuritic plaques staining pattern, $A\beta_{4\text{-}x}$ was found predominantly in the dense plaque cores. Differences were observed also in terms of vascular depositions. $A\beta_{1\text{-}x}$ accumulation in vessels was generally more prominent than $A\beta_{4\text{-}x}$ and more abundant in meningeal vessels, while $A\beta_{4\text{-}x}$ peptides deposited relatively more in parenchymal vessels than in meningeal ones. Such heterogeneity and diverse distribution suggest a possible different involvement of these Aβ variants in the etiology and pathology of the disease.

In addition to being one of the most abundant N-terminally truncated species, $A\beta_{4\text{-}42}$ was reported having a comparable toxicity to full-length $A\beta_{1\text{-}42}$. Despite several studies supporting an important role of $A\beta_{4\text{-}42}$ in AD pathology, it is at present not fully

understood how changes in the generation and clearance of these peptides would affect the disease, nor how they relate to the main neuropathological hallmarks of AD, extracellular amyloid plaques and hyperphosphorylated tau deposits. We aimed to address and provide more insight on these topics in the following projects.

In sporadic cases of AD, the increased amyloid deposition is believed to be related, among other things, to a reduced clearance of Aβ peptides. Neprilysin (NEP) is one of the most characterized Aβ-degrading enzymes, able to digest full-length Aβ peptides. In the first part of Project II, we tested whether $A\beta_{4\text{-}42}$ peptides are susceptible to hydrolysis by NEP. We showed that $A\beta_{4\text{-}42}$ peptides, along with $A\beta_{4\text{-}40}$, are indeed subjected to digestion by recombinant NEP *in-vitro*. Interestingly, NEP appeared to hydrolyze $A\beta_{4\text{-}x}$ peptides at higher rates than the full-length counterpart. To assess whether $A\beta_{4\text{-}42}$ peptides are hydrolyzed by NEP *in-vivo*, endogenous NEP was removed in the Tg4-42^{het} mouse model of AD, expressing exclusively $A\beta_{4\text{-}42}$ peptides, by crossing with NEP knock-out mice (NEP$^{-/-}$). When lacking endogenous NEP, Tg4-42^{het} mice showed increased $A\beta_{4\text{-}42}$ accumulation at young age, indicating that $A\beta_{4\text{-}42}$ peptides are indeed also degraded by NEP *in-vivo*. The generation of $A\beta_{4\text{-}x}$ in AD brains is still not fully unraveled. Among the proteases linked with the generation of N-truncated peptides, ADAMTS4 was reported to produce $A\beta_{4\text{-}x}$ both *in-vitro* and *in-vivo*. To study how the absence of endogenous ADAMTS4 would affect $A\beta_{4\text{-}x}$ pathology, 5xFAD mice on a full ADMATS4 knock-out (ADAMTS4$^{-/-}$) background were previously generated. Upon absence of endogenous ADAMTS4 metalloprotease, reduced $A\beta_{4\text{-}x}$ concentrations were previously reported in brain lysates of 5xFAD mice. In the second part of Project II, we further characterized the effects of an ADAMTS4$^{-/-}$ background on the behavior and amyloid pathology of 5xFAD mice. The absence of endogenous ADAMTS4 led to the rescue of motor deficits in 9-month-old 5xFAD mice but working memory deficits that characterize the AD line at this time point remained unaltered. The ADAMTS4 metalloprotease was found to be

exclusively expressed in oligodendrocytes, which could explain why the main effects of its absence were observed on a motor level. These changes were accompanied by a reduction of $A\beta_{4-x}$ pathology in the gray matter of the cervical spinal cord. We observed that Aβ thread-like structures, which can be found in brain and spinal cord of 5xFAD and linked to the development of axonopathy, were composed of both $A\beta_{1-x}$ and $A\beta_{4-x}$ in the grey matter, while only $A\beta_{4-x}$-positive threads could be observed in the white matter of the spinal cord. In 5xFAD/ADAMTS4$^{-/-}$, the $A\beta_{4-x}$-positive threads appeared to be greatly reduced in the gray matter and absent in the white matter. $A\beta_{1-x}$ plaque and threads pathology remained, on the other hand, unchanged, supporting the specific activity of ADAMTS4 in generating $A\beta_{4-x}$ N-truncated peptides.

In Project III, we aimed to address the relationship between insoluble fibrillar plaques and soluble $A\beta_{4-42}$ oligomers *in-vivo*. To this end, we crossed the already mentioned 5xFAD and Tg4-42^{hom} mouse models of AD to generate FAD/Tg4-42^{hom} mice. While the 5xFAD mouse model of AD is characterized by abundant extracellular amyloid pathology in brain and spinal cord, it presents with no neurodegeneration nor deficits in the test here employed at the analyzed ages of 3 and 6 months. On the other hand, the Tg4-42^{hom} line presents intraneuronal accumulation of soluble $A\beta_{4-42}$ but no extracellular plaques deposits, strong hippocampal neurodegeneration, and cognitive deficits at 6 months of age. In the first part of the project, we focused on the motor phenotype and spinal cord pathology of FAD/Tg4-42^{hom} mice. When extracellular amyloid pathology and intraneuronal accumulation of $A\beta_{4-42}$ co-existed, we observed an aggravation of motor performances in FAD/Tg4-42^{hom} mice. Tg4-42^{hom} mice presented with a significant α-MNs degeneration but a further loss of α-MNs could be measured in the cervical spinal cord of FAD/Tg4-42^{hom} mice. It is questionable whether this aggravation is the result of the cumulative loss of the Tg4-42^{hom} and 5xFAD parental lines. The increased motor deficits and loss of MNs could not be related to extracellular amyloid pathology as FAD/Tg4-

42^{hom} mice showed a surprising reduction of the load of extracellular amyloid deposits and of insoluble Aβ concentrations in the spinal cord. Since both Aβ$_{1-x}$ and Aβ$_{4-x}$ variants were reduced, we assumed that the general reduction of production could be the consequence of the decreased number of MNs in the filial line. An apparent increment of MNs accumulating intracellular Aβ seen in FAD/Tg4-42^{hom} mice could explain the aggravated phenotype, but quantitative measurements would be necessary to confirm this hypothesis. In the second part of the project, we focused on cognition and hippocampal pathology. Extracellular amyloid pathology did not worsen spatial memory deficits in the Tg4-42^{hom} line and even appeared to be beneficial to recognition memory. The rescue of recognition impairments was accompanied by a decreased neurodegeneration of pyramidal neurons in the distal CA1, a hippocampal subfield connected with the formation of non-spatial memory. No changes in the proximal CA1, connected with spatial memory, were observed, which is in line with the lack of alteration of spatial memory deficits in the MWM task. Generally, no changes in hippocampal extracellular amyloid pathology could be observed in 5xFAD mice after the co-expression of Aβ$_{4-42}$ peptides, but measurements of Aβ$_{4-x}$ levels in the hippocampus showed an increased concentration in the hippocampal insoluble fraction of FAD/Tg4-42^{hom} mice. This result, together with the partial cognition rescue and increased neuron numbers, might suggest a possible buffering effect of insoluble amyloid plaques on the toxic Aβ$_{4-42}$ oligomers of the Tg4-42^{hom} line. The measurement of an alleged reduction of soluble Aβ$_{4-42}$ oligomers in the CA1 pyramidal neurons of FAD/Tg4-42^{hom} mice would be the essential next step to corroborate this hypothesis. Unfortunately, because of the experimental design and technical possibilities it was not possible to perform such measurements. Semiquantitative analysis of Aβ$_{4-x}$ immunoreactivity in the CA1 pyramidal layer showed increased Aβ load in 6-month-old FAD/Tg4-42^{hom} mice compared to Tg4-42^{hom} littermates, which we believe secondary to the increased number of neurons at this time point. Overall, extracellular amyloid deposits could not be related to an aggravation of motor

nor cognitive behavior in the FAD/Tg4-42^{hom} mice. The rescue of recognition memory and hippocampal neurodegeneration, together with the increased amount of insoluble Aβ_{4-x} levels in FAD/Tg4-42^{hom} mice, supports the hypothesis of buffering properties of amyloid plaques.

In the last project, we analyzed the *in-vivo* association between soluble Aβ_{4-42} peptides and tau pathology by crossing the already mentioned Tg4-42^{hom} line with the MAPT (PS19) mouse model of tauopathy. Aβ is believed to act upstream in the pathological cascade of events, triggering the formation of tau aggregation in neurofibrillary tangles (NFTs) and the subsequent neurodegeneration. This hypothesis is supported by the study of line co-expressing human mutated APP and transgenic tau, showing that extracellular Aβ deposits have an aggravating effect on tau pathology. The contribution of soluble Aβ peptides is, however, still under investigated. In our study, co-expression of Aβ_{4-42} peptides and mutant human tau caused partial worsening of motor performances and increased spatial memory impairments, while recognition memory and anxiety-like behavior appeared to be unaffected. The observed aggravations, however, could not be explained by increased hippocampal CA1 neurodegeneration nor increased tau pathology in MAPT/Tg4-42^{hom} mice. Neuron loss and hyperphosphorylated tau immunoreactivity were indeed generally comparable between the filial and parental lines. The lack of exacerbation of tau pathology and neurodegeneration might suggest that the singular additive detrimental effects of Aβ_{4-42} and transgenic tau could be the cause of the observed behavioral changes. Alterations in other brain regions or physio-pathological pathways not analyzed here could lie behind the aggravated behavioral phenotypes of MAPT/Tg4-42^{hom} mice. Alternatively, since several APP/tau transgenic lines reported aggravated pathologies, human APP overexpression and extracellular amyloid plaques might be fundamental for an enhanced formation of neurofibrillary tangles.

6 BIBLIOGRAPHY

Abramowski D., Rabe S., Upadhaya A. R., Reichwald J., Danner S., Staab D., Capetillo-Zarate E., Yamaguchi H., Saido T. C., Wiederhold K. H., Thal D. R., and Staufenbiel M. 2012. "Transgenic Expression of Intraneuronal Aβ42 But Not Aβ40 Leads to Cellular Aβ Lesions, Degeneration, and Functional Impairment without Typical Alzheimer's Disease Pathology." *The Journal of Neuroscience* 32 (4):1273-1283. doi: 10.1523/jneurosci.4586-11.2012.

Aggarwal N. T., Wilson R. S., Beck T. L., Bienias J. L., and Bennett D. A. 2006. "Motor dysfunction in mild cognitive impairment and the risk of incident Alzheimer disease." *Arch Neurol* 63 (12):1763-9. doi: 10.1001/archneur.63.12.1763

Ahmed T., Van der Jeugd A., Blum D., Galas M. C., D'Hooge R., Buee L., and Balschun D. 2014. "Cognition and hippocampal synaptic plasticity in mice with a homozygous tau deletion." *Neurobiol Aging* 35 (11):2474-2478. doi: 10.1016/j.neurobiolaging.2014.05.005.

Ait-Bouziad N., Lv G., Mahul-Mellier A. L., Xiao S., Zorludemir G., Eliezer D., Walz T., and Lashuel H. A. 2017. "Discovery and characterization of stable and toxic Tau/phospholipid oligomeric complexes." *Nat Commun* 8 (1):1678. doi: 10.1038/s41467-017-01575-4.

Aizenstein H. J., Nebes R. D., Saxton J. A., Price J. C., Mathis C. A., Tsopelas N. D., Ziolko S. K., James J. A., Snitz B. E., Houck P. R., Bi W., Cohen A. D., Lopresti B. J., Dekosky S. T., Halligan E. M., and Klunk W. E. 2008. "Frequent amyloid deposition without significant cognitive impairment among the elderly." *Arch Neurol* 65 (11):1509-17. doi: 10.1001/archneur.65.11.1509.

Alexandru A., Jagla W., Graubner S., Becker A., Bauscher C., Kohlmann S., Sedlmeier R., Raber K. A., Cynis H., Ronicke R., Reymann K. G., Petrasch-Parwez E., Hartlage-Rubsamen M., Waniek A., Rossner S., Schilling S., Osmand A. P., Demuth H. U., and von Horsten S. 2011. "Selective Hippocampal Neurodegeneration in Transgenic Mice Expressing Small Amounts of Truncated A{beta} Is Induced by Pyroglutamate-A{beta} Formation." *J Neurosci* 31 (36):12790-12801. doi: 10.1523/JNEUROSCI.1794-11.2011.

Allinson T. M., Parkin E. T., Turner A. J., and Hooper N. M. 2003. "ADAMs family members as amyloid precursor protein alpha-secretases." *J Neurosci Res* 74 (3):342-52. doi: 10.1002/jnr.10737.

Almeida C. G., Takahashi R. H., and Gouras G. K. 2006. "Beta-amyloid accumulation impairs multivesicular body sorting by inhibiting the ubiquitin-proteasome system." *J Neurosci* 26 (16):4277-88. doi: 10.1523/JNEUROSCI.5078-05.2006.

Almeida C. G., Tampellini D., Takahashi R. H., Greengard P., Lin M. T., Snyder E. M., and Gouras G. K. 2005. "Beta-amyloid accumulation in APP mutant neurons reduces PSD-95 and GluR1 in synapses." *Neurobiol Dis* 20 (2):187-98. doi: 10.1016/j.nbd.2005.02.008

Alonso A., Zaidi T., Novak M., Grundke-Iqbal I., and Iqbal K. 2001. "Hyperphosphorylation induces self-assembly of tau into tangles of paired helical filaments/straight filaments." *Proc Natl Acad Sci U S A* 98 (12):6923-8. doi: 10.1073/pnas.121119298.

Alzheimer A. 1907. "Über eine eigenartige Erkrankung der Hirnrinde." *Allg. Zeitsch. Psychiatrie Psychisch-gerichtliches Med.* 64:146-148.

Andreadis A. 2005. "Tau gene alternative splicing: expression patterns, regulation and modulation of function in normal brain and neurodegenerative diseases." *Biochim Biophys Acta* 1739 (2-3):91-103. doi: 10.1016/j.bbadis.2004.08.010.

Antonios G., Borgers H., Richard B. C., Brauß A., Meißner J., Weggen S., Pena V., Pillot T., Davies S. L., Bakrania P., Matthews D., Brownlees J., Bouter Y., and Bayer T. A. 2015. "Alzheimer therapy with an antibody against N-terminal Abeta 4-X and pyroglutamate Abeta 3-X." *Scientific Reports* 5:17338. doi: 10.1038/srep17338.

Antonios G., Saiepour N., Bouter Y., Richard B., Paetau A., Verkkoniemi-Ahola A., Lannfelt L., Ingelsson M., Kovacs G., Pillot T., Wirths O., and Bayer T. 2013. "N-truncated Abeta starting with position four: early intraneuronal accumulation and rescue of toxicity using NT4X-167, a novel monoclonal antibody." *Acta Neuropathologica Communications* 1 (1):56.

Aoki M., Volkmann I., Tjernberg L. O., Winblad B., and Bogdanovic N. 2008. "Amyloid beta-peptide levels in laser capture microdissected cornu ammonis 1 pyramidal neurons of Alzheimer's brain." *Neuroreport* 19 (11):1085-9. doi: 10.1097/WNR.0b013e328302c858.

Apte S. S. 2009. "A disintegrin-like and metalloprotease (reprolysin-type) with thrombospondin type 1 motif (ADAMTS) superfamily: functions and mechanisms." *J Biol Chem* 284 (46):31493-7. doi: 10.1074/jbc.R109.052340.

Arendash G. W., King D. L., Gordon M. N., Morgan D., Hatcher J. M., Hope C. E., and Diamond D. M. 2001. "Progressive, age-related behavioral impairments in transgenic mice carrying both mutant amyloid precursor protein and presenilin-1 transgenes." *Brain Res.* 891 (1-2):42-53. doi: 10.1016/s0006-8993(00)03186-3.

Arispe N., Pollard H. B., and Rojas E. 1993. "Giant multilevel cation channels formed by Alzheimer disease amyloid beta-protein [A beta P-(1-40)] in bilayer membranes." *Proc Natl Acad Sci U S A* 90 (22):10573-7. doi: 10.1073/pnas.90.22.10573.

Backman L., Jones S., Berger A. K., Laukka E. J., and Small B. J. 2004. "Multiple cognitive deficits during the transition to Alzheimer's disease." *J Intern Med* 256 (3):195-204. doi: 10.1111/j.1365-2796.2004.01386.x.

Bancher C., Lassmann H., Breitschopf H., and Jellinger K. A. 1997. "Mechanisms of cell death in Alzheimer's disease." *J Neural Transm Suppl* 50:141-52. doi: 10.1007/978-3-7091-6842-4_14.

Bertram L., and Tanzi R. E. 2005. "The genetic epidemiology of neurodegenerative disease." *J Clin Invest* 115 (6):1449-57. doi: 10.1172/JCI24761.

Beyer I., Rezaei-Ghaleh N., Klafki H. W., Jahn O., Haußmann U., Wiltfang J., Zweckstetter M., and Knölker H. J. 2016. "Solid-Phase Synthesis and Characterization of N-Terminally Elongated Aβ(−3–x)-Peptides." *Chemistry* 22 (25):8685-8693. doi: 10.1002/chem.201600892.

Bi X., Gall C. M., Zhou J., and Lynch G. 2002. "Uptake and pathogenic effects of amyloid beta peptide 1-42 are enhanced by integrin antagonists and blocked by NMDA receptor antagonists." *Neuroscience* 112 (4):827-40. doi: 10.1016/s0306-4522(02)00132-x.

Blair J. A., Wang C., Hernandez D., Siedlak S. L., Rodgers M. S., Achar R. K., Fahmy L. M., Torres S. L., Petersen R. B., Zhu X., Casadesus G., and Lee H.-G. 2016. "Individual Case Analysis of Postmortem Interval Time on Brain Tissue Preservation." *PloS one* 11 (3):e0151615-e0151615. doi: 10.1371/journal.pone.0151615.

Bloom G. S. 2014. "Amyloid-β and tau: The trigger and bullet in alzheimer disease pathogenesis." *JAMA Neurology*. doi: 10.1001/jamaneurol.2013.5847.

Boekhoorn K., Terwel D., Biemans B., Borghgraef P., Wiegert O., Ramakers G. J., de Vos K., Krugers H., Tomiyama T., Mori H., Joels M., van Leuven F., and Lucassen P. J. 2006. "Improved long-term potentiation and memory in young tau-P301L transgenic mice before onset of hyperphosphorylation and tauopathy." *J Neurosci* 26 (13):3514-23. doi: 10.1523/JNEUROSCI.5425-05.2006.

Bories C., Arsenault D., Lemire M., Tremblay C., De Koninck Y., and Calon F. 2017. "Transgenic autoinhibition of p21-activated kinase exacerbates synaptic impairments and fronto-dependent behavioral deficits in an animal model of Alzheimer's disease." *Aging (Albany NY)* 9 (5):1386-1403. doi: 10.18632/aging.101239.

Bouter C., Henniges P., Franke T. N., Irwin C., Sahlmann C. O., Sichler M. E., Beindorff N., Bayer T. A., and Bouter Y. 2019. "18F-FDG-PET Detects Drastic Changes in Brain Metabolism in the Tg4–42 Model of Alzheimer's Disease." *Frontiers in Aging Neuroscience* 10 (425). doi: 10.3389/fnagi.2018.00425.

Bouter Y., Dietrich K., Wittnam J. L., Rezaei-Ghaleh N., Pillot T., Papot-Couturier S., Lefebvre T., Sprenger F., Wirths O., Zweckstetter M., and Bayer T. A. 2013. "N-truncated amyloid beta (Abeta) 4-42 forms stable aggregates and induces acute and long-lasting behavioral deficits." *Acta Neuropathol* 126 (2):189-205. doi: 10.1007/s00401-013-1129-2.

Bouter Y., Kacprowski T., Rossler F., Jensen L. R., Kuss A. W., and Bayer T. A. 2020. "miRNA Alterations Elicit Pathways Involved in Memory Decline and Synaptic Function in the Hippocampus of Aged Tg4-42 Mice." *Front Neurosci* 14:580524. doi: 10.3389/fnins.2020.580524.

Bouter Y., Kacprowski T., Weissmann R., Dietrich K., Borgers H., Brauss A., Sperling C., Wirths O., Albrecht M., Jensen L. R., Kuss A. W., and Bayer T. A. 2014. "Deciphering the molecular profile of plaques, memory decline and neuron loss in two mouse models for Alzheimer's disease by deep sequencing." *Front Aging Neurosci* 6:75. doi: 10.3389/fnagi.2014.00075.

Braak H., and Braak E. 1991. "Neuropathological stageing of Alzheimer-related changes." *Acta Neuropathol (Berl)* 82 (4):239-59. doi: 10.1007/BF00308809.

Braak H., and Braak E. 1997. "Diagnostic criteria for neuropathologic assessment of Alzheimer's disease." *Neurobiol Aging* 18 (4 Suppl):S85-8. doi: 10.1016/s0197-4580(97)00062-6.

Bramblett G. T., Goedert M., Jakes R., Merrick S. E., Trojanowski J. Q., and Lee V. M. 1993. "Abnormal tau phosphorylation at Ser396 in Alzheimer's disease recapitulates development and contributes to reduced microtubule binding." *Neuron* 10 (6):1089-99. doi: 10.1016/0896-6273(93)90057-x.

Braun D., and Feinstein D. L. 2019. "The locus coeruleus neuroprotective drug vindeburnol normalizes behavior in the 5xFAD transgenic mouse model of Alzheimer's disease." *Brain Res* 1702:29-37. doi: 10.1016/j.brainres.2017.12.028.

Broadbent N. J., Gaskin S., Squire L. R., and Clark R. E. 2010. "Object recognition memory and the rodent hippocampus." *Learning & Memory* 17 (1):5-11. doi: 10.1101/lm.1650110.

Broadbent N. J., Squire L. R., and Clark R. E. 2004. "Spatial memory, recognition memory, and the hippocampus." *Proceedings of the National Academy of Sciences of the United States of America* 101 (40):14515-14520. doi: 10.1073/pnas.0406344101.

Brody D. L., Jiang H., Wildburger N., and Esparza T. J. 2017. "Non-canonical soluble amyloid-beta aggregates and plaque buffering: controversies and future directions for target discovery in Alzheimer's disease." *Alzheimer's Research & Therapy* 9 (1):62. doi: 10.1186/s13195-017-0293-3.

Brun A., and Englund E. 1986. "A white matter disorder in dementia of the Alzheimer type: A pathoanatomical study." *Annals of Neurology* 19 (3):253-262. doi: 10.1002/ana.410190306.

Bu G., Cam J., and Zerbinatti C. 2006. "LRP in amyloid-beta production and metabolism." *Ann N Y Acad Sci* 1086:35-53. doi: 10.1196/annals.1377.005.

Buchman A. S., and Bennett D. A. 2011. "Loss of motor function in preclinical Alzheimer's disease." *Expert Review of Neurotherapeutics* 11 (5):665-676. doi: 10.1586/ern.11.57.

Cabrera E., Mathews P., Mezhericher E., Beach T. G., Deng J., Neubert T. A., Rostagno A., and Ghiso J. 2018. "Aβ truncated species: Implications for brain clearance mechanisms and amyloid plaque deposition." *Biochim Biophys Acta* 1864 (1):208-225. doi: 10.1016/j.bbadis.2017.07.005.

Campion D., Dumanchin C., Hannequin D., Dubois B., Belliard S., Puel M., Thomas-Anterion C., Michon A., Martin C., Charbonnier F., Raux G., Camuzat A., Penet C., Mesnage V., Martinez M., Clerget-Darpoux F., Brice A., and Frebourg T. 1999. "Early-onset autosomal dominant Alzheimer disease: prevalence, genetic heterogeneity, and mutation spectrum." *Am J Hum Genet* 65 (3):664-70. doi: 10.1086/302553.

Cao X., and Südhof T. C. 2001. "A Transcriptively Active Complex of APP with Fe65 and Histone Acetyltransferase Tip60." *Science* 293 (5527):115-120. doi: 10.1126/science.1058783.

Carson J. A., and Turner A. J. 2002. "β-Amyloid catabolism: roles for neprilysin (NEP) and other metallopeptidases?" *J Neurochem* 81 (1):1-8. doi: 10.1046/j.1471-4159.2002.00855.x.

Casas C., Sergeant N., Itier J. M., Blanchard V., Wirths O., van der Kolk N., Vingtdeux V., van de Steeg E., Ret G., Canton T., Drobecq H., Clark A., Bonici B., Delacourte A., Benavides J., Schmitz C., Tremp G., Bayer T. A., Benoit P., and Pradier L. 2004. "Massive CA1/2 neuronal loss with intraneuronal and N-terminal truncated Abeta42 accumulation in a novel Alzheimer transgenic model." *Am J Pathol* 165 (4):1289-300. doi: 10.1016/S0002-9440(10)63388-3.

Caspersen C., Wang N., Yao J., Sosunov A., Chen X., Lustbader J. W., Xu H. W., Stern D., McKhann G., and Yan S. D. 2005. "Mitochondrial Abeta: a potential focal point for neuronal metabolic dysfunction in Alzheimer's disease." *Faseb J* 19 (14):2040-1. doi: 10.1096/fj.05-3735fje.

Castellano J. M., Kim J., Stewart F. R., Jiang H., Demattos R. B., Patterson B. W., Fagan A. M., Morris J. C., Mawuenyega K. G., Cruchaga C., Goate A. M., Bales K. R., Paul S. M., Bateman R. J., and Holtzman D. M. 2011. "Human apoE Isoforms Differentially Regulate Brain Amyloid-{beta} Peptide Clearance." *Sci Transl Med* 3 (89):89ra57. doi: 10.1126/scitranslmed.3002156.

Cataldo A. M., Petanceska S., Terio N. B., Peterhoff C. M., Durham R., Mercken M., Mehta P. D., Buxbaum J., Haroutunian V., and Nixon R. A. 2004. "Abeta localization in abnormal endosomes: association with earliest Abeta elevations in AD and Down syndrome." *Neurobiol Aging.* 25 (10):1263-72. doi: 10.1016/j.neurobiolaging.2004.02.027.

Cataldo J. K., Prochaska J. J., and Glantz S. A. 2010. "Cigarette smoking is a risk factor for Alzheimer's Disease: an analysis controlling for tobacco industry affiliation." *J Alzheimers Dis* 19 (2):465-80. doi: 10.3233/JAD-2010-1240.

Chabrier M. A., Blurton-Jones M., Agazaryan A. A., Nerhus J. L., Martinez-Coria H., and Laferla F. M. 2012. "Soluble abeta promotes wild-type tau pathology in vivo." *J Neurosci* 32 (48):17345-50. doi: 10.1523/JNEUROSCI.0172-12.2012.

Chalermpalanupap T., Schroeder J. P., Rorabaugh J. M., Liles L. C., Lah J. J., Levey A. I., and Weinshenker D. 2018. "Locus Coeruleus Ablation Exacerbates Cognitive Deficits, Neuropathology, and Lethality in P301S Tau Transgenic Mice." *J Neurosci* 38 (1):74-92. doi: 10.1523/JNEUROSCI.1483-17.2017.

Chapman P. F., White G. L., Jones M. W., Cooper-Blacketer D., Marshall V. J., Irizarry M., Younkin L., Good M. A., Bliss T. V., Hyman B. T., Younkin S. G., and Hsiao K. K. 1999. "Impaired synaptic plasticity and learning in aged amyloid precursor protein transgenic mice." *Nat Neurosci* 2 (3):271-6. doi: 10.1038/6374.

Chong S. A., Benilova I., Shaban H., De Strooper B., Devijver H., Moechars D., Eberle W., Bartic C., Van Leuven F., and Callewaert G. 2011. "Synaptic dysfunction in hippocampus of transgenic mouse models of Alzheimer's disease: a multi-electrode array study." *Neurobiol Dis* 44 (3):284-91. doi: 10.1016/j.nbd.2011.07.006.

Chu T.-H., Cummins K., Sparling J. S., Tsutsui S., Brideau C., Nilsson K. P. R., Joseph J. T., and Stys P. K. 2017. "Axonal and myelinic pathology in 5xFAD Alzheimer's mouse spinal cord." *PLOS ONE* 12 (11):e0188218. doi: 10.1371/journal.pone.0188218.

Chung J. A., and Cummings J. L. 2000. "Neurobehavioral and neuropsychiatric symptoms in Alzheimer's disease: characteristics and treatment." *Neurol Clin* 18 (4):829-46. doi: 10.1016/s0733-8619(05)70228-0.

Chyung J. H., Raper D. M., and Selkoe D. J. 2005. "Gamma-secretase exists on the plasma membrane as an intact complex that accepts substrates and effects intramembrane cleavage." *J Biol Chem* 280 (6):4383-92. doi: 10.1074/jbc.M409272200.

Cirrito J. R., May P. C., O'Dell M. A., Taylor J. W., Parsadanian M., Cramer J. W., Audia J. E., Nissen J. S., Bales K. R., Paul S. M., DeMattos R. B., and Holtzman D. M. 2003. "In vivo assessment of brain interstitial fluid with microdialysis reveals plaque-associated changes in amyloid-beta metabolism and half-life." *J Neurosci* 23 (26):8844-53. doi: 10.1523/JNEUROSCI.23-26-08844.2003

Cirrito J. R., Yamada K. A., Finn M. B., Sloviter R. S., Bales K. R., May P. C., Schoepp D. D., Paul S. M., Mennerick S., and Holtzman D. M. 2005. "Synaptic Activity Regulates Interstitial Fluid Amyloid-β Levels In Vivo." *Neuron* 48 (6):913-922. doi: 10.1016/j.neuron.2005.10.028.

Cleary J. P., Walsh D. M., Hofmeister J. J., Shankar G. M., Kuskowski M. A., Selkoe D. J., and Ashe K. H. 2005. "Natural oligomers of the amyloid-beta protein specifically disrupt cognitive function." *Nat Neurosci* 8 (1):79-84. doi: 10.1038/nn1372.

Coleman P. D., and Flood D. G. 1987. "Neuron numbers and dendritic extent in normal aging and Alzheimer's disease." *Neurobiol Aging* 8 (6):521-45. doi: 10.1016/0197-4580(87)90127-8.

Corder E. H., Saunders A. M., Risch N. J., Strittmatter W. J., Schmechel D. E., Gaskell P. C., Jr., Rimmler J. B., Locke P. A., Conneally P. M., Schmader K. E., and et al. 1994. "Protective effect of apolipoprotein E type 2 allele for late onset Alzheimer disease." *Nat Genet* 7 (2):180-4. doi: 10.1038/ng0694-180.

Corder E. H., Saunders A. M., Strittmatter W. J., Schmechel D. E., Gaskell P. C., Small G. W., Roses A. D., Haines J. L., and Pericak-Vance M. A. 1993. "Gene dose of apolipoprotein E type 4 allele and the risk of Alzheimer's disease in late onset families." *Science* 261 (5123):921-3. doi: 10.1126/science.8346443.

D'Andrea M. R., Nagele R. G., Wang H. Y., Peterson P. A., and Lee D. H. 2001. "Evidence that neurones accumulating amyloid can undergo lysis to form amyloid plaques in Alzheimer's disease." *Histopathology* 38 (2):120-34. doi: 10.1046/j.1365-2559.2001.01082.x.

Dahlgren K. N., Manelli A. M., Stine W. B., Jr., Baker L. K., Krafft G. A., and LaDu M. J. 2002. "Oligomeric and fibrillar species of amyloid-beta peptides differentially affect neuronal viability." *J Biol Chem* 277 (35):32046-53. doi: 10.1074/jbc.M201750200.

Dawson H. N., Ferreira A., Eyster M. V., Ghoshal N., Binder L. I., and Vitek M. P. 2001. "Inhibition of neuronal maturation in primary hippocampal neurons from tau deficient mice." *J Cell Sci* 114 (Pt 6):1179-87. doi: 10.1242/jcs.114.6.1179.

De Strooper B., and Karran E. 2016. "The Cellular Phase of Alzheimer's Disease." *Cell* 164 (4):603-615. doi: 10.1016/j.cell.2015.12.056.

Delaere P., Duyckaerts C., Masters C., Beyreuther K., Piette F., and Hauw J. J. 1990. "Large amounts of neocortical beta A4 deposits without neuritic plaques nor tangles in a psychometrically assessed, non-demented person." *Neurosci Lett* 116 (1-2):87-93. doi: 10.1016/0304-3940(90)90391-l.

Devi L., Alldred M. J., Ginsberg S. D., and Ohno M. 2010. "Sex- and brain region-specific acceleration of beta-amyloidogenesis following behavioral stress in a mouse model of Alzheimer's disease." *Mol Brain* 3:34. doi: 10.1186/1756-6606-3-34.

Devi L., and Ohno M. 2010. "Phospho-eIF2alpha level is important for determining abilities of BACE1 reduction to rescue cholinergic neurodegeneration and memory defects in 5XFAD mice." *PLoS ONE* 5 (9):e12974. doi: 10.1371/journal.pone.0012974.

Devi L., and Ohno M. 2016. "Cognitive benefits of memantine in Alzheimer's 5XFAD model mice decline during advanced disease stages." *Pharmacol Biochem Behav* 144:60-6. doi: 10.1016/j.pbb.2016.03.002.

Dickson D. W., Crystal H. A., Mattiace L. A., Masur D. M., Blau A. D., Davies P., Yen S. H., and Aronson M. K. 1992. "Identification of normal and pathological aging in prospectively studied nondemented elderly humans." *Neurobiol Aging* 13 (1):179-89. doi: 10.1016/0197-4580(92)90027-u.

Dietrich K., Bouter Y., Muller M., and Bayer T. A. 2018. "Synaptic Alterations in Mouse Models for Alzheimer Disease-A Special Focus on N-Truncated Abeta 4-42." *Molecules* 23 (4). doi: 10.3390/molecules23040718.

Dougherty J. J., Wu J., and Nichols R. A. 2003. "Beta-amyloid regulation of presynaptic nicotinic receptors in rat hippocampus and neocortex." *J Neurosci* 23 (17):6740-7. doi: 10.1523/JNEUROSCI.23-17-06740.2003

Dovey H. F., Suomensaari-Chrysler S., Lieberburg I., Sinha S., and Keim P. S. 1993. "Cells with a familial Alzheimer's disease mutation produce authentic beta-peptide." *Neuroreport* 4 (8):1039-42. doi: 10.1097/00001756-199308000-00011.

Drechsel D. N., Hyman A. A., Cobb M. H., and Kirschner M. W. 1992. "Modulation of the dynamic instability of tubulin assembly by the microtubule-associated protein tau." *Mol Biol Cell* 3 (10):1141-54. doi: 10.1091/mbc.3.10.1141.

Duarte A. I., Candeias E., Alves I. N., Mena D., Silva D. F., Machado N. J., Campos E. J., Santos M. S., Oliveira C. R., and Moreira P. I. 2020. "Liraglutide Protects Against Brain Amyloid-beta1-42 Accumulation in Female Mice with Early Alzheimer's Disease-Like Pathology by Partially Rescuing Oxidative/Nitrosative Stress and Inflammation." *Int J Mol Sci* 21 (5). doi: 10.3390/ijms21051746.

Duyckaerts C., Delatour B., and Potier M. C. 2009. "Classification and basic pathology of Alzheimer disease." *Acta Neuropathol* 118 (1):5-36. doi: 10.1007/s00401-009-0532-1 [doi].

Duyckaerts C., Potier M. C., and Delatour B. 2008. "Alzheimer disease models and human neuropathology: similarities and differences." *Acta Neuropathol* 115 (1):5-38. doi: 10.1007/s00401-007-0312-8.

Eckenweber F., Medina-Luque J., Blume T., Sacher C., Biechele G., Wind K., Deussing M., Briel N., Lindner S., Boening G., von Ungern-Sternberg B., Unterrainer M., Albert N. L., Zwergal A., Levin J., Bartenstein P., Cumming P., Rominger A., Hoglinger G. U., Herms J., and Brendel M. 2020. "Longitudinal TSPO expression in tau transgenic P301S mice predicts increased tau accumulation and deteriorated spatial learning." *J Neuroinflammation* 17 (1):208. doi: 10.1186/s12974-020-01883-5.

Eckert A., Nisbet R., Grimm A., and Götz J. 2014. "March separate, strike together — Role of phosphorylated TAU in mitochondrial dysfunction in Alzheimer's disease." *Biochimica et Biophysica Acta (BBA) - Molecular Basis of Disease* 1842 (8):1258-1266. doi: 10.1016/j.bbadis.2013.08.013.

Eimer W. A., and Vassar R. 2013. "Neuron loss in the 5XFAD mouse model of Alzheimer's disease correlates with intraneuronal Abeta42 accumulation and Caspase-3 activation." *Mol Neurodegener* 8 (1):2. doi: 10.1186/1750-1326-8-2.

Esparza T. J., Gangolli M., Cairns N. J., and Brody D. L. 2018. "Soluble amyloid-beta buffering by plaques in Alzheimer disease dementia versus high-pathology controls." *PLOS ONE* 13 (7):e0200251. doi: 10.1371/journal.pone.0200251.

Esparza T. J., Zhao H., Cirrito J. R., Cairns N. J., Bateman R. J., Holtzman D. M., and Brody D. L. 2013. "Amyloid-beta oligomerization in Alzheimer dementia versus high-pathology controls." *Ann Neurol* 73 (1):104-19. doi: 10.1002/ana.23748.

Farrer L. A., Cupples L. A., Haines J. L., Hyman B., Kukull W. A., Mayeux R., Myers R. H., Pericak-Vance M. A., Risch N., and van Duijn C. M. 1997. "Effects of age, sex, and ethnicity on the association between apolipoprotein E genotype and Alzheimer disease. A meta-analysis. APOE and Alzheimer Disease Meta Analysis Consortium." *JAMA* 278 (16):1349-56. doi: 10.1001/jama.1997.03550160069041.

Farris W., Schütz S. G., Cirrito J. R., Shankar G. M., Sun X., George A., Leissring M. A., Walsh D. M., Qiu W. Q., Holtzman D. M., and Selkoe D. J. 2007. "Loss of Neprilysin Function Promotes Amyloid Plaque Formation and Causes Cerebral Amyloid Angiopathy." *Am J Pathol* 171 (1):241-251. doi: 10.2353/ajpath.2007.070105.

Fein J. A., Sokolow S., Miller C. A., Vinters H. V., Yang F., Cole G. M., and Gylys K. H. 2008. "Co-localization of amyloid beta and tau pathology in Alzheimer's disease synaptosomes." *Am J Pathol* 172 (6):1683-92. doi: 10.2353/ajpath.2008.070829.

Fernandez-Vizarra P., Fernandez A. P., Castro-Blanco S., Serrano J., Bentura M. L., Martinez-Murillo R., Martinez A., Rodrigo J., Encinas J. M., Munoz P., Alonso D., Gomez M. B., Sanchez J., Rios-Tejada F., Salas E., Lisazoain I., Leza J. C., Lopez J. C., Manuel Encinas J., Lorenzo P., Pedrosa J. A., Peinado M. A., Richart A., Santacana M., Cuttitta F., Uttenthal L. O., Bosca L., Rodriguez I., and Ruiz-Cabello J. 2004. "Intra- and extracellular Abeta and PHF in clinically evaluated cases of Alzheimer's disease." *Histol Histopathol* 19 (3):823-44. doi: 10.14670/HH-19.823

Ferretti L., McCurry S. M., Logsdon R., Gibbons L., and Teri L. 2001. "Anxiety and Alzheimer's disease." *J Geriatr Psychiatry Neurol* 14 (1):52-8. doi: 10.1177/089198870101400111.

Filali M., Lalonde R., Theriault P., Julien C., Calon F., and Planel E. 2012. "Cognitive and non-cognitive behaviors in the triple transgenic mouse model of Alzheimer's disease expressing mutated APP, PS1, and Mapt (3xTg-AD)." *Behav Brain Res* 234 (2):334-42. doi: 10.1016/j.bbr.2012.07.004.

Fischer D., Mukrasch M. D., Biernat J., Bibow S., Blackledge M., Griesinger C., Mandelkow E., and Zweckstetter M. 2009. "Conformational changes specific for pseudophosphorylation at serine 262 selectively impair binding of tau to microtubules." *Biochemistry* 48 (42):10047-55. doi: 10.1021/bi901090m.

Fogel H., Frere S., Segev O., Bharill S., Shapira I., Gazit N., O'Malley T., Slomowitz E., Berdichevsky Y., Walsh D. M., Isacoff E. Y., Hirsch J. A., and Slutsky I. 2014. "APP homodimers transduce an

amyloid-beta-mediated increase in release probability at excitatory synapses." *Cell Rep* 7 (5):1560-1576. doi: 10.1016/j.celrep.2014.04.024.

Forstl H., and Kurz A. 1999. "Clinical features of Alzheimer's disease." *Eur Arch Psychiatry Clin Neurosci* 249 (6):288-90. doi: 10.1007/s004060050101.

Frandemiche M. L., De Seranno S., Rush T., Borel E., Elie A., Arnal I., Lante F., and Buisson A. 2014. "Activity-dependent tau protein translocation to excitatory synapse is disrupted by exposure to amyloid-beta oligomers." *J Neurosci* 34 (17):6084-97. doi: 10.1523/JNEUROSCI.4261-13.2014.

Fratiglioni L., Paillard-Borg S., and Winblad B. 2004. "An active and socially integrated lifestyle in late life might protect against dementia." *The Lancet Neurology* 3 (6):343-353. doi: 10.1016/S1474-4422(04)00767-7.

Friese A., Kaltschmidt J. A., Ladle D. R., Sigrist M., Jessell T. M., and Arber S. 2009. "Gamma and alpha motor neurons distinguished by expression of transcription factor Err3." *Proc Natl Acad Sci U S A* 106 (32):13588-93. doi: 10.1073/pnas.0906809106.

Galante D., Corsaro A., Florio T., Vella S., Pagano A., Sbrana F., Vassalli M., Perico A., and D'Arrigo C. 2012. "Differential toxicity, conformation and morphology of typical initial aggregation states of Abeta1-42 and Abetapy3-42 beta-amyloids." *Int J Biochem Cell Biol* 44 (11):2085-93. doi: 10.1016/j.biocel.2012.08.010.

Garcia-Osta A., and Alberini C. M. 2009. "Amyloid beta mediates memory formation." *Learn Mem* 16 (4):267-72. doi: 10.1101/lm.1310209.

Gendron T. F., and Petrucelli L. 2009. "The role of tau in neurodegeneration." *Mol Neurodegener* 4:13. doi: 10.1186/1750-1326-4-13.

Gerth J., Kumar S., Rijal Upadhaya A., Ghebremedhin E., von Arnim C. A. F., Thal D. R., and Walter J. 2018. "Modified amyloid variants in pathological subgroups of β-amyloidosis." *Annals of clinical and translational neurology* 5 (7):815-831. doi: 10.1002/acn3.577.

Giannakopoulos P., Herrmann F. R., Bussiere T., Bouras C., Kovari E., Perl D. P., Morrison J. H., Gold G., and Hof P. R. 2003. "Tangle and neuron numbers, but not amyloid load, predict cognitive status in Alzheimer's disease." *Neurology* 60 (9):1495-500. doi: 10.1212/01.wnl.0000063311.58879.01.

Giuliani A., Beggiato S., Baldassarro V. A., Mangano C., Giardino L., Imbimbo B. P., Antonelli T., Calza L., and Ferraro L. 2013. "CHF5074 restores visual memory ability and pre-synaptic cortical acetylcholine release in pre-plaque Tg2576 mice." *J Neurochem* 124 (5):613-20. doi: 10.1111/jnc.12136.

Goedert M., and Spillantini M. G. 2000. "Tau mutations in frontotemporal dementia FTDP-17 and their relevance for Alzheimer's disease." *Biochim Biophys Acta* 1502 (1):110-21. doi: 10.1016/s0925-4439(00)00037-5.

Goedert M., Spillantini M. G., Jakes R., Rutherford D., and Crowther R. A. 1989. "Multiple isoforms of human microtubule-associated protein tau: sequences and localization in neurofibrillary tangles of Alzheimer's disease." *Neuron* 3 (4):519-26. doi: 10.1016/0896-6273(89)90210-9.

Goldgaber D., Lerman M. I., McBride W. O., Saffiotti U., and Gajdusek D. C. 1987. "Isolation, characterization, and chromosomal localization of human brain cDNA clones coding for the precursor of the amyloid of brain in Alzheimer's disease, Down's syndrome and aging." *J Neural Transm Suppl* 24:23-8.

Gomes L. A., Hipp S. A., Rijal Upadhaya A., Balakrishnan K., Ospitalieri S., Koper M. J., Largo-Barrientos P., Uytterhoeven V., Reichwald J., Rabe S., Vandenberghe R., von Arnim C. A. F., Tousseyn T., Feederle R., Giudici C., Willem M., Staufenbiel M., and Thal D. R. 2019. "Abeta-induced acceleration of Alzheimer-related tau-pathology spreading and its association with prion protein." *Acta Neuropathol* 138 (6):913-941. doi: 10.1007/s00401-019-02053-5.

Gomez-Isla T., Hollister R., West H., Mui S., Growdon J. H., Petersen R. C., Parisi J. E., and Hyman B. T. 1997. "Neuronal loss correlates with but exceeds neurofibrillary tangles in Alzheimer's disease." *Ann Neurol* 41 (1):17-24. doi: 10.1002/ana.410410106.

Gomez-Isla T., Price J. L., McKeel D. W., Jr., Morris J. C., Growdon J. H., and Hyman B. T. 1996. "Profound loss of layer II entorhinal cortex neurons occurs in very mild Alzheimer's disease." *J Neurosci.* 16 (14):4491-500. doi: 10.1523/JNEUROSCI.16-14-04491.1996.

Gotz J., Chen F., van Dorpe J., and Nitsch R. M. 2001. "Formation of neurofibrillary tangles in P301l tau transgenic mice induced by Abeta 42 fibrils." *Science* 293 (5534):1491-5. doi: 10.1126/science.1062097

Gouras G. K., Tsai J., Naslund J., Vincent B., Edgar M., Checler F., Greenfield J. P., Haroutunian V., Buxbaum J. D., Xu H., Greengard P., and Relkin N. R. 2000. "Intraneuronal Abeta42 accumulation in human brain." *Am J Pathol* 156 (1 Jan):15-20. doi: 10.1016/s0002-9440(10)64700-1.

Grueninger F., Bohrmann B., Czech C., Ballard T. M., Frey J. R., Weidensteiner C., von Kienlin M., and Ozmen L. 2010. "Phosphorylation of Tau at S422 is enhanced by Abeta in TauPS2APP triple transgenic mice." *Neurobiol Dis* 37 (2):294-306. doi: 10.1016/j.nbd.2009.09.004.

Grundke-Iqbal I., Iqbal K., George L., Tung Y. C., Kim K. S., and Wisniewski H. M. 1989. "Amyloid protein and neurofibrillary tangles coexist in the same neuron in Alzheimer disease." *Proc Natl Acad Sci U S A* 86 (8):2853-7. doi: 10.1073/pnas.86.8.2853.

Grundke-Iqbal I., Iqbal K., Quinlan M., Tung Y. C., Zaidi M. S., and Wisniewski H. M. 1986. "Microtubule-associated protein tau. A component of Alzheimer paired helical filaments." *J Biol Chem* 261 (13):6084-9. doi: 10.1016/S0021-9258(17)38495-8.

Gulisano W., Maugeri D., Baltrons M. A., Fa M., Amato A., Palmeri A., D'Adamio L., Grassi C., Devanand D. P., Honig L. S., Puzzo D., and Arancio O. 2018. "Role of Amyloid-beta and Tau Proteins in Alzheimer's Disease: Confuting the Amyloid Cascade." *J Alzheimers Dis* 64 (s1):S611-S631. doi: 10.3233/JAD-179935.

Haass C., Hung A. Y., Schlossmacher M. G., Teplow D. B., and Selkoe D. J. 1993. "beta-Amyloid peptide and a 3-kDa fragment are derived by distinct cellular mechanisms." *J Biol Chem* 268 (5):3021-4. doi: 10.1016/S0021-9258(18)53650-4.

Haass C., Koo E. H., Mellon A., Hung A. Y., and Selkoe D. J. 1992. "Targeting of cell-surface beta-amyloid precursor protein to lysosomes: alternative processing into amyloid-bearing fragments." *Nature* 357 (6378):500-3. doi: 10.1038/357500a0.

Haass C., and Selkoe D. J. 2007. "Soluble protein oligomers in neurodegeneration: lessons from the Alzheimer's amyloid [beta]-peptide." *Nat Rev Mol Cell Biol* 8 (2):101-112. doi: 10.1038/nrm2101.

Haglund M., Kalaria R., Slade J., and Englund E. 2006. "Differential deposition of amyloid β peptides in cerebral amyloid angiopathy associated with Alzheimer's disease and vascular dementia." *Acta Neuropathologica* 111 (5):430-435. doi: 10.1007/s00401-006-0054-z.

Halliday G. M., Double K. L., Macdonald V., and Kril J. J. 2003. "Identifying severely atrophic cortical subregions in Alzheimer's disease." *Neurobiol Aging* 24 (6):797-806. doi: 10.1016/s0197-4580(02)00227-0.

Harada A., Oguchi K., Okabe S., Kuno J., Terada S., Ohshima T., Sato-Yoshitake R., Takei Y., Noda T., and Hirokawa N. 1994. "Altered microtubule organization in small-calibre axons of mice lacking tau protein." *Nature* 369 (6480):488-91. doi: 10.1038/369488a0.

Hardy J., and Allsop D. 1991. "Amyloid deposition as the central event in the aetiology of Alzheimer's disease." *Trends Pharmacol Sci* 12 (10):383-8. doi: 10.1016/0165-6147(91)90609-v.

Hardy J., and Selkoe D. J. 2002. "The amyloid hypothesis of Alzheimer's disease: progress and problems on the road to therapeutics." *Science.* 297 (5580):353-6. doi: 10.1126/science.1072994.

Harrison J. R., and Owen M. J. 2016. "Alzheimer's disease: the amyloid hypothesis on trial." *Br J Psychiatry* 208 (1):1-3. doi: 10.1192/bjp.bp.115.167569.

Hart D. J., Craig D., Compton S. A., Critchlow S., Kerrigan B. M., McIlroy S. P., and Passmore A. P. 2003. "A retrospective study of the behavioural and psychological symptoms of mid and late phase Alzheimer's disease." *Int J Geriatr Psychiatry* 18 (11):1037-42. doi: 10.1002/gps.1013.

Hartley D., Blumenthal T., Carrillo M., DiPaolo G., Esralew L., Gardiner K., Granholm A.-C., Iqbal K., Krams M., Lemere C., Lott I., Mobley W., Ness S., Nixon R., Potter H., Reeves R., Sabbagh M., Silverman W., Tycko B., Whitten M., and Wisniewski T. 2015. "Down syndrome and Alzheimer's disease: Common pathways, common goals." *Alzheimer's & dementia : the journal of the Alzheimer's Association* 11 (6):700-709. doi: 10.1016/j.jalz.2014.10.007.

Hashimoto M., Bogdanovic N., Volkmann I., Aoki M., Winblad B., and Tjernberg L. O. 2010. "Analysis of microdissected human neurons by a sensitive ELISA reveals a correlation between elevated intracellular concentrations of Abeta42 and Alzheimer's disease neuropathology." *Acta Neuropathol* 119 (5):543-54. doi: 10.1007/s00401-010-0661-6.

Hatch R. J., Wei Y., Xia D., and Gotz J. 2017. "Hyperphosphorylated tau causes reduced hippocampal CA1 excitability by relocating the axon initial segment." *Acta Neuropathol* 133 (5):717-730. doi: 10.1007/s00401-017-1674-1.

Haußmann U., Jahn O., Linning P., Janßen C., Liepold T., Portelius E., Zetterberg H., Bauer C., Schuchhardt J., Knölker H.-J., Klafki H., and Wiltfang J. 2013. "Analysis of Amino-Terminal Variants of Amyloid-

β Peptides by Capillary Isoelectric Focusing Immunoassay." *Analytical Chemistry* 85 (17):8142-8149. doi: 10.1021/ac401055y.

Henkins K. M., Sokolow S., Miller C. A., Vinters H. V., Poon W. W., Cornwell L. B., Saing T., and Gylys K. H. 2012. "Extensive p-tau pathology and SDS-stable p-tau oligomers in Alzheimer's cortical synapses." *Brain Pathol* 22 (6):826-33. doi: 10.1111/j.1750-3639.2012.00598.x.

Héraud C., Goufak D., Ando K., Leroy K., Suain V., Yilmaz Z., De Decker R., Authelet M., Laporte V., Octave J.-N., and Brion J.-P. 2014. "Increased misfolding and truncation of tau in APP/PS1/tau transgenic mice compared to mutant tau mice." *Neurobiol Dis* 62:100-112. doi: 10.1016/j.nbd.2013.09.010.

Hof P. R., Cox K., and Morrison J. H. 1990. "Quantitative analysis of a vulnerable subset of pyramidal neurons in Alzheimer's disease: I. Superior frontal and inferior temporal cortex." *J Comp Neurol* 301 (1):44-54. doi: 10.1002/cne.903010105.

Holtzman D. M., Morris J. C., and Goate A. M. 2011. "Alzheimer's disease: the challenge of the second century." *Sci Transl Med* 3 (77):77sr1. doi: 10.1126/scitranslmed.3002369.

Hong M., Zhukareva V., Vogelsberg-Ragaglia V., Wszolek Z., Reed L., Miller B. I., Geschwind D. H., Bird T. D., McKeel D., Goate A., Morris J. C., Wilhelmsen K. C., Schellenberg G. D., Trojanowski J. Q., and Lee V. M. 1998. "Mutation-specific functional impairments in distinct tau isoforms of hereditary FTDP-17." *Science* 282 (5395):1914-7. doi: 10.1126/science.282.5395.1914.

Hoover B. R., Reed M. N., Su J., Penrod R. D., Kotilinek L. A., Grant M. K., Pitstick R., Carlson G. A., Lanier L. M., Yuan L. L., Ashe K. H., and Liao D. 2010. "Tau mislocalization to dendritic spines mediates synaptic dysfunction independently of neurodegeneration." *Neuron* 68 (6):1067-81. doi: 10.1016/j.neuron.2010.11.030.

Hoozemans J. J., Chafekar S. M., Baas F., Eikelenboom P., and Scheper W. 2006. "Always around, never the same: pathways of amyloid beta induced neurodegeneration throughout the pathogenic cascade of Alzheimer's disease." *Curr Med Chem.* 13 (22):2599-605. doi: 10.2174/092986706778201585.

Hornung K., Zampar S., Engel N., Klafki H., Liepold T., Bayer T. A., Wiltfang J., Jahn O., and Wirths O. 2019. "N-Terminal Truncated Abeta4-42 Is a Substrate for Neprilysin Degradation in vitro and in vivo." *J Alzheimers Dis* 67 (3):849-858. doi: 10.3233/jad-181134.

Howell S., Nalbantoglu J., and Crine P. 1995. "Neutral endopeptidase can hydrolyze β-amyloid(1–40) but shows no effect on β-amyloid precursor protein metabolism." *Peptides* 16 (4):647-652. doi: 10.1016/0196-9781(95)00021-B.

Hsia A. Y., Masliah E., McConlogue L., Yu G. Q., Tatsuno G., Hu K., Kholodenko D., Malenka R. C., Nicoll R. A., and Mucke L. 1999. "Plaque-independent disruption of neural circuits in Alzheimer's disease mouse models." *Proc Natl Acad Sci U S A* 96 (6):3228-33.

Hsieh H., Boehm J., Sato C., Iwatsubo T., Tomita T., Sisodia S., and Malinow R. 2006. "AMPAR Removal Underlies Aβ-Induced Synaptic Depression and Dendritic Spine Loss." *Neuron* 52 (5):831-843. doi: 10.1016/j.neuron.2006.10.035.

Hu X., Li X., Zhao M., Gottesdiener A., Luo W., and Paul S. 2014. "Tau pathogenesis is promoted by Abeta1-42 but not Abeta1-40." *Mol Neurodegener* 9 (1):52. doi: 10.1186/1750-1326-9-52.

Huang C. W., Lui C. C., Chang W. N., Lu C. H., Wang Y. L., and Chang C. C. 2009. "Elevated basal cortisol level predicts lower hippocampal volume and cognitive decline in Alzheimer's disease." *J Clin Neurosci* 16 (10):1283-6. doi: 10.1016/j.jocn.2008.12.026.

Hudry E., Wu H. Y., Arbel-Ornath M., Hashimoto T., Matsouaka R., Fan Z., Spires-Jones T. L., Betensky R. A., Bacskai B. J., and Hyman B. T. 2012. "Inhibition of the NFAT pathway alleviates amyloid beta neurotoxicity in a mouse model of Alzheimer's disease." *J Neurosci* 32 (9):3176-92. doi: 10.1523/JNEUROSCI.6439-11.2012.

Hulette C. M., Welsh-Bohmer K. A., Murray M. G., Saunders A. M., Mash D. C., and McIntyre L. M. 1998. "Neuropathological and neuropsychological changes in "normal" aging: evidence for preclinical Alzheimer disease in cognitively normal individuals." *J Neuropathol Exp Neurol* 57 (12):1168-74. doi: 10.1097/00005072-199812000-00009.

Hurtado D. E., Molina-Porcel L., Iba M., Aboagye A. K., Paul S. M., Trojanowski J. Q., and Lee V. M. 2010. "A{beta} accelerates the spatiotemporal progression of tau pathology and augments tau amyloidosis in an Alzheimer mouse model." *Am J Pathol* 177 (4):1977-88. doi: 10.2353/ajpath.2010.100346.

Hüttenrauch M., Baches S., Gerth J., Bayer T. A., Weggen S., and Wirths O. 2015. "Neprilysin Deficiency Alters the Neuropathological and Behavioral Phenotype in the 5XFAD Mouse Model of Alzheimer's Disease." *J Alzheimers Dis* 44:1291-1302. doi: 10.3233/jad-142463.

Hüttenrauch M., Brauss A., Kurdakova A., Borgers H., Klinker F., Liebetanz D., Salinas-Riester G., Wiltfang J., Klafki H. W., and Wirths O. 2016. "Physical activity delays hippocampal neurodegeneration and rescues memory deficits in an Alzheimer disease mouse model." *Transl Psychiatry* 6:e800. doi: 10.1038/tp.2016.65.

Hüttenrauch M., Walter S., Kaufmann M., Weggen S., and Wirths O. 2017. "Limited Effects of Prolonged Environmental Enrichment on the Pathology of 5XFAD Mice." *Mol Neurobiol* 54 (8):6542-6555. doi: 10.1007/s12035-016-0167-x.

Itagaki S., McGeer P. L., Akiyama H., Zhu S., and Selkoe D. 1989. "Relationship of microglia and astrocytes to amyloid deposits of Alzheimer disease." *J Neuroimmunol* 24 (3):173-82. doi: 10.1016/0165-5728(89)90115-x.

Ittner A., and Ittner L. M. 2018. "Dendritic Tau in Alzheimer's Disease." *Neuron* 99 (1):13-27. doi: 10.1016/j.neuron.2018.06.003.

Ittner L. M., and Gotz J. 2011. "Amyloid-beta and tau--a toxic pas de deux in Alzheimer's disease." *Nat Rev Neurosci* 12 (2):65-72. doi: 10.1038/nrn2967.

Ittner L. M., Ke Y. D., Delerue F., Bi M., Gladbach A., van Eersel J., Wolfing H., Chieng B. C., Christie M. J., Napier I. A., Eckert A., Staufenbiel M., Hardeman E., and Gotz J. 2010. "Dendritic function of tau mediates amyloid-beta toxicity in Alzheimer's disease mouse models." *Cell* 142 (3):387-97. doi: 10.1016/j.cell.2010.06.036.

Iwata N., Mizukami H., Shirotani K., Takaki Y., Muramatsu S., Lu B., Gerard N. P., Gerard C., Ozawa K., and Saido T. C. 2004. "Presynaptic localization of neprilysin contributes to efficient clearance of amyloid-beta peptide in mouse brain." *J Neurosci* 24 (4):991-8. doi: 10.1523/jneurosci.4792-03.2004.

Iwata N., Tsubuki S., Takaki Y., Watanabe K., Sekiguchi M., Hosoki E., Kawashima-Morishima M., Lee H. J., Hama E., Sekine-Aizawa Y., and Saido T. C. 2000. "Identification of the major Abeta1-42-degrading catabolic pathway in brain parenchyma: suppression leads to biochemical and pathological deposition." *Nat Med* 6 (2):143-50. doi: 10.1038/72237.

Jack C. R., Jr., Dickson D. W., Parisi J. E., Xu Y. C., Cha R. H., O'Brien P. C., Edland S. D., Smith G. E., Boeve B. F., Tangalos E. G., Kokmen E., and Petersen R. C. 2002. "Antemortem MRI findings correlate with hippocampal neuropathology in typical aging and dementia." *Neurology* 58 (5):750-7. doi: 10.1212/wnl.58.5.750.

Jack C. R., Jr., Shiung M. M., Weigand S. D., O'Brien P. C., Gunter J. L., Boeve B. F., Knopman D. S., Smith G. E., Ivnik R. J., Tangalos E. G., and Petersen R. C. 2005. "Brain atrophy rates predict subsequent clinical conversion in normal elderly and amnestic MCI." *Neurology* 65 (8):1227-31. doi: 10.1212/01.wnl.0000180958.22678.91.

Jankowsky J. L., and Zheng H. 2017. "Practical considerations for choosing a mouse model of Alzheimer's disease." *Molecular Neurodegeneration* 12 (1):89. doi: 10.1186/s13024-017-0231-7.

Jansen I. E., Savage J. E., Watanabe K., Bryois J., Williams D. M., Steinberg S., Sealock J., Karlsson I. K., Hagg S., Athanasiu L., Voyle N., Proitsi P., Witoelar A., Stringer S., Aarsland D., Almdahl I. S., Andersen F., Bergh S., Bettella F., Bjornsson S., Braekhus A., Brathen G., de Leeuw C., Desikan R. S., Djurovic S., Dumitrescu L., Fladby T., Hohman T. J., Jonsson P. V., Kiddle S. J., Rongve A., Saltvedt I., Sando S. B., Selbaek G., Shoai M., Skene N. G., Snaedal J., Stordal E., Ulstein I. D., Wang Y., White L. R., Hardy J., Hjerling-Leffler J., Sullivan P. F., van der Flier W. M., Dobson R., Davis L. K., Stefansson H., Stefansson K., Pedersen N. L., Ripke S., Andreassen O. A., and Posthuma D. 2019a. "Genome-wide meta-analysis identifies new loci and functional pathways influencing Alzheimer's disease risk." *Nat Genet* 51 (3):404-413. doi: 10.1038/s41588-018-0311-9.

Jansen I. E., Savage J. E., Watanabe K., Bryois J., Williams D. M., Steinberg S., Sealock J., Karlsson I. K., Hägg S., Athanasiu L., Voyle N., Proitsi P., Witoelar A., Stringer S., Aarsland D., Almdahl I. S., Andersen F., Bergh S., Bettella F., Bjornsson S., Brækhus A., Bråthen G., de Leeuw C., Desikan R. S., Djurovic S., Dumitrescu L., Fladby T., Hohman T. J., Jonsson P. V., Kiddle S. J., Rongve A., Saltvedt I., Sando S. B., Selbæk G., Shoai M., Skene N. G., Snaedal J., Stordal E., Ulstein I. D., Wang Y., White L. R., Hardy J., Hjerling-Leffler J., Sullivan P. F., van der Flier W. M., Dobson R., Davis L. K., Stefansson H., Stefansson K., Pedersen N. L., Ripke S., Andreassen O. A., and Posthuma D. 2019b. "Genome-wide meta-analysis identifies new loci and functional pathways influencing Alzheimer's disease risk." *Nature Genetics*. doi: 10.1038/s41588-018-0311-9.

Jarrett J. T., Berger E. P., and Lansbury P. T., Jr. 1993. "The carboxy terminus of the beta amyloid protein is critical for the seeding of amyloid formation: implications for the pathogenesis of Alzheimer's disease." *Biochemistry* 32 (18):4693-7. doi: 10.1021/bi00069a001.

Jawhar S., Trawicka A., Jenneckens C., Bayer T. A., and Wirths O. 2012. "Motor deficits, neuron loss, and reduced anxiety coinciding with axonal degeneration and intraneuronal Abeta aggregation in the

5XFAD mouse model of Alzheimer's disease." *Neurobiol Aging* 33 (1):196.e29-196.e40. doi: 10.1016/j.neurobiolaging.2010.05.027

Jawhar S., Wirths O., Schilling S., Graubner S., Demuth H. U., and Bayer T. A. 2011. "Overexpression of Glutaminyl Cyclase, the Enzyme Responsible for Pyroglutamate Abeta Formation, Induces Behavioral Deficits, and Glutaminyl Cyclase Knock-out Rescues the Behavioral Phenotype in 5XFAD Mice." *J Biol Chem* 286 (6):4454-60. doi: 10.1074/jbc.M110.185819.

Jho Y. S., Zhulina E. B., Kim M. W., and Pincus P. A. 2010. "Monte carlo simulations of tau proteins: effect of phosphorylation." *Biophys J* 99 (8):2387-97. doi: 10.1016/j.bpj.2010.06.056.

Jin M., Shepardson N., Yang T., Chen G., Walsh D., and Selkoe D. J. 2011. "Soluble amyloid beta-protein dimers isolated from Alzheimer cortex directly induce Tau hyperphosphorylation and neuritic degeneration." *Proc Natl Acad Sci U S A* 108 (14):5819-24. doi: 10.1073/pnas.1017033108.

Kalaria R. N. 2001. "Advances in molecular genetics and pathology of cerebrovascular disorders." *Trends Neurosci* 24 (7):392-400. doi: 10.1016/s0166-2236(00)01836-1.

Kamenetz F., Tomita T., Hsieh H., Seabrook G., Borchelt D., Iwatsubo T., Sisodia S., and Malinow R. 2003. "APP processing and synaptic function." *Neuron* 37 (6):925-37. doi: 10.1016/s0896-6273(03)00124-7.

Kang J., Lemaire H. G., Unterbeck A., Salbaum J. M., Masters C. L., Grzeschik K. H., Multhaup G., Beyreuther K., and Muller-Hill B. 1987. "The precursor of Alzheimer's disease amyloid A4 protein resembles a cell-surface receptor." *Nature* 325:733-736. doi: 10.1038/325733a0.

Kanning K. C., Kaplan A., and Henderson C. E. 2010. "Motor neuron diversity in development and disease." *Annu Rev Neurosci* 33:409-40. doi: 10.1146/annurev.neuro.051508.135722.

Karl T., Pabst R., and von Horsten S. 2003. "Behavioral phenotyping of mice in pharmacological and toxicological research." *Exp Toxicol Pathol.* 55 (1):69-83. doi: 10.1078/0940-2993-00301.

Katzman R., Aronson M., Fuld P., Kawas C., Brown T., Morgenstern H., Frishman W., Gidez L., Eder H., and Ooi W. L. 1989. "Development of dementing illnesses in an 80-year-old volunteer cohort." *Annals of Neurology* 25 (4):317-324. doi: doi:10.1002/ana.410250402.

Kayed R., and Lasagna-Reeves C. A. 2013. "Molecular mechanisms of amyloid oligomers toxicity." *J Alzheimers Dis* 33 Suppl 1:S67-78. doi: 10.3233/JAD-2012-129001.

Kellogg E. H., Hejab N. M. A., Poepsel S., Downing K. H., DiMaio F., and Nogales E. 2018. "Near-atomic model of microtubule-tau interactions." *Science* 360 (6394):1242-1246. doi: 10.1126/science.aat1780.

Kim J., Basak J. M., and Holtzman D. M. 2009. "The role of apolipoprotein E in Alzheimer's disease." *Neuron* 63 (3):287-303. doi: 10.1016/j.neuron.2009.06.026.

Kimura R., Devi L., and Ohno M. 2010. "Partial reduction of BACE1 improves synaptic plasticity, recent and remote memories in Alzheimer's disease transgenic mice." *J Neurochem* 113 (1):248-61. doi: 10.1111/j.1471-4159.2010.06608.x.

King M. E., Kan H. M., Baas P. W., Erisir A., Glabe C. G., and Bloom G. S. 2006. "Tau-dependent microtubule disassembly initiated by prefibrillar beta-amyloid." *J Cell Biol* 175 (4):541-6. doi: 10.1083/jcb.200605187.

Kitagishi Y., Nakanishi A., Ogura Y., and Matsuda S. 2014. "Dietary regulation of PI3K/AKT/GSK-3beta pathway in Alzheimer's disease." *Alzheimers Res Ther* 6 (3):35. doi: 10.1186/alzrt265.

Klafki H. W., Rieper P., Matzen A., Zampar S., Wirths O., Vogelgsang J., Osterloh D., Rohdenburg L., Oberstein T. J., Jahn O., Beyer I., Lachmann I., Knölker H.-J., and Wiltfang J. 2020. "Development and Technical Validation of an Immunoassay for the Detection of APP(669-711) (Aβ(-3-40)) in Biological Samples." *International journal of molecular sciences* 21 (18):6564. doi: 10.3390/ijms21186564.

Knowles R. B., Wyart C., Buldyrev S. V., Cruz L., Urbanc B., Hasselmo M. E., Stanley H. E., and Hyman B. T. 1999. "Plaque-induced neurite abnormalities: implications for disruption of neural networks in Alzheimer's disease." *Proc Natl Acad Sci U S A* 96 (9):5274-9. doi: 10.1073/pnas.96.9.5274.

Koffie R. M., Hashimoto T., Tai H. C., Kay K. R., Serrano-Pozo A., Joyner D., Hou S., Kopeikina K. J., Frosch M. P., Lee V. M., Holtzman D. M., Hyman B. T., and Spires-Jones T. L. 2012. "Apolipoprotein E4 effects in Alzheimer's disease are mediated by synaptotoxic oligomeric amyloid-beta." *Brain* 135 (Pt 7):2155-68. doi: 10.1093/brain/aws127.

Koffie R. M., Meyer-Luehmann M., Hashimoto T., Adams K. W., Mielke M. L., Garcia-Alloza M., Micheva K. D., Smith S. J., Kim M. L., Lee V. M., Hyman B. T., and Spires-Jones T. L. 2009. "Oligomeric amyloid beta associates with postsynaptic densities and correlates with excitatory synapse loss near senile plaques." *Proc Natl Acad Sci U S A* 106 (10):4012-7. doi: 10.1073/pnas.0811698106.

Kosik K. S., Joachim C. L., and Selkoe D. J. 1986. "Microtubule-associated protein tau (tau) is a major antigenic component of paired helical filaments in Alzheimer disease." *Proc Natl Acad Sci U S A* 83 (11):4044-8. doi: 10.1073/pnas.83.11.4044.

Kruger L., and Mandelkow E. M. 2016. "Tau neurotoxicity and rescue in animal models of human Tauopathies." *Curr Opin Neurobiol* 36:52-8. doi: 10.1016/j.conb.2015.09.004.

Kuchibhotla K. V., Goldman S. T., Lattarulo C. R., Wu H. Y., Hyman B. T., and Bacskai B. J. 2008. "Abeta plaques lead to aberrant regulation of calcium homeostasis in vivo resulting in structural and functional disruption of neuronal networks." *Neuron* 59 (2):214-25. doi: 10.1016/j.neuron.2008.06.008.

Kuhn P. H., Wang H., Dislich B., Colombo A., Zeitschel U., Ellwart J. W., Kremmer E., Rossner S., and Lichtenthaler S. F. 2010. "ADAM10 is the physiologically relevant, constitutive alpha-secretase of the amyloid precursor protein in primary neurons." *EMBO J* 29 (17):3020-32. doi: 10.1038/emboj.2010.167.

Kunkle B. W., Grenier-Boley B., Sims R., Bis J. C., Damotte V., Naj A. C., Boland A., Vronskaya M., van der Lee S. J., Amlie-Wolf A., Bellenguez C., Frizatti A., Chouraki V., Martin E. R., Sleegers K., Badarinarayan N., Jakobsdottir J., Hamilton-Nelson K. L., Moreno-Grau S., Olaso R., Raybould R., Chen Y., Kuzma A. B., Hiltunen M., Morgan T., Ahmad S., Vardarajan B. N., Epelbaum J., Hoffmann P., Boada M., Beecham G. W., Garnier J.-G., Harold D., Fitzpatrick A. L., Valladares O.,

Moutet M.-L., Gerrish A., Smith A. V., Qu L., Bacq D., Denning N., Jian X., Zhao Y., Del Zompo M., Fox N. C., Choi S.-H., Mateo I., Hughes J. T., Adams H. H., Malamon J., Sanchez-Garcia F., Patel Y., Brody J. A., Dombroski B. A., Naranjo M. C. D., Daniilidou M., Eiriksdottir G., Mukherjee S., Wallon D., Uphill J., Aspelund T., Cantwell L. B., Garzia F., Galimberti D., Hofer E., Butkiewicz M., Fin B., Scarpini E., Sarnowski C., Bush W. S., Meslage S., Kornhuber J., White C. C., Song Y., Barber R. C., Engelborghs S., Sordon S., Voijnovic D., Adams P. M., Vandenberghe R., Mayhaus M., Cupples L. A., Albert M. S., De Deyn P. P., Gu W., Himali J. J., Beekly D., Squassina A., Hartmann A. M., Orellana A., Blacker D., Rodriguez-Rodriguez E., Lovestone S., Garcia M. E., Doody R. S., Munoz-Fernadez C., Sussams R., Lin H., Fairchild T. J., Benito Y. A., Holmes C., Karamujić-Čomić H., Frosch M. P., Thonberg H., Maier W., Roschupkin G., Ghetti B., Giedraitis V., Kawalia A., Li S., Huebinger R. M., Kilander L., Moebus S., Hernández I., Kamboh M. I., Brundin R., Turton J., Yang Q., Katz M. J., Concari L., Lord J., Beiser A. S., Keene C. D., Helisalmi S., Kloszewska I., Kukull W. A., Koivisto A. M., Lynch A., Tarraga L., Larson E. B., Haapasalo A., Lawlor B., Mosley T. H., Lipton R. B., Solfrizzi V., Gill M., Longstreth W. T., Montine T. J., Frisardi V., Diez-Fairen M., Rivadeneira F., Petersen R. C., Deramecourt V., Alvarez I., Salani F., Ciaramella A., Boerwinkle E., Reiman E. M., Fievet N., Rotter J. I., Reisch J. S., Hanon O., Cupidi C., Andre Uitterlinden A. G., Royall D. R., Dufouil C., Maletta R. G., de Rojas I., Sano M., Brice A., Cecchetti R., George-Hyslop P. S., Ritchie K., Tsolaki M., Tsuang D. W., Dubois B., Craig D., Wu C.-K., Soininen H., Avramidou D., Albin R. L., Fratiglioni L., Germanou A., Apostolova L. G., Keller L., Koutroumani M., Arnold S. E., Panza F., Gkatzima O., Asthana S., Hannequin D., Whitehead P., Atwood C. S., Caffarra P., Hampel H., Quintela I., Carracedo Á., Lannfelt L., Rubinsztein D. C., Barnes L. L., Pasquier F., Frölich L., Barral S., McGuinness B., Beach T. G., Johnston J. A., Becker J. T., Passmore P., Bigio E. H., Schott J. M., Bird T. D., Warren J. D., Boeve B. F., Lupton M. K., Bowen J. D., Proitsi P., Boxer A., Powell J. F., Burke J. R., Kauwe J. S. K., Burns J. M., Mancuso M., Buxbaum J. D., Bonuccelli U., Cairns N. J., McQuillin A., Cao C., Livingston G., Carlson C. S., Bass N. J., Carlsson C. M., Hardy J., Carney R. M., Bras J., Carrasquillo M. M., Guerreiro R., Allen M., Chui H. C., Fisher E., Masullo C., Crocco E. A., DeCarli C., Bisceglio G., Dick M., Ma L., Duara R., Graff-Radford N. R., Evans D. A., Hodges A., Faber K. M., Scherer M., Fallon K. B., Riemenschneider M., Fardo D. W., Heun R., Farlow M. R., Kölsch H., Ferris S., Leber M., Foroud T. M., Heuser I., Galasko D. R., Giegling I., Gearing M., Hüll M., Geschwind D. H., Gilbert J. R., Morris J., Green R. C., Mayo K., Growdon J. H., Feulner T., Hamilton R. L., Harrell L. E., Drichel D., Honig L. S., Cushion T. D., Huentelman M. J., Hollingworth P., Hulette C. M., Hyman B. T., Marshall R., Jarvik G. P., Meggy A., Abner E., Menzies G. E., Jin L.-W., Leonenko G., Real L. M., Jun G. R., Baldwin C. T., Grozeva D., Karydas A., Russo G., Kaye J. A., Kim R., Jessen F., Kowall N. W., Vellas B., Kramer J. H., Vardy E., LaFerla F. M., Jöckel K.-H., Lah J. J., Dichgans M., Leverenz J. B., Mann D., Levey A. I., Pickering-Brown S., and Lieberman A. P. 2019. "Genetic meta-analysis of diagnosed Alzheimer's disease identifies new risk loci and implicates Aβ, tau, immunity and lipid processing." *Nature Genetics* 51 (3):414-430. doi: 10.1038/s41588-019-0358-2.

Kutoku Y., Ohsawa Y., Kuwano R., Ikeuchi T., Inoue H., Ataka S., Shimada H., Mori H., and Sunada Y. 2015. "A second pedigree with amyloid-less familial Alzheimer's disease harboring an identical mutation in the amyloid precursor protein gene (E693delta)." *Intern Med* 54 (2):205-8. doi: 10.2169/internalmedicine.54.3021.

Lacor P. N., Buniel M. C., Chang L., Fernandez S. J., Gong Y., Viola K. L., Lambert M. P., Velasco P. T., Bigio E. H., Finch C. E., Krafft G. A., and Klein W. L. 2004. "Synaptic targeting by Alzheimer's-related amyloid beta oligomers." *J Neurosci* 24 (45):10191-200. doi: 10.1523/JNEUROSCI.3432-04.2004.

Lalancette-Hebert M., Sharma A., Lyashchenko A. K., and Shneider N. A. 2016. "Gamma motor neurons survive and exacerbate alpha motor neuron degeneration in ALS." *Proc Natl Acad Sci U S A* 113 (51):E8316-E8325. doi: 10.1073/pnas.1605210113.

Lalonde R. 2002. "The neurobiological basis of spontaneous alternation." *Neurosci. Biobehav. Rev.* 26:91-104. doi: 10.1016/s0149-7634(01)00041-0.

Lalonde R., Dumont M., Staufenbiel M., Sturchler-Pierrat C., and Strazielle C. 2002. "Spatial learning, exploration, anxiety, and motor coordination in female APP23 transgenic mice with the Swedish mutation." *Brain Res.* 956 (1):36-44. doi: 10.1016/s0006-8993(02)03476-5.

Lalonde R., Lewis T. L., Strazielle C., Kim H., and Fukuchi K. 2003. "Transgenic mice expressing the betaAPP695SWE mutation: effects on exploratory activity, anxiety, and motor coordination." *Brain Res* 977 (1):38-45. doi: 10.1016/s0006-8993(03)02694-5.

Lalonde R., and Strazielle C. 2007. "Brain regions and genes affecting postural control." *Prog Neurobiol* 81 (1):45-60. doi: 10.1016/j.pneurobio.2006.11.005.

Lambert M. P., Barlow A. K., Chromy B. A., Edwards C., Freed R., Liosatos M., Morgan T. E., Rozovsky I., Trommer B., Viola K. L., Wals P., Zhang C., Finch C. E., Krafft G. A., and Klein W. L. 1998. "Diffusible, nonfibrillar ligands derived from Abeta1-42 are potent central nervous system neurotoxins." *Proc Natl Acad Sci U S A* 95 (11):6448-53. doi: 10.1073/pnas.95.11.6448.

Lance-Jones C. 1982. "Motoneuron cell death in the developing lumbar spinal cord of the mouse." *Brain Res* 256 (4):473-9. doi: 10.1016/0165-3806(82)90192-4.

Lazarevic V., Fieńko S., Andres-Alonso M., Anni D., Ivanova D., Montenegro-Venegas C., Gundelfinger E. D., Cousin M. A., and Fejtova A. 2017. "Physiological Concentrations of Amyloid Beta Regulate Recycling of Synaptic Vesicles via Alpha7 Acetylcholine Receptor and CDK5/Calcineurin Signaling." *Frontiers in Molecular Neuroscience* 10 (221). doi: 10.3389/fnmol.2017.00221.

Leissring M. A., Farris W., Chang A. Y., Walsh D. M., Wu X., Sun X., Frosch M. P., and Selkoe D. J. 2003. "Enhanced Proteolysis of β-Amyloid in APP Transgenic Mice Prevents Plaque Formation, Secondary Pathology, and Premature Death." *Neuron* 40 (6):1087-1093. doi: 10.1016/S0896-6273(03)00787-6.

Leroy K., Ando K., Laporte V., Dedecker R., Suain V., Authelet M., Heraud C., Pierrot N., Yilmaz Z., Octave J. N., and Brion J. P. 2012. "Lack of Tau Proteins Rescues Neuronal Cell Death and Decreases Amyloidogenic Processing of APP in APP/PS1 Mice." *Am J Pathol* 181 (6):1928-1940. doi: 10.1016/j.ajpath.2012.08.012.

Lesne S., Koh M. T., Kotilinek L., Kayed R., Glabe C. G., Yang A., Gallagher M., and Ashe K. H. 2006. "A specific amyloid-beta protein assembly in the brain impairs memory." *Nature* 440 (7082):352-7. doi: 10.1038/nature04533.

Levenga J., Krishnamurthy P., Rajamohamedsait H., Wong H., Franke T. F., Cain P., Sigurdsson E. M., and Hoeffer C. A. 2013. "Tau pathology induces loss of GABAergic interneurons leading to altered synaptic plasticity and behavioral impairments." *Acta Neuropathol Commun* 1:34. doi: 10.1186/2051-5960-1-34.

Lewis H., Beher D., Cookson N., Oakley A., Piggott M., Morris C. M., Jaros E., Perry R., Ince P., Kenny R. A., Ballard C. G., Shearman M. S., and Kalaria R. N. 2006. "Quantification of Alzheimer pathology in ageing and dementia: age-related accumulation of amyloid-beta(42) peptide in vascular dementia." *Neuropathol Appl Neurobiol* 32 (2):103-18. doi: 10.1111/j.1365-2990.2006.00696.x.

Lewis J., Dickson D. W., Lin W. L., Chisholm L., Corral A., Jones G., Yen S. H., Sahara N., Skipper L., Yager D., Eckman C., Hardy J., Hutton M., and McGowan E. 2001. "Enhanced neurofibrillary degeneration in transgenic mice expressing mutant tau and APP." *Science* 293 (5534):1487-91. doi: 10.1126/science.1058189.

Li J. M., Xue Z. Q., Deng S. H., Luo X. G., Patrylo P. R., Rose G. W., Cai H., Cai Y., and Yan X. X. 2013. "Amyloid plaque pathogenesis in 5XFAD mouse spinal cord: retrograde transneuronal modulation after peripheral nerve injury." *Neurotox Res* 24 (1):1-14. doi: 10.1007/s12640-012-9355-2.

Li S., Hong S., Shepardson N. E., Walsh D. M., Shankar G. M., and Selkoe D. 2009. "Soluble oligomers of amyloid Beta protein facilitate hippocampal long-term depression by disrupting neuronal glutamate uptake." *Neuron* 62 (6):788-801. doi: 10.1016/j.neuron.2009.05.012.

Li X., Song D., and Leng S. X. 2015. "Link between type 2 diabetes and Alzheimer's disease: from epidemiology to mechanism and treatment." *Clin Interv Aging* 10:549-60. doi: 10.2147/CIA.S74042.

Lichtenthaler S. F., Wang R., Grimm H., Uljon S. N., Masters C. L., and Beyreuther K. 1999. "Mechanism of the cleavage specificity of Alzheimer's disease gamma-secretase identified by phenylalanine-scanning mutagenesis of the transmembrane domain of the amyloid precursor protein." *Proc Natl Acad Sci U S A* 96 (6):3053-8. doi: 10.1073/pnas.96.6.3053.

Lindwall G., and Cole R. D. 1984. "Phosphorylation affects the ability of tau protein to promote microtubule assembly." *J Biol Chem* 259 (8):5301-5. doi: 10.1016/S0021-9258(17)42989-9.

Liu K., Doms R. W., and Lee V. M. 2002. "Glu11 site cleavage and N-terminally truncated A beta production upon BACE overexpression." *Biochemistry* 41 (9):3128-36. doi: 10.1021/bi015800g.

Liu M., Wang L., Gao J., Dong Q., Perry G., Ma X., and Wang X. 2019. "Inhibition of Calpain Protects Against Tauopathy in Transgenic P301S Tau Mice." *J Alzheimers Dis* 69 (4):1077-1087. doi: 10.3233/JAD-190281.

Lopez-Noguerola J. S., Giessen N. M. E., Ueberuck M., Meissner J. N., Pelgrim C. E., Adams J., Wirths O., Bouter Y., and Bayer T. A. 2018a. "Synergistic Effect on Neurodegeneration by N-Truncated Abeta4-42 and Pyroglutamate Abeta3-42 in a Mouse Model of Alzheimer's Disease." *Front Aging Neurosci* 10:64. doi: 10.3389/fnagi.2018.00064.

Lopez-Noguerola J. S., Giessen N. M. E., Ueberück M., Meißner J. N., Pelgrim C. E., Adams J., Wirths O., Bouter Y., and Bayer T. A. 2018b. "Synergistic Effect on Neurodegeneration by N-Truncated Aβ4−42 and Pyroglutamate Aβ3−42 in a Mouse Model of Alzheimer's Disease." *Front Aging Neurosci* 10:64. doi: 10.3389/fnagi.2018.00064.

Love S., and Miners J. S. 2016. "Cerebrovascular disease in ageing and Alzheimer's disease." *Acta Neuropathol* 131 (5):645-58. doi: 10.1007/s00401-015-1522-0.

Lu B., Gerard N. P., Kolakowski L. F., Jr., Bozza M., Zurakowski D., Finco O., Carroll M. C., and Gerard C. 1995. "Neutral endopeptidase modulation of septic shock." *J Exp Med* 181 (6):2271-5. doi: 10.1084/jem.181.6.2271.

Luong T. N., Carlisle H. J., Southwell A., and Patterson P. H. 2011. "Assessment of motor balance and coordination in mice using the balance beam." *J Vis Exp* (49). doi: 10.3791/2376.

Maggio J. E., Stimson E. R., Ghilardi J. R., Allen C. J., Dahl C. E., Whitcomb D. C., Vigna S. R., Vinters H. V., Labenski M. E., and Mantyh P. W. 1992. "Reversible in vitro growth of Alzheimer disease beta-amyloid plaques by deposition of labeled amyloid peptide." *Proc Natl Acad Sci U S A* 89 (12):5462-6. doi: 10.1073/pnas.89.12.5462.

Maloney J. A., Bainbridge T., Gustafson A., Zhang S., Kyauk R., Steiner P., van der Brug M., Liu Y., Ernst J. A., Watts R. J., and Atwal J. K. 2014. "Molecular mechanisms of Alzheimer disease protection by the A673T allele of amyloid precursor protein." *J Biol Chem* 289 (45):30990-1000. doi: 10.1074/jbc.M114.589069.

Marioni R. E., Harris S. E., Zhang Q., McRae A. F., Hagenaars S. P., Hill W. D., Davies G., Ritchie C. W., Gale C. R., Starr J. M., Goate A. M., Porteous D. J., Yang J., Evans K. L., Deary I. J., Wray N. R., and Visscher P. M. 2018. "GWAS on family history of Alzheimer's disease." *Translational Psychiatry* 8 (1):99. doi: 10.1038/s41398-018-0150-6.

Marquez-Sterling N. R., Lo A. C., Sisodia S. S., and Koo E. H. 1997. "Trafficking of cell-surface beta-amyloid precursor protein: evidence that a sorting intermediate participates in synaptic vesicle recycling." *J Neurosci* 17 (1):140-51. doi: 10.1523/JNEUROSCI.17-01-00140.1997.

Maruyama M., Shimada H., Suhara T., Shinotoh H., Ji B., Maeda J., Zhang M. R., Trojanowski J. Q., Lee V. M., Ono M., Masamoto K., Takano H., Sahara N., Iwata N., Okamura N., Furumoto S., Kudo Y., Chang Q., Saido T. C., Takashima A., Lewis J., Jang M. K., Aoki I., Ito H., and Higuchi M. 2013. "Imaging of tau pathology in a tauopathy mouse model and in Alzheimer patients compared to normal controls." *Neuron* 79 (6):1094-108. doi: 10.1016/j.neuron.2013.07.037.

Masliah E., Mallory M., Hansen L., DeTeresa R., Alford M., and Terry R. 1994. "Synaptic and neuritic alterations during the progression of Alzheimer's disease." *Neurosci Lett* 174 (1):67-72. doi: 10.1016/0304-3940(94)90121-x.

Masliah E., Terry R. D., Mallory M., Alford M., and Hansen L. A. 1990. "Diffuse plaques do not accentuate synapse loss in Alzheimer's disease." *Am J Pathol* 137 (6):1293-7.

Masters C. L., Multhaup G., Simms G., Pottgiesser J., Martins R. N., and Beyreuther K. 1985a. "Neuronal origin of a cerebral amyloid: neurofibrillary tangles of Alzheimer's disease contain the same protein as the amyloid of plaque cores and blood vessels." *Embo J* 4 (11):2757-63. doi: 10.1002/j.1460-2075.1985.tb04000.x.

Masters C. L., Simms G., Weinman N. A., Multhaup G., McDonald B. L., and Beyreuther K. 1985b. "Amyloid plaque core protein in Alzheimer disease and Down syndrome." *Proc Natl Acad Sci U S A* 82 (12):4245-9. doi: 10.1073/pnas.82.12.4245.

Masurkar A. V. 2018. "Towards a circuit-level understanding of hippocampal CA1 dysfunction in Alzheimer's disease across anatomical axes." *Journal of Alzheimer's disease & Parkinsonism* 8 (1):412. doi: 10.4172/2161-0460.1000412.

Mattson M. P. 1994. "Calcium and neuronal injury in Alzheimer's disease. Contributions of beta-amyloid precursor protein mismetabolism, free radicals, and metabolic compromise." *Ann N Y Acad Sci* 747:50-76. doi: 10.1111/j.1749-6632.1994.tb44401.x.

Mattson M. P., Cheng B., Davis D., Bryant K., Lieberburg I., and Rydel R. E. 1992. "beta-Amyloid peptides destabilize calcium homeostasis and render human cortical neurons vulnerable to excitotoxicity." *J Neurosci* 12 (2):376-89. doi: 10.1523/JNEUROSCI.12-02-00376.1992.

Mayeux R., and Stern Y. 2012. "Epidemiology of Alzheimer Disease." *Cold Spring Harbor Perspectives in Medicine* 2 (8). doi: 10.1101/cshperspect.a006239.

McLean C. A., Cherny R. A., Fraser F. W., Fuller S. J., Smith M. J., Beyreuther K., Bush A. I., and Masters C. L. 1999. "Soluble pool of Abeta amyloid as a determinant of severity of neurodegeneration in Alzheimer's disease." *Ann Neurol* 46 (6):860-6. doi: 10.1002/1531-8249(199912)46:6<860::aid-ana8>3.0.co;2-m.

Medina M., and Avila J. 2015. "Further understanding of tau phosphorylation: implications for therapy." *Expert Rev Neurother* 15 (1):115-22. doi: 10.1586/14737175.2015.1000864.

Meissner J. N., Bouter Y., and Bayer T. A. 2015. "Neuron Loss and Behavioral Deficits in the TBA42 Mouse Model Expressing N-Truncated Pyroglutamate Amyloid-beta3-42." *J Alzheimers Dis* 45 (2):471-482. doi: 10.3233/jad-142868.

Mikhail F., Calingasan N., Parolari L., Subramanian A., Yang L., and Flint Beal M. 2015. "Lack of exacerbation of neurodegeneration in a double transgenic mouse model of mutant LRRK2 and tau." *Hum Mol Genet* 24 (12):3545-56. doi: 10.1093/hmg/ddv105.

Miravalle L., Calero M., Takao M., Roher A. E., Ghetti B., and Vidal R. 2005. "Amino-terminally truncated Abeta peptide species are the main component of cotton wool plaques." *Biochemistry* 44 (32):10810-21. doi: 10.1021/bi0508237.

Mital M., Bal W., Frączyk T., and Drew S. C. 2018. "Interplay between Copper, Neprilysin, and N-Truncation of β-Amyloid." *Inorganic Chemistry*. doi: 10.1021/acs.inorgchem.8b00391.

Moore B. D., Chakrabarty P., Levites Y., Kukar T. L., Baine A. M., Moroni T., Ladd T. B., Das P., Dickson D. W., and Golde T. E. 2012. "Overlapping profiles of abeta peptides in the Alzheimer's disease and pathological aging brains." *Alzheimers Res Ther* 4 (3):18. doi: 10.1186/alzrt121.

Moreno H., Yu E., Pigino G., Hernandez A. I., Kim N., Moreira J. E., Sugimori M., and Llinas R. R. 2009. "Synaptic transmission block by presynaptic injection of oligomeric amyloid beta." *Proc Natl Acad Sci U S A* 106 (14):5901-6. doi: 10.1073/pnas.0900944106.

Morgan D., Munireddy S., Alamed J., DeLeon J., Diamond D. M., Bickford P., Hutton M., Lewis J., McGowan E., and Gordon M. N. 2008. "Apparent behavioral benefits of tau overexpression in P301L tau transgenic mice." *J Alzheimers Dis* 15 (4):605-14. doi: 10.3233/jad-2008-15407.

Mori C., Spooner E. T., Wisniewsk K. E., Wisniewski T. M., Yamaguch H., Saido T. C., Tolan D. R., Selkoe D. J., and Lemere C. A. 2002. "Intraneuronal Abeta42 accumulation in Down syndrome brain." *Amyloid* 9 (2):88-102. doi: 10.3109/13506120208995241.

Morris M., Maeda S., Vossel K., and Mucke L. 2011. "The many faces of tau." *Neuron* 70 (3):410-26. doi: 10.1016/j.neuron.2011.04.009.

Morris R. 1984. "Developments of a water-maze procedure for studying spatial learning in the rat." *J Neurosci Methods.* 11 (1):47-60. doi: 10.1016/0165-0270(84)90007-4.

Moser M. B., Moser E. I., Forrest E., Andersen P., and Morris R. G. 1995. "Spatial learning with a minislab in the dorsal hippocampus." *Proc Natl Acad Sci U S A* 92 (21):9697-701. doi: 10.1073/pnas.92.21.9697.

Mountjoy C. Q., Roth M., Evans N. J., and Evans H. M. 1983. "Cortical neuronal counts in normal elderly controls and demented patients." *Neurobiol Aging* 4 (1):1-11. doi: 10.1016/0197-4580(83)90048-9.

Mucke L., Masliah E., Yu G. Q., Mallory M., Rockenstein E. M., Tatsuno G., Hu K., Kholodenko D., Johnson-Wood K., and McConlogue L. 2000. "High-Level Neuronal Expression of Abeta 1-42 in Wild-Type Human Amyloid Protein Precursor Transgenic Mice: Synaptotoxicity without Plaque Formation." *J Neurosci* 20 (11):4050-4058. doi: 10.1523/JNEUROSCI.20-11-04050.2000.

Mukhin V. N., Pavlov K. I., and Klimenko V. M. 2017. "Mechanisms of Neuron Loss in Alzheimer's Disease." *Neuroscience and Behavioral Physiology* 47 (5):508-516. doi: 10.1007/s11055-017-0427-x.

Nagele R. G., D'Andrea M. R., Anderson W. J., and Wang H. Y. 2002. "Intracellular accumulation of beta-amyloid(1-42) in neurons is facilitated by the alpha 7 nicotinic acetylcholine receptor in Alzheimer's disease." *Neuroscience* 110 (2):199-211. doi: 10.1016/s0306-4522(01)00460-2.

Naseri N. N., Wang H., Guo J., Sharma M., and Luo W. 2019. "The complexity of tau in Alzheimer's disease." *Neurosci Lett* 705:183-194. doi: 10.1016/j.neulet.2019.04.022.

Nasrabady S. E., Rizvi B., Goldman J. E., and Brickman A. M. 2018. "White matter changes in Alzheimer's disease: a focus on myelin and oligodendrocytes." *Acta Neuropathologica Communications* 6 (1):22. doi: 10.1186/s40478-018-0515-3.

Nelson P. T., Alafuzoff I., Bigio E. H., Bouras C., Braak H., Cairns N. J., Castellani R. J., Crain B. J., Davies P., Tredici K. D., Duyckaerts C., Frosch M. P., Haroutunian V., Hof P. R., Hulette C. M., Hyman B. T., Iwatsubo T., Jellinger K. A., Jicha G. A., Kövari E., Kukull W. A., Leverenz J. B., Love S., Mackenzie I. R., Mann D. M., Masliah E., McKee A. C., Montine T. J., Morris J. C., Schneider J. A., Sonnen J. A., Thal D. R., Trojanowski J. Q., Troncoso J. C., Wisniewski T., Woltjer R. L., and Beach T. G. 2012. "Correlation of Alzheimer Disease Neuropathologic Changes With Cognitive Status: A Review of the Literature." *Journal of Neuropathology & Experimental Neurology* 71 (5):362-381. doi: 10.1097/NEN.0b013e31825018f7.

Nixon R. A., and Cataldo A. M. 2006. "Lysosomal system pathways: genes to neurodegeneration in Alzheimer's disease." *J Alzheimers Dis* 9 (3 Suppl):277-89. doi: 10.3233/jad-2006-9s331.

Nixon R. A., Wegiel J., Kumar A., Yu W. H., Peterhoff C., Cataldo A., and Cuervo A. M. 2005. "Extensive involvement of autophagy in Alzheimer disease: an immuno-electron microscopy study." *J Neuropathol Exp Neurol* 64 (2):113-22. doi: 10.1093/jnen/64.2.113.

O'Leary T. P., Mantolino H. M., Stover K. R., and Brown R. E. 2020. "Age-related deterioration of motor function in male and female 5xFAD mice from 3 to 16 months of age." *Genes, Brain and Behavior* 19 (3):e12538. doi: 10.1111/gbb.12538.

O'Leary T. P., Robertson A., Chipman P. H., Rafuse V. F., and Brown R. E. 2018. "Motor function deficits in the 12 month-old female 5xFAD mouse model of Alzheimer's disease." *Behav Brain Res* 337:256-263. doi: 10.1016/j.bbr.2017.09.009.

Oakley H., Cole S. L., Logan S., Maus E., Shao P., Craft J., Guillozet-Bongaarts A., Ohno M., Disterhoft J., Van Eldik L., Berry R., and Vassar R. 2006. "Intraneuronal beta-amyloid aggregates, neurodegeneration, and neuron loss in transgenic mice with five familial Alzheimer's disease mutations: potential factors in amyloid plaque formation." *J Neurosci.* 26 (40):10129-40. doi: 10.1523/JNEUROSCI.1202-06.2006

Oddo S., Billings L., Kesslak J. P., Cribbs D. H., and LaFerla F. M. 2004. "Abeta Immunotherapy Leads to Clearance of Early, but Not Late, Hyperphosphorylated Tau Aggregates via the Proteasome." *Neuron* 43 (3):321-32. doi: 10.1016/j.neuron.2004.07.003.

Ohia-Nwoko O., Montazari S., Lau Y. S., and Eriksen J. L. 2014. "Long-term treadmill exercise attenuates tau pathology in P301S tau transgenic mice." *Mol Neurodegener* 9 (1):54. doi: 10.1186/1750-1326-9-54.

Ohno M., Chang L., Tseng W., Oakley H., Citron M., Klein W. L., Vassar R., and Disterhoft J. F. 2006. "Temporal memory deficits in Alzheimer's mouse models: rescue by genetic deletion of BACE1." *Eur J Neurosci* 23 (1):251-60. doi: 10.1111/j.1460-9568.2005.04551.x.

Ohno M., Cole S. L., Yasvoina M., Zhao J., Citron M., Berry R., Disterhoft J. F., and Vassar R. 2007. "BACE1 gene deletion prevents neuron loss and memory deficits in 5XFAD APP/PS1 transgenic mice." *Neurobiol Dis* 26 (1):134-45. doi: 10.1016/j.nbd.2006.12.008.

Oikawa N., and Walter J. 2019. "Presenilins and γ-Secretase in Membrane Proteostasis." *Cells* 8 (3):209.

Ownby R. L., Crocco E., Acevedo A., John V., and Loewenstein D. 2006. "Depression and risk for Alzheimer disease: systematic review, meta-analysis, and metaregression analysis." *Arch Gen Psychiatry* 63 (5):530-8. doi: 10.1001/archpsyc.63.5.530.

Palop J. J., and Mucke L. 2010. "Amyloid-beta-induced neuronal dysfunction in Alzheimer's disease: from synapses toward neural networks." *Nat Neurosci* 13 (7):812-8. doi: 10.1038/nn.2583.

Park J., Jang M., and Chang S. 2013. "Deleterious effects of soluble amyloid-beta oligomers on multiple steps of synaptic vesicle trafficking." *Neurobiol Dis* 55:129-39. doi: 10.1016/j.nbd.2013.03.004.

Pastor P., Roe C. M., Villegas A., Bedoya G., Chakraverty S., Garcia G., Tirado V., Norton J., Rios S., Martinez M., Kosik K. S., Lopera F., and Goate A. M. 2003. "Apolipoprotein Eepsilon4 modifies

Alzheimer's disease onset in an E280A PS1 kindred." *Ann Neurol* 54 (2):163-9. doi: 10.1002/ana.10636.

Peters O. M., Shelkovnikova T., Tarasova T., Springe S., Kukharsky M. S., Smith G. A., Brooks S., Kozin S. A., Kotelevtsev Y., Bachurin S. O., Ninkina N., and Buchman V. L. 2013. "Chronic administration of Dimebon does not ameliorate amyloid-beta pathology in 5xFAD transgenic mice." *J Alzheimers Dis* 36 (3):589-96. doi: 10.3233/jad-130071.

Pettersson A. F., Olsson E., and Wahlund L. O. 2005. "Motor function in subjects with mild cognitive impairment and early Alzheimer's disease." *Dement Geriatr Cogn Disord.* 19 (5-6):299-304. . doi: 10.1159/000084555.

Pickett E. K., Herrmann A. G., McQueen J., Abt K., Dando O., Tulloch J., Jain P., Dunnett S., Sohrabi S., Fjeldstad M. P., Calkin W., Murison L., Jackson R. J., Tzioras M., Stevenson A., d'Orange M., Hooley M., Davies C., Colom-Cadena M., Anton-Fernandez A., King D., Oren I., Rose J., McKenzie C. A., Allison E., Smith C., Hardt O., Henstridge C. M., Hardingham G. E., and Spires-Jones T. L. 2019. "Amyloid Beta and Tau Cooperate to Cause Reversible Behavioral and Transcriptional Deficits in a Model of Alzheimer's Disease." *Cell Rep* 29 (11):3592-3604 e5. doi: 10.1016/j.celrep.2019.11.044.

Pike C. J., Cummings B. J., and Cotman C. W. 1995. "Early association of reactive astrocytes with senile plaques in Alzheimer's disease." *Exp Neurol* 132 (2):172-9. doi: 10.1016/0014-4886(95)90022-5.

Pimenova A. A., Raj T., and Goate A. M. 2018. "Untangling Genetic Risk for Alzheimer's Disease." *Biol Psychiatry* 83 (4):300-310. doi: 10.1016/j.biopsych.2017.05.014.

Plant L. D., Boyle J. P., Smith I. F., Peers C., and Pearson H. A. 2003. "The production of amyloid beta peptide is a critical requirement for the viability of central neurons." *J Neurosci* 23 (13):5531-5. doi: 10.1523/JNEUROSCI.23-13-05531.2003.

Plassman B. L., Williams J. W., Jr., Burke J. R., Holsinger T., and Benjamin S. 2010. "Systematic review: factors associated with risk for and possible prevention of cognitive decline in later life." *Ann Intern Med* 153 (3):182-93. doi: 10.7326/0003-4819-153-3-201008030-00258.

Poirier R., Wolfer D. P., Welzl H., Tracy J., Galsworthy M. J., Nitsch R. M., and Mohajeri M. H. 2006. "Neuronal neprilysin overexpression is associated with attenuation of Aβ-related spatial memory deficit." *Neurobiol Dis* 24 (3):475-483. doi: 10.1016/j.nbd.2006.08.003.

Polydoro M., Acker C. M., Duff K., Castillo P. E., and Davies P. 2009. "Age-dependent impairment of cognitive and synaptic function in the htau mouse model of tau pathology." *J Neurosci* 29 (34):10741-9. doi: 10.1523/JNEUROSCI.1065-09.2009.

Poorkaj P., Bird T. D., Wijsman E., Nemens E., Garruto R. M., Anderson L., Andreadis A., Wiederholt W. C., Raskind M., and Schellenberg G. D. 1998. "Tau is a candidate gene for chromosome 17 frontotemporal dementia." *Ann Neurol* 43 (6):815-25. doi: 10.1002/ana.410430617.

Portelius E., Bogdanovic N., Gustavsson M. K., Volkmann I., Brinkmalm G., Zetterberg H., Winblad B., and Blennow K. 2010. "Mass spectrometric characterization of brain amyloid beta isoform signatures in familial and sporadic Alzheimer's disease." *Acta Neuropathol* 120 (2):185-93. doi: 10.1007/s00401-010-0690-1.

Portelius E., Lashley T., Westerlund A., Persson R., Fox N. C., Blennow K., Revesz T., and Zetterberg H. 2015. "Brain Amyloid-Beta Fragment Signatures in Pathological Ageing and Alzheimer's Disease by Hybrid Immunoprecipitation Mass Spectrometry." *Neurodegenerative Diseases* 15 (1):50-57. doi: 10.1159/000369465.

Powis R. A., and Gillingwater T. H. 2016. "Selective loss of alpha motor neurons with sparing of gamma motor neurons and spinal cord cholinergic neurons in a mouse model of spinal muscular atrophy." *J Anat* 228 (3):443-51. doi: 10.1111/joa.12419.

Price J. L., and Morris J. C. 1999. "Tangles and plaques in nondemented aging and "preclinical" Alzheimer's disease." *Ann Neurol* 45 (3):358-68. doi: 10.1002/1531-8249(199903)45:3<358::aid-ana12>3.0.co;2-x.

Priller C., Bauer T., Mitteregger G., Krebs B., Kretzschmar H. A., and Herms J. 2006. "Synapse formation and function is modulated by the amyloid precursor protein." *J Neurosci* 26 (27):7212-21. doi: 10.1523/JNEUROSCI.1450-06.2006.

Pruvost M., Lépine M., Leonetti C., Etard O., Naveau M., Agin V., Docagne F., Maubert E., Ali C., Emery E., and Vivien D. 2017. "ADAMTS-4 in oligodendrocytes contributes to myelination with an impact on motor function." *Glia* 65 (12):1961-1975. doi: 10.1002/glia.23207.

Purro S. A., Dickins E. M., and Salinas P. C. 2012. "The Secreted Wnt Antagonist Dickkopf-1 Is Required for Amyloid β-Mediated Synaptic Loss." *The Journal of Neuroscience* 32 (10):3492-3498. doi: 10.1523/jneurosci.4562-11.2012.

Puzzo D., Piacentini R., Fa M., Gulisano W., Li Puma D. D., Staniszewski A., Zhang H., Tropea M. R., Cocco S., Palmeri A., Fraser P., D'Adamio L., Grassi C., and Arancio O. 2017. "LTP and memory impairment caused by extracellular Abeta and Tau oligomers is APP-dependent." *Elife* 6. doi: 10.7554/eLife.26991.

Puzzo D., Privitera L., Fa M., Staniszewski A., Hashimoto G., Aziz F., Sakurai M., Ribe E. M., Troy C. M., Mercken M., Jung S. S., Palmeri A., and Arancio O. 2011. "Endogenous amyloid-beta is necessary for hippocampal synaptic plasticity and memory." *Ann Neurol* 69 (5):819-30. doi: 10.1002/ana.22313.

Puzzo D., Privitera L., Leznik E., Fa M., Staniszewski A., Palmeri A., and Arancio O. 2008. "Picomolar amyloid-beta positively modulates synaptic plasticity and memory in hippocampus." *J Neurosci* 28 (53):14537-45. doi: 10.1523/JNEUROSCI.2692-08.2008.

Qiang L., Yu W., Andreadis A., Luo M., and Baas P. W. 2006. "Tau protects microtubules in the axon from severing by katanin." *J Neurosci* 26 (12):3120-9. doi: 10.1523/JNEUROSCI.5392-05.2006.

Qiu C., Kivipelto M., and von Strauss E. 2009. "Epidemiology of Alzheimer's disease: occurrence, determinants, and strategies toward intervention." *Dialogues Clin Neurosci* 11 (2):111-28. doi: 10.31887/DCNS.2009.11.2/cqiu.

Rapoport M., Dawson H. N., Binder L. I., Vitek M. P., and Ferreira A. 2002. "Tau is essential to beta -amyloid-induced neurotoxicity." *Proc Natl Acad Sci U S A* 99 (9):6364-9. doi: 10.1073/pnas.092136199.

Regan P., Piers T., Yi J. H., Kim D. H., Huh S., Park S. J., Ryu J. H., Whitcomb D. J., and Cho K. 2015. "Tau phosphorylation at serine 396 residue is required for hippocampal LTD." *J Neurosci* 35 (12):4804-12. doi: 10.1523/JNEUROSCI.2842-14.2015.

Reinert J., Richard B. C., Klafki H. W., Friedrich B., Bayer T. A., Wiltfang J., Kovacs G. G., Ingelsson M., Lannfelt L., Paetau A., Bergquist J., and Wirths O. 2016. "Deposition of C-terminally truncated Aβ species Aβ37 and Aβ39 in Alzheimer's disease and transgenic mouse models." *Acta Neuropathologica Communications* 4 (1):1-12. doi: 10.1186/s40478-016-0294-7.

Reisberg B., Ferris S. H., de Leon M. J., and Crook T. 1982. "The Global Deterioration Scale for assessment of primary degenerative dementia." *Am J Psychiatry* 139 (9):1136-9. doi: 10.1176/ajp.139.9.1136.

Reitz C., Brayne C., and Mayeux R. 2011. "Epidemiology of Alzheimer disease." *Nat Rev Neurol* 7 (3):137-52. doi: 10.1038/nrneurol.2011.2.

Reitz C., and Mayeux R. 2014. "Alzheimer disease: epidemiology, diagnostic criteria, risk factors and biomarkers." *Biochem Pharmacol* 88 (4):640-51. doi: 10.1016/j.bcp.2013.12.024.

Ribe E. M., Perez M., Puig B., Gich I., Lim F., Cuadrado M., Sesma T., Catena S., Sanchez B., Nieto M., Gomez-Ramos P., Moran M. A., Cabodevilla F., Samaranch L., Ortiz L., Perez A., Ferrer I., Avila J., and Gomez-Isla T. 2005. "Accelerated amyloid deposition, neurofibrillary degeneration and neuronal loss in double mutant APP/tau transgenic mice." *Neurobiol Dis.* 20 (3):814-22. . doi: 10.1016/j.nbd.2005.05.027.

Richard B. C., Kurdakova A., Baches S., Bayer T. A., Weggen S., and Wirths O. 2015. "Gene Dosage Dependent Aggravation of the Neurological Phenotype in the 5XFAD Mouse Model of Alzheimer's Disease." *J Alzheimers Dis* 45:1223-1236. doi: 10.3233/jad-143120.

Roberson E. D., Halabisky B., Yoo J. W., Yao J., Chin J., Yan F., Wu T., Hamto P., Devidze N., Yu G. Q., Palop J. J., Noebels J. L., and Mucke L. 2011. "Amyloid-beta/Fyn-induced synaptic, network, and cognitive impairments depend on tau levels in multiple mouse models of Alzheimer's disease." *J Neurosci* 31 (2):700-11. doi: 10.1523/JNEUROSCI.4152-10.2011.

Roberson E. D., Scearce-Levie K., Palop J. J., Yan F., Cheng I. H., Wu T., Gerstein H., Yu G. Q., and Mucke L. 2007. "Reducing endogenous tau ameliorates amyloid beta-induced deficits in an Alzheimer's disease mouse model." *Science* 316 (5825):750-4. doi: 10.1126/science.1141736.

Roher A. E., Chaney M. O., Kuo Y. M., Webster S. D., Stine W. B., Haverkamp L. J., Woods A. S., Cotter R. J., Tuohy J. M., Krafft G. A., Bonnell B. S., and Emmerling M. R. 1996. "Morphology and toxicity of Abeta-(1-42) dimer derived from neuritic and vascular amyloid deposits of Alzheimer's disease." *J Biol Chem* 271 (34):20631-5. doi: 10.1074/jbc.271.34.20631.

Rovelet-Lecrux A., Hannequin D., Raux G., Le Meur N., Laquerriere A., Vital A., Dumanchin C., Feuillette S., Brice A., Vercelletto M., Dubas F., Frebourg T., and Campion D. 2006. "APP locus duplication causes autosomal dominant early-onset Alzheimer disease with cerebral amyloid angiopathy." *Nat Genet* 38 (1):24-6. doi: 10.1038/ng1718.

Saitoh T., Sundsmo M., Roch J. M., Kimura N., Cole G., Schubert D., Oltersdorf T., and Schenk D. B. 1989. "Secreted form of amyloid beta protein precursor is involved in the growth regulation of fibroblasts." *Cell* 58 (4):615-22. doi: 10.1016/0092-8674(89)90096-2.

Saul A., Lashley T., Revesz T., Holton J., Ghiso J. A., Coomaraswamy J., and Wirths O. 2013a. "Abundant pyroglutamate-modified ABri and ADan peptides in extracellular and vascular amyloid deposits in familial British and Danish dementias." *Neurobiol Aging* 34:1416-1425. doi: 10.1016/j.neurobiolaging.2012.11.014.

Saul A., Sprenger F., Bayer T. A., and Wirths O. 2013b. "Accelerated tau pathology with synaptic and neuronal loss in a novel triple transgenic mouse model of Alzheimer's disease." *Neurobiol Aging* 34 (11):2564-2573. doi: 10.1016/j.neurobiolaging.2013.05.003.

Savastano A., Klafki H., Haussmann U., Oberstein T. J., Muller P., Wirths O., Wiltfang J., and Bayer T. A. 2016. "N-Truncated Abeta 2-X Starting with Position Two in Sporadic Alzheimer's Disease Cases and Two Alzheimer Mouse Models." *J Alzheimers Dis* 49 (1):101-110. doi: 10.3233/jad-150349.

Saydoff J. A., Olariu A., Sheng J., Hu Z., Li Q., Garcia R., Pei J., Sun G. Y., and von Borstel R. 2013. "Uridine prodrug improves memory in Tg2576 and TAPP mice and reduces pathological factors associated with Alzheimer's disease in related models." *J Alzheimers Dis* 36 (4):637-57. doi: 10.3233/JAD-130059.

Scarmeas N., Albert M., Brandt J., Blacker D., Hadjigeorgiou G., Papadimitriou A., Dubois B., Sarazin M., Wegesin D., Marder K., Bell K., Honig L., and Stern Y. 2005. "Motor signs predict poor outcomes in Alzheimer disease." *Neurology.* 64 (10):1696-703. doi: 10.1212/01.WNL.0000162054.15428.E9.

Scarmeas N., Hadjigeorgiou G. M., Papadimitriou A., Dubois B., Sarazin M., Brandt J., Albert M., Marder K., Bell K., Honig L. S., Wegesin D., and Stern Y. 2004. "Motor signs during the course of Alzheimer disease." *Neurology* 63 (6):975-82. doi: 10.1212/01.wnl.0000138440.39918.0c.

Schaffert L. N., and Carter W. G. 2020. "Do Post-Translational Modifications Influence Protein Aggregation in Neurodegenerative Diseases: A Systematic Review." *Brain Sci* 10 (4). doi: 10.3390/brainsci10040232.

Scheff S. W., Price D. A., Schmitt F. A., DeKosky S. T., and Mufson E. J. 2007. "Synaptic alterations in CA1 in mild Alzheimer disease and mild cognitive impairment." *Neurology* 68 (18):1501-8. doi: 10.1212/01.wnl.0000260698.46517.8f.

Schilling S., Lauber T., Schaupp M., Manhart S., Scheel E., Bohm G., and Demuth H. U. 2006. "On the seeding and oligomerization of pGlu-amyloid peptides (in vitro)." *Biochemistry* 45 (41):12393-9. doi: 10.1021/bi0612667.

Schilling S., Zeitschel U., Hoffmann T., Heiser U., Francke M., Kehlen A., Holzer M., Hutter-Paier B., Prokesch M., Windisch M., Jagla W., Schlenzig D., Lindner C., Rudolph T., Reuter G., Cynis H., Montag D., Demuth H. U., and Rossner S. 2008. "Glutaminyl cyclase inhibition attenuates pyroglutamate Abeta and Alzheimer's disease-like pathology." *Nat Med* 14 (10):1106-11. doi: 10.1038/nm.1872.

Schmittgen T. D., and Livak K. J. 2008. "Analyzing real-time PCR data by the comparative C(T) method." *Nat Protoc* 3 (6):1101-8. doi: 10.1038/nprot.2008.73.

Schneider F., Baldauf K., Wetzel W., and Reymann K. G. 2014. "Behavioral and EEG changes in male 5xFAD mice." *Physiology & Behavior* 135 (0):25-33. doi: 10.1016/j.physbeh.2014.05.041.

Schneider F., Baldauf K., Wetzel W., and Reymann K. G. 2015. "Effects of methylphenidate on the behavior of male 5xFAD mice." *Pharmacol Biochem Behav* 128:68-77. doi: 10.1016/j.pbb.2014.11.006.

Schwab C., Klegeris A., and McGeer P. L. 2010. "Inflammation in transgenic mouse models of neurodegenerative disorders." *Biochimica et Biophysica Acta (BBA) - Molecular Basis of Disease* 1802 (10):889-902. doi: 10.1016/j.bbadis.2009.10.013.

Selkoe D. J. 2008. "Soluble oligomers of the amyloid beta-protein impair synaptic plasticity and behavior." *Behav Brain Res* 192 (1):106-13. doi: 10.1016/j.bbr.2008.02.016.

Sellers K. J., Elliott C., Jackson J., Ghosh A., Ribe E., Rojo A. I., Jarosz-Griffiths H. H., Watson I. A., Xia W., Semenov M., Morin P., Hooper N. M., Porter R., Preston J., Al-Shawi R., Baillie G., Lovestone S., Cuadrado A., Harte M., Simons P., Srivastava D. P., and Killick R. 2018. "Amyloid beta synaptotoxicity is Wnt-PCP dependent and blocked by fasudil." *Alzheimers Dement* 14 (3):306-317. doi: 10.1016/j.jalz.2017.09.008.

Seo J., Kritskiy O., Watson L. A., Barker S. J., Dey D., Raja W. K., Lin Y. T., Ko T., Cho S., Penney J., Silva M. C., Sheridan S. D., Lucente D., Gusella J. F., Dickerson B. C., Haggarty S. J., and Tsai L. H. 2017. "Inhibition of p25/Cdk5 Attenuates Tauopathy in Mouse and iPSC Models of Frontotemporal Dementia." *J Neurosci* 37 (41):9917-9924. doi: 10.1523/JNEUROSCI.0621-17.2017.

Seo J. S., Leem Y. H., Lee K. W., Kim S. W., Lee J. K., and Han P. L. 2010. "Severe motor neuron degeneration in the spinal cord of the Tg2576 mouse model of Alzheimer disease." *J Alzheimers Dis* 21 (1):263-76. doi: 10.3233/JAD-2010-091528.

Sergeant N., Bombois S., Ghestem A., Drobecq H., Kostanjevecki V., Missiaen C., Wattez A., David J. P., Vanmechelen E., Sergheraert C., and Delacourte A. 2003. "Truncated beta-amyloid peptide species in pre-clinical Alzheimer's disease as new targets for the vaccination approach." *J Neurochem.* 85 (6):1581-91. doi: 10.1046/j.1471-4159.2003.01818.x.

Serrano-Pozo A., Frosch M. P., Masliah E., and Hyman B. T. 2011a. "Neuropathological Alterations in Alzheimer Disease." *Cold Spring Harbor Perspectives in Medicine* 1 (1). doi: 10.1101/cshperspect.a006189.

Serrano-Pozo A., Mielke M. L., Gomez-Isla T., Betensky R. A., Growdon J. H., Frosch M. P., and Hyman B. T. 2011b. "Reactive glia not only associates with plaques but also parallels tangles in Alzheimer's disease." *Am J Pathol* 179 (3):1373-84. doi: 10.1016/j.ajpath.2011.05.047.

Seward M. E., Swanson E., Norambuena A., Reimann A., Cochran J. N., Li R., Roberson E. D., and Bloom G. S. 2013. "Amyloid-beta signals through tau to drive ectopic neuronal cell cycle re-entry in Alzheimer's disease." *J Cell Sci* 126 (Pt 5):1278-86. doi: 10.1242/jcs.1125880.

Sgourakis N. G., Yan Y., McCallum S. A., Wang C., and Garcia A. E. 2007. "The Alzheimer's peptides Abeta40 and 42 adopt distinct conformations in water: a combined MD / NMR study." *Journal of molecular biology* 368 (5):1448-1457. doi: 10.1016/j.jmb.2007.02.093.

Shankar G. M., Bloodgood B. L., Townsend M., Walsh D. M., Selkoe D. J., and Sabatini B. L. 2007. "Natural oligomers of the Alzheimer amyloid-beta protein induce reversible synapse loss by modulating an NMDA-type glutamate receptor-dependent signaling pathway." *J Neurosci* 27 (11):2866-75. doi: 10.1523/JNEUROSCI.4970-06.2007.

Shankar G. M., Li S., Mehta T. H., Garcia-Munoz A., Shepardson N. E., Smith I., Brett F. M., Farrell M. A., Rowan M. J., Lemere C. A., Regan C. M., Walsh D. M., Sabatini B. L., and Selkoe D. J. 2008. "Amyloid-beta protein dimers isolated directly from Alzheimer's brains impair synaptic plasticity and memory." *Nat Med* 14 (8):837-42. doi: 10.1038/nm1782.

Shao C. Y., Mirra S. S., Sait H. B., Sacktor T. C., and Sigurdsson E. M. 2011. "Postsynaptic degeneration as revealed by PSD-95 reduction occurs after advanced Abeta and tau pathology in transgenic mouse models of Alzheimer's disease." *Acta Neuropathol* 122 (3):285-92. doi: 10.1007/s00401-011-0843-x.

Shimada H., Ataka S., Tomiyama T., Takechi H., Mori H., and Miki T. 2011. "Clinical course of patients with familial early-onset Alzheimer's disease potentially lacking senile plaques bearing the E693Delta mutation in amyloid precursor protein." *Dement Geriatr Cogn Disord* 32 (1):45-54. doi: 10.1159/000330017.

Shipton O. A., Leitz J. R., Dworzak J., Acton C. E., Tunbridge E. M., Denk F., Dawson H. N., Vitek M. P., Wade-Martins R., Paulsen O., and Vargas-Caballero M. 2011. "Tau protein is required for amyloid {beta}-induced impairment of hippocampal long-term potentiation." *J Neurosci* 31 (5):1688-92. doi: 10.1523/jneurosci.2610-10.2011.

Shirotani K., Tsubuki S., Iwata N., Takaki Y., Harigaya W., Maruyama K., Kiryu-Seo S., Kiyama H., Iwata H., Tomita T., Iwatsubo T., and Saido T. C. 2001. "Neprilysin degrades both amyloid beta peptides 1-40 and 1-42 most rapidly and efficiently among thiorphan- and phosphoramidon-sensitive endopeptidases." *J Biol Chem* 276 (24):21895-901. doi: 10.1074/jbc.M008511200.

Shukla V., Skuntz S., and Pant H. C. 2012. "Deregulated Cdk5 activity is involved in inducing Alzheimer's disease." *Arch Med Res* 43 (8):655-62. doi: 10.1016/j.arcmed.2012.10.015.

Sichler M. E., Low M. J., Schleicher E. M., Bayer T. A., and Bouter Y. 2019. "Reduced Acoustic Startle Response and Prepulse Inhibition in the Tg4-42 Model of Alzheimer's Disease." *J Alzheimers Dis Rep* 3 (1):269-278. doi: 10.3233/ADR-190132.

Simic G., Kostovic I., Winblad B., and Bogdanovic N. 1997. "Volume and number of neurons of the human hippocampal formation in normal aging and Alzheimer's disease." *J Comp Neurol* 379 (4):482-94. doi: 10.1002/(sici)1096-9861(19970324)379:4<482::aid-cne2>3.0.co;2-z.

Skoog I., and Gustafson D. 2006. "Update on hypertension and Alzheimer's disease." *Neurol Res* 28 (6):605-11. doi: 10.1179/016164106X130506.

Skovronsky D. M., Doms R. W., and Lee V. M. 1998. "Detection of a novel intraneuronal pool of insoluble amyloid beta protein that accumulates with time in culture." *J Cell Biol* 141 (4):1031-9. doi: 10.1083/jcb.141.4.1031.

Small S. A., and Duff K. 2008. "Linking Abeta and tau in late-onset Alzheimer's disease: a dual pathway hypothesis." *Neuron* 60 (4):534-42. doi: 10.1016/j.neuron.2008.11.007.

Snyder E. M., Nong Y., Almeida C. G., Paul S., Moran T., Choi E. Y., Nairn A. C., Salter M. W., Lombroso P. J., Gouras G. K., and Greengard P. 2005. "Regulation of NMDA receptor trafficking by amyloid-beta." *Nat Neurosci* 8 (8):1051-8. doi: 10.1038/nn1503.

Sola C., Mengod G., Probst A., and Palacios J. M. 1993. "Differential regional and cellular distribution of beta-amyloid precursor protein messenger RNAs containing and lacking the Kunitz protease inhibitor domain in the brain of human, rat and mouse." *Neuroscience* 53 (1):267-95. doi: 10.1016/0306-4522(93)90304-x.

Spires-Jones T. L., and Hyman B. T. 2014. "The intersection of amyloid beta and tau at synapses in Alzheimer's disease." *Neuron* 82 (4):756-71. doi: 10.1016/j.neuron.2014.05.004.

Spires T. L., Meyer-Luehmann M., Stern E. A., McLean P. J., Skoch J., Nguyen P. T., Bacskai B. J., and Hyman B. T. 2005. "Dendritic spine abnormalities in amyloid precursor protein transgenic mice demonstrated by gene transfer and intravital multiphoton microscopy." *J Neurosci* 25 (31):7278-87. doi: 10.1523/JNEUROSCI.1879-05.2005.

Squire L. R., Wixted J. T., and Clark R. E. 2007. "Recognition memory and the medial temporal lobe: a new perspective." *Nat Rev Neurosci* 8 (11):872-83. doi: 10.1038/nrn2154.

Stancu I.-C., Ris L., Vasconcelos B., Marinangeli C., Goeminne L., Laporte V., Haylani L. E., Couturier J., Schakman O., Gailly P., Pierrot N., Kienlen-Campard P., Octave J.-N., and Dewachter I. 2014a. "Tauopathy contributes to synaptic and cognitive deficits in a murine model for Alzheimer's disease." *The FASEB Journal*. doi: 10.1096/fj.13-246702.

Stancu I. C., Vasconcelos B., Terwel D., and Dewachter I. 2014b. "Models of beta-amyloid induced Tau-pathology: the long and "folded" road to understand the mechanism." *Mol Neurodegener* 9:51. doi: 10.1186/1750-1326-9-51.

Stazi M., and Wirths O. 2021. "Chronic Memantine Treatment Ameliorates Behavioral Deficits, Neuron Loss, and Impaired Neurogenesis in a Model of Alzheimer's Disease." *Mol Neurobiol* 58 (1):204-216. doi: 10.1007/s12035-020-02120-z.

Steiner H., Fukumori A., Tagami S., and Okochi M. 2018. "Making the final cut: pathogenic amyloid-β peptide generation by γ-secretase." *Cell Stress* 2 (11):292-310. doi: 10.15698/cst2018.11.162.

Steinerman J. R., Irizarry M., Scarmeas N., Raju S., Brandt J., Albert M., Blacker D., Hyman B., and Stern Y. 2008. "Distinct pools of beta-amyloid in Alzheimer disease-affected brain: a clinicopathologic study." *Arch Neurol* 65 (7):906-12. doi: 10.1001/archneur.65.7.906.

Sterniczuk R., Antle M. C., Laferla F. M., and Dyck R. H. 2010. "Characterization of the 3xTg-AD mouse model of Alzheimer's disease: part 2. Behavioral and cognitive changes." *Brain Res* 1348:149-55. doi: 10.1016/j.brainres.2010.06.011.

Stover K. R., Campbell M. A., Van Winssen C. M., and Brown R. E. 2015. "Analysis of motor function in 6-month-old male and female 3xTg-AD mice." *Behav Brain Res* 281:16-23. doi: 10.1016/j.bbr.2014.11.046.

Sun Y., Guo Y., Feng X., Jia M., Ai N., Dong Y., Zheng Y., Fu L., Yu B., Zhang H., Wu J., Yu X., Wu H., and Kong W. 2020. "The behavioural and neuropathologic sexual dimorphism and absence of MIP-3alpha in tau P301S mouse model of Alzheimer's disease." *J Neuroinflammation* 17 (1):72. doi: 10.1186/s12974-020-01749-w.

Sungura R., Onyambu C., Mpolya E., Sauli E., and Vianney J. M. 2021. "The extended scope of neuroimaging and prospects in brain atrophy mitigation: A systematic review." *Interdisciplinary Neurosurgery* 23:100875. doi: 10.1016/j.inat.2020.100875.

Sydow A., Van der Jeugd A., Zheng F., Ahmed T., Balschun D., Petrova O., Drexler D., Zhou L., Rune G., Mandelkow E., D'Hooge R., Alzheimer C., and Mandelkow E. M. 2011. "Tau-induced defects in synaptic plasticity, learning, and memory are reversible in transgenic mice after switching off the toxic Tau mutant." *J Neurosci* 31 (7):2511-25. doi: 10.1523/JNEUROSCI.5245-10.2011.

Tai H. C., Serrano-Pozo A., Hashimoto T., Frosch M. P., Spires-Jones T. L., and Hyman B. T. 2012. "The synaptic accumulation of hyperphosphorylated tau oligomers in Alzheimer disease is associated with dysfunction of the ubiquitin-proteasome system." *Am J Pathol* 181 (4):1426-35. doi: 10.1016/j.ajpath.2012.06.033.

Takahashi M., Miyata H., Kametani F., Nonaka T., Akiyama H., Hisanaga S., and Hasegawa M. 2015. "Extracellular association of APP and tau fibrils induces intracellular aggregate formation of tau." *Acta Neuropathol* 129 (6):895-907. doi: 10.1007/s00401-015-1415-2.

Takahashi R. H., Almeida C. G., Kearney P. F., Yu F., Lin M. T., Milner T. A., and Gouras G. K. 2004. "Oligomerization of Alzheimer's beta-amyloid within processes and synapses of cultured neurons and brain." *J Neurosci* 24 (14):3592-9. doi: 10.1523/JNEUROSCI.5167-03.2004

Takahashi R. H., Milner T. A., Li F., Nam E. E., Edgar M. A., Yamaguchi H., Beal M. F., Xu H., Greengard P., and Gouras G. K. 2002. "Intraneuronal Alzheimer Abeta42 accumulates in multivesicular bodies and is associated with synaptic pathology." *Am J Pathol* 161 (5):1869-79. doi: 10.1016/s0002-9440(10)64463-x.

Takashima A., Noguchi K., Sato K., Hoshino T., and Imahori K. 1993. "Tau protein kinase I is essential for amyloid beta-protein-induced neurotoxicity." *Proc Natl Acad Sci U S A* 90 (16):7789-93. doi: 10.1073/pnas.90.16.7789.

Takeuchi H., Iba M., Inoue H., Higuchi M., Takao K., Tsukita K., Karatsu Y., Iwamoto Y., Miyakawa T., Suhara T., Trojanowski J. Q., Lee V. M. Y., and Takahashi R. 2011. "P301S Mutant Human Tau Transgenic Mice Manifest Early Symptoms of Human Tauopathies with Dementia and Altered Sensorimotor Gating." *PLoS ONE* 6 (6):e21050. doi: 10.1371/journal.pone.0021050.

Takuma K., Fang F., Zhang W., Yan S., Fukuzaki E., Du H., Sosunov A., McKhann G., Funatsu Y., Nakamichi N., Nagai T., Mizoguchi H., Ibi D., Hori O., Ogawa S., Stern D. M., Yamada K., and Yan S. S. 2009. "RAGE-mediated signaling contributes to intraneuronal transport of amyloid-beta and neuronal dysfunction." *Proc Natl Acad Sci U S A* 106 (47):20021-6. doi: 10.1073/pnas.0905686106.

Tanaka S., Nakamura S., Ueda K., Kameyama M., Shiojiri S., Takahashi Y., Kitaguchi N., and Ito H. 1988. "Three types of amyloid protein precursor mRNA in human brain: their differential expression in Alzheimer's disease." *Biochem Biophys Res Commun* 157 (2):472-9. doi: 10.1016/s0006-291x(88)80273-0.

Tanzi R. E. 2012. "The Genetics of Alzheimer Disease." *Cold Spring Harb Perspect Med* 2 (10). doi: 10.1101/cshperspect.a006296.

Tarasoff-Conway J. M., Carare R. O., Osorio R. S., Glodzik L., Butler T., Fieremans E., Axel L., Rusinek H., Nicholson C., Zlokovic B. V., Frangione B., Blennow K., Ménard J., Zetterberg H., Wisniewski T., and de Leon M. J. 2015. "Clearance systems in the brain—implications for Alzheimer disease." *Nature Reviews Neurology* 11:457. doi: 10.1038/nrneurol.2015.119.

Tekirian T. L., Yang A. Y., Glabe C., and Geddes J. W. 1999. "Toxicity of pyroglutaminated amyloid beta-peptides 3(pE)-40 and -42 is similar to that of A beta1-40 and -42." *J Neurochem.* 73 (4):1584-9. doi: 10.1046/j.1471-4159.1999.0731584.x.

Thal D. R., Rub U., Orantes M., and Braak H. 2002. "Phases of A beta-deposition in the human brain and its relevance for the development of AD." *Neurology* 58 (12):1791-800. doi: 10.1212/wnl.58.12.1791.

Thies E., and Mandelkow E.-M. 2007. "Missorting of Tau in Neurons Causes Degeneration of Synapses That Can Be Rescued by the Kinase MARK2/Par-1." *The Journal of Neuroscience* 27 (11):2896-2907. doi: 10.1523/jneurosci.4674-06.2007.

Tomiyama T., Matsuyama S., Iso H., Umeda T., Takuma H., Ohnishi K., Ishibashi K., Teraoka R., Sakama N., Yamashita T., Nishitsuji K., Ito K., Shimada H., Lambert M. P., Klein W. L., and Mori H. 2010. "A mouse model of amyloid-b oligomers: their contribution to synaptic alteration, abnormal tau phosphorylation, glial activation, and neuronal loss in vivo." *J Neurosci* 30 (14):4845-56. doi: 10.1523/JNEUROSCI.5825-09.2010.

Tomiyama T., Nagata T., Shimada H., Teraoka R., Fukushima A., Kanemitsu H., Takuma H., Kuwano R., Imagawa M., Ataka S., Wada Y., Yoshioka E., Nishizaki T., Watanabe Y., and Mori H. 2008. "A new amyloid beta variant favoring oligomerization in Alzheimer's-type dementia." *Ann Neurol* 63 (3):377-87. doi: 10.1002/ana.21321.

Turner P. R., O'Connor K., Tate W. P., and Abraham W. C. 2003. "Roles of amyloid precursor protein and its fragments in regulating neural activity, plasticity and memory." *Prog Neurobiol* 70 (1):1-32. doi: 10.1016/s0301-0082(03)00089-3.

Urbanc B., Cruz L., Le R., Sanders J., Ashe K. H., Duff K., Stanley H. E., Irizarry M. C., and Hyman B. T. 2002. "Neurotoxic effects of thioflavin S-positive amyloid deposits in transgenic mice and Alzheimer's disease." *Proc Natl Acad Sci U S A.* 99 (22):13990-5. doi: 10.1073/pnas.222433299.

Vagnozzi A. N., Giannopoulos P. F., and Pratico D. 2018. "Brain 5-lipoxygenase over-expression worsens memory, synaptic integrity, and tau pathology in the P301S mice." *Aging Cell* 17 (1). doi: 10.1111/acel.12695.

Valla J., Yaari R., Wolf A. B., Kusne Y., Beach T. G., Roher A. E., Corneveaux J. J., Huentelman M. J., Caselli R. J., and Reiman E. M. 2010. "Reduced posterior cingulate mitochondrial activity in expired young adult carriers of the APOE epsilon4 allele, the major late-onset Alzheimer's susceptibility gene." *J Alzheimers Dis* 22 (1):307-13. doi: 10.3233/JAD-2010-100129.

Van der Jeugd A., Hochgrafe K., Ahmed T., Decker J. M., Sydow A., Hofmann A., Wu D., Messing L., Balschun D., D'Hooge R., and Mandelkow E. M. 2012. "Cognitive defects are reversible in inducible mice expressing pro-aggregant full-length human Tau." *Acta Neuropathol* 123 (6):787-805. doi: 10.1007/s00401-012-0987-3.

Van der Jeugd A., Vermaercke B., Halliday G. M., Staufenbiel M., and Gotz J. 2016. "Impulsivity, decreased social exploration, and executive dysfunction in a mouse model of frontotemporal dementia." *Neurobiol Learn Mem* 130:34-43. doi: 10.1016/j.nlm.2016.01.007.

Vasconcelos B., Stancu I.-C., Buist A., Bird M., Wang P., Vanoosthuyse A., Van Kolen K., Verheyen A., Kienlen-Campard P., Octave J.-N., Baatsen P., Moechars D., and Dewachter I. 2016. "Heterotypic seeding of Tau fibrillization by pre-aggregated Abeta provides potent seeds for prion-like seeding and propagation of Tau-pathology in vivo." *Acta Neuropathologica* 131 (4):549-569. doi: 10.1007/s00401-015-1525-x.

Vassar R., Bennett B. D., Babu-Khan S., Kahn S., Mendiaz E. A., Denis P., Teplow D. B., Ross S., Amarante P., Loeloff R., Luo Y., Fisher S., Fuller J., Edenson S., Lile J., Jarosinski M. A., Biere A. L., Curran E., Burgess T., Louis J. C., Collins F., Treanor J., Rogers G., and Citron M. 1999. "Beta-secretase cleavage of Alzheimer's amyloid precursor protein by the transmembrane aspartic protease BACE." *Science* 286 (5440):735-41. doi: 10.1126/science.286.5440.735.

von Rotz R. C., Kohli B. M., Bosset J., Meier M., Suzuki T., Nitsch R. M., and Konietzko U. 2004. "The APP intracellular domain forms nuclear multiprotein complexes and regulates the transcription of its own precursor." *J Cell Sci* 117 (Pt 19):4435-48. doi: 10.1242/jcs.01323.

Vorhees C. V., and Williams M. T. 2006. "Morris water maze: procedures for assessing spatial and related forms of learning and memory." *Nat Protoc* 1 (2):848-58. doi: 10.1038/nprot.2006.116.

Vossel K. A., Zhang K., Brodbeck J., Daub A. C., Sharma P., Finkbeiner S., Cui B., and Mucke L. 2010. "Tau reduction prevents Abeta-induced defects in axonal transport." *Science* 330 (6001):198. doi: 10.1126/science.1194653.

Wagner J. M., Sichler M. E., Schleicher E. M., Franke T. N., Irwin C., Low M. J., Beindorff N., Bouter C., Bayer T. A., and Bouter Y. 2019. "Analysis of Motor Function in the Tg4-42 Mouse Model of Alzheimer's Disease." *Front Behav Neurosci* 13:107. doi: 10.3389/fnbeh.2019.00107.

Walsh D. M., Klyubin I., Fadeeva J. V., Cullen W. K., Anwyl R., Wolfe M. S., Rowan M. J., and Selkoe D. J. 2002. "Naturally secreted oligomers of amyloid beta protein potently inhibit hippocampal long-term potentiation in vivo." *Nature* 416 (6880):535-9. doi: 10.1038/416535a.

Walter S., Jumpertz T., Hüttenrauch M., Ogorek I., Gerber H., Storck S. E., Zampar S., Dimitrov M., Lehmann S., Lepka K., Berndt C., Wiltfang J., Becker-Pauly C., Beher D., Pietrzik C. U., Fraering P. C., Wirths O., and Weggen S. 2019. "The metalloprotease ADAMTS4 generates N-truncated Aβ4–x species and marks oligodendrocytes as a source of amyloidogenic peptides in Alzheimer's disease." *Acta Neuropathologica* 137 (2):239-257. doi: 10.1007/s00401-018-1929-5.

Wang H. W., Pasternak J. F., Kuo H., Ristic H., Lambert M. P., Chromy B., Viola K. L., Klein W. L., Stine W. B., Krafft G. A., and Trommer B. L. 2002. "Soluble oligomers of beta amyloid (1-42) inhibit long-term potentiation but not long-term depression in rat dentate gyrus." *Brain Res* 924 (2):133-40. doi: 10.1016/s0006-8993(01)03058-x.

Wang J., Dickson D. W., Trojanowski J. Q., and Lee V. M. 1999. "The levels of soluble versus insoluble brain Abeta distinguish Alzheimer's disease from normal and pathologic aging." *Exp Neurol* 158 (2):328-37. doi: 10.1006/exnr.1999.7085.

Wang Y., and Mandelkow E. 2016. "Tau in physiology and pathology." *Nat Rev Neurosci* 17 (1):5-21. doi: 10.1038/nrn.2015.1.

Weggen S., and Beher D. 2012. "Molecular consequences of amyloid precursor protein and presenilin mutations causing autosomal-dominant Alzheimer's disease." *Alzheimer's Research & Therapy* 4 (2):9. doi: 10.1186/alzrt107.

Wegiel J., Kuchna I., Nowicki K., Frackowiak J., Mazur-Kolecka B., Imaki H., Wegiel J., Mehta P. D., Silverman W. P., Reisberg B., Deleon M., Wisniewski T., Pirttilla T., Frey H., Lehtimaki T., Kivimaki T., Visser F. E., Kamphorst W., Potempska A., Bolton D., Currie J. R., and Miller D. L. 2007. "Intraneuronal Abeta immunoreactivity is not a predictor of brain amyloidosis-beta or neurofibrillary degeneration." *Acta Neuropathol (Berl)* 113 (4):389-402. doi: 10.1007/s00401-006-0191-4.

Weidemann A., Konig G., Bunke D., Fischer P., Salbaum J. M., Masters C. L., and Beyreuther K. 1989. "Identification, biogenesis, and localization of precursors of Alzheimer's disease A4 amyloid protein." *Cell* 57 (1):115-26. doi: 10.1016/0092-8674(89)90177-3.

Weingarten M. D., Lockwood A. H., Hwo S. Y., and Kirschner M. W. 1975. "A protein factor essential for microtubule assembly." *Proc Natl Acad Sci U S A* 72 (5):1858-62. doi: 10.1073/pnas.72.5.1858.

Weller R. O., Preston S. D., Subash M., and Carare R. O. 2009. "Cerebral amyloid angiopathy in the aetiology and immunotherapy of Alzheimer disease." *Alzheimers Res Ther* 1 (2):6. doi: 10.1186/alzrt6.

West M. J., Coleman P. D., Flood D. G., and Troncoso J. C. 1994. "Differences in the pattern of hippocampal neuronal loss in normal ageing and Alzheimer's disease." *Lancet* 344 (8925):769-72. doi: 10.1016/s0140-6736(94)92338-8.

Whitson J. S., Selkoe D. J., and Cotman C. W. 1989. "Amyloid beta protein enhances the survival of hippocampal neurons in vitro." *Science* 243 (4897):1488-90. doi: 10.1126/science.2928783.

Whitwell J. L., Josephs K. A., Murray M. E., Kantarci K., Przybelski S. A., Weigand S. D., Vemuri P., Senjem M. L., Parisi J. E., Knopman D. S., Boeve B. F., Petersen R. C., Dickson D. W., and Jack C. R., Jr. 2008.

"MRI correlates of neurofibrillary tangle pathology at autopsy: a voxel-based morphometry study." *Neurology* 71 (10):743-9. doi: 10.1212/01.wnl.0000324924.91351.7d.

WHO. 2017. Global action plan on the public health response to dementia 2017–2025. Geneva: World Health Organization.

WHO. 2019. Risk reduction of cognitive decline and dementia: WHO guidelines. Geneva: World Health Organization.

Wietrzych M., Meziane H., Sutter A., Ghyselinck N., Chapman P. F., Chambon P., and Krężel W. 2005. "Working memory deficits in retinoid X receptor γ-deficient mice." *Learning & Memory* 12 (3):318-326. doi: 10.1101/lm.89805.

Wildburger N. C., Esparza T. J., LeDuc R. D., Fellers R. T., Thomas P. M., Cairns N. J., Kelleher N. L., Bateman R. J., and Brody D. L. 2017. "Diversity of Amyloid-beta Proteoforms in the Alzheimer's Disease Brain." *Scientific Reports* 7 (1):9520. doi: 10.1038/s41598-017-10422-x.

Wiltfang J., Smirnov A., Schnierstein B., Kelemen G., Matthies U., Klafki H. W., Staufenbiel M., Huther G., Ruther E., and Kornhuber J. 1997. "Improved electrophoretic separation and immunoblotting of beta-amyloid (A beta) peptides 1-40, 1-42, and 1-43." *Electrophoresis* 18 (3-4):527-32. doi: 10.1002/elps.1150180332.

Wirths O., and Bayer T. A. 2008. "Motor impairment in Alzheimer's disease and transgenic Alzheimer's disease mouse models." *Genes Brain Behav* 7 Suppl 1:1-5. doi: 10.1111/j.1601-183X.2007.00373.x

Wirths O., Breyhan H., Cynis H., Schilling S., Demuth H. U., and Bayer T. A. 2009. "Intraneuronal pyroglutamate-Abeta 3-42 triggers neurodegeneration and lethal neurological deficits in a transgenic mouse model." *Acta Neuropathol* 118 (4):487-496. doi: 10.1007/s00401-009-0557-5.

Wirths O., Multhaup G., and Bayer T. A. 2004. "A modified beta-amyloid hypothesis: intraneuronal accumulation of the beta-amyloid peptide - the first step of a fatal cascade." *J Neurochem* 91 (3):513-20. doi: 10.1111/j.1471-4159.2004.02737.x.

Wirths O., Walter S., Kraus I., Klafki H. W., Stazi M., Oberstein T. J., Ghiso J., Wiltfang J., Bayer T. A., and Weggen S. 2017. "N-truncated Aβ4–x peptides in sporadic Alzheimer's disease cases and transgenic Alzheimer mouse models." *Alzheimers Res Ther* 9 (1):80. doi: 10.1186/s13195-017-0309-z.

Wirths O., and Zampar S. 2019. "Emerging roles of N- and C-terminally truncated Aβ species in Alzheimer's disease." *Expert Opinion on Therapeutic Targets* 23 (12):991-1004. doi: 10.1080/14728222.2019.1702972.

Wirths O., and Zampar S. 2020. "Neuron Loss in Alzheimer's Disease: Translation in Transgenic Mouse Models." *Int J Mol Sci* 21 (21). doi: 10.3390/ijms21218144.

Wirths O., Zampar S., and Weggen S. 2019. "N-Terminally Truncated Abeta Peptide Variants in Alzheimer's Disease." In *Alzheimer's Disease*, edited by T. Wisniewski. Brisbane (AU), doi: 10.15586/alzheimersdisease.2019.ch7.

Wisniewski K. E., Wisniewski H. M., and Wen G. Y. 1985. "Occurrence of neuropathological changes and dementia of Alzheimer's disease in Down's syndrome." *Ann Neurol* 17 (3):278-82. doi: 10.1002/ana.410170310.

Wittnam J. L., Portelius E., Zetterberg H., Gustavsson M. K., Schilling S., Koch B., Demuth H.-U., Blennow K., Wirths O., and Bayer T. A. 2012. "Pyroglutamate Amyloid β (Aβ) Aggravates Behavioral Deficits in Transgenic Amyloid Mouse Model for Alzheimer Disease." *J Biol Chem* 287 (11):8154-8162. doi: 10.1074/jbc.M111.308601.

Wu H. Y., Hudry E., Hashimoto T., Kuchibhotla K., Rozkalne A., Fan Z., Spires-Jones T., Xie H., Arbel-Ornath M., Grosskreutz C. L., Bacskai B. J., and Hyman B. T. 2010. "Amyloid beta induces the morphological neurodegenerative triad of spine loss, dendritic simplification, and neuritic dystrophies through calcineurin activation." *J Neurosci* 30 (7):2636-49. doi: 10.1523/JNEUROSCI.4456-09.2010.

Wyss-Coray T. 2006. "Inflammation in Alzheimer disease: driving force, bystander or beneficial response?" *Nat Med* 12 (9):1005-15. doi: 10.1038/nm1484.

Wyss-Coray T., and Rogers J. 2012. "Inflammation in Alzheimer Disease—A Brief Review of the Basic Science and Clinical Literature." *Cold Spring Harbor Perspectives in Medicine* 2 (1). doi: 10.1101/cshperspect.a006346.

Xie Y., Yao Z., Chai H., Wong W. M., and Wu W. 2003. "Potential roles of Alzheimer precursor protein A4 and beta-amyloid in survival and function of aged spinal motor neurons after axonal injury." *J Neurosci Res* 73 (4):557-64. doi: 10.1002/jnr.10667.

Yamin G. 2009. "NMDA receptor-dependent signaling pathways that underlie amyloid beta-protein disruption of LTP in the hippocampus." *J Neurosci Res* 87 (8):1729-36. doi: 10.1002/jnr.21998.

Yankner B. A., Duffy L. K., and Kirschner D. A. 1990. "Neurotrophic and neurotoxic effects of amyloid beta protein: reversal by tachykinin neuropeptides." *Science* 250 (4978):279-82. doi: 10.1126/science.2218531.

Yatin S. M., Aksenova M., Aksenov M., Markesbery W. R., Aulick T., and Butterfield D. A. 1998. "Temporal relations among amyloid beta-peptide-induced free-radical oxidative stress, neuronal toxicity, and neuronal defensive responses." *J Mol Neurosci* 11 (3):183-97. doi: 10.1385/JMN:11:3:183.

Yin Y., Gao D., Wang Y., Wang Z. H., Wang X., Ye J., Wu D., Fang L., Pi G., Yang Y., Wang X. C., Lu C., Ye K., and Wang J. Z. 2016. "Tau accumulation induces synaptic impairment and memory deficit by calcineurin-mediated inactivation of nuclear CaMKIV/CREB signaling." *Proc Natl Acad Sci U S A* 113 (26):E3773-81. doi: 10.1073/pnas.1604519113.

Yoshida H., and Ihara Y. 1993. "Tau in paired helical filaments is functionally distinct from fetal tau: assembly incompetence of paired helical filament-tau." *J Neurochem* 61 (3):1183-6. doi: 10.1111/j.1471-4159.1993.tb03642.x.

Yoshikai S., Sasaki H., Doh-ura K., Furuya H., and Sakaki Y. 1990. "Genomic organization of the human amyloid beta-protein precursor gene." *Gene* 87 (2):257-63. doi: 10.1016/0378-1119(90)90310-n.

Yoshiyama Y., Higuchi M., Zhang B., Huang S. M., Iwata N., Saido T. C., Maeda J., Suhara T., Trojanowski J. Q., and Lee V. M. 2007. "Synapse loss and microglial activation precede tangles in a P301S tauopathy mouse model." *Neuron* 53 (3):337-51. doi: 10.1016/j.neuron.2007.01.010.

Zakharova N. V., Bugrova A. E., Kononikhin A. S., Indeykina M. I., Popov I. A., and Nikolaev E. N. 2018. "Mass spectrometry analysis of the diversity of Abeta peptides: difficulties and future perspectives for AD biomarker discovery." *Expert Rev Proteomics* 15 (10):773-775. doi: 10.1080/14789450.2018.1525296.

Zampar S., Klafki H. W., Sritharen K., Bayer T. A., Wiltfang J., Rostagno A., Ghiso J., Miles L. A., and Wirths O. 2020. "N-terminal heterogeneity of parenchymal and vascular amyloid-beta deposits in Alzheimer's disease." *Neuropathol Appl Neurobiol* 46 (7):673-685. doi: 10.1111/nan.12637.

Zampar S., and Wirths O. 2020. "Immunotherapy Targeting Amyloid-beta Peptides in Alzheimer's Disease." In *Alzheimer's Disease: Drug Discovery*, edited by X. Huang. Brisbane (AU), doi: 10.36255/exonpublications.alzheimersdisease.2020.ch2.

Zampar S., and Wirths O. 2021. "Characterization of a Mouse Model of Alzheimer's Disease Expressing Aβ4-42 and Human Mutant Tau." *International Journal of Molecular Sciences* 22 (10):5191. doi: 10.3390/ijms22105191.

Zempel H., Thies E., Mandelkow E., and Mandelkow E. M. 2010. "Abeta oligomers cause localized Ca(2+) elevation, missorting of endogenous Tau into dendrites, Tau phosphorylation, and destruction of microtubules and spines." *J Neurosci* 30 (36):11938-50. doi: 10.1523/JNEUROSCI.2357-10.2010.

Zhang H., Liu D., Wang Y., Huang H., Zhao Y., and Zhou H. 2017. "Meta-analysis of expression and function of neprilysin in Alzheimer's disease." *Neurosci Lett* 657:69-76. doi: 10.1016/j.neulet.2017.07.060.

Zhang Y., Chen K., Sloan S. A., Bennett M. L., Scholze A. R., O'Keeffe S., Phatnani H. P., Guarnieri P., Caneda C., Ruderisch N., Deng S., Liddelow S. A., Zhang C., Daneman R., Maniatis T., Barres B. A., and Wu J. Q. 2014. "An RNA-sequencing transcriptome and splicing database of glia, neurons, and vascular cells of the cerebral cortex." *J Neurosci* 34 (36):11929-47. doi: 10.1523/jneurosci.1860-14.2014.

Zhao D., Watson J. B., and Xie C. W. 2004. "Amyloid beta prevents activation of calcium/calmodulin-dependent protein kinase II and AMPA receptor phosphorylation during hippocampal long-term potentiation." *J Neurophysiol* 92 (5):2853-8. doi: 10.1152/jn.00485.2004.

Zhao X., Kotilinek L. A., Smith B., Hlynialuk C., Zahs K., Ramsden M., Cleary J., and Ashe K. H. 2016. "Caspase-2 cleavage of tau reversibly impairs memory." *Nat Med* 22 (11):1268-1276. doi: 10.1038/nm.4199.

Zhou L., McInnes J., Wierda K., Holt M., Herrmann A. G., Jackson R. J., Wang Y. C., Swerts J., Beyens J., Miskiewicz K., Vilain S., Dewachter I., Moechars D., De Strooper B., Spires-Jones T. L., De Wit J., and Verstreken P. 2017. "Tau association with synaptic vesicles causes presynaptic dysfunction." *Nat Commun* 8:15295. doi: 10.1038/ncomms15295.

Zou L.-B., Mouri A., Iwata N., Saido T. C., Wang D., Wang M.-W., Mizoguchi H., Noda Y., and Nabeshima T. 2006. "Inhibition of Neprilysin by Infusion of Thiorphan into the Hippocampus Causes an Accumulation of Amyloid β and Impairment of Learning and Memory." *J Pharmacol Exp Ther* 317 (1):334-340. doi: 10.1124/jpet.105.095687.

7 ACKNOWLEDGEMENTS

In the first place I want to express my gratitude to my supervisor, Prof. Dr. Oliver Wirths. Because of your example, support and guidance I have learned and grown tremendously. Thank you for mentoring me with your scientific knowledge and for letting me develop my independence and critical sense.

I thank the members of my thesis committee: Prof. Dr. Tiago Outeiro, thank you for agreeing to be the second reviewer for my thesis, for your valuable input during my progress reports and for your support. Thank you, Prof. Dr. Fred Wouters, for your time and very helpful discussions.

Thanks to the GGNB office and member of the CMBP program, especially to Prof. Dr. Michael Hörner, Prof. Dr. Thomas Dresbach, Dr. Kirsten Pöhlker and Franziska Kühne.

Furthermore, I would like to thank Dr. Hans Klafki for his guidance through part of my research, for his scientific rigor and his friendly jokes. Thank you, Petra Rieper, for the technical and emotional support, I loved sharing the office with you. I would also like to thank Petra Tucholla for the laboratory assistance and practical support during the first part of my doctoral studies.

To the current and former lab members, and to the students I had the pleasure to supervise, thank you for having being part of this journey. I learned a lot because all of you.

Thanks to Justin and Tomoko, for the unforgettable dinners and evenings together. Göttingen would have not been the same without you. Grazie ad Antonio, Daniele, Fabio, Gabriele e Giuseppe per avermi fatto sentire a casa in un paese straniero. Un ringraziamento speciale a Martina, mia collega di avventure e sventure. La tua presenza

ha portato allegria e leggerezza in laboratorio e fuori. Sono grata di aver potuto condividere questa esperienza con te.

Un enorme grazie alla mia famiglia. Siete sempre stati i miei principali sostenitori e avete gioito di ogni mio piccolo traguardo. Un pensiero speciale ai miei nonni e alle mie nonne, vicini e lontani. Grazie ad Anna ed Enzo, per il supporto continuo.

Leonardo, non è possibile condensare in poche righe tutto quello che abbiamo provato e vissuto negli ultimi dieci anni. Sei l'unico che può capire davvero. Grazie per essere il mio costante punto di riferimento. Sei il mio passato, presente e futuro. Al nostro prossimo capitolo di questa vita.

A Edoardo, per spingermi ogni giorno ad essere migliore. Mi stai insegnando ciò che è davvero importante nella vita. Spero che un giorno tu sarai orgoglioso di me.

8 APPENDIX

8.1 List of figures

8.2 List of tables

8.3 List of abbreviations

Abbreviation	Description
Aβ	Amyloid-β
ABC	Avidin-biotin complex
AβOs	Amyloid-β oligomers
AD	Alzheimer's disease
ADAM	A disintegrin and metalloprotease
ADAMTS	A disintegrin-like and metalloprotease with thrombospondin type 1 motif
ADE	Aβ-degrading enzyme
AICD	APP intracellular domain
ALS	Amyotrophic lateral sclerosis
ANOVA	Analysis of variance
APO	Apolipoprotein E
APP	Amyloid precursor protein
ATP	Adenosine triphosphate
BACE1	β -site APP cleaving enzyme
BBB	Blood-brain barrier
CA1-3	Cornu ammonis area 1-3
CAA	Cerebral amyloid angiopathy
cDNA	Complementary DNA
ChAT	Choline acetyltransferase
CIEF	Capillary Isoelectric Focusing
CSF	Cerebrospinal fluid
CTF	Carboxyl-terminal fragment
DAB	3,3′-diaminobenzidine
DAPI	4′,6-diamidin-2-phenylindol
DG	Dentate gyrus
DI	Discrimination index
DMSO	Dimethyl sulfoxide
DNA	Deoxyribonucleic acid
DS	Down syndrome
EC	Entorhinal cortex
ELISA	Enzyme-linked immunosorbent assay
EPM	Elevated plus maze
EO-FAD	Early-onset familial Alzheimer's disease
ER	Endoplasmic reticulum
FAD	Familial Alzheimer's disease

FCS	Fetal cow serum
FTD	Frontotemporal dementia
GOI	Gene of interest
GWAS	Genome-wide association studies
HEPES	4-(2-hydroxyethyl)-1-piperazineethanesulfonic acid
Het	Heterozygous
Hom	Homozygous
HRP	Horseradish peroxidase
Iba1	Ionized calcium-binding adapter molecule 1
LOAD	Late-onset Alzheimer's disease
LTD	Long-term depression
LTP	Long-term potentiation
MAPT	Microtubule-associated protein tau
MBD	Microtubule-binding domain
MCI	Mild cognitive impairment
MN	Motoneuron
MRI	Magnetic resonance imaging
mRNA	Messenger RNA
MWM	Morris Water Maze
NDC	Non-demented controls
NEP	Neprilysin
NFT	Neurofibrillary tangle
NOR	Novel object recognition
OF	Open field
PA	Phosphoramidon
PBS	Phosphate buffered saline
PCR	Polymerase chain reaction
PHF	Paired helical filament
PMI	Post-mortem interval
PrP	Prion protein
PSEN	Presenilin
pTau	Phosphorylated tau
qRT-PCR	quantitative Real-Time PCR
RNA	Ribonucleic acid
RT	Room temperature
sAPP	Soluble APP fragment
SD	Standard deviation
SDS	Sodium dodecyl sulfate
SDS-buffer	Tris/NaCl/SDS buffer
TBE buffer	Tris/borate/EDTA buffer

TBS-buffer	Tris/NaCl buffer
TFA	Trifluoroacetic acid
TRH	Thyrotropin-releasing hormone
WT	Wild type